Structural aspects of the plasmalemmal Amyloid Precursor Protein cluster

---

- DISSERTATION -

zur Erlangung des Doktorgrades (Dr. rer. nat.)

der

Mathematisch-Naturwissenschaftlichen Fakultät

der

Rheinischen Friedrich-Wilhelms-Universität Bonn

vorgelegt von

Dennis de Coninck

aus

Stein, die Niederlande

Bonn, August 2020

Angefertigt mit Genehmigung der
Mathematisch-Naturwissenschaftlichen Fakultät der
Rheinischen Friedrich-Wilhelms-Universität Bonn

1. Gutachter

Herr Prof. Dr. rer. nat. Thorsten Lang

2. Gutachter

Herr Prof. Dr. rer. nat. Jochen Walter

Tag der Mündlichen Prüfung:

15 Dezember 2020

Erscheinungsjahr:

2021

Anmerkung/Annotation

Teile dieser Arbeit wurden bereits vorab veröffentlicht:
Parts of this work have been published in advance:

De Coninck, D., Schmidt, T.H., Schloetel, J.G., Lang, T. (2018) “Packing Density of the Amyloid Precursor Protein in the Cell Membrane.” In: *Biophysical Journal* 114(5), pp. 1128-1141.
DOI: https://doi.org/10.1016/j.bpj.2018.01.009

Everything not saved will be lost.

Nintendo “Quit Screen” message

Table of Contents

List of Figures 8
List of Tables 9
Abbreviations 10
1. Introduction 13
1.1. Epidemiology and impact of AD 13
1.2. Pathophysiology of AD 15
1.2.1. Environmental factors 16
1.2.2. Genetic factors 17
1.2.3. Etiology 20
1.3. The APP family 23
1.3.1. Physiological role 23
1.4. The amyloid precursor protein 25
1.4.1. Structure 25
1.4.2. Proteolytic processing and cellular transport 27
1.4.3. Cellular functions 30
1.4.4. Plasmalemmal organization 32
1.4.5. Mutations 34
2. Rationale and aims of the study 38
3. Materials and Methods 40
3.1. Materials 40
3.1.1. General instruments 40
3.1.2. Microscopes 41
3.1.3. Chemicals and consumables 42
3.1.4. Buffers and solutions 43
3.1.5. Culture media and reagents 44
3.1.6. Cell lines 44
3.1.7. Antibodies 45
3.1.8. Plasmids 45
3.1.9. Kits 46
3.1.10. Software 47

3.2. Methods 47
3.2.1. Cloning of expression plasmids 47
3.2.2. Bacterial expression of His_6-APP_{695} 49
3.2.3. Ni-NTA purification of His_6-APP_{695} 50
3.2.4. Protein biotinylation 51
3.2.5. SDS-PAGE 51
3.2.6. In-gel stainings 52
3.2.7. Western blotting 52
3.2.8. Cell culture of SH-SY5Y and HepG2 cells 53
3.2.9. Preparation of cover slips for microscopy 54
3.2.10. Microscopy 56
3.2.11. Image analysis 57
4. Results 60
4.1. Packing density of plasmalemmal APP clusters 60
4.1.1. Expression and purification of recombinant APP_{695} 60
4.1.2. APP content of SH-SY5Y plasma membranes 66
4.1.3. Molecular density of APP in the plasma membrane 70
4.1.4. Validation of the methodology for visualization of plasmalemmal APP 74
4.1.5. Size and molecular density of the plasmalemmal APP clusters 81
4.2. Significance of the A673T mutant for plasmalemmal APP 92
4.2.1. Effect of the A673T mutation on APP clustering 92
4.2.2. Functional differences of the APP variants 99
5. Discussion 104
5.1. Validity of the model systems 104
5.2. Caveats of standard fixation protocols 105
5.3. Accuracy of the plasmalemmal copy number 107
5.4. Implications of APP overexpression 110
5.5. Microscopic approaches to the molecular cluster density 111
5.6. Impact of the A673T mutation on clustering and processing 115
5.7. Conclusion 118
5.8. Outlook 120
6. References 122
7. Summary 165
8. Acknowledgments 167

List of Figures

Figure	Title	Page
	Introduction	
Figure 1	Future impact of AD	15
Figure 2	Genetics of AD	21
Figure 3	Structure of APP and Aβ	28
Figure 4	Intracellular trafficking and processing of APP	31
Figure 5	AD-related Aβ-proximal APP mutations	37
	Results	
Figure 6	Bacterial expression of recombinant APP_{695}	64
Figure 7	Purification of recombinant APP_{695}	66
Figure 8	Concentration of recombinant APP_{695}	67
Figure 9	SH-SY5Y total cellular protein content	68
Figure 10	APP copy number per cell	69
Figure 11	Plasmalemmal APP fraction	71
Figure 12	Effect of fixation on cell blebbing	72
Figure 13	SH-SY5Y membrane surface area	74
Figure 14	Purity of plasma membrane sheets	77
Figure 15	Validity of APP overexpression and the C-terminal antibody	80
Figure 16	Reliable analysis and immobilization of plasmalemmal APP	82
Figure 17	Detection of APP under variable labelling conditions	85
Figure 18	Labelling condition-dependent brightness of APP maxima	86
Figure 19	Monomeric fraction of plasmalemmal APP	88
Figure 20	Density and size of APP clusters in the plasma membrane	92
Figure 21	Influence of the A673T mutation on APP cluster size	95
Figure 22	Plasmalemmal distribution of APP_{WT} and APP_{A673T}	97
Figure 23	Mobility of APP_{WT} and APP_{A673T} in the plasma membrane	99
Figure 24	Relevance of APP processing for plasmalemmal mobility	100
Figure 25	Sorting of APP_{WT} and APP_{A673T} into clathrin structures	102
Figure 26	α-processing of APP_{WT} and APP_{A673T}	104
	Discussion	
Figure 27	Interaction between monomer fraction and cluster density	114
Figure 28	Molecular density of the average APP cluster	121

List of Tables

Table	Title	Page
Table 1	General instruments	42
Table 2	Chemicals and consumables	44
Table 3	Buffers and solutions	45
Table 4	Culture media and reagents	46
Table 5	Antibodies	47
Table 6	Plasmids	47
Table 7	Kits	48
Table 8	Software	49

Abbreviations

(D)PBS	(Dulbecco's) phosphate buffered saline
(α/β)-CTF	alpha or beta C-terminal fragment
a.u.	arbitrary units
aa	amino acid
AICD	Amyloid Precursor Protein intra-cellular domain
APLP1/2	Amyloid Precursor-like Protein 1 or 2
APP	Amyloid Precursor Protein
APS	ammonium persulfate
Aβ	Amyloid-beta
BACE1/2	beta-site Amyloid Precursor Protein cleaving enzyme 1 or 2
BCA	bicinchoninic acid
BSA	bovine serum albumin
ddH_2O	double-distilled water
DMSO	dimethylsulfoxid
DNA	deoxyribonucleic acid
DTT	dithiothreitol
EDTA	ethylenediaminetetraacetic acid
EGTA	ethylene glycol-bis(2-aminoethylether)-N,N,N,N-tetraacetic acid
emGFP	emerald Green Fluorescent Protein
ER	endoplasmic reticulum
FCS	fetal calf serum
FRAP	fluorescence recovery after photobleaching
FRET	Förster resonance energy transfer
FWHM	full width at half maximum
GFP	Green Fluorescent Protein
gSTED	time-gated stimulated emission depletion
h or hr	hour
IF	immonufluorescence
iPSC	induced pluripotent stem cell
JMD	juxtamembrane domain
LB medium	Luria-Bertani medium according to Lennox
m or min	minute
mCh	monomeric Cherry; mFruits family of monomeric Red Fluorescent Proteins

mOsm	milliosmole
PAGE	polyacrylamide gel electrophoresis
PALM	photo-activated localization microscopy
PCC	Pearson correlation coefficient
PCR	polymerase chain reaction
PFA	paraformaldehyde
PLL	poly-L-lysine
PLP	paraformaldehyde-lysine-periodate
PM	plasma membrane
PMSF	phenylmethylsulfonyl fluoride
PSEN1/2	Presenilin 1 or 2
RIPA	radioimmunoprecipitation assay buffer
RNA	ribonucleic acid
ROI	region of interest
s or sec	second
sAPP(α/β)	soluble amyloid precursor protein alpha or beta
SDS	sodium dodecyl sulphate
TAE	Tris-acetate-EDTA
TBS	Tris buffered saline
TIRF	total internal reflection fluorescence
TMD	Transmembrane domain
TMA-DPH	1-(4-trimethyl-ammoniumphenyl)-6-phenyl-1,3,5-hexatriene-p-toluolsulfonate
WB	western blot

1. Introduction

1.1. Epidemiology and impact of AD

Nowadays, Alzheimer's Disease (AD) is the dominant cause of dementia and accounts for between 60-70% of all dementia cases (World Health Organization 2019). Its incidence in western countries is primarily dependent on age, starting with an incidence rate of about 3 per 1000 person-years between the ages of 65 and 69 and approximately doubling every 5 years thereafter (Bermejo-Pareja et al. 2008). Independent of age, women are about two times more likely to be diagnosed with AD, although whether this has a biological reason or is merely due to education or survival bias remains to be elucidated (Hebert et al. 2013; Andersen et al. 1999; Chêne et al. 2015; Rocca et al. 2014). It also appears that there are racial and ethnic differences in the number of individuals diagnosed with AD. In the United States of America (USA), African-Americans seem to have the highest risk for developing AD, followed by Hispanic-Americans, then European-Americans and finally Asian-Americans (Mayeda et al. 2016). There are strong indications, however, that these differences are more likely caused by variations in health, lifestyle and socio-economic risk factors typical for the ethnical group the individual belongs to than by racial disparity of genetic factors (Yaffe et al. 2013; Chin et al. 2011). In 2017, prevalence of AD in the USA is estimated to be around 5.5 million people, of which 5.3 million are above the age of 65. This means that about 10% of the people above the age of 65 in the USA have been diagnosed with AD (Hebert et al. 2013). Prevalence in Europe does not differ much from the USA with about 7% of all people above the age of 65 diagnosed with AD in 2016 (Niu et al. 2017).

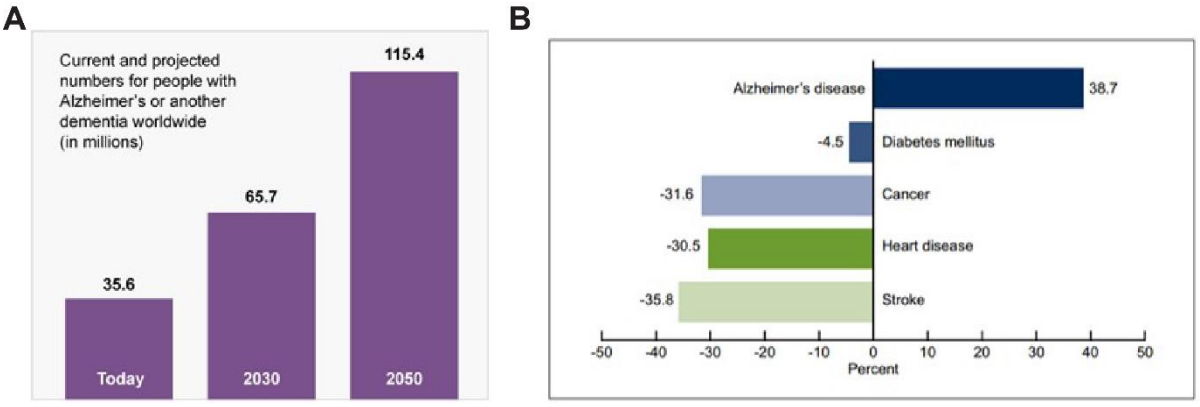

Figure 1. Future impact of AD

(A) The current and projected number of people suffering from AD or another dementia worldwide. Graph taken from the "World Alzheimer Report 2009" (Alzheimer's Disease International 2009). **(B)** Change in mortality rates between 2000 and 2010 of prominent diseases affecting the population of the USA. Graph taken from the "Mortality From Alzheimer's Disease in the United States: Data for 2000 and 2010" NCHS Data Brief No. 116 (Betzaida Tejada-Vera 2013).

Considering that AD is generally underdiagnosed, underreported and rather comprises the later stages of the underlying disease, it can be projected that the prevalence of AD is probably much higher than the officially reported numbers (Bradford et al. 2009; Zaleta et al. 2012). Furthermore, the relative number of people above the age of 65 is expected to grow rapidly in coming years due to increasing medical knowledge, quality of healthcare and the fact that the 'baby boom generation' has started to enter these age ranges (Administration on Aging, Administration for Community Living 2016; Statistisches Bundesamt). Taken together, it is probable that incidence and prevalence of AD will keep rising in the coming years (Figure 1A).

Even though the consequences of AD are often underestimated by the general population, its impact on an individual's health is considerable and the socio-economic burden on all levels of our society enormous. Scientists today are able to gauge the significance of diseases more accurately by not just evaluating the number of people affected by the disease, but also include information such as the years of life lost and the years of life spent in a state of disability as a result of the pathology. Regardless of the exact method used, no other major pathology rose in rank as fast as AD in the last 30 years, exemplifying the ever-increasing severity and influence of the affliction (Alzheimer's Association Report 2017). Alzheimer's disease is becoming a more common cause of death, and it is the only top 10 cause of death that cannot be prevented, cured or even slowed at the moment. Whereas deaths as a result of stroke, heart disease, cancer and even diabetes mellitus have decreased steadily from the year 2000 onward, confirmed mortalities due to AD have increased by almost two-fold in the same timespan (Figure 1B) (Kenneth D. Kochanek et al. 2016; Arialdi M. Minino et al. 2002). As the disease itself does not directly cause death, a person is considered to have died from AD if it is acknowledged as the underlying cause of death, which is defined by the World Health Organization as "the disease or injury which initiated the train of events leading directly to death" (World Health Organization 2004). To elaborate, as AD progresses, it will unequivocally result in complications such as swallowing disorders, malnutrition and immobility. In turn, these complications increase the risk for more severe ailments like dehydration and pneumonia that, especially in the elderly, can eventually lead to death. Thus, after AD is positively diagnosed, life expectancy of an affected individual typically ranges from three to ten years, with less than 3% of individuals surviving for over 14 years past diagnosis (Mölsä et al. 1995; Zanetti et al. 2009). While the total number of survival years is higher the earlier AD is diagnosed, especially the younger victims have a significantly reduced life expectancy compared to the same-age healthy population (Dodge et al. 2003). Furthermore, men have a considerably worse survival prognosis than women (Ganguli et al. 2005).

AD-related mortalities, although increasing in both absolute and relative numbers, are not the main reason for the pathology's immense socio-economic burden on individuals, families and modern

society as a whole. AD is also one of the leading causes of morbidity nowadays. This state of poor health, disability and dependence, which a victim usually has to live through for many years, is the main reason for the tremendous impact of AD. Affected individuals spend on average 40% of the total number of years they have to live with AD in the most severe state of the dementia and much of this time is usually spend in a specialized clinic or facility. Of the general population only 4% is expected to be in a nursing home at age 80 compared to 75% of the people diagnosed with AD (Arrighi et al. 2010). Even if a demented individual lives at home or in a residential setting, support from direct-care workers, like nurse, home health and personal or home care aides is essential. As a result of the required long-term and intensive care for individuals suffering from dementia, it is one of the most expensive conditions for modern society (Hurd et al. 2013). In total the USA will spend an estimated 259 billion dollars on professional medical care and aid for all individuals with Alzheimer's or other dementias in 2017 (Alzheimer's Association Report 2017). However, older people are generally dependent on additional support that in 83% of all cases in the USA comes from family members or close friends (Friedman et al. 2015). Almost half of these unpaid caregivers, which are more than 15 million people, do so for someone suffering from dementia. This adds up to an astounding 18.2 billion hours or 230.1 billion dollars of unpaid service in 2016, almost mirroring the cost of professional care for demented individuals (Wolff et al. 2016). If one than also takes into consideration that, because of their often intimate relationship, informal caregivers of the demented are twice as likely to suffer from emotional, financial and physical difficulties compared to caregivers of people without dementia, the full range of the impact of AD on society becomes apparent. Although the ratio between professional and unpaid caregiver cost is probably skewed towards the professional side, there is no reason to assume that total expenditure per individual for demented people in Europe differs much from the costs in the USA (Ferri et al. 2005).

1.2. Pathophysiology of AD

The apparent cognitive, behavioral and neuropsychiatric symptoms associated with AD are a result of neuropathological abnormalities that precede and eventually cause the dementia and worsen the more the disease progresses. Macroscopically, these abnormalities are characterized by atrophy of affected brain regions, primarily the temporal and parietal lobe, brainstem nuclei and parts of the frontal cortex and cingulate gyrus (Wenk 2003; Braak and Del Tredici 2012). The cerebral atrophy is a result of processes that act on the cellular scale. It is generally accepted that microvascular damage, inflammation caused by microgliosis and neuronal and synaptic dysfunction are the key mechanisms eventually culminating in neuron loss (Nochlin et al. 1993). However, it is still unclear in what order these mechanisms emerge and how they interact. Additionally, it remains to be elucidated which players and pathways can cause or modulate these mechanisms on the molecular scale. Initially, the

culprits were believed to be the two most important clinico-pathological features of AD: the extracellular amyloid deposits consisting of aggregated amyloid-beta peptide (Aβ) and the intracellular neurofibrillary tangles comprised of aggregated Tau protein. However, as Alois Alzheimer already noticed when he analyzed the brain of his second patient, Johann F., it is possible to suffer from AD without showing the intracellular Tau tangles (Alois Alzheimer 1911). It is also possible to develop AD without displaying amyloid plaques and mentally healthy individuals can present with either Aβ plaques, Tau tangles or both, without any symptoms or indications even hinting towards an underlying dementia (Gefen et al. 2015). These discrepancies, especially the latter, suggest that Aβ plaques and Tau tangles cannot be the primary causative effectors in AD. But what then is the underlying cause for Alzheimer's? To date this question has, unfortunately, not been conclusively answered. However, many factors that either can or cannot affect AD initiation, progression or both have been uncovered over the years.

1.2.1. Environmental factors

By meta-analyzing multiple studies and assembling an online database of epidemiological reports, multiple environmental risk and protective factors have been identified over the years. Two very prominent risk factors are without a doubt age and head injury, but because these are not modifiable, they are perhaps the least interesting ones for pharmaceutical research (Ferri et al. 2005; Sundström et al. 2007). Nevertheless, because aging is a slow, continuous and gradual transition, whereas head injury happens suddenly modifying processes in the brain abruptly, these two risk factors show that inherently different mechanisms can lead to the same outcome and thus underline the complexity of AD. Important modifiable lifestyle risk factors for dementia are smoking (Lee et al. 2010) and midlife obesity (Beydoun et al. 2008), while alcohol intake (Anstey et al. 2009), physical activity (Hamer and Chida 2009) and 'cognitive reserve', a combination of the beneficial effects of mental activity, education and occupation (Valenzuela and Sachdev 2006), are protective factors. Diet is also implicated to have a direct effect on the onset and progression of dementia. Diets with high cholesterol, saturated fats and simple carbohydrates appear to increase disease risk (Kanoski and Davidson 2011). Mediterranean and Japanese diets conversely seem to be beneficial, apparently because of their positive impact on the cardiovascular system (Hu et al. 2013; Solfrizzi et al. 2008). Additionally, caffeine and flavonoids have also been shown to protect against AD, even though their mode of action has not yet been elucidated (Santos et al. 2010; Nehlig 2013). Many other dietary components, like vitamins (vitamin A, multiple B vitamins, vitamin C and alpha-tocopherol), minerals (selenium and zinc), specific fatty acids (omega-3 and docosahexaenoic acid), curcumin, ginkgo and cannabinoids, have been evaluated over the years (Essa et al. 2016), but to date not even one has been conclusively shown to alter disease initiation or progression significantly. Besides lifestyle conditions,

medical conditions are also implicated to influence AD susceptibility. Notably, stroke (Savva and Stephan 2010), diabetes (Lu et al. 2009), midlife hypertension (Qiu et al. 2005) and midlife hypercholesterolemia (Anstey et al. 2008; Kivipelto and Solomon 2006) seem to increase the chance of developing dementia. Of course, one must take care with interpreting these determinants, as there is a good chance that lifestyle factors affect medical conditions at least to a certain degree and vice versa. Medication is another important group of environmental factors that can influence AD and can be subdivided in two categories, medication that is given specifically to treat AD and medication that is prescribed for other ailments but seems to have an effect on AD. As Alzheimer's is incurable as it stands, its medical treatment is purely palliative and offers only symptomatic relieve. There are 5 medications that are approved by the FDA and are given to alleviate some of the cognitive problems that accompany the pathology: one NMDA receptor antagonist (memantine) and four acetylcholinesterase inhibitors (donepezil, rivastigmine, tacrine and galantamine). However, none of these have been shown to even delay the progression of AD (Casey et al. 2010). Long-term usage of non-steroidal anti-inflammatory drugs (NSAIDs), on the other hand, has previously been shown to reduce the probability of AD occurrence (Szekely et al. 2007). Unfortunately, after more stringent verification, it appears that their use just reduces the inflammation surrounding the senile plaques and thus does not counter the underlying pathology (Imbimbo 2009). Although many AD associated risk factors are also cardiovascular disease risk factors (smoking, diet, diabetes and midlife obesity, hypertension and cholesterolemia), statins, which are a class of lipid-lowering medications that are effective in treating cardiovascular disease, have been unable to prevent or improve AD pathology (McGuinness et al. 2014). The last 50 years or so a lot of research has focused on the effects of lifestyle choices, environmental factors and many types of drugs on AD, but, regrettably, it has not made us much wiser about the molecular origins of or the mechanisms involved in the pathology. For this reason, although only a small portion of the AD cases have a clear genetic cause, researchers have looked especially to genetics to elucidate more of the mystery surrounding AD.

1.2.2. Genetic factors

To be able to discuss the underlying mechanisms responsible for AD initiation and progression, it is helpful to first define the various categorizations of the disease. The most common, but least meaningful distinction is a relic of the past and is based on the age of onset of the disease. Early-onset Alzheimer's disease (EOAD) is diagnosed before the age of 65 and accounts for roughly 5-10% of all AD cases; whereas late-onset Alzheimer's disease (LOAD) is diagnosed after the age 65 and accounts for the remainder of cases (Figure 2A) (Zhu et al. 2015). A second and more useful classification is based on heritability and distinguishes between familial Alzheimer's disease and sporadic Alzheimer's disease. In familial Alzheimer's disease (FAD) certain germline mutations in one of three genes causes

the autosomal dominant, inheritable form of AD with nearly complete penetrance (Waring and Rosenberg 2008; Williamson et al. 2009). These three genes are APP, presenilin 1 (PSEN1) and presenilin 2 (PSEN2), which are responsible for 10-15%, 30-70% and <5% of the FAD cases respectively (Bird 1993-2020). Some FAD cases show no known identifiable pathogenic variant of either of these genes, making it likely that other genes can be causative as well. Essentially all cases of FAD are also early-onset and usually comprise some of the earliest diagnoses of AD, sometimes even before the age of 20. However, FAD is quite uncommon as it only constitutes between 2 and 35% of EOAD cases which boils down to between 0.1 and 3.5% of the total AD cases (Campion et al. 1999; Harvey et al. 2003; Mendez 2012). The other incidences of EOAD share the same traits as LOAD and are grouped together in what is called sporadic Alzheimer's disease (SAD). In SAD genetic predispositions are common, however, in contrast to the FAD inducing mutations, none of the SAD associated polymorphisms show full penetrance towards development of AD (Figure 2B). Nevertheless, although these generally occur only rarely, a few mutation-harboring loci related to SAD can substantially increase the risk for developing the pathology. The most famous risk factor for SAD is the APOEε4 allele of which between 40 and 80% of individuals diagnosed with AD possess at least one (Mahley et al. 2006). Heterozygote carriers of the APOEε4 allele have an increased risk to develop AD of approximately 3 times, whereas in homozygotes the risk is increased to 15 times higher in comparison to non-carriers (Farrer et al. 1997). On the other hand, the ε2 allele of APOE has been described as protective against AD (Corder et al. 1994). Three genes that have also been shown to possess rare coding variants with moderate to large effects on the risk to develop SAD are ADAM10, TREM2 and PLD3 (Guerreiro et al. 2013; Jonsson et al. 2013; Kim et al. 2009; Suh et al. 2013; Cruchaga et al. 2014), even though PLD3 has recently been questioned again quite convincingly (Fazzari et al. 2017). It should be remarked here that the three genes implicated in causing FAD (APP, PSEN1 and PSEN2) can also harbor mutations that do not confer full penetrance towards development of AD and can therefore additionally be classified as risk genes for SAD. By virtue of genome-wide association studies (GWAS), meta-analyses of large LOAD consortium data sets and gene-regulatory pathway reconstructions, many other genes that correlate to the development of SAD have been identified over the years (Bertram et al. 2008; Harold et al. 2009; Hollingworth et al. 2011; Lambert et al. 2013; Lambert et al. 2009; Naj et al. 2011; Zhang et al. 2013). To describe and examine them all in detail is beyond the scope of this work, however, it is interesting to note the diversity of molecular pathways the risk genes play a role in (Figure 2B). APOE, CLU, ABCA7 and SLC24A4 are, in some way or another, involved in cholesterol metabolism. Other risk loci as, for example, TREM2, CR1, CD33, MS4A, HLA-DRB5, INPP5D, EPHA1 and again CLU, have been correlated with neuroinflammation and regulation of the immune response. BIN1, PICALM, CD2AP, SORL1, RIN3, PTK2B, MEF2C and again EPHA1 operate in endocytosis and synaptic function. Some genes, like DSG2,

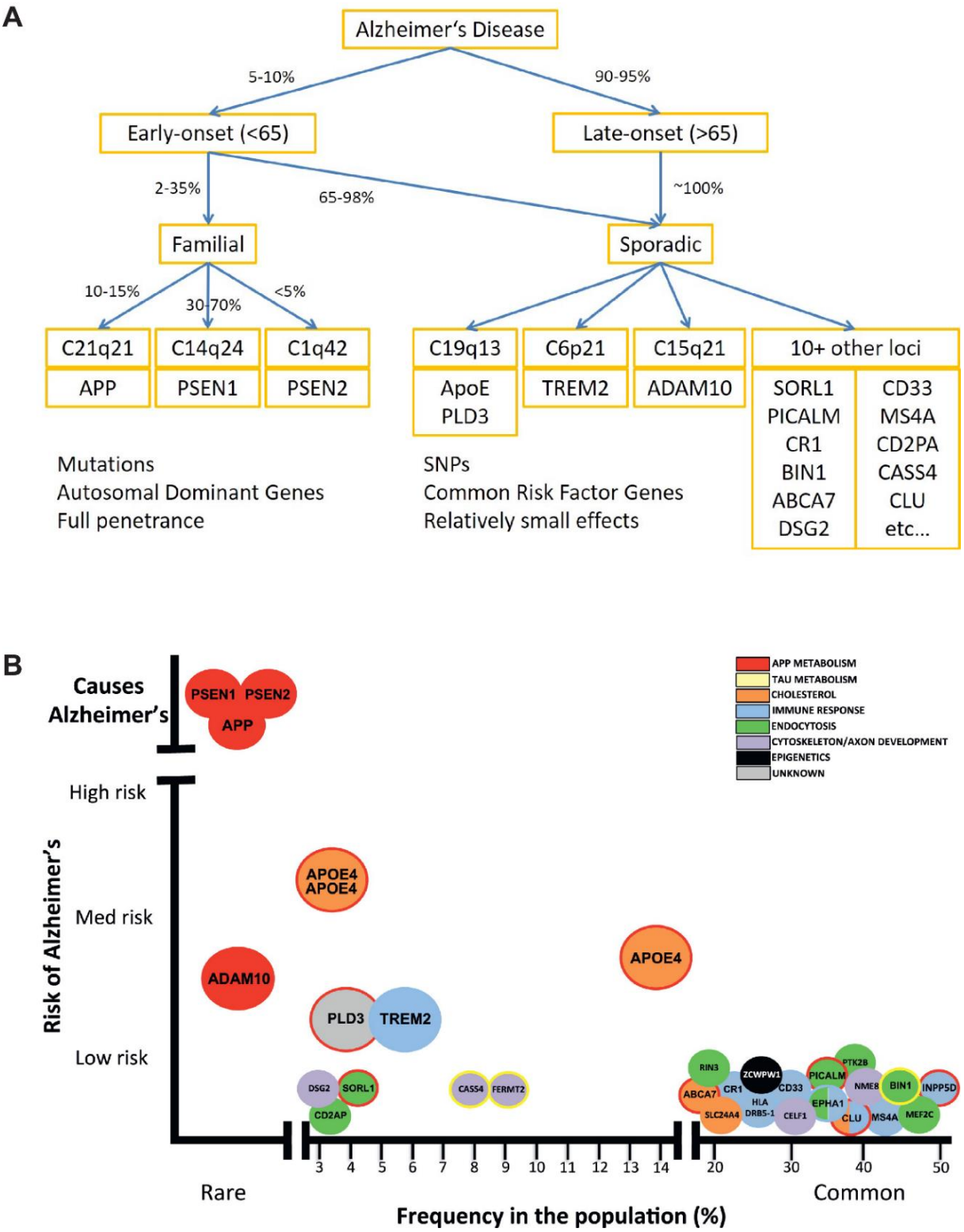

Figure 2. Genetics of AD

(A) A diagram of how AD can be subdivided based on age of onset and genetic disposition with the likelihoods in percentages for each of the classifications. The bottom of the graph displays genes that are typically associated with the respective classification and several keywords that describe their typical mode of action. **(B)** A graph that shows the relationship between the risk potential to develop AD against the frequency that they are found in the population for many genes that are typically associated with AD. Graph taken from a review by Celeste M. Karch and Alison M. Goate (Karch and Goate 2015).

CASS4, FERMT2, CELF1 and NME8, are responsible for cytoskeleton function and axonal transport. Finally, a single gene that coordinates epigenetic regulation, ZCWPW1, has also been implicated to play a role in AD. For a few of these risk genes, CASS4, FERMT2 and BIN1, it has been shown that they play a role in the metabolism of Tau as well.

Thus, many genes have been associated with AD, however, the major common denominator involved in AD must be APP. Many AD risk genes, like ADAM10, APOE, PLD3, SORL1, ABCA7, PICALM, CLU, INPP5D, and the only other major causative genes PSEN1 and 2, have all been shown to be involved in the processing of APP and it is likely more will be added to this list in the future. Additionally, the correlation between Alzheimer's disease and Down syndrome (DS) initiated the search for a gene on chromosome 21 in the first place (Glenner and Wong 1984a). The triplication of the long arm of the 21st chromosome results in elevated expression levels of APP and subsequently also Aβ. To date, no other genes have been found that are localized to the triplicated area and have also been implicated to play a role in AD. That heightened levels of APP are indeed causative in the early and widespread incidence of AD in DS patients is, therefore, plausible. Furthermore, it is unlikely accidental that this is the same protein giving rise to the senile plaques that were so imperative for the identification and segregation of AD. All in all, the genetic evidence that APP is not only involved in AD, but is also one of the key players, is quite convincing.

1.2.3. Etiology

Already since Alois Alzheimer first described his disease and differentiated it from other dementias based on histopathological hallmarks, there have been many theories as to its actual cause. Because of the arguments given above, it seems logical that the most famous and, for a long time, widely regarded as the best fitting hypothesis for the molecular mechanism behind AD revolves around Aβ and, by extent, to APP. Ever since its first postulation by John Hardy and Gerry Higgins in 1992, the 'Amyloid cascade hypothesis' was and is one of the central models for Alzheimer's disease (Hardy and Higgins 1992). It focusses around the senile or amyloid plaques in the brains of AD patients that for a long time were thought to have been the primary cause of AD and consist mostly of insoluble aggregated Aβ peptides (Glenner and Wong 1984b). The Aβ peptide is a part of APP which is released after a specific processing cascade, linking a primary pathological hallmark to the convincing genetic information regarding APP. However, there is plenty of criticism and opposition against the amyloid cascade hypothesis, not in the least of John Hardy himself (Hardy 2009; Karran and Strooper 2016; Hillen 2019; Kametani and Hasegawa 2018). As mentioned before, individuals can display considerable Aβ plaque burden without showing typical AD symptoms and disease progression does not correlate well with the number or size of amyloid depositions (Gefen et al. 2015; Katzman et al. 1988; Aizenstein

et al. 2008; Villemagne et al. 2011; Perrin et al. 2009). Moreover, although several Aβ species can induce neuronal death *in vitro* (Lambert et al. 1998; Walsh et al. 2002), their effects are rather marginal especially compared to the impact of tau mutations (Oddo et al. 2003; Lewis et al. 2001; Lewis et al. 2000). One important point of the amyloid cascade hypothesis is that amyloid toxicity should induce tangle dysfunction. It was indeed demonstrated that Aβ stimulates tau hyper-phosphorylation and that both synergistically can induce neuronal cell death (Ittner and Götz 2011). However, certain lines of evidence indicate that tangle formation actually precedes amyloid deposition (Braak and Braak 1991; Schönheit et al. 2004). Moreover, mouse strains harboring single or multiple mutations in APP and/or PSEN1/2, which undeniably produce increased levels of Aβ, demonstrate no significant effects on tangle pathology and only a relatively minor loss of neurons (Drummond and Wisniewski 2017). Ablation of tau seems to reduce Aβ neurotoxicity *in vitro* and a decrease of tau levels in transgenic AD mice alleviates synaptic loss and cognitive impairment (Ittner et al. 2010; Rapoport et al. 2002; Roberson et al. 2007). Conversely, introducing tau mutations in AD mice stimulates and hastens tangle pathology and neurodegeneration (Lewis et al. 2001; Oddo et al. 2003). All in all, it seems that tau is at the very least on the same level as Aβ in the neurotoxic cascade and many addendums to the amyloid cascade hypothesis have been made since to incorporate this knowledge.

It seems clear that Aβ is not the sole causative agent in AD initiation and progression, but that Aβ plays an important role in the disease cannot be denied. That plaque burden does not correlate well to AD state has already been discussed and it could also be shown that monomeric Aβ possesses no neurotoxic effects whatsoever (Crews and Masliah 2010). The levels of Aβ in cerebrospinal fluid samples, however, correlated better to disease severity (McDonald et al. 2012). Thus, the focus shifted towards smaller soluble Aβ oligomers (Krafft and Klein 2010; Viola et al. 2008). These lower order aggregates were demonstrated to be able to induce cell death and hamper neuronal signaling (Lambert et al. 1998; Walsh et al. 2002). Additionally, they are associated with an altered ion homeostasis, oxidative stress, Tau hyperphosphorylation, inhibition of essential kinases and many other pathological effects (Renner et al. 2010; O'Brien and Wong 2011; Sakono and Zako 2010). Especially significant for AD are the described inhibition of long-term potentiation, reinforcement of long-term depression and restriction of synaptic plasticity exerted by these soluble Aβ oligomers (Shankar et al. 2008; Townsend et al. 2006; Hsieh et al. 2006). It should be noted that many different forms of Aβ oligomers have been described over time, from dimers up to 24-mers that can aggregate further to protofibrils and finally the full multi-faceted fibrillary plaques. Furthermore, intermediary forms can be more or less dense giving rise to different molecular conformations and the potential capacity of bigger species to release smaller species back into the extracellular environment (Benilova et al. 2012). The relationship between the different species and the parameters governing the potential interconversion between

them are still vigorously discussed. Nevertheless, even if only some of the Aβ subspecies possess neurotoxic effects, Aβ oligomerization seems way more dynamic than originally assumed, suggesting that multiple forms of Aβ aggregates could potentially contribute to AD initiation or progression. Additional support for the amyloid cascade hypothesis comes from animal models, especially transgenic mice. Some of the typical characteristics of AD, like memory deficits, a decline in neuronal plasticity and development of amyloid plaques were demonstrated to be recapitulated by transgenic APP and/or PSEN1/2 mouse models (Puzzo et al. 2014; Li et al. 2016; Sasaguri et al. 2017). Furthermore, some of these features, such as cognitive impairment and loss of synaptic plasticity, could be rescued by immunological, pharmacological and genetic interventions aimed at decreasing Aβ levels in the brains of several of these transgenic mouse models (Götz et al. 2004; Li et al. 2013; Morgan et al. 2000; Janus et al. 2000; Dodart et al. 2002), suggesting the validity of at least part of the hypothesis.

One of the biggest problems with the amyloid cascade hypothesis is that it predicted that decreasing circulating and/or deposited Aβ would improve AD state and that such results, albeit maybe to a lesser extent than initially expected, were up until now only obtained in animal models. In other words, a lot of research has focused on these transgenic mouse strains and promising results have been obtained, but it seems increasingly likely that they are not adequate models for the human pathology. First, the transgenic mice all carry mutations that are related to FAD, which only reflects 5-10% of all AD. Because it manifests at a much younger age and is associated with different neuropathological features and a distinct disease progression than SAD (Farrer et al. 1990; Komarova and Thalhauser 2011; Stopford et al. 2008), it is not the best system for modelling most AD cases. Even for FAD, the transgenic animals are not a perfect model as they all rely on overexpression of mutated disease-related proteins, of which there is no proof in AD patients. Additionally, they do not show the extensive neurodegeneration and tangle pathology that is generally observed in the human disease. It is therefore also not surprising that to date all clinical trials that aimed to reduce Aβ burden either by immunization or by inhibiting the enzymes that process APP have failed (Huang et al. 2020). Thus, although a lot has been learned about the formation of amyloid deposits, the biochemistry of Aβ, the significance of tau and the generation of tangles, it does not seem to be sufficient and most prominent researchers in the field are convinced that major pivotal information is still lacking. Two key aspects that are often recited to be required are to understand the normal biological function of APP and all of its splice products (Hardy 2009) and to elucidate all the mechanisms that govern the “decision making process” whether APP undergoes amyloidogenic or non-amyloidogenic processing (Karran and Strooper 2016). Thus, although focus seems to shift away from Aβ, it is still widely believed that APP is at the heart of AD.

1.3. The APP family

After its identification in 1987 as the precursor protein of the Aβ peptide (Kang et al. 1987; Robakis et al. 1987; Tanzi et al. 1987; Goldgaber et al. 1987), an enormous amount of funding and time has been allocated to uncovering its features, life cycle, associated mechanisms and modulators. Although the Aβ sequence is unique to human APP, research has looked extensively to related proteins to learn more about APP's physiological functions and interactions. APP belongs to a rather small gene family that, besides APP, contains APP-like proteins of which mammals possess two, APLP1 and APLP2 (Strooper and Annaert 2000). APP and APP-like proteins are highly conserved transmembrane proteins with large, extracellular N-terminal domains and small, intracellular C-terminal domains (Kaden et al. 2012). Furthermore, all its members undergo comparable proteolytic processing by several secretases (Eggert et al. 2004). The evolutionary simplest organisms in which ancestors of APP have been identified are bilaterians that, strikingly, also developed one of the earliest forms of a nervous system with functional synapses. For example, the fruit fly *Drosophila melanogaster* possesses the single amyloid precursor protein-like (Appl) gene (Martin-Morris and White 1990) and the roundworm *Caenorhabditis elegans* the amyloid precursor-like 1 (apl-1) gene (Daigle and Li 1993). The next step in the evolutionary ladder is characterized by duplications, which created paralogs to the ancestral APP-like genes. The zebrafish *Danio rerio* carries four APP genes: two homologues to APP (appa and appb) and one each to APLP1 (aplp1) and APLP2 (aplp2) (Joshi et al. 2009; Liao et al. 2012). The clawed frog *Xenopus laevis* also expresses four APP genes of which one is a homolog to APLP1 (aplp1), but, in contrast to the zebrafish, only one to APP (app) and two to APLP2 (aplp2a and aplp2b) (van den Hurk et al. 2001; Okado and Okamoto 1992). More recently in evolution, the chicken *Gallus gallus* has lost the APLP1 homolog all together and is left with APP and APLP2 only (Shariati and Strooper 2013), suggesting that the duplications have been subject to stringent evolutionary selection pressure. Finally, the evolutionary course of the APP family ends in mammals, be it mouse (*Mus musculus*), dog (*Canis lupus familiaris*) or human (*Homo sapiens*), which all have three paralogs: APP, APLP1 and APLP2 (Zheng and Koo 2011).

1.3.1. Physiological role

Most of our understanding about the physiological role of APP and its family members comes from loss-of-function studies in three well-characterized experimental animal models: *C. elegans, D. melanogaster* and *M. musculus*. This is not surprising as the evolutionary conservation of APP homologues in these three species is remarkable. Although there are some deviations in function between single family members of different organisms and within the same organism, the information convincingly suggests that the APP family plays a role in the central nervous system and especially in its development. In *C. elegans*, the single APP-like gene apl-1 is associated with several metabolic

processes, such as body size and egg-laying rate (Ewald et al. 2012). It is also imperative to the reach transitional molt and lack of apl-1 results in developmental lethality at all larval stages (Hornsten et al. 2007). That the defect emerges due to neurological abnormalities is supported by the fact that apl-1 null mutants are also hypersensitive to acetylcholinesterase inhibitors that act in the synaptic junctions (Wiese et al. 2010). Interestingly, both the developmental lethality and the hypersensitivity can be rescued by re-introduction of just the soluble extracellular domain of APL-1, suggesting that a receptor for this domain must exist (Wiese et al. 2010; Hornsten et al. 2007). Opposed to *C. elegans*, *D. melanogaster* Appl null mutants are viable and fertile and Appl expression is first detected during axogenesis in developing neurons (Luo et al. 1990). They do show subtle phenotypes, however, as neuromuscular junctions of mutant flies feature reduced numbers of boutons, whereas APPL-overexpressing larvae have more boutons (Torroja et al. 1999). Additionally, APPL was shown to be able to affect neurite arborization by signaling through the Abelson tyrosine kinase (Abl) pathway (Leyssen et al. 2005). Loss of APPL was recently shown to cripple axonal outgrowth in fly mushroom bodies due to interactions with the planar polarity pathway for which heterozygosity for the Abl kinase significantly ameliorated the axonal phenotype again (Soldano et al. 2013). It should be noted that, in contrast to *C. elegans'* APL-1, all the mentioned properties of APPL depend on a highly conserved YENPTY motif residing on its small intracellular N-terminal domain (Torroja et al. 1999; Leyssen et al. 2005). Because mammals possess three APP family members, the situation is more complex. In mice, single knock-out (KO) animals for either App, Aplp1 or Aplp2 produce viable and fertile offspring (Zheng et al. 1995; Müller et al. 1994; Koch et al. 1997; Heber et al. 2000). However, KO of App results in disturbed forelimb strength, a decreased body weight and behavioral impairments, such as debilitated spatial learning, crippled locomotor activity and an abated urge to explore (Zheng et al. 1995; Dawson et al. 1999; Müller et al. 1994; Tremml et al. 1998). Staining of App null mice showed an early age-related decrease in synaptic markers and increased gliosis markers (Zheng et al. 1995; Seabrook et al. 1999; Yang et al. 2009). Additionally, a gliosis-dependent impairment of long-term potentiation, possibly due to increased expression of specific calcium channels which regulate GABAergic synaptic activity in inhibitory neurons, could also be observed in App KO these mice (Seabrook et al. 1999; Yang et al. 2009). Upregulation of the other two family members, Aplp1 and Aplp2, to compensate for the loss of App was not observed (Zheng et al. 1995; Heber et al. 2000). Aplp1 or Aplp2 KO produced far less extensive handicaps with only a minor decrease in body weight reported for Aplp1 animals (Heber et al. 2000; Koch et al. 1997). Interestingly, although the combined KO of App and Aplp1 results in viable and fertile offspring with no additional abnormalities on top of the aforementioned ones for single KOs (Heber et al. 2000), the combination of ablations of App with Aplp2, Aplp1 with Aplp2 or all three simultaneously culminates in a virtually complete penetrance of early perinatal lethality (Heber et al. 2000; Koch et al. 1997; Herms et al. 2004). It can, therefore, be concluded that App, Aplp1 and

Aplp2 are partially functionally redundant and partially functionally unique. The fact that Aplp2 alone is apparently enough to support viability but only the combined presence of App and Aplp1 grants survivability, implies that Aplp2 is the most vital paralog. However, sole ablation of Aplp2 seems to have no phenotype at all, suggesting that App and Aplp1 together have all the functionality of Aplp2, whereas Aplp2 cannot possess all functional aspects of especially App as single KO of App results in quite a serious phenotype.

1.4. The amyloid precursor protein

In humans, APP resides on chromosome 21 and consists of at least 18 exons that code for 3.3 to 3.5 kb of RNA transcripts (Robakis et al. 1987; Yoshikai et al. 1991). APP is a typical type I transmembrane protein, which means that it crosses the lipid membrane only once and that its transmembrane domain has an α-helical structure. It is anchored to the lipid membrane with a stop-transfer anchor sequence with its N-terminal side directed towards the lumen of the endoplasmic reticulum (ER) during synthesis. After maturation and translocation to the cellular plasma membrane, the N-terminal part will be extracellular, while the C-terminus resides in the cytosol. Three major isoforms are recognized in mammals, APP_{770}, APP_{751} and APP_{695}, which are designated based on the number of amino acids (aa) they comprise. Whereas APP is ubiquitously expressed in all tissues, its expression levels and the isoform(s) that are preferentially expressed depend on the tissue, respective cell type, developmental stage and environmental circumstances. Nevertheless, it can safely be said that APP_{695} the dominant isoform in human neurons and the central nervous system is (Wertkin et al. 1993; Bayer et al. 1999; Beyreuther et al. 1993; Belyaev et al. 2010). Therefore, and given that this work focusses on the dynamics of APP oligomerization in neurons, from here on out the characteristics and life cycle of APP will be described with regard to a neuronal setting.

1.4.1. Structure

APP is a relatively large single-pass membrane protein with several structurally and functionally distinct domains (Figure 3). Its largest isoform, APP_{770}, possesses both the KPI and Ox domains, whereas APP_{751} only harbors the KPI domain and APP_{695} has neither. KPI is short for “Kunitz-type protease inhibitor” and this functional unit has been associated with modulation of serine proteases that regulate blood coagulation and wound repair (van Nostrand et al. 1991), but might also suppress neuronal growth (Wang and Reiser 2003). The 19 aa stretch denoted Ox is identical to part of the Ox-2 antigen, a lymphoid and neuronal cell-surface glycoprotein, and is, thus, likely involved in cell-surface binding and recognition (Clark et al. 1985). Of the parts common to all isoforms, the cysteine-rich E1 and the α-helix-rich E2 regions constitute structurally distinct sections that possess multiple functional domains. E1 shares little homology with non-APP family proteins and consists of a growth-factor like

domain (GFLD) and a metal-binding domain (MBD). Part of the GFLD can bind heparin and is, therefore, called heparin-binding domain (HBD) (Small et al. 1994; Rossjohn et al. 1999). Immediately bordering the HBD is a hydrophobic pocket (HP) for which multiple functions have been suggested. It is implicated to facilitate dimerization upon heparin binding (Gralle et al. 2006; Dahms et al. 2010) but could also form a protein binding site that facilitates binding of ligands or ECM components like proteoglycans or acts like a growth factor (Small et al. 1994; Rossjohn et al. 1999). Although the MBD's main function

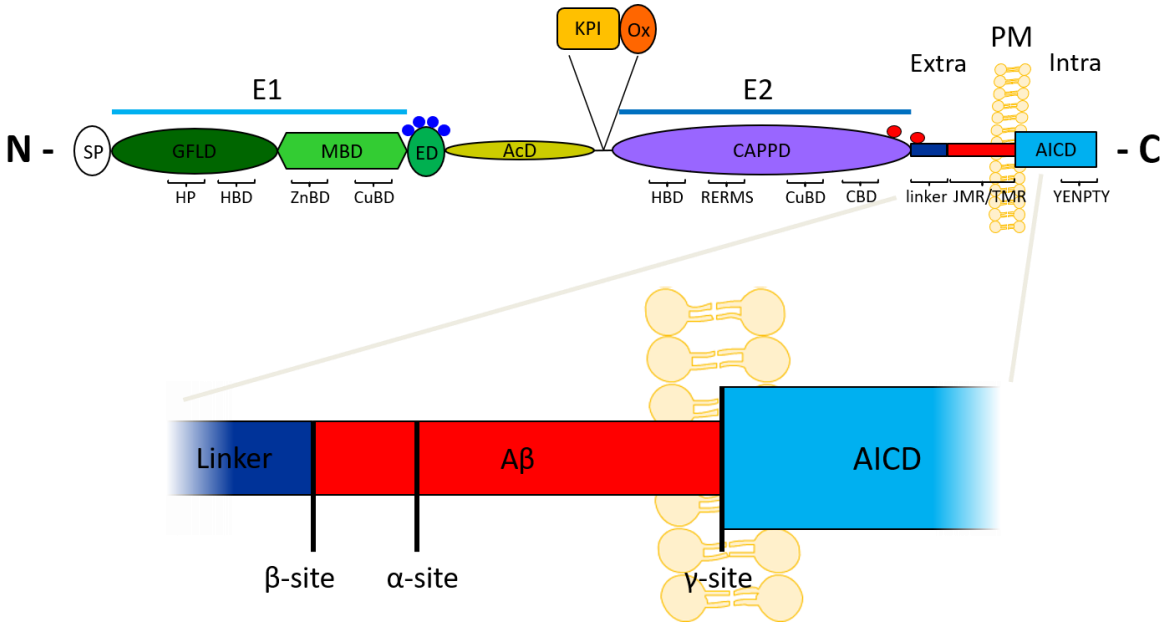

Figure 3. Structure of APP and Aβ

The upper part of the cartoon presents the lay-out of the various domains of APP featuring the functional units below the main structure using braces to mark their locations and sizes. The lower part shows an enlargement of the Aβ region with the canonical α-, β- and γ-cleavage sites.

seems to be Cu^{2+} binding and reduction using its copper-binding domain (CuBD) (Bush et al. 1993; Multhaup et al. 1996), it also contains a peptide sequence than can probably bind Zn^{2+} (ZnBD), but might require contribution of aa residues from other domains to do so (Ciuculescu et al. 2005). C-terminal from the E1 region a short aa sequence unique to APP, called the extension domain (ED), harbors 4 putative serine phosphorylation sites of which the function has not been conclusively determined (Walter et al. 1997; Walter et al. 2000). The function of the low complexity, acidic stretch downstream of the ED, which is called the acidic domain (AcD) and consists of more than 50% aspartate and glutamate, has also not been elucidated yet. However, it has been suggested to possibly play a role in mitochondrial membrane translocation (Anandatheerthavarada et al. 2003). E2 is also often called the central APP domain (CAPPD) and consists exclusively of α-helices (Dulubova et al. 2004). Due to its structure it is thought to readily dimerize and mediate APP self-oligomerization (Xue et al. 2011), which is convincingly contradicted by previous work from our group (Schreiber et al. 2012). The E2 region contains another HBD (Multhaup et al. 1994; Clarris et al. 1997), a CuBD that can supposedly

also bind Zn^{2+} (Dahms et al. 2012), a collagen binding domain (CBD) that can also bind laminin (Beher et al. 1996; Narindrasorasak et al. 1992) and the pentapeptide RERMS, which is proposed to mediate growth promoting effects of APP (Ninomiya et al. 1993). Intriguingly, interaction of RERMS with its designated receptor is only feasible when the peptide is liberated from E2 or the α-helical structure becomes unfolded somehow. Past the E2 region, the mostly disordered linker region is separated from the juxtamembrane domain (JMD) by the putative β-secretase cleavage site (Gralle et al. 2002; Sandbrink et al. 1994). More-or-less in the middle of the JMD the α-cleavage site is encountered, while halfway the mostly α-helical transmembrane domain (TMD) the γ-secretase cleavage site marks the beginning of the APP intracellular domain (AICD). Of note, the notorious Aβ peptide associated with AD is produced when APP is sequentially processed at the β- and γ-cleavage sites and is colored red in Figure 4. Not much is known about the exact conformation of the JMD in the full-length protein, however, elucidation of the crystal structure of the C-terminal part of APP that remains after β-cleavage, suggested that the α-cleavage site sits directly on the membrane surface. This is due to a few residues between the α-site and the transmembrane helix that organize in a small additional helical structure, called the N-helix, which causes this region to fold back onto the membrane (Barrett et al. 2012). The N-helix is connected to the TMD with the short N-loop and a combination of residues belonging to all 3 structures have been implicated to form a cholesterol-binding site (Beel et al. 2010; Barthet et al. 2011). Besides having a simple α-helical structure, the TMD is characterized by the presence of 4 GxxxG/A motifs that have been associated with homodimerization of APP (Munter et al. 2007). Finally, the AICD is mainly interesting because of its highly conserved YENPTY motif that allows interaction with many adaptor and effector proteins of which Fe65 is probably the most well-known (Bressler et al. 1996; Borg et al. 1996; Fiore et al. 1995; Müller et al. 2008). Clathrin-mediated endocytosis of APP has been shown to be mediated by this motif as well (Perez et al. 1999; Ring et al. 2007; Lai et al. 1995). Release into the cytosol upon proteolytic cleavage has been proposed to allow the AICD to signal to several potential target proteins (Rotz et al. 2004) and influence actin cytoskeleton dynamics (Müller et al. 2007). Also, although multiple phosphorylation sites have been identified, the specific implications of these targets either remain unknown or are controversially discussed (Ando et al. 2001; Chang et al. 2006; Gandy et al. 1988; Scheinfeld et al. 2002).

1.4.2. Proteolytic processing and cellular transport

As an integral type I membrane protein with a signal peptide for plasma membrane localization, most APP traverses the typical route from ER, via Golgi apparatus to the cellular plasma membrane. (Figure 4). During maturation, APP is not only N- and O-glycosylated, ectodomain and cytoplasmic phosphorylated and tyrosine sulfated, but intramolecular disulfide bridges are created as well. After sorting to the ER and Golgi, APP molecules have been shown to be transported in synaptic vesicles to

the axonal plasma membranes of neuronal cells by fast axonal transport (Koo et al. 1990; Groemer et al. 2011), which fits well with the observation that APP processing and release are known to occur in response to neuronal stimulation (Cirrito et al. 2008; Cirrito et al. 2005). After arriving at the cellular plasma membrane, an APP molecule can essentially undergo either of two competitive processing mechanisms. The canonical pathway is defined by proteolytic cleavage at the plasma membrane by one of the many possible α-secretases at the well conserved α-cleavage site in the middle of the Aβ domain (see Figure 3, bottom half). Because α-processing thus prohibits generation of the Aβ peptide it is also called the non-amyloidogenic pathway. Most α-secretases are zinc metalloproteases such as ADAM9, ADAM10 (also a major genetic risk factor, see Figure 2B), TACE/ADAM17, ADAM19 and MDC-9 (O'Brien and Wong 2011), while interestingly BACE2 has also been described to be an α-secretase (Allinson et al. 2003; Basi et al. 2003). Some of these, like ADAM10, are thought to be constitutively active in the cellular plasma membrane, whereas others, like TACE/ADAM17, have been suggested to be inducible. Processing by α-secretases is highly accurate and always takes place between the lysine and leucine at position 686 and 687 (APP_{770} numbering). The released 100-110 kDa soluble fragment is called sAPPα, for soluble APP cleaved at the α-site. Following processing by α-secretases, the remaining transmembrane α-C-terminal fragment (α-CTF, also called C83) is almost immediately cleaved by the γ-secretase in its TMD (Barthet et al. 2011). This results in a small N-terminal fragment called p3, which is released in the extracellular environment, and the larger C-terminal AICD, which is released in the cytosol. The γ-secretase is multiprotein complex consisting of 4 proteins: either presenilin 1 or 2 (PSEN1/2), the type I transmembrane glycoprotein nicastrin (NCT) and 2 multipass transmembrane proteins called anterior pharynx defective (APH)-1a or -2b and PSEN enhancer (PEN)-2. PSEN1 and 2 contain the catalytic unit required for the intramembranous proteolysis and are the only genes besides APP of which mutations show full penetrance towards development of AD (see Figure 2B). It has been proposed that the ectodomain of Nct is able to target the aminoterminal stubs of the CTF fragments (Bergmans et al. 2010). The γ-secretase is a promiscuous enzyme with over 90 different substrates that do not share obvious common features (Beel and Sanders 2008; Haapasalo and Kovacs 2011). Knowledge of the mechanisms how the γ-secretase can discriminate between substrates, with the exception of the requirement that most of the substrate's ectodomain must have been shed (Lichtenthaler et al. 2011), is still lacking. Additionally, processing by the γ-secretase is not precise and, at least for APP, a sequential process, whereby cleavage starts at the C-terminal side of the TMD and gradually proceeds upstream. At least 3 mutually exclusive sequential cleavage paths have been distinguished to date, which generate p3 peptides of different lengths (Sastre et al. 2001; Qi-Takahara et al. 2005; Weidemann et al. 2002; Takami et al. 2009).

On the other hand, in the amyloidogenic pathway, APP starts to oligomerize and eventually forms complexes of more than a few molecules (Figure 4, red arrow). Clustering of APP results in the recruitment of Clathrin, which leads to coated bud formation of the cell membrane and eventually reinternalization via Clathrin-mediated endocytosis (Cirrito et al. 2008; Schreiber et al. 2012) bringing APP molecules together with β- and γ-secretases into the endosomal compartment (Kinoshita et al. 2003; Rushworth and Hooper 2010). Subsequent acidification of the vesicle lumen activates the β-secretases, which induces processing of APP at the β-site thereby producing sAPPβ and a still membrane-bound β-C-terminal fragment (β-CTF, also called C99). In experiments that hinder surface

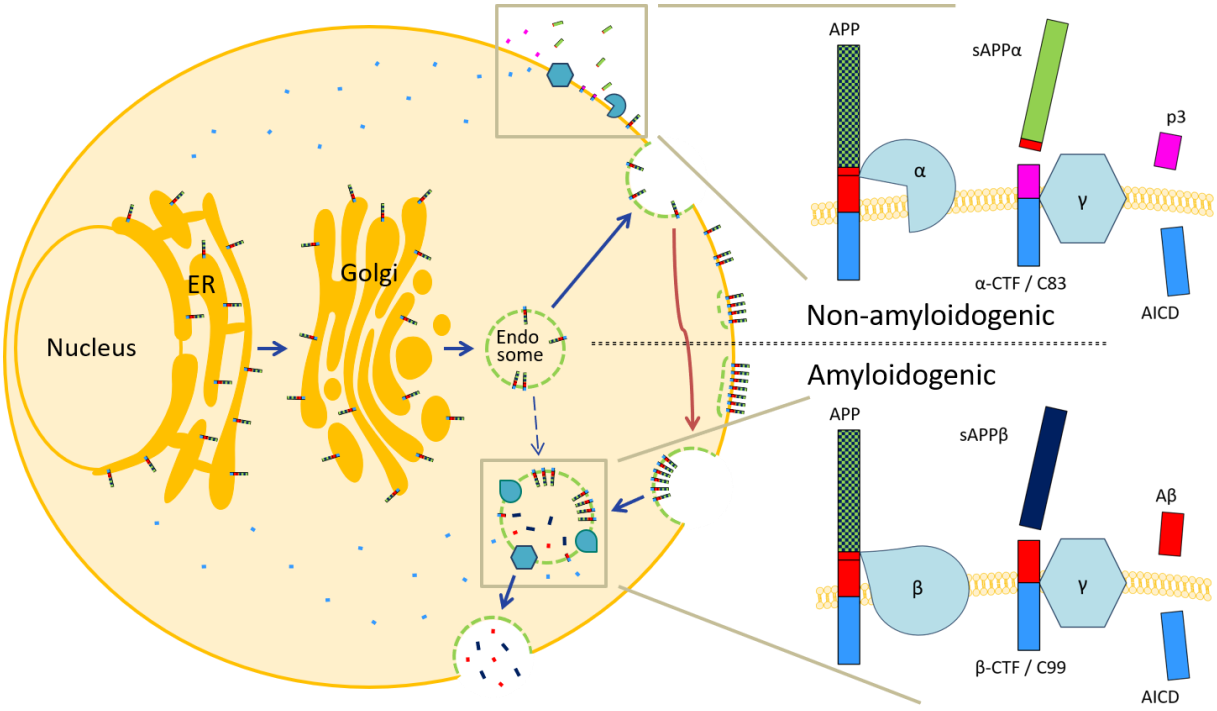

Figure 4. Intracellular trafficking and processing of APP

APP is trafficked from the nucleus to the endoplasmic reticulum (ER) and then via the Golgi apparatus (Golgi) to the plasma membrane in endosomes. Here it can either be shedded via sequential α- and γ-cleavage, which is called the non-amyloidogenic pathway (upper-right zoom-in), or start to cluster (red arrow). Following membrane oligomerization, APP is reinternalized via Clathrin-mediated endocytosis back into the endosomal compartment. Here, APP can either be sequentially cleaved by β- and γ- secretases, which is called the amyloidogenic pathway (lower-right zoom-in), or degraded when the endosomes are matured to lysosomes. After amyloidogenic processing, the endosomes fuse with the plasma membrane releasing the contents, including Aβ, into the extracellular environment. A minor fraction of the APP is already β-cleaved before being expressed on the cellular membrane at all (dashed blue arrow). Adapted from a review of Richard J. O'Brien and Philip C. Wong (O'Brien and Wong 2011).

endocytosis, 80% of β-proteolysis was prevented, demonstrating that this is the major mechanism behind β-cleavage (Koo and Squazzo 1994). Two pepsin-like β-site APP-cleaving enzymes (BACE) have been identified so far, BACE1 and 2, of which only BACE1 seems to possess β-site proteolytic activity (Cai et al. 2001). Analogous to α-processing, β-cleavage is quickly complemented by proteolysis by the

γ-secretase, which can also be found in the endosomal compartment (Parvathy et al. 1999; Fukumori et al. 2006). The resultant fragments are the amyloidogenic Aβ peptide, which is together with sAPPβ contained in the endocytic vesicle lumen, and the same AICD described earlier, which is released in the cytosol. In parallel to the p3 fragment, because of the γ-secretase's somewhat inaccurate sequential processing mechanism, Aβ peptides of between 37 to 49 aa can be produced (Sastre et al. 2001; Qi-Takahara et al. 2005; Weidemann et al. 2002; Takami et al. 2009). Strikingly, almost all mutations in PSEN1 or 2 that affect AD development and progression occur in one of its 9 transmembrane domains and lead to an increased ratio of the less soluble and more pathogenic $A\beta_{42}$ compared to $A\beta_{40}$, the two major Aβ species (Shen and Kelleher 2007). Following β/γ-processing, the vesicles can either progress to lysosomes (Haass et al. 1992), which destroys their content, or recycled back to the cellular plasma membrane, which releases both sAPPβ and Aβ to the extracellular space (Koo and Squazzo 1994).

Several aspects of this generally accepted model deserve comment at this point. First, although APP is encoded with a plasma membrane localization signal, presumably only a fraction of its total pool can be found in the plasma membrane at any given time. Protein must constantly be replaced because of APP's reportedly rapid turnover of between 30 minutes to 1 hour (Herreman et al. 2003; Lyckman et al. 1998), resulting in a significant subset of APP molecules that are undergoing maturation in the ER, Golgi and related cell organelles at any time. Because of the rapid proteolytic α-cleavage at the plasma membrane and Clathrin-mediated endocytosis from the plasma membrane, APP molecules only reside at the cellular plasma membrane for a relatively short time (Gralle and Ferreira 2007; Lee et al. 2008). Furthermore, it is believed that APP is stored in intracellular vesicles before being incorporated in the plasma membrane and exposed to the extracellular environment (Mills and Reiner 1999; Hung et al. 1993). On a few occasions, reviews mention the fraction of APP that is supposed to inhabit the cellular membrane and usually give a value between 10 and 20%. However, interestingly not a single review gives any reference to original research that supports these values (Haass et al. 2012; Thinakaran and Koo 2008; O'Brien and Wong 2011). Secondly, a potentially significant portion of APP might be shunted directly from the Golgi to the endosomal compartment (Figure 4, dashed arrow) and activity of BACE1 could be demonstrated in the Golgi (Greenfield et al. 1999; Huse et al. 2002). Both mechanisms would allow production of Aβ without possible regulation by α-secretases at the site of the cellular plasma membrane and might therefore be important for AD.

1.4.3. Cellular functions

Because the exact functions of APP and its family members on the scale of a whole organism have been difficult to unravel, investigation of the role of APP on a smaller scale using *in vitro* and *ex vivo* experimental methodologies seems logical. Examination of the conserved domains in the extracellular

part of the APP family members strongly indicates a role for APP as an adhesion molecule. It has been shown that APP can interact with itself in both cis and trans alignments (Gralle and Ferreira 2007; Scheuermann et al. 2001; Soba et al. 2005; Wang and Ha 2004). Especially the trans dimers could be important in cell-cell-interactions between neurons and glial cells during brain development (Trapp and Hauer 1994). APP has also been implicated to relay environmental information by binding ECM substrates, like collagen type I and laminin, and thereby regulate neurite growth (Reinhard et al. 2005; Small et al. 1999; Turner et al. 2003). Because of the similarities between APP's and Notch's processing, APP was suggested to be a cell surface receptor already shortly after its discovery (Kang et al. 1987). More recently, several groups have proposed that it can bind its own processing product, the Aβ peptide (Lorenzo et al. 2000; Shaked et al. 2006). Nowadays, many possible ligands have been identified, among others the neuronal glycoprotein F-spondin, heparin and netrin-1, a soluble protein that has a function in axonal growth (Zheng and Koo 2011; Ho and Südhof 2004; Lourenço et al. 2009). Whether APP is a cell surface receptor or not remains to be confirmed to this day, however, that APP plays a role in neuronal processes seems generally accepted. It has been linked to neuronal excitation and synaptic plasticity, synaptogenesis, neurite growth and dendritic branching. Additionally, APP is supposed to be a carrier receptor involved in axonal vesicle transport (Kamal et al. 2000; Kamal et al. 2001; Lazarov et al. 2005; Matsuda et al. 2003). Via its metal-binding domains, APP could theoretically modulate ion homeostasis in cells and tissues, as, for example, the copper-binding domain binds Cu^{2+} ions and reduces them to Cu^{+} ions (Multhaup et al. 1996; Hesse et al. 1994), although more work is needed in this area to validate this notion. The Aβ domain within the full-length protein has been implicated to influence the axonal distribution of APP in hippocampal neurons (Tienari et al. 1996). Besides the intact, full-length APP, its cleavage products might also have physiological functions of their own. Zinc and iron ion balances have been associated with the Aβ peptide as changes thereof have been correlated to AD progression (Maynard et al. 2005; Roberts et al. 2012). Furthermore, it has been proposed that the Aβ peptide has a protective function against oxidative stress (Baruch-Suchodolsky and Fischer 2009; Zou et al. 2002). In murine astrocytes the peptide is also suggested to stimulate the transport of cholesterol and Caveolin from the cellular plasma membrane to the Golgi apparatus (Igbavboa et al. 2009). There are two forms of the soluble extracellular N-terminal domain, sAPPα and sAPPβ, depending on which enzyme processed the full-length APP. The latter has been connected to promoting axonal pruning via caspase activation in the brain (Nikolaev et al. 2009), whereas the former has been shown to have positive effects on the survivability of neurons in culture (Mattson 1997). The lethal phenotype of the APP/APLP2 double KO can even be rescued by the genetic knock-in of sAPPα alone (Weyer et al. 2011). The AICD, on the other hand, has been implicated to induce apoptosis via activation of GSK-3β following binding with Fe65 (Ghosal et al. 2009; Zheng and Koo 2011). Additionally, interaction of APP with the apoptosis factor p53 and tumor necrosis factor

alpha (TNFα) corroborate the idea of its involvement in programmed cell death (Bamberger et al. 2003; Pardossi-Piquard and Checler 2012). The AICD has been suggested to bind proteins like JIP, Dab and Shc/GRP2 and thereby activate G protein-coupled signal transduction cascades (Reinhard et al. 2005). It has also been found to localize to the nucleus where it can regulate transcription of certain genes, among others the EGFR, LRP1, p53, BACE and APP itself (Pardossi-Piquard and Checler 2012).

1.4.4. Plasmalemmal organization

Previous work has shown that APP is distributed heterogeneously across the plasma membranes of neuronal cells and that at least a subpopulation is organized in relatively large multi-protein clusters consisting of a considerable number of APP molecules (Schneider et al. 2008). The driving forces behind this behavior and its function or implication remain obscure to this day. However, by drawing comparisons to other membrane proteins, a few potential purposes can be suggested. For many transmembrane proteins it has been shown that oligomerization is required to fulfill their role as membrane receptors and relay a signal across the cellular plasma membrane efficiently (Cebecauer et al. 2010; Lang and Rizzoli 2010; Kornberg et al. 1991). On the other hand, aggregation could be a mechanism to "store" membrane proteins in a biochemically inactive state, thereby regulating the amount of protein that is able to exert its intended function (Bar-On et al. 2009; Zilly et al. 2011). Possibly related to this could be the suggestion that once relatively big molecular complexes are formed they should remain within their membrane compartments longer, an effect called 'oligomerization-induced trapping' (Kusumi et al. 2005). Multimerization could also just confer protection against degradation and denaturation because of a reduced surface area available for interactions (Goodsell and Olson 2000; Ali and Imperiali 2005). Lastly, clustering has also been implicated to induce or enhance various forms of internalization that are either Clathrin-dependent or independent, like, for example, transcytosis (Hofman et al. 2010; Cureton et al. 2012; Galmes et al. 2013; Yu et al. 2015). Whatever non-pathological, biological functions APP oligomerization might possess; its connection to Clathrin-dependent endocytosis seems to play a pivotal role in the underlying pathological mechanisms that could be causative in AD. The amyloidogenic pathway is initiated when full-length APP molecules somehow escape α-processing and start to cluster together. Whether oligomerization of APP itself is the major mechanism allowing it to evade α-cleavage by sterically hindering α-secretases to access the APP molecules or APP evades α-processing via other means and clustering is just a secondary mechanism that then becomes possible has yet to be elucidated. Nevertheless, aggregation of APP eventually causes it to be reinternalized via Clathrin-mediated endocytosis into the early endosomal compartment where APP is then cleaved by the β- and γ-secretases. (Cirrito et al. 2008; Schreiber et al. 2012; Schneider et al. 2008).

One important aspect of amyloidogenic processing seems to be related to cholesterol, as the multiple environmental and genetic risk factors associated with it suggest. First of all, it could be shown that a subpopulation of plasmalemmal APP molecules resides in sphingolipid- and cholesterol-rich microdomains (Ehehalt et al. 2003; Rushworth and Hooper 2010). The juxtamembranous cholesterol-binding site has been suggested to be able to direct localization of APP towards these microdomains upon binding of cholesterol (Beel et al. 2010; Barrett et al. 2012) and they are known for their capacity to induce clustering of the proteins that they contain (Lingwood and Simons 2010). Within these microdomains APP can already form functional complexes with both the β- and γ-secretases that also reside there (Rushworth and Hooper 2010), whereas α-secretases are thought to primarily resides in more cholesterol-poor regions of the plasma membrane (Ehehalt et al. 2003; Kojro et al. 2001). Moreover, it could be shown that α-processing is hampered when α-secretases are stimulated to locate to cholesterol-rich microdomains (Harris et al. 2009). Cholesterol has also been implicated to encourage amyloidogenesis by increasing both β- and γ-secretase activity through either directly affecting substrate binding, catalysis rate and/or product dissociation (Beel et al. 2010). Finally, the cholesterol in these microdomains seems to be a requirement for the Clathrin-dependent endocytosis that precedes amyloidogenic processing of APP (Schneider et al. 2008; Ehehalt et al. 2003; Cossec et al. 2010). However, not only cholesterol influences APP's behavior in the cellular plasma membrane, the extracellular matrix could also contribute to its plasmalemmal multimerization. APP possesses heparin- and collagen-binding domains that are known to be involved in the formation of both cis- and trans-dimers (Beher et al. 1996; Gralle and Ferreira 2007). Furthermore, protein-protein interactions appear to be important for APP oligomerization as well. Interactions of its C-terminus with the plasmalemmal scaffold protein Flotillin-2 have been proposed to affect the size of APP clusters (Schneider et al. 2008). At least 4 other possible interfaces for protein-protein interactions that could promote APP aggregation have been proposed. The E1 and E2 domains have both been implicated to at least promote dimerization (Beher et al. 1996; Scheuermann et al. 2001; Wang and Ha 2004). The third interface lies within the TMD and is comprised of tandem GxxxG/A aa sequences that are known to be classical dimerization motifs (Senes et al. 2004; Munter et al. 2007). The last interface consists of the first 5 aa of the Aβ region within the full-length APP. Deletion of the entire N-terminus up until the first aa of the Aβ region still allowed oligomerization of a significant subpopulation of APP molecules; whereas additional removal of the next 5 aa almost completely abrogated plasmalemmal cluster formation (Schreiber et al. 2012). Considering how famous Aβ is for its capacity to aggregate, the fact that the Aβ domain also mediates oligomerization of the full-length APP is maybe not extremely unexpected. However, given the recent pleas of prominent scientists in the field to investigate the biological functions of APP processing and how could be regulated (Hardy 2009; Karran and Strooper 2016), it is surprising that there still are remarkably few publications that address these mechanisms.

These findings also implicate several aspects that should be interesting in this respect. Firstly, almost the entire extracellular part of APP, which includes the E1 and E2 domains, is apparently not required for formation of higher-order APP clusters. Secondly, oligomerization of APP is a requirement for amyloidogenic cleavage, which means that the Aβ region can modulate its own formation. Thirdly, if a stretch of only 5 aa is so important for protein complexing, mutations within this region or near it might affect APP's clustering dynamics directly.

1.4.5. Mutations

As already extensively discussed in chapter *1.2.2. Genetic factors*, there are many mutations that are linked to early-onset FAD, most of which occur in the PSEN1 gene and a minor fraction in PSEN2. For almost all these mutations, there is convincing evidence that they in some way influence processing of APP and usually increase the proportion of $A\beta_{42}$ in relation to $A\beta_{40}$ (Shen and Kelleher 2007). It is, therefore, to be expected that many of the 60 mutations in APP affect the same mechanism. Especially the numerous pathological mutations that occur around the multiple cleavage sites of the γ-secretase (aa 705-724 using APP_{770} numbering) suggest this much (Figure 5) and practically all of them have been shown to alter the $A\beta_{42}$ to $A\beta_{40}$ ratio in some way (Kumar-Singh et al. 2000; Cruts et al. 2003; Ancolio et al. 1999; Guerreiro et al. 2010; Eckman et al. 1997; Murrell et al. 1991; Chartier-Harlin et al. 1991; Goate et al. 1991; Murrell et al. 2000; Hsu et al. 2018; Ghidoni et al. 2009; Wang et al. 2015; Kwok et al. 2000; Theuns et al. 2006). The next set of mutations appears in aa 692, 693 and 694 using APP_{770} numbering or aa 21, 22 and 23 of the Aβ domain (Figure 5) and their resulting phenotypes are more diverse. The Flemish mutation (A692G) increases total production of Aβ *in vitro* (Haass et al. 1994; Jonghe et al. 1998), but likely decreases the $A\beta_{42}$ to $A\beta_{40}$ ratio (Tian et al. 2010). This is interesting, because evidently this mutation not only affects γ-secretase processing but is also able to drive APP cleavage towards the amyloidogenic pathway. Conversely, the E693G, also called Arctic, mutation decreases total Aβ generation *in vivo* (Nilsberth et al. 2001), again showing that a single mutation somehow controls in what direction APP processing transpires. It is still a pathologic mutation, however, because Arctic Aβ is more susceptible to form protofibrils (Nilsberth et al. 2001) and is more resistant to neprilysin-mediated degradation (Tsubuki et al. 2003). Appearing at the same position as the Arctic mutation are the Dutch (E693Q) and the Italian (E693K) mutations, which both do not elicit AD but rather cerebral amyloid angiopathy (CAA) (Bugiani et al. 2010; van Broeckhoven et al. 1990). CAA is a disease where Aβ peptides deposit in cerebral and meningeal vascular endothelial walls, which can develop alongside AD, but can also establish without any indications of cognitive decline or dementia at all (Sharma et al. 2018). Dutch mutation has no effect on Aβ levels (Watson et al. 1999), but accelerates peptide aggregation (Wisniewski et al. 1991) and consequently increased levels of β-conformation and a preferential accumulation in cerebral vessel walls (Miravalle et al. 2000). The

Italian mutant has not been extensively investigated, but it seems that it decreases the $A\beta_{42}$ to $A\beta_{40}$ ratio significantly while slightly decreasing total Aβ levels (Nilsberth et al. 2001). The final variant that occurs at that same site is the Osaka mutant (E693Δ), wherein the glutamic acid at this position is deleted. Carriers display strong cognitive impairments with unusually low levels of amyloid deposition (Shimada et al. 2011), although the mutant Aβ seems to be resistant against neprilysin and insulin-degrading enzyme (Tomiyama et al. 2008). Synthetic mutant peptides showed enhanced oligomerization without any fibrillization at all, while still exerting stronger inhibitory effects on LTP than wild-type peptides (Tomiyama et al. 2008), demonstrating again that lower order oligomers are the toxic species. The last mutant in this group is the Iowa variant (D694N), which exhibited a different peptide structure than other Aβ peptides *in vitro* (Krone et al. 2008). The altered structure manifests

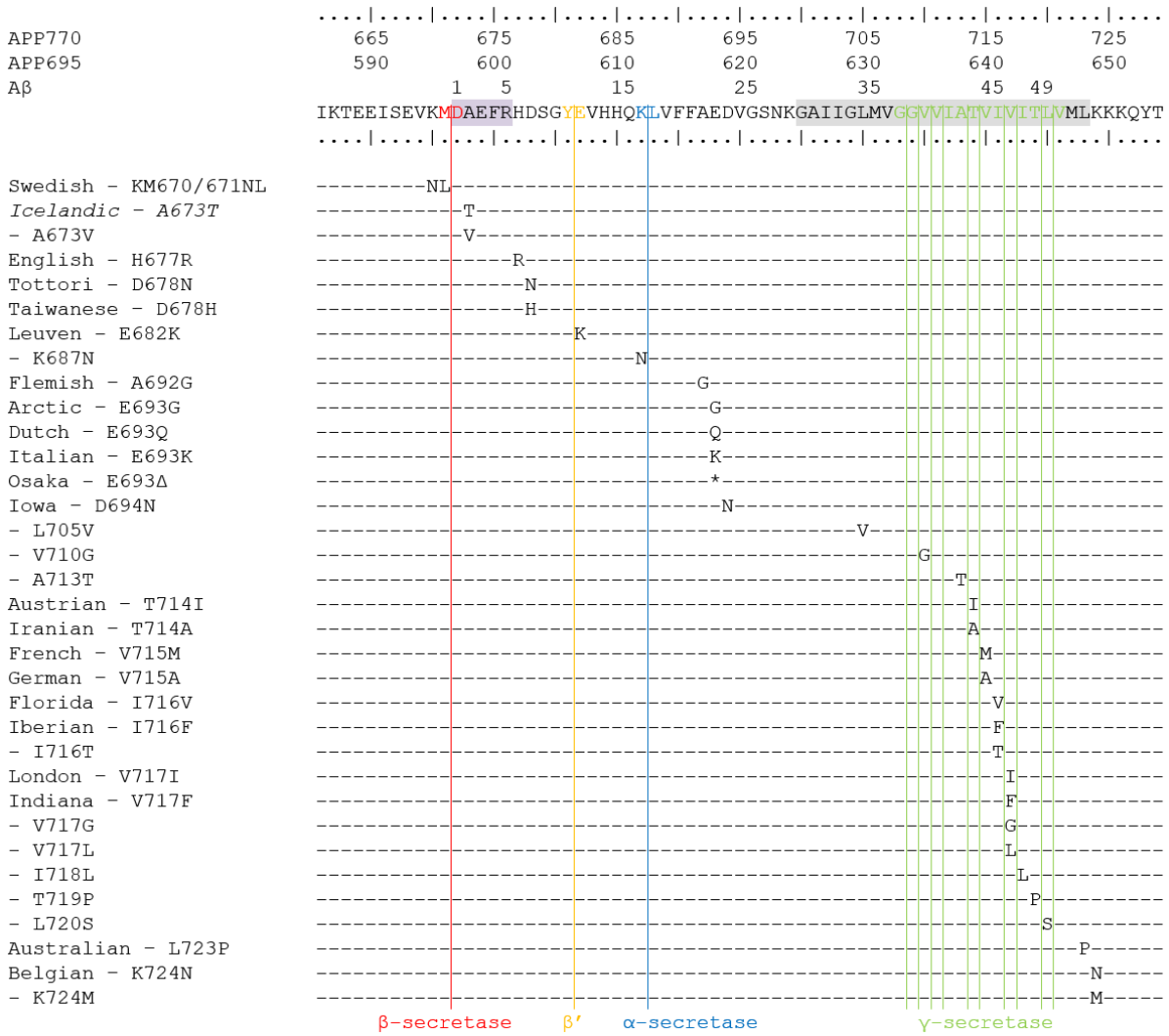

Figure 5. AD-related Aβ-proximal APP mutations

This list shows all APP mutations close to the Aβ domain that convey pathogenicity towards AD, apart from the protective Icelandic (A673T) mutation (in italics). β-, α- and γ-cleavage sites have been color coded in red, blue and green respectively and the potential alternative β'-cleavage site orange. The first 5 aa of the Aβ region that were proven crucial for APP clustering have been outlined in and purple box and the putative transmembrane domain in a grey box. Made using the APP mutation database available on alzorum.org (Alzforum).

by promoting fibrillogenesis and increasing Aβ-induced toxicity (van Nostrand et al. 2002), which culminates in an increased risk for both AD and CAA (Grabowski et al. 2001). Up until now only a single mutation was found proximal to the α-cleavage site, the K687N mutant. This mutation increases resistance for neprilysin-mediated degradation and makes APP a poor substrate for α-secretases and, thus, reduces α-processing and increases Aβ production (Kaden et al. 2012a). Intriguingly, in a pure form the Aβ42 variant of this mutant displayed less toxicity in vitro, while a mixture of both wild-type and K687N Aβ42 was even more toxic than wild-type Aβ42 peptide alone (Kaden et al. 2012a). The Leuven mutation occurs at aa 682 of APP770 and has to date been found in a single patient. It is interesting nonetheless, while it is suggested to be pathogenic because it shifts cleavage of APP away from a potential alternative splice site of the β-secretase BACE1 that lies between aa 681 and 682 by making it a worse substrate (Zhou et al. 2011). Processing at this β'-site apparently protects against amyloidogenisis by decreasing the amount of available substrate for canonical β-secretase activity (Kimura et al. 2016), a mechanism that is remarkably comparable to the K687N mutant. The Tottori (D678N) and Taiwanese (D678M) mutants occur at the same site and both increase and accelerate Aβ oligomerization causing a greater cytotoxic capacity compared to wild-type Aβ (Chen et al. 2012; Ono et al. 2010). Interestingly, the Taiwanese mutation does seem to elevate total Aβ production and $A\beta_{42}$ to $A\beta_{40}$ ratio (Chen et al. 2012); whereas the Tottori mutation does not affect Aβ generation at all (Hori et al. 2007). It is unclear whether the English mutation (H677R) is pathogenic, as only one patient has been described so far and his noncarrier sibling had a similar neuropathological progress (Janssen et al. 2003). In vitro, no effect on Aβ production could be found (Hori et al. 2007), but mutant peptides showed quicker oligomerization dynamics and increased neurotoxicity (Ono et al. 2010).

The following two mutations again appear at the same site, the A673T and A673V variants. The A673T mutant was first described in 1993 and was called the Icelandic mutation because it appears to be restricted mainly to Scandinavian and especially Icelandic populations (Peacock et al. 1993). It is to date the first and only APP mutation associated with protection against age-related cognitive decline (Jonsson et al. 2012), making it an extremely interesting variant to study. There are several publications that suggest that the A673T mutation makes APP a worse substrate for BACE1, with up to 40% less production of mutant Aβ compared to wild-type *in vitro* (Jonsson et al. 2012; Benilova et al. 2014; Maloney et al. 2014). This is not surprising as it is in close proximity to the β-secretase cleavage site and lies on the second residues of the 5 aa stretch that was found to be pivotal in cluster formation (Schreiber et al. 2012). Furthermore, mutant A673T Aβ seems to be less prone to aggregate (Benilova et al. 2014; Maloney et al. 2014), with indications that especially $A\beta_{42}$ is not able to form higher-order oligomers anymore (Zheng et al. 2015). However, neuronal toxicity of mutant $A\beta_{40}$ and $A\beta_{42}$ at various concentrations did not seem increased compared to wild-type peptides (Maloney et al. 2014).

Remarkably, in an independent study, APP harboring the A673T mutations conferred protection against TGF-β2 induced cell death when overexpressed in neurons (Hashimoto and Matsuoka 2014). On the other hand, the A673V elicits pathogenicity presumably while it makes APP a better substrate for BACE1, however, there seems to be some discussion concerning the aggregation dynamics of its mutant Aβ peptides. When overexpressed *in vitro*, the A673V mutation increased β-processing, while the ratios of $A\beta_{42}$ to $A\beta_{40}$ remained comparable to wild-type (Di Fede et al. 2009). These findings could be confirmed in murine primary neurons and human induced pluripotent stem cell (iPSC)-derived neurons (Benilova et al. 2014; Maloney et al. 2014). Although Aβ carrying the mutation show an increased aggregation, a mixture of mutant and wild-type peptides aggregated more slowly and demonstrated less cytotoxicity on neuroblastoma cells compared to either peptide alone (Di Fede et al. 2009; Di Fede et al. 2012). This suggests that a single mutant allele, i.e. heterozygous carriers, might actually be protected against AD. The last mutation that is discussed here is maybe also the most famous one and is called the Swedish mutation (KM670/671NL). It is a double mutation where two aa, lysine (K) and methionine (M), are substituted to asparagine (N) and leucine (L) on position 670 and 671 respectively and the only mutation so far that is located directly adjacent to the β-secretase cleavage site. This mutation has often been shown to elevate production of especially $A\beta_{40}$ and $A\beta_{42}$ without affecting their ratio (Nilsberth et al. 2001; Scheuner et al. 1996; Cai et al. 1993) and is frequently used in transgenic mouse models, such as Tg2576, J20 and 3xTg, and as a positive control to test novel APP mutations against.

2. Rationale and aims of the study

Previous work of Schneider et al. (Schneider et al. 2008) and Schreiber et al. (Schreiber et al. 2012) demonstrated that at least a subpopulation of APP resides in the plasma membranes of murine and rat neuronal cells and human hepatic cells as clusters. Antibody-induced augmented aggregation of APP clusters led to an increased clathrin-mediated endocytosis of APP and an escalation of Aβ production. On the other hand, depletion of cholesterol from the plasma membrane or N-terminal deletion of the full-length protein only when the first 5 amino acids of the Aβ domain were also included severely hampered cluster formation and, by extent, clathrin-mediated endocytosis.

These observations indicate a pivotal role of plasmalemmal APP oligomerization for promoting amyloidogenic processing. This raises the question how APP can evade non-amyloidogenic cleavage, as it is generally accepted that this precedes the amyloidogenic pathway. Our hypothesis is that APP clusters are so crowded that α-secretases simply cannot reach the molecules closer to the centers of these complexes. Therefore, the first aim of this study was to investigate the structure of the plasmalemmal APP cluster, with specific attention for the molecular packing density. To this end, precise biochemical experiments should elucidate the plasmalemmal copy number of APP in human neuronal SH-SY5Y cells. That the used cell system is of human origin is imperative, as the past has made clear that AD-related mechanisms are notoriously difficult to model in other organisms. Standard dilutions of purified recombinant APP will be utilized to examine the APP copy number per SH-SY5Y cell by quantitative western blotting. After resolving the plasmalemmal APP fraction employing a membrane biotinylation assay, quantification of the plasma membrane surface area of SH-SY5Y cells via confocal optical sectioning will be performed. Subsequently, the fraction of monomeric APP will be investigated using plasma membrane sheets in combination with high-sensitivity epifluorescence microscopy. Determination of the cluster size via time-gated stimulated emission depletion (gSTED) microscopy should then finally allow calculation of the molecular density within an APP cluster. Additional relevant information about APP, such as the total protein content of SH-SY5Y cells and the effect of APP overexpression on clustering, will be addressed along the way as well.

The fact that the only mutation in APP that has ever been described to be protective against AD, the A673T variant, occurs on the second residue of the 5 amino acid region that is so essential for APP clustering, suggests that this mutation might also influence clustering dynamics and, hence, which cleavage pathway follows. Thus, we posit the hypothesis that the A673T mutation interferes with plasmalemmal APP oligomerization, thereby affecting its processing by secretases either directly or indirectly. The second aim of this study is, consequently, the exploration of changes that the A673T

mutation exerts on plasmalemmal APP clustering and processing. Accordingly, wild-type and A673T is to be overexpressed in human HepG2 and SH-SY5Y cells and their oligomerization characteristics evaluated and compared. Analogues to the first aim, cluster size and plasmalemmal distribution will be analyzed employing gSTED and high-sensitivity epifluorescence microscopy, respectively. Moreover, the potential difference in mobility in the plasma membrane of both wild-type and A673T APP will be probed utilizing fluorescence recovery after photobleaching microscopy. The A673T mutant will be scrutinized functionally by assessing its correlation to clathrin-related structures with colocalization microscopy. Finally, the rate of α-cleavage will be probed by exploiting pharmacological inhibition of the γ-secretase and quantifying the levels of produced α-CTF relative to the wild-type protein via semi-quantitative western blotting.

3. Materials and Methods

3.1. Materials

Standard chemicals and reagents used in this study were purchased from *Carl Roth* (Karlsruhe, Germany), *Sigma Aldrich* (Hamburg, Germany), *Merck* (Darmstadt, Germany), *NEB* (Ipswich, USA), or *Thermo Fisher Scientific* (Waltham, USA) unless stated otherwise. All consumables for cell culture were obtained from *Sarstedt* (Nuembrecht, Germany), other consumables were from *Carl Roth* (Karlsruhe, Germany), *VWR* (Darmstadt, Germany), *Labomedic* (Bonn, Germany), *Eppendorf* (Hamburg, Germany), or *Bio-Rad* (Munich, Germany). Glass coverslips for microscopy were purchased from *Paul Marienfeld* (Lauda-Koenigshofen, Germany). Cell culture media and reagents were obtained from *PAN Biotech* (Aidenbach, Germany) and *Biochrom* (Berlin, Germany).

3.1.1. General instruments

Table 1. General instruments

Instrument	Manufacturer/Source	Specifications
biophotometer	GeneQuant 100 (*GE Healthcare Europe GmbH*, Freiburg, Germany)	quantification of bacterial growth (OD_{600})
bright-field microscope	Inverted microscope ECLIPSE TS100, CFI60 Infinity Optical System (*Nikon*, Tokyo, Japan)	cell culture
cell electroporation	Neon Transfection System (*Thermo Fisher Scientific*, Waltham, USA)	transfection of eukaryotic cells with DNA plasmids
flow cytometer	Guava easyCyte 5 (*Merck*, Darmstadt, Germany)	counting of eukaryotic cells
gel electrophoresis	Mini-PROTEAN Tetra Cell with Mini Trans-Blot Module (*Bio-Rad*, Hercules, USA)	SDS-PAGE and protein transfer on nitrocellulose membranes
infrared imaging system	Odyssey® CLx Imaging System (*Li-Cor,* Lincoln, USA)	imaging of in-gel stainings and western blots
microplate reader	Infinite® 200 PRO multimode microplate reader (*Tecan*, Maennedorf, Switzerland)	determination of protein concentration by BCA assay
sonicator	Bandelin Sonoplus HD2070 with a MS 73 probe (*Bandelin Sonoplus*, Berlin, Germany)	lysis of bacteria and unroofing of adherent cells
spectrophotometer	NanoDrop2000 (*Thermo Fisher Scientific*, Waltham, USA)	DNA concentration measurements
thermocyclers	TPersonal and TProfessional basic gradient (*Biometra*, Goettingen, Germany)	standard PCR

3.1.2. Microscopes

Epifluorescence microscopes: For epifluorescence microscopy, an Olympus IX81-ZDC inverted fluorescence microscope with a 60x 1.49 NA apochromat objective (*Olympus*, Hamburg, Germany) was used with additional magnification (1.6x and 2x lenses). A MT20E illumination system (*Olympus*) with a 150W xenon lamp and the filter sets DAPI HC (F36-500), EGFP HC (F36-525), TRITC HC (F36-503) and Cy5 ET (F46-009) (*AHF Analysentechnik*, Tuebingen, Germany) were used for fluorescence excitation and detection. For imaging, the 16-bit EMCCD camera ImagEM C9100-13 (*Hamamatsu Photonics*, Hamamatsu, Japan) with 512 x 512 pixels (16 µm x 16 µm pixel size) was coupled to the microscope. The microscope was controlled via the CellR® (*Olympus*) software.

Confocal microscope for optical sectioning: For optical sectioning, a Zeiss AXIO Observer Z1 inverted fluorescence microscope with an LSM 710 confocal system and an LCI Plan-Neofluar 1.3 NA 63x Imm Corr DIC M27 water immersion objective (*Zeiss*) was employed. A 30 mW 405 nm diode laser (*Zeiss*) was used for excitation, whereas fluorescent emission was detected with a 2-channel QUASAR PMT (*Zeiss*) with variable wavelength transmission. The microscope was controlled via the ZEN 2011 (*Zeiss*) software.

Confocal microscope for FRAP measurements: FRAP measurements were carried out using an Olympus FluoView1000 confocal microscope equipped with a UPlanSAPO 60x NA 1.35 oil immersion objective (*Olympus*), a 30 mW 488 nm argon, a 1 mW 543 nm HeNe-Green laser and a climate chamber (*Evotec*, Hamburg, Germany). Standard photomultiplier detectors (*Olympus*) and a selectable wavelength filter allowed specific fluorescent detection. The microscope was controlled by the Fluoview 3.0 software (*Olympus*).

STED microscopes: gSTED microscopy was performed on an easy3D STED microscope (*Abberior Instruments*, Göttingen, Germany). The microscope was equipped with an easy 3D module and an UPlanSApo 100x (1.4 NA) oil immersion objective on an Olympus IX83 confocal microscope body (*Olympus*). For detection of fluorescence, pulsed 485 nm, 561 nm and 640 nm excitation lasers (*Abberior Instruments*), a pulsed 775nm STED laser (*MPBC*, Montreal, Canada), 500-520 nm, 580-630 nm and 650-720 nm filter sets (*Abberior Instruments*) and single photon counting avalanche photodiodes as detectors (*Excelitas*, Waltham, USA) were used. The microscope was controlled by the Imspector software (*Abberior Instruments*).

Additionally, gSTED microscopy was performed on a TCS SP8 gated-STED microscope (*Leica*, Mannheim, Germany) equipped with an HCX PL APO 100x (1.4 NA) oil immersion objective, a pulsed white-light laser for fluorescent excitation, a 592 nm continuous wave (CW) laser for STED and hybrid detectors (HyD) for single-photon detection (*Leica*). The microscope was controlled by the Leica Application Suite for Advanced Fluorescence (LAS-AF; *Leica*).

3.1.3. Chemicals and consumables

Table 2. Chemicals and consumables

0.2 µm nitrocellulose membranes (Roti-NC)	#HP40.1, *Carl Roth*, Karlsruhe, Germany
10K molecular weight cutoff Slide-A-Lyzer Dialysis Cassette	#66380, *Thermo Fisher Scientific*, Waltham, USA
22 mm square, No. 1.5 high-precision coverslips	#0107052, *Paul Marienfeld*, Lauda Koenigshofen, Germany
25 mm round, No.1 coverslips	#0111650, *Paul Marienfeld*, Lauda Koenigshofen, Germany
BSA	#8076, *Carl Roth*, Karlsruhe, Germany
cOmplete protease inhibitor cocktail	#11697498001, *Sigma Aldrich*, Hamburg, Germany
Coomassie Brilliant Blue G-250	#20279, *Thermo Fisher Scientific*, Waltham, USA
DAPT	#D5942, *Sigma Aldrich*, Hamburg, Germany
DNase I	#M0303, *NEB*, Ipswich, USA
Fast Green FCF	#F7252, *Sigma Aldrich*, Hamburg, Germany
Fast-DiO	#D3898, *Thermo Fisher Scientific*, Waltham, USA
Inhibitor Cocktail Plus	#3751.1, *Carl Roth*, Karlsruhe, Germany
IPTG	#BP1755100, *Thermo Fisher Scientific*, Waltham, USA
L-lysine (HCl)	#L5626, *Sigma Aldrich*, Hamburg, Germany
lysozyme	#8259, *Carl Roth*, Karlsruhe, Germany
p2 cosmetics nail polish (transparent)	*DM*, Vienna, Austria
Na-metaperiodate	#S1878, *Sigma Aldrich*, Hamburg, Germany
Neubauer counting chamber	#0640030, *Paul Marienfeld*, Lauda Koenigshofen, Germany
Ni-NTA beads (50% slurry)	#745400, *Macherey-Nagel*, Dueren, Germany
Non-neutralized Albumin Fraction V	#2834, *Carl Roth*, Karlsruhe, Germany
Odyssey Blocking Buffer	#927-40000, *Li-Cor*, Lincoln, USA
PLL	#P1524, *Sigma Aldrich*, Hamburg, Germany
ProLong Gold	#P36930, *Thermo Fisher Scientific*, Waltham, USA
RIPA lysis buffer system	#sc24948, *Santa Cruz*, Dallas, USA
RNase H	#M0297, *NEB*, Ipswich, USA
Tetraspec microspheres	#T7284, *Thermo Fisher Scientific*, Waltham, USA
TMA-DPH	#T204, *Thermo Fisher Scientific*, Waltham, USA

3.1.4. Buffers and solutions

All buffers and solutions were prepared in fully double distilled water (ddH_2O) unless noted otherwise and autoclaved or sterile filtered when possible.

Table 3. Buffers and solutions

1% PLP	1% (w/v) PFA, 75 mM L-lysine (HCl), 10 mM Na-metaperiodate, 1.045 mM $CaCl_2$, 0.706 mM $MgCl_2$ in DPBS
10% SDS running gel	32.64% (v/v) 1:37.5 bis:acrylamid, 371 mM Tris-HCl (pH 8.8), 0.1% (w/v) SDS, 0.1% (w/v) APS, 0.01% (v/v) TEMED
20x PLL stock solution	2 mg/ml PLL
4% SDS stacking gel	12.85% (v/v) 1:37.5 bis:acrylamid, 124 mM Tris-HCl (pH 6.8), 0.1% (w/v) SDS, 0.1% (w/v) APS, 0.02% (v/v) TEMED
4x Laemmli	8% (w/v) SDS, 40% (w/v) glycerol, 0.008% (w/v) bromophenol blue, 250 mM Tris-HCl, 20% (v/v) β-mercaptoethanol (added before use), pH 6.8
Cell counting buffer	2% (v/v) FCS, 1 mM EDTA in DPBS
Colloidal Coomassie gel destaining solution	10% (v/v) EtOH, 2% (v/v) orthophosphoric acid
Colloidal Coomassie gel staining buffer	0.02% (w/v) Coomassie BB G-250, 5% (w/v) $Al_2(SO_4)_3$*14-18H_2O, 10% (v/v) EtOH, 2% (v/v) orthophosphoric acid
DPBS++	DPBS containing 1.045 mM $CaCl_2$ and 0.706 mM $MgCl_2$
Elution buffer for Ni-NTA protein purification	50 mM NaH_2PO_4, 500 mM NaCl, 300 mM imidazole, pH 8
Fast Green gel destaining solution	30% (v/v) MeOH, 7% (v/v) acetic acid
Fast Green gel staining buffer	0.001% (w/v) Fast Green FCF, 30% (v/v) MeOH, 7% (v/v) acetic acid
Lysis buffer for Ni-NTA protein purification	washing buffer with 10 mM imidazole, 15 mM β-mercaptoethanol, 1 mM PMSF, 1 mg/ml lysozyme and cOmplete protease inhibitors, pH 8
PBS	137 mM NaCl, 2.7 mM KCl, 1.76 mM KH_2PO_4, 10 mM Na_2HPO_4, pH 7.4
PBS-T	PBS containing 0.1% (v/v) Tween-20
PFA stock solution	16% (w/v) PFA added to pre-warmed 55°C ddH_2O while stirring, solution cleared with 1 M NaOH, aliquoted and stored at -20°C
Ringer solution	130 mM NaCl, 4 mM KCl, 1 mM $CaCl_2$, 1 mM $MgCl_2$, 48 mM D(+)glucose, 10 mM HEPES-NaOH, pH 7.4
SDS running buffer	25 mM Tris, 0.1% (w/v) SDS, 192 mM glycine
TAE buffer	40 mM Tris, 1 mM EDTA and 0.11% (v/v) acetic acid
TBS	50 mM Tris-HCl, 150 mM NaCl, pH 7.4
TMA-DPH working solution	10% (v/v) of a saturated TMA-DPH/PBS solution in PBS
Towbin buffer	25 mM Tris, 192 mM glycine, 20% (v/v) methanol
Washing buffer for Ni-NTA protein purification	50 mM NaH_2PO_4, 500 mM NaCl, 1% (v/v) Tween-20, various concentrations of imidazole, pH 8

3.1.5. Culture media and reagents

Table 4. Culture media and reagents

HepG2 growth medium	MEM Eagle (#P04-08509, *PAN Biotech*) supplemented with 10% (v/v) FCS (#S0615, *Biochrom*), 2 mM stable glutamine (#P04-82100, *PAN Biotech*) and 1% (v/v) penicillin/streptomycin (#P06-07100, *PAN Biotech*)
SH-SY5Y growth medium	DMEM:F12 (#P04-41500, *PAN Biotech*) supplemented with 10% (v/v) FCS (#S0615, *Biochrom*) and 1% (v/v) penicillin/streptomycin (#P06-07100, *PAN Biotech*)
DPBS, w/o: Ca and Mg	Dulbecco's PBS without Ca^{2+} and Mg^{2+} (#P04-36500, *PAN Biotech*)
DPBS, (10x) w: Ca and Mg	10x Dulbecco's PBS with Ca^{2+} and Mg^{2+} (#P04-37500, *PAN Biotech*)
Trypsin/EDTA	Trypsin (0.05%) with 0.02% EDTA in PBS, without Ca^{2+} and Mg^{2+} (#P10-0231SP, *PAN Biotech*)
LB medium	2% (w/v) LB (#X964, *Carl Roth*, Karlsruhe, Germany); for plates medium 2% (w/v) agar was added

3.1.6. Cell lines

HepG2 cells: HepG2 cells are human liver hepatocellular cells isolated from a hepatoblastoma. For this study they were acquired at passage 19 from *CLS*, Eppelheim, Germany, (#300198).

SH-SY5Y cells: SH-SY5Y cells are thrice subcloned for neuroblast-like cell populations from its SK-N-SH parental cell line, which are human neuroblastoma cells derived from a bone marrow metastatic site. SH-SY5Y were purchased at passage 26 from *LGC Standards*, Wesel, Germany (#ATCC-CRL-2266).

XL10-Gold Ultracompetent cells: XL10-Gold cells were regularly used for all cloning and screening purposes. The cells were purchased from *Agilent Technologies*, Waldbronn, Germany (#200314).

Rosetta™ 2(DE3)pLysS Competent Cells: Rosetta 2 bacteria were used to express eukaryotic proteins with the intent of purifying the product afterwards. The cells were purchased from *Merck*, Darmstadt, Germany (#71403).

ArcticExpress-(DE3)RP Competent Cells: ArcticExpress RP bacteria were used to express eukaryotic proteins with the intent of purifying the product afterwards. The cells were purchased from *Agilent Technologies*, Waldbronn, Germany (#230194).

3.1.7. Antibodies

Table 5. Primary and secondary antibodies

Depending on manufacturer's instructions antibodies were either stored whole at 4°C or aliquoted and stored at -20°C. After dilution in a staining buffer, antibodies were briefly sonicated unless otherwise noted.

Primary		
goat anti-Clathrin HC (C-20)	polyclonal	#sc6579, *Santa Cruz*, Dallas, USA
mouse anti-APP (C1/6.1)	monoclonal	#802801, *BioLegend*, San Diego, USA
mouse anti-Histidine tag (AD1.1.10)	monoclonal	#MCA1396, *Bio-Rad*, Hercules, USA
rabbit anti-Calnexin	polyclonal	#ab22595, *Abcam*, Cambridge, UK
rabbit anti-Caveolin	polyclonal	#ab2910, *Abcam*, Cambridge, UK
rabbit anti-GFP	polyclonal	#ab290, *Abcam*, Cambridge, UK
rabbit anti-Rab11	polyclonal	#ab3612, *Abcam*, Cambridge, UK
rabbit anti-Rab5	polyclonal	#ab18211, *Abcam*, Cambridge, UK
Secondary		
donkey anti-goat Alexa Fluor 488	polyclonal	#A-11055, *Thermo Fisher Scientific*, Waltham, USA
donkey anti-goat Alexa Fluor 594	polyclonal	#A-11058, *Thermo Fisher Scientific*, Waltham, USA
donkey anti-mouse Alexa Fluor 594	polyclonal	#A-21203, *Thermo Fisher Scientific*, Waltham, USA
donkey anti-mouse Alexa Fluor 647	polyclonal	#A-31571, *Thermo Fisher Scientific*, Waltham, USA
donkey anti-rabbit Alexa Fluor 488	polyclonal	#A-21206, *Thermo Fisher Scientific*, Waltham, USA
goat anti-mouse IRDye® 800CW	polyclonal	#926-32210, *Li-Cor*, Lincoln, USA
goat anti-rabbit Alexa Fluor 488	polyclonal	#A-11034, *Thermo Fisher Scientific*, Waltham, USA
goat anti-rabbit IRDye® 680RD	polyclonal	#925-68071, *Li-Cor*, Lincoln, USA

3.1.8. Plasmids

Table 6. Plasmids

Backbone vectors	**Source**	**Notes**
pGEM®-T Easy	#A1360, *Promega*, Mannheim, Germany	PCR cloning and easy ligation vector suitable for blue/white colony selection
pET-15b	#69661, *Merck*, Darmstadt, Germany	bacterial expression vector carrying an N-terminal His-tag followed by a thrombin site

pcDNA™6.2/C-emGFP-DEST	#V35520, *Thermo Fisher Scientific*, Waltham, USA	Gateway® mammalian expression vector carrying a C-terminal emerald GFP
pmCherry-C1	#632524, *Takara Bio Europe*, St-Germain-en-Laye, France	mammalian expression vector carrying an N-terminal mCherry fluorescent protein
Expression plasmids		
pcDNA6.2-APP$_{695}$-emGFP	kindly provided by Arne Schreiber (Schreiber et al. 2012)	human APP$_{695}$ (NM_201414) C-terminally fused to emGFP with the linker sequence KGGRADPAFLYKVVDAVN
pET-15b-APP$_{695}$	Dennis de Coninck	APP$_{695}$ from pcDNA6.2-APP$_{695}$-emGFP cloned into the pET-15b expression vector
pcDNA6.2-APP$_{A673T}$-emGFP	Dennis de Coninck	pcDNA6.2-APP$_{695}$-emGFP point mutated to create the A673T mutant
pcDNA6.2-APP$_{β\text{-}CTF}$-emGFP	Dennis de Coninck	pcDNA6.2-APP$_{695}$-emGFP of which AA22-596 were deleted
pcDNA6.2-APP$_{α\text{-}CTF}$-emGFP	Dennis de Coninck	pcDNA6.2-APP$_{695}$-emGFP of which AA22-612 were deleted
pcDNA6.2-mCh-APP$_{695}$-emGFP	Dennis de Coninck	pcDNA6.2-APP$_{695}$-emGFP with the addition of an N-terminal mCherry tag
pcDNA6.2-mCh-APP$_{A673T}$-emGFP	Dennis de Coninck	pcDNA6.2-mCh-APP$_{695}$-emGFP point mutated to create the A673T mutant

3.1.9. Kits

Kits were used according to the manufacturer's instructions unless specified otherwise.

Table 7. Kits

Neon™ Transfection System 100 µL kit	#MPK10096, *Thermo Fisher Scientific*, Waltham, USA
NucleoBond Xtra Midi®	#740410, *Macherey-Nagel*, Dueren, Germany
NucleoSpin Gel and PCR clean-up®	#740609, *Macherey-Nagel*, Dueren, Germany
NucleoSpin Plasmid®	#740588, *Macherey-Nagel*, Dueren, Germany
OneTaq® DNA Polymerase kit	#M0480S, *NEB*, Ipswich, USA
Pierce™ BCA Protein Assay kit	#23225, *Thermo Fisher Scientific*, Waltham, USA
Pierce™ Cell Surface Protein Isolation kit	#10230104, *Thermo Fisher Scientific*, Waltham, USA
Q5® High-Fidelity PCR kit	#E0555S, *NEB*, Ipswich, USA
Q5® Site-Directed Mutagenesis kit	#E0554S, *NEB*, Ipswich, USA

3.1.10. Software

Table 8. Software

ImageJ (incl. MBF and Fiji bundles)	developed by Wayne Rasband (NIH)	western blot and immunocytochemical image analysis
ApE	developed by Wayne Davis	DNA sequence editor
BioEdit	developed by Tom Hall	DNA sequence editor
Imaris	*Bitplane AG*, Zurich, Switzerland	3D modelling software
Microsoft Office 2010/2016/2019/365	*Microsoft Corporation*, Redmond, USA	writing, data analysis and organization, creating and editing figures
Graphpad Prism 6	*Graphpad Software LLC*, La Jolla, USA	data analysis and organization, creating and editing graphs
Métamorphose 2	developed by Ianaré Sévi	batch organization and renaming of files and folders
Photoshop and Illustrater CS5	*Adobe Systems Incorporated*, San Jose, USA	creating and editing figures and graphs

Appliances listed in *3.1.1. General instruments* were operated with the accompanying equipment software of the manufacturers when applicable.

3.2. Methods

Experiments were carried out at room temperature unless specified otherwise.

3.2.1. Cloning of expression plasmids

All restriction enzymes were purchased from NEB, Ipswich (MA), USA and were used with the accompanied buffers and according to the manufacturer's instructions. DNA amplification via polymerase chain reaction (PCR) was performed with Q5® High-Fidelity DNA polymerase (NEB, #M0491S). Primers for PCR were designed manually and purchased from MWG-Biotech, Ebersberg, Germany. The optimal annealing temperatures for PCR reaction was calculated using the NEB Tm calculator tool (http://tmcalculator.neb.com/). By default, plasmids were dephosphorylated after restriction digests using Antarctic Phosphatase (NEB, #M0289S) prior to ligation with T4 DNA ligase (NEB, #M0202T) according to the manufacturer's instructions. For plasmid amplification, *E.coli* XL10-Gold® (Stratagene, San Diego, USA, # 200314) were transformed and selectively grown in LB medium and/or on LB-agar plates containing the antibiotic carbenicillin (an analogue of ampicillin) at 100 µg/ml. Screening for correct clones was performed by colony PCR using OneTaq® DNA polymerase. Alternatively, a restriction digestion of purified plasmids was performed. All constructs were finally verified by sequencing (GATC, Konstanz, Germany). Products of PCRs and restriction digestions were routinely separated by electrophoresis using TAE buffer and agarose gels. DNA bands cut-out from

agarose gels and PCR products were purified using the NucleoSpin Gel and PCR clean-up® (Macherey-Nagel, Dueren, Germany, #740609). DNA plasmids were purified from LB cultures of transformed bacteria using either the NucleoSpin Plasmid® kit (Macherey-Nagel, #740588) for volumes up to 3 ml or the NucleoBond Xtra Midi® kit (Macherey-Nagel, #740410) for larger volumes.

pcDNA6.2-APP_{695}-emGFP: All plasmids used in this work were based on a single construct described previously (Schreiber et al. 2012). This construct contains the complete human APP_{695} protein without STOP codon (NCBI reference sequence NM_201414) which has been introduced into the Vivid Colors pcDNA6.2/C-emGFP-DEST vector backbone (Thermo Fisher Scientific, #V35520) using the site-specific recombination properties of bacteriophage lambda. Specifically, this means that the APP_{695} coding sequence is followed by a linker region {5'-AAGGGTGGGCGCGCCGACCCAGCTTTCTTGTACAAAGTGGTTGATGCTGTTAAC-3'} and finally the humanized emerald Green Fluorescent Protein (emGFP) tag.

pET-15b-His_6-Thr-APP_{695}: The bacterial expression vector for human APP_{695} was amplified from this construct by PCR using a forward primer that introduces a N-terminal NdeI restriction site {5'-TATTATCATATGCTGCCCGGTTTGGCACTGCTC-3'} and a C-terminal primer that introduces a BlpI restriction site and two STOP codons {5'-ATATTAGCTCAGCTTATTAGTTCTGCATCTGCTCAAAG-3'}. Thus, APP_{695} was amplified without the linker sequence and the emGFP-tag, but with flanking NdeI and BlpI restriction sites and two STOP codons just before the C-terminal BlpI restriction site. After restriction digestion of both the APP_{695} amplicon and the pET-15b vector (Merck, Novagen, #69661-3) with NdeI and BlpI, the vector was dephosphorylated and the coding sequence ligated into the multiple cloning site of the pET-15b vector creating a bacterial expression plasmid with a N-terminal His_6-tag followed by a thrombin cleavage site and finally the human APP_{695} coding sequence. Of note BlpI is called Bpu1102I in Thermo Fisher Scientific and Fermentas nomenclature.

pcDNA6.2-mCherry-APP_{695}-emGFP: For the creation of the double tagged APP-fusion proteins containing a N-terminal mCherry fluorescent tag in addition to the C-terminal emGFP tag, the mCherry tag was inserted into the N-terminal APP_{695} coding sequence using the unique KpnI restriction site at amino acid position 19-21. mCherry was lifted from the pmCherry-N1 plasmid (Takara Bio, Clontech Laboratories, #632523) using a forward primer that introduces a KpnI restriction site followed by the sequence 'CACT' before the START codon of mCherry {5'-ATTATTGGTACCCACTATGGTGAGCAAGGGCGAGG-3'} and a reverse primer that introduces a secondary KpnI restriction site and the sequence 'CTGGA' between the C-terminus of mCherry and the KpnI restriction site {5'-TTATTAGGTACCTCCAGCTTGTACAGCTCGTCCATGC-3'}. This way, in the final product, the first 5 amino acids after the signaling peptide are retained before the mCherry coding sequence

starts and the complete APP_{695} coding sequence without the signaling peptide follows the inserted mCherry tag. After restriction digestion of both the amplicon and the target vector, the target vector was dephosphorylated and the amplicon ligated into the vector.

APP_{A673T} mutants: The APP mutants of both the single tagged and double tagged APP-fusion proteins were produced using non-overlapping primers that introduce base pair substitutions and the Q5 Site-Directed Mutagenesis kit (NEB, #E0554S) as per manufacturer's instructions. Specifically, for the APP_{A673T} mutant a forward primer {5'- GAAGTGAAGATGGATACAGAATTCCGACATGAC-3'} and a reverse primer {5'- AGAGATCTCCTCCGTCTTGATATTTGTCAAC-3'} that anneal back-to-back were employed. After amplification, the parent vectors are degraded and the amplicons phosphorylated and ligated all in a single step. Using these two primer pairs the plasmids pcDNA6.2-APP_{A673T}-emGFP and pcDNA6.2-mCh-APP_{A673T}-emGFP were made using pcDNA6.2-APP_{695}-emGFP and pcDNA6.2-mCherry-APP_{695}-emGFP described above as parent vectors.

pcDNA6.2-$APP_{\beta\text{-CTF}}$-emGFP and pcDNA6.2-$APP_{\alpha\text{-CTF}}$-emGFP: The two APP C-terminal fragment coding vectors were created using pcDNA6.2-APP695-emGFP as the parent vector and by making use of the same kit and similar methodology as the site-directed mutagenesis approach described above. The difference is that these primer pairs do not introduce base pair substitutions and, more importantly, do not anneal back-to-back, which results in a gap between the 5' sides of the primers. The part of the sequence covered by this gap is not amplified and is therefore absent and thus deleted in the final product. Two different forward primers, one for generating the plasmid that codes for APP's β-secretase cleaved C-terminal fragment (β-CTF) {5'- GATGCAGAATTCCGACATGACTCAGG-3'} and one for the α-CTF {5'- TTGGTGTTCTTTGCAGAAGATGTG-3'}, and one reverse primer {5'- GGGTACCTCCAGCGCC-3'} that can be used for both constructs, were designed and used to amplify the deletion constructs. Finally, the same post-amplification methodology as was utilized in the site-directed mutagenesis described above was used to create the final CTF coding vectors.

3.2.2. Bacterial expression of His_6-APP_{695}

Rosetta™ 2(DE3)pLysS (Rosetta 2) competent cells (Merck, Novagen, #71403) or ArcticExpress-(DE3)RP (AE-RP) competent cells (Agilent Technologies, #230194) were transformed with the pET-15b-His_6-Thr-APP_{695} expression vector as per manufacturer's instructions and plated on agar plates containing the appropriate antibiotics for the bacteria and the plasmid. The next day, starter colonies from both species of competent cells were inoculated under selection pressure with the corresponding antibiotics with bacteria from single colonies and incubated overnight at either 37°C for Rosetta 2 cells or 30°C for AE-RP cells. The next morning, the cultures were diluted in antibiotic-free LB broth medium to OD_{600} = 0.1 in a final volume of 2 L and grown to OD_{600} = 0.6 at 37°C and 30°C respectively. The

cultures were cooled down to 30°C for Rosetta 2 cells and to 12°C for AE-RP cells and protein expression was induced by the addition of 0.1, 0.25, 0.5 or 1 mM IPTG (Fisher Scientific, #BP1755100). During a total incubation time of either 6 hours on 30°C for Rosetta 2 cells or 16 hours at 12°C for AE-RP cells, multiple samples were taken at specific timepoints to measure culture density by OD_{600} or to assess protein expression using colloidal Coomassie in-gel stainings and western blotting.

3.2.3. Ni-NTA purification of His_6-APP_{695}

Following expression of His_6-APP_{695}, cells were pelleted by centrifugation at 4,000 x g for 10 min at 4°C, followed by a wash with pre-cooled PBS (137 mM NaCl, 2.7 mM KCl, 10 mM Na_2HPO_4, 1.76 mM KH_2PO_4, pH 7.4) after which they were pelleted again. The pellet was resuspended in ice-cold lysis buffer (50 mM NaH_2PO_4, 500 mM NaCl, 1% Tween-20, 10 mM imidazole, 15 mM β-mercaptoethanol, 1 mM PMSF, 1 mg/ml lysozyme and protease inhibitors (cOmplete Protease Inhibitor Cocktail; Sigma-Aldrich, #11697498001), pH 8) using 5 ml lysis buffer per gram wet weight. The solution was incubated for 15 min with agitation at 4°C before adding DNAse I (NEB, #M0303) and RNAse H (NEB, #M0297), followed by incubation for 15 min at 4°C. Then, the solution was sonicated for 1 min on ice at 40% power (100% cycle; using a Bandolin Sonoplus HD2070 with a MS 73 probe) and then for 5 min at 40% power (10% cycle). Including a short pause between sessions, these sonication steps were repeated until the solution cleared up. From the almost clear solution, insoluble material was removed by centrifugation at 10,000 x g for 30 min at 4°C. To equilibrate the Ni-NTA beads (50% slurry) (Macherey-Nagel, Protino, #745400), they were washed three times with washing buffer (50 mM NaH_2PO_4, 500 mM NaCl, 1% Tween-20, pH 8). Next, they were added to the cleared lysate solution (1 ml of beads per 10 ml of cleared lysate) and the mixture was incubated overnight at 4°C with agitation. The beads were harvested by centrifugation at 500 x g for 5 min at 4°C, and the bead pellet was washed 4 times in ice-cold washing buffer containing increasingly higher concentrations of imidazole (20, 30, 40 and 50 mM) with each washing step. Beads in 50 mM imidazole containing washing buffer were transferred into a column. The bound protein was eluted from the beads with 15 ml elution buffer (50 mM NaH_2PO_4, 500 mM NaCl, 300 mM imidazole, pH 8), which was collected as 1 ml fractions. The protein content of the fractions was measured using the Pierce BCA Protein Assay kit (Thermo Fisher Scientific, #23225) following the manufacturer's instructions. The three fractions containing the highest protein concentration were identified and pooled. For dialysis, the solution was transferred into a 10K MWCO Slide-A-Lyzer Dialysis Cassette (Thermo Fisher Scientific, #66380). Dialysis was performed in 500 ml PBS with stirring at 4°C for 8 hr replacing the PBS every 2 hr, resulting in a $(3/500)^4$ = ~7.71×10^8 times dilution of the original buffer. After supplementing the protein solution with 50% w/v glycerol and 0.05% w/v sodium azide (final concentrations), it was aliquoted and stored at -80°C.

3.2.4. Protein biotinylation

To label extracellular plasmalemmal proteins, the Pierce Cell Surface Protein Isolation kit (Thermo Fisher Scientific, #10230104) was employed following the manufacturer's instructions (using the following buffers from the kit: 'Quenching Solution', 'Lysis Buffer', 'Wash Buffer' and 'Elution Buffer'). Briefly, four T75 cell culture flasks of adherent cells grown to 90% confluency were washed twice with DPBS pre-cooled to 4°C. Then, each flask was incubated with 10 ml pre-cooled DPBS supplemented with 250 µg/ml Sulfo-NHS-SS-Biotin. The flasks were gently agitated on a rocking platform for 30 min at 4°C. Afterwards, the reaction was stopped by the addition of 500 µl 'Quenching Solution'. The biotinylated cells were mechanically detached using a cell scraper, pelleted by centrifugation (1000 x g for 3 min), washed once with 5 ml pre-cooled TBS, and pelleted again. The cell pellet was resuspended in 566 µl pre-cooled 'Lysis Buffer' with protease inhibitors added (Inhibitor Cocktail Plus, Roth, #3751.1). For lysis, the cells were incubated on ice over a period of 15 min, vortexing every 5 min for 5 sec. Then another 15 min incubation period on ice followed, this time applying a 1 sec sonication burst at 5% power (Bandolin Sonoplus HD2070, with a MS 73 probe) every 5 min. The insoluble material was removed by centrifugation at 10,000 x g for 2 min at 4°C. For isolation of the biotinylated material, 500 µl of NeutrAvidin Agarose beads (50% slurry) were transferred into a spin column. The beads were washed three times by the addition of 500 µl 'Wash Buffer', followed by centrifugation at 1,000 x g for 1 min. Then, the lysate was incubated with the NeutrAvidin Agarose beads for at least 1 hr at room temperature with end-over-end rotation. Next, the column was centrifuged at 1,000 x g for 1 min and the flow-through collected. The column was washed 4 times as described above using 'Wash Buffer' supplemented with protease inhibitors (Inhibitor Cocktail Plus, Roth, #3751.1). The flow-throughs from the washes were collected. To elute the bound protein, the column was incubated with 500 µl 'Elution Buffer' containing 66.67 mM DTT for 1 hr with end-over-end rotation. The eluate was collected by centrifugation at 1,000 x g for 1 min. A second elution step was performed overnight to ensure all bound protein was collected. All fractions were stored at -20°C until analyzed by western blotting.

3.2.5. SDS-PAGE

Protein samples were mixed with 4x Lämmli buffer and incubated at 95°C for 10 min with agitation. Samples were run in SDS running buffer (25 mM Tris, 0.1% w/v SDS, 192 mM glycine, pH 8.3 in ddH_2O) using 10% poly-acrylamide running gels (4.1 ml ddH_2O, 3.3 ml 1:37.5 bis:acrylamide, 2.5 ml 1.5 M Tris-HCl (pH 8.8), 100 µl 10% w/v SDS, 100 µl 10% w/v APS, 10 µl TEMED) with a 4% stacking gel (3.05 ml ddH_2O, 0.65 ml 1:37.5 bis:acrylamide, 1.25 ml 0.5 M Tris-HCl (pH 6.8), 50 µl 10% w/v SDS, 50 µl 10% w/v APS, 10 µl TEMED) mounted in BioRad Mini-PROTEAN Tetra Cells. After the samples had left the stacking gel, the voltage was raised from initially 70 V to 100 V. After the run and removal of the gel

from the glass slides, gels were washed in ddH_2O for 5 min with agitation and either used for in-gel stainings or for western blot analysis.

3.2.6. In-gel stainings

Gels were washed an additional 2 times for 10 min with agitation in ddH_2O and stained overnight with either colloidal Coomassie (0.02% w/v Coomassie Brilliant Blue G-250 (Thermo Fisher Scientific, #20279) in ddH_2O supplemented with 5% w/v $Al_2(SO_4)_3$*xH_2O (x ≈14-18), 10% v/v EtOH, and 2% v/v orthophosphoric acid) or with Fast Green (0.001% w/v Fast Green FCF (Sigma-Aldrich, #F7252) in ddH_2O supplemented with 30% v/v MeOH and 7% v/v acetic acid). After staining, gels were washed three times for 5 min in ddH_2O and destained for 1 hr with agitation in destaining solution (10% v/v EtOH with 2% v/v orthophosphoric acid in ddH_2O for colloidal Coomassie gels and 30% v/v MeOH with 7% v/v acetic acid in ddH_2O for Fast Green gels). Finally, the gels were washed again twice for 5 min in ddH_2O and imaged using the 700 nm channel of a Li-Cor Odyssey Classic Imaging System with settings recommended for imaging of in-gel stainings (resolution: 338.983 µm; quality: highest; focus offset: 0.5; intensity: 5 (at 700 nm)).

3.2.7. Western blotting

After the final wash following SDS-PAGE, gels were equilibrated in ice-cold Towbin buffer (25 mM Tris, 192 mM glycine, 20% v/v MeOH, pH 8.3 in ddH_2O) for 10 min with agitation. Nitrocellulose membranes (0.2 µm pore-size; Carl Roth, Roti-NC, #HP40.1) were also equilibrated in ice-cold Towbin buffer for 30 min. Transfer was performed in a BioRad Mini-PROTEAN Tetra Cell with a Mini Trans-Blot Module in Towbin buffer under constant agitation and cooling at 100 V constant for 2 hr. After protein transfer, the membranes were washed twice with PBS for 5 min with agitation and blocked with a 1:1 mixture of PBS and Odyssey Blocking Buffer (Li-Cor, #927-40000) for 1 hour with agitation. Next, membranes were incubated with agitation with a suitable concentration of primary antibody in 5 ml 1:1 PBS:Odyssey Blocking Buffer containing 0.1% v/v Tween-20 for either 2-3 hr at room temperature or overnight at 4°C. Membranes were washed 5 times in PBS-T (PBS containing 0.1% v/v Tween-20) for 10 min with agitation. For detection, membranes were incubated with a suitable concentration of secondary antibody in 5 ml 1:1 PBS:Odyssey Blocking Buffer containing 0.1% v/v Tween-20 for 1 hr at room temperature with agitation. Finally, membranes were washed three times with PBS-T and twice with PBS for 5 min with agitation. Bands were detected using the 700 and 800 nm channels of a Li-Cor Odyssey Classic Imaging System with recommended settings for imaging of western blot membranes (resolution: 84.674 µm; quality: medium; focus offset: 0; intensity: 3 (at 700 nm) and 6 to 7.5 (at 800 nm)).

3.2.8. Cell culture of SH-SY5Y and HepG2 cells

All general cell culture procedures and transfections were performed under a sterile laminar flow cell culture hood (BDK, Sonnenbühl, Germany). Cells were cultivated at 37°C and 5% CO_2 in a cell incubator (Binder, Tuttlingen, Germany). Both SH-SY5Y and HepG2 cells were never used past total passage 40 and were regularly tested for mycoplasma contamination (GATC mycoplasma check, SKU#B50400400).

Thawing: Cryostocks of cells were instantly transferred into a 37°C water bath, thawed for 2 min and resuspended in pre-warmed cell specific medium. The cell suspension was centrifuged for 3 min at 200 x g. The supernatant was discarded and the cell pellet resuspended in pre-warmed medium. Cells were transferred to a cell culture flask and were used for experiments after passaging at least 3 times after thawing.

Freezing: For cryo-conservation of cells, cell suspensions were adjusted to 10^7 cells per ml freezing medium (70% (v/v) medium, 20% (v/v) FCS, 10% (v/v) dimethylsulfoxid (DMSO)). Aliquots of 1 ml cell suspension per cryo vial were transferred to a cryo-freezing container for a gradual reduction in temperature to below −80°C before storage in liquid nitrogen.

Passaging: SH-SY5Y cells were cultured in DMEM:F12 (PAN Biotech, #P04-41500) supplemented with 10% heat-inactivated FBS (Biochrom AG, #S0615) and 1% penicillin-streptomycin (PAN Biotech, #06-07100). HepG2 cells were cultured in EMEM (PAN Biotech, #P04-08509) supplemented with 2 mM L-glutamine (PAN Biotech, #04-82100), 1 mM sodium pyruvate (PAN Biotech, #04-43100), 10% heat-inactivated FBS and 1% penicillin-streptomycin. For both cell types, the medium was routinely replaced every 3 days and both were passaged before reaching a maximal confluency of 90%. Passaging was performed by a brief wash with DPBS without Ca^{2+} and Mg^{2+} (PAN Biotech, #P04-36500) pre-heated to 37°C and an incubation with Trypsin/EDTA (PAN Biotech, #P10-0231SP) at 37°C for 3 min for SH-SY5Y cells and for 8 min for HepG2 cells. To stop the protease activity, cell specific growth medium was added and the cell suspension of the detached cells was centrifuged for 3 min at 200 x g. The supernatant was removed and cells were resuspended in their appropriate medium. Next, cells were either counted using a Neubauer chamber for transfection or seeding on coverslips, or directly transferred to a new cell culture flask for further cultivation. SH-SY5Y cells were routinely reseeded using a dilution of 1:4 while never exceeding a dilution of 1:10, whereas HepG2 cells were routinely diluted 1:10 for reseeding while never exceeding a dilution of 1:30.

Harvesting, counting and cell lysis: For harvesting, cells were washed 3 times in DPBS without Ca^{2+} and Mg^{2+} pre-cooled to 4°C and mechanically detached using a cell scraper followed by collection in

ice-cold DPBS. Cells were pelleted, resuspended in 10 ml of pre-cooled DPBS and quantified without further dilution by manually counting the cells in a Neubauer chamber as per manufacturer's instructions (per sample filling both sides of the chamber with two separate dilutions and counting all four 4x4 squares). Alternatively, cells were diluted 1:30 in cell counting buffer (2% v/v FBS, 1 mM EDTA in DPBS) and quantified by a flow cytometer (Guava easyCyte 5), which collected samples of at least 10,000 intact cells (i.e. by excluding all counts with a diameter <1 µm based on forward scatter). For lysis, the cells were pelleted, resuspended in RIPA buffer containing protease and phosphatase inhibitors (Santa Cruz, #sc-24948; pre-cooled to 4°C) and rigorously vortexed. The samples were rotated for 30 min at 4°C, followed by a 10 min incubation in an ice-cold ultrasound bath. After centrifugation at 14,000 x g for 10 min at 4°C, the supernatant was collected and stored at -20°C. The protein content of each lysate was determined using the Pierce BCA Protein Assay kit (Thermo Fisher Scientific, #23225) following the manufacturer's instructions.

Electroporation: For overexpression of specific (fusion-)proteins, the corresponding expression vectors were electroporated into the cells using the Neon Transfection System (Thermo Fisher Scientific, Invitrogen). In brief, the cells were detached from the culture flasks, counted and pelleted. For electroporation of SH-SY5Y cells, 1 x 10^6 cells were resuspended in 125 µl Buffer R containing 10 µg plasmid DNA. 100 µl of the cell-DNA mixture was taken up in a 100 µl Neon electroporation tip attached to the Neon pipette, which was inserted into a Neon electroporation tube filled with 3 ml E2 buffer. Finally, a single pulse of 1,100 V with a 50 msec width was applied to electroporate the cells. For HepG2 cells, 3 x 10^6 cells were resuspended in 125 µl Buffer R containing 5 µg plasmid DNA, after which a single pulse of 1,200 V and a width of 50 msec was used. Electroporated SH-SY5Y or HepG2 cells were transferred into cell culture medium without antibiotics and either seeded on PLL-coated cover slips or in 6-well plates and generally analyzed 20-24 hours post-electroporation unless otherwise noted. For the α-processing assay, HepG2 cells were treated with 10 µM DAPT starting 4 hours post-electroporation. After another 14 hours cells were lysed using RIPA lysis buffer and analyzed by western blotting.

3.2.9. Preparation of cover slips for microscopy

For analysis by epifluorescence or confocal microscopy, cells were mounted on 25 mm diameter round glass cover slips with a thickness of "1" (0.13-0.16 mm; Marienfeld, #0111650). For super-resolution gSTED microscopy, 22 mm square high precision cover slips with a thickness of "1.5H" (0.170 mm +/- 0.005 mm; Marienfeld, #0107052) were used. Please note that both varieties of cover slips have a surface area of about 5 cm².

Cleaning and coating of cover slips: The cover slips were cleaned by consecutive washes with agitation in 1 M HCl, in 1 M NaOH and in 100% ethanol for 1 hr each. In between each wash step, cover slips were rinsed thoroughly in ddH_2O. After the last wash step, the ethanol was discarded and the cover slips were sterilized and dried at 180°C. The cover slips were distributed in 6-well plates and coated for 30 min with 500 µl 100 µg/ml PLL in ddH_2O solution per cover slip. After removal of the PLL solution, the cover slips were dried and subsequently sterilized by exposure to UV light for 20 min.

Seeding of cells on PLL-coated cover slips: Electroporated cells were taken up in antibiotic-free cell culture medium and seeded at a density of 1×10^5 cells per cm^2 (i.e. 5×10^5 per cover slip) by pipetting 500 µl menisci onto the PLL-coated cover slips. Non-electroporated cells were taken up in cell culture medium with antibiotics and seeded at a density of 6×10^4 cells per cm^2 (i.e. 3×10^5 per cover slip) similarly to electroporated cells. After a 1-2 hr incubation to allow the cells to recover and attach, cell culture medium with antibiotics was added to a final volume of 2 ml per well. The cells were either used for generating membrane sheets or directly for experiments at least 22 hr after seeding.

Generation of membrane sheets: Cover slips with overexpressing or non-overexpressing cells were washed twice with ice-cold DPBS++ and transferred to the middle of a glass petri-dish filled with ice-cold DPBS++. A sonicator tip was positioned directly above the cover slip at a 5 mm distance, and a 100 msec sonication pulse that removes the upper parts of the cells was applied (~15% power for SH-SY5Y cells, ~80% power for HepG2 cells; Bandolin Sonoplus HD2070 with a MS 73 probe), leaving behind the intact and functional basal plasma membranes. The plasma membrane sheets were rinsed once more with ice-cold DPBS++ before fixation.

Paraformaldehyde-based fixation: Cover slips with intact cells (which were first rinsed twice with either RT or ice-cold DPBS++) or plasma membrane sheets were fixated for 30 min with either 4% paraformaldehyde (PFA; 4% w/v PFA in DPBS++, pH 7.4), 1% PFA or 1% periodate-lysine-paraformaldehyde (PLP; 1% w/v PFA, 10 mM sodium-metaperiodate, 75 mM L-lysine in DPBS++, pH 7.4) either at room temperature or pre-cooled to 4°C. To stop fixation, the coverslips were rinsed once with 50 mM NH_4Cl in PBS and then incubated for 20 min with agitation in 50 mM NH_4Cl in PBS. Finally, the cover slips were rinsed once and washed twice with PBS for 5 min with agitation.

Immunolabeling of fixated plasma membrane sheets: After the final wash steps following fixation, fixated plasma membrane sheets were blocked with 2.5% BSA in PBS for 1 hr with agitation. The coverslips were labeled with primary antibody diluted 1:200 (unless otherwise noted) in 1% BSA in PBS overnight at 4°C and washed 5 times with 0.5% BSA in PBS for 10 min with agitation. Next, labeled proteins were detected with secondary antibody diluted 1:200 in 1% BSA in PBS. Lastly, the cover slips were washed four times with PBS for 5 min with agitation. For stochastic labelling experiments, diluted

antibody solutions were subjected to a pre-cooled sonication bath for 5 min before applying them to the plasma membrane sheets.

3.2.10. Microscopy

For confocal and epifluorescence microscopy, cover slips were mounted in wet microscopy chambers filled with an imaging buffer consisting of a saturated TMA-DPH (Thermo Fisher Scientific, Invitrogen, #T204) solution in PBS which was diluted 1:10 in PBS. For gSTED microscopy, cover slips were first counterstained by incubating with 0.5 µM Fast-DiO (Thermo Fisher Scientific, #D3898) in PBS for 10 min with agitation, followed by washing three times with PBS for 5 min with agitation. Finally, the cover slips were mounted on microscopy slides using a drop (~15 µl) of ProLong Gold (Thermo Fisher Scientific, #P36930), left to harden in the dark for 24 hr at room temperature and sealed using transparent nail polish without alcohols (DM, p2 cosmetics).

Confocal optical sectioning: SH-SY5Y cells were prepared as described above with the exception that the cells were seeded at a much lower density (5 x 10^3 cells per cm^2; 25 x 10^3 per cover slip). The cells were fixated in 1% PFA in DPBS++ pre-cooled to 4°C. The Zeiss AXIO Observer Z1 inverted confocal microscope was employed using 10% laser power of the 405 nm diode laser and detecting fluorescence from 415-464 nm for visualization of TMA-DPH, a pixel depth of 8-bit, a lateral pixel size of 260 nm, axial sectioning steps of 240 nm, 2x line averaging and a pinhole size of 45 µm.

Epifluorescence microscopy: Epifluorescence microscopy was performed either on the Olympus IX-81 inverted microscope or on the Axio Observer D1 inverted microscope. On the Olympus microscope, the DAPI HC filter set was used to excite and detect TMA-DPH, the EGFP HC filter set for emGFP and Alexa Fluor 488, the TRITC HC filter set for mCherry and Alexa Fluor 594 and the Cy5 ET filter set for Alexa Fluor 647. The acquisition time was set to either 50 or 100 ms and the lamp power was chosen so that the detected fluorescence covered about 2/3 of the dynamic range of the camera when using an EM-GAIN of 20 and a GAIN of 1. Moreover, recordings were routinely obtained using both the 1.6x and 2x magnification lenses, yielding a pixel size of 83.33 nm. For optical sectioning, axial sectioning steps of 500 nm were used. For experiments requiring optimal signal-to-noise ratios, 10 images were taken in quick succession and afterwards averaged.

Time-gated STED microscopy: For super-resolution microscopy, cover slips mounted on microscopy slides were imaged with either the 4-channel easy3D STED microscope or the white-light laser TCS SP8 gated-STED microscope. On the easy3D STED microscope, Fast-DiO was excited with the 485 nm laser at 60 µW power and the 500-520 nm filter set and Alexa Fluor 594 with the 561 nm laser at 60 µW power and the 580-630 nm filter set. For depletion of Alexa Fluor 594, the pulsed 775 nm

depletion laser was employed at 700 mW in 2D mode. For all images, pixel size was 15 nm and the pinhole size 60 µm. gSTED micrographs were recorded with 10 line accumulations and time-gated detection with 1.25 ns delay and 8 ns gate width. Confocal images were recorded with time-gated detection with 78.13 ps delay and 8 ns gate width.

On the TCS SP8 gated-STED microscope, Alexa Fluor 488 was excited using 20% power of the white-light laser set to 488 nm, while depletion was accomplished using 40% power of the 592 nm CW-STED laser. Images were recorded at 200 Hz, pixel size was adjusted to 20.04 nm and pixel dwell time to 0.6 µs. gSTED micrographs were recorded with 10 line accumulations and time-gated detection between 1 and 6.5 ns. Confocal images were recorded without time-gated detection.

Confocal FRAP microscopy: For fluorescence recovery after photobleaching (FRAP), live SH-SY5Y and HepG2 cells were imaged in Ringer solution at 37°C in the climate chamber of the Olympus Fluoview 1000 laser scanning microscope for a maximum of 1 hr per cover slip. emGFP was excited with the 488 nm laser and mCherry with the 543 nm laser, detection was performed by using adjusting the selectable wavelength filter to 500-524 nm for emGFP and 600-630 nm for mCherry. The focal plane was adjusted to the plane of the basal plasma membrane, the scanning field was set to 100 x 100 pixels with a pixel size of 207 nm and images were taken at 1 Hz. After the first three frames, a region measuring 15 x 15 pixels was photobleached for one frame at 100% laser power of both the 488 and 543 nm lasers. Recovery of fluorescence was monitored for an additional 116 frames post-bleach.

3.2.11. Image analysis

Microscopic images and images from the Odyssey® CLx Imaging System of in-gel stainings and western blotting were routinely analyzed using the ImageJ software or more extensive distributions of ImageJ, like Fiji and the McMaster Biophotonics Facility (MBF) collection of plugins and macros for ImageJ, unless specified otherwise.

In-gel stainings and western blots: Corresponding bands were quantified in relation to each other using the ImageJ 'Gels' tool under the 'Analyze' menu. In brief, each lane containing one or multiple bands of interest was delineated by a rectangular ROI that covered all the bands of that lane. For each lane, the ROIs are of equal width and height and have the same x-position. Next, these ROIs are transformed into lane profile plots in which the grey values of every pixel per horizontal line of the ROI are summed and displayed in a graph where the summed intensities are plotted on the x-axis and each line position on the y-axis. By using the 'Straight Line' tool, base lines can be drawn at the height of the background signal so that each peak defines a closed area corresponding to a band of interest. The 'Wand' tool can then be used to measure the area under the curve (AUC) of each closed-off peak, which is a good approximation for the background corrected intensity of each band. These analyses

were always performed on images without 'scale' (i.e. no relationship between pixels and units of length such as centimeters) and using uncalibrated optical densities (ODs).

Plasma membrane surface area measurements: Z-image stacks of the imaged SH-SY5Y cells. Specifically, image stacks of solitary cells were cropped in such a way that residual signals from adjacent cells were removed, as these would form additional objects after creating 3D models. Additionally, the image stacks were smoothed employing the 'Smooth' filter under the 'Process' menu. Next, the cleaned image stacks were loaded into the Imaris software (Bitplane AG 2015) and 3D cell models were created without thresholding. As a result, pixel interpolation and creation of voxels occurred. The voxel size was calibrated with reference to the imaging settings (260 nm pixel size and 240 nm axial step size). Using the 'Surface Creation Tool', each cell was thresholded manually to find the highest threshold resulting in a surface model in which neurites remain intact and no holes or disruptions in the cell surface occur. From these surface models, parameters like, for example, cell surface area, cell volume and roundness can directly be obtained. To control for bias when setting the surface thresholds, each cell was re-analyzed with a 5% and 10% increase and decrease in threshold level.

Average fluorescence intensity, relative standard deviation, and correlation coefficient: For each composite image, one ROI was placed within the PM sheet (ROI_{sheet}) and one ROI was placed next to the PM sheet (ROI_{BG}) in the membrane counterstain channel to ensure an unbiased selection of which area is to be analyzed. The fluorescence intensity of both ROIs was then determined in the channel(s) of interest using the option 'Mean Gray Value' of the 'Measure' tool in the 'Analyze' menu of ImageJ. The mean gray value of the ROI_{BG} was subtracted from that of the ROI_{sheet} to obtain its average fluorescent intensity. The relative standard deviation was calculated by dividing the standard deviation (option 'Standard Deviation of the 'Measure' tool) of a ROI_{sheet} by its corresponding background corrected average fluorescence intensity. The correlation coefficient within a ROI_{sheet} was determined using the ImageJ plugin 'Intensity Correlation Analysis' (Li et al. 2004), which can perform a pixel-wise Pearson correlation coefficient (PCC) between two channels of a composite image. To correct for the shift between channels resulting from light path aberrations due to not perfectly aligned laser couplings and/or filter cubes, tetraspeck microspheres (ThermoFisher Scientific, #T7284) were used as a spatial reference.

Maxima analysis: For unbiased analysis, ROIs were placed as described above. Maxima were recognized and counted within each ROI using the 'Find Maxima' algorithm. A threshold of 3 gray values for all gSTED recordings (signal dynamic range: 0-200 gray values) and 30 gray values for all epifluorescence images (signal dynamic range: 2,150-11,000 gray values) was chosen to eliminate

instrument noise. For quantification of the maxima per µm², the number of maxima was normalized to the total area per ROI. Next, circular ROIs with a diameter of 5 pixels were centered on the detected maxima. The mean intensities of all maxima within a ROI were determined and corrected with the average fluorescence intensity of the ROI_{BG} (see above). Additionally, a horizontal and a vertical line scan with a length of 31 pixels for gSTED microscopy or 15 pixels for epifluorescence microscopy and a width of 3 pixels (which were averaged) were placed through each maximum. Both line scans were fitted with a Gaussian function and, based on fit quality, either the horizontal or the vertical fit was chosen and used to extract the full width at half maximum (FWHM). Fits with an R-squared value < 0.90 and fits that were too far off-center (peak outside of pixel 10-20 for gSTED and 5-10 for epifluorescence microscopy), which accounted for less than 2% of all maxima in all samples, were excluded from the analysis. This macro was kindly provided by Dr. Jan-Gero Schloetel.

Correction of maxima intensity distributions: Per sample, the maxima (see above) from all biological replicates were pooled and distributed into bins with a width of 75 intensity counts and the number of maxima per µm² was determined for each bin. For each bin, the maxima per µm² of the control sample (no primary antibody) were subtracted from the maxima per µm² of the routinely labeled (1:200 dilution of primary antibody) and the stochastically labeled (1:8000 dilution of primary antibody) samples to correct for non-specific signals.

FRAP analysis: Inside the scanning field 3 ROIs of 15 x 15 pixels were marked: one corresponding to the photobleached region (ROI_{bleach}), one covering an unbleached region within the overexpressing cell ($ROI_{control}$) and one beside the cell (ROI_{BG}). The average fluorescence intensity of ROI_{BG} was used to correct for background fluorescence in both ROI_{bleach} and $ROI_{control}$. The pre-bleach fluorescence intensity (average of the 3 pre-bleach frames) of $ROI_{control}$ was compared to the fluorescence intensity of the last 3 frames (frames 118-120) and the measurement was discarded if the difference was bigger than 15%. Similarly, if the difference between the fluorescent intensity of the pre-bleach frames and the first frame after photobleaching of ROI_{bleach} was less than 80%, the measurement was also discarded. For quantification of the fluorescent recovery after photobleaching, the post-bleach frames were normalized to the average fluorescent intensity of the 3 pre-bleach frames and plotted against the time. Per experimental day and sample, plotted values were averaged and fitted to a hyperbolic function with a fixed offset (γ_0) to obtain the half time recovery ($t_{1/2}$) and the maximal recovery (Rec_{max}):

$$\gamma_t = \gamma_0 + \frac{Rec_{max} \times t}{t_{1/2} + t}$$

4. Results

4.1. Packing density of plasmalemmal APP clusters

The initial aim of this project was to determine the molecular density of APP within its plasmalemmal protein cluster as accurately as possible. To allow for this high level of precision in molecular quantification, a methodology based on a combination of chemistry-based molecular biological techniques and state-of-the-art microscopy has been shown before to be highly successful and was therefore also preferred here (Sieber et al. 2007). The biggest challenge of this aim, however, was not the required exactness, but the fact that the desired quantification was absolute and not relative, as usually is the case. This 'absoluteness' means that experimental results generally cannot be correlated to a control situation, which prohibits comparative statistical analyses in most cases, though often parallels to published values can be drawn. Additionally, within the framework of this project most quantifications are dependent on each other, which could theoretically amplify uncertainties especially if multiple experiments are unintentionally similarly biased. Because of these reasons, it was imperative to keep technical variability to a minimum and approximate any absolute biological parameters as closely as possible. This was achieved, among others, by using suitable calibrated standards, evaluating many more technical and biological replicates than are typically used in molecular biological experiments and correlating our results to comparable systems found in the literature wherever possible.

4.1.1. Expression and purification of recombinant APP_{695}

To acquire the best possible standard to normalize the amount of endogenous APP to in quantitative western blots, it was decided to express human APP_{695} in bacterial cells and extract it via Ni-NTA affinity purification of a His-tag fused N-terminally to the APP coding sequence. The pET-15b backbone, which is a bacterial expression vector based on the pBR322 plasmid, seemed perfect as it carries an N-terminal His_6-tag followed by a thrombin cleavage site and the multiple cloning site (Figure 6A). After cloning the APP_{695} coding sequence into the pET-15b backbone, the expression vector encoding the recombinant protein shown at the bottom of Figure 6 panel A was used to express APP in bacterial cells. Initially, the Rosetta 2 (DE3) host strain was chosen, as it is naturally compatible with the pET expression vectors and can be selectively and quantitatively triggered to express the protein of interest by IPTG addition allowing fine-tuning of expression timepoint and levels. Additionally, it contains a vector that codes for 7 tRNAs that are rare in bacteria but abundant in eukaryotes, making it especially suitable for expression of eukaryotic genes. After transformation and overnight expansion

of the Rosetta 2 culture, expression of APP was induced by addition of 1 mM of IPTG and the culture incubated at 30°C for 6 hours taking a sample every hour for analysis. To check for expression of His_6-APP_{695}, colloidal Coomassie in-gel stainings in combination with western blotting against the His-tag were employed. However, expression of the recombinant protein could not be detected, and bacterial cultures did not seem to proliferate anymore after induction (data not shown). To provide an indication whether APP toxicity could be the culprit, bacterial growth was monitored by measuring OD_{600} to see whether induced cells were still able to proliferate. Induction with as little as 0.1 mM IPTG was already enough to severely hamper bacterial expansion compared to the uninduced control, whereas higher IPTG concentrations completely abrogated culture growth (Figure 6B). This suggested that expression of recombinant APP burdened the bacterial cells immensely, also prohibiting them to produce useful quantities of the recombinant protein. To circumvent this problem another bacterial host strain, namely ArcticExpress (DE3) RP (AE-RP), was used. This host strain also possesses a lacUV5 promoter, offering compatibility with pET vectors and enabling precise control of protein expression by IPTG, and genes encoding 2 rare tRNAs especially suitable for expression of heterologous mammalian proteins with a GC-rich coding sequence. However, the major advantage with AE-RP cells is that exogenous proteins can still be efficiently expressed and processed using low-temperature cultivation due to the co-expression of cold-adapted chaperonins Cpn10 and Cpn60. Production of heterologous proteins in bacterial cells at temperatures between 4 and 12°C attenuates protein expression rates and increases recovery of soluble protein (Ferrer et al. 2003). Before induction with IPTG, the overnight AE-RP culture transformed with the APP expression vector was cooled down to 12°C and kept at this temperature for expression of the recombinant protein. In contrast to the Rosetta 2 cells at 30°C, especially the lower IPTG concentrations allowed the AE-RP cells to continue to propagate after induction (Figure 6C), indicating that the toxic effect of heterologous APP expression was constrained to an acceptable level. Of course, culture expansion was not the primary goal of this endeavor, production of the APP fusion protein was. Therefore, AE-RP cells transformed with the expression vector were induced with 0.1 mM IPTG after which a sample was taken from the culture on selected timepoints. Using colloidal Coomassie in-gel stainings, it could clearly be shown that abundance of a protein running at the predicted height the APP fusion protein should also run at, i.e. ~120 kDa, steadily increased over time (Figure 6D). To make sure that this protein was the protein of interest and that no truncated fragments or degradation producs were present, western blot analysis was performed on a subset of the collected samples. Detection with an anti-His antibody demonstrated that the accumulating protein indeed possessed a His-tag, indicating that this had to be the expressed APP fusion protein (Figure 6E). Furthermore, the His-tag was only detected at about 120 kDa, suggesting that no C-terminally truncated fragments had been produced and that the fusion protein was not degraded at some point

during the process. Thus, these conditions were chosen to launch the scaled-up version of the expression process with the goal of purification.

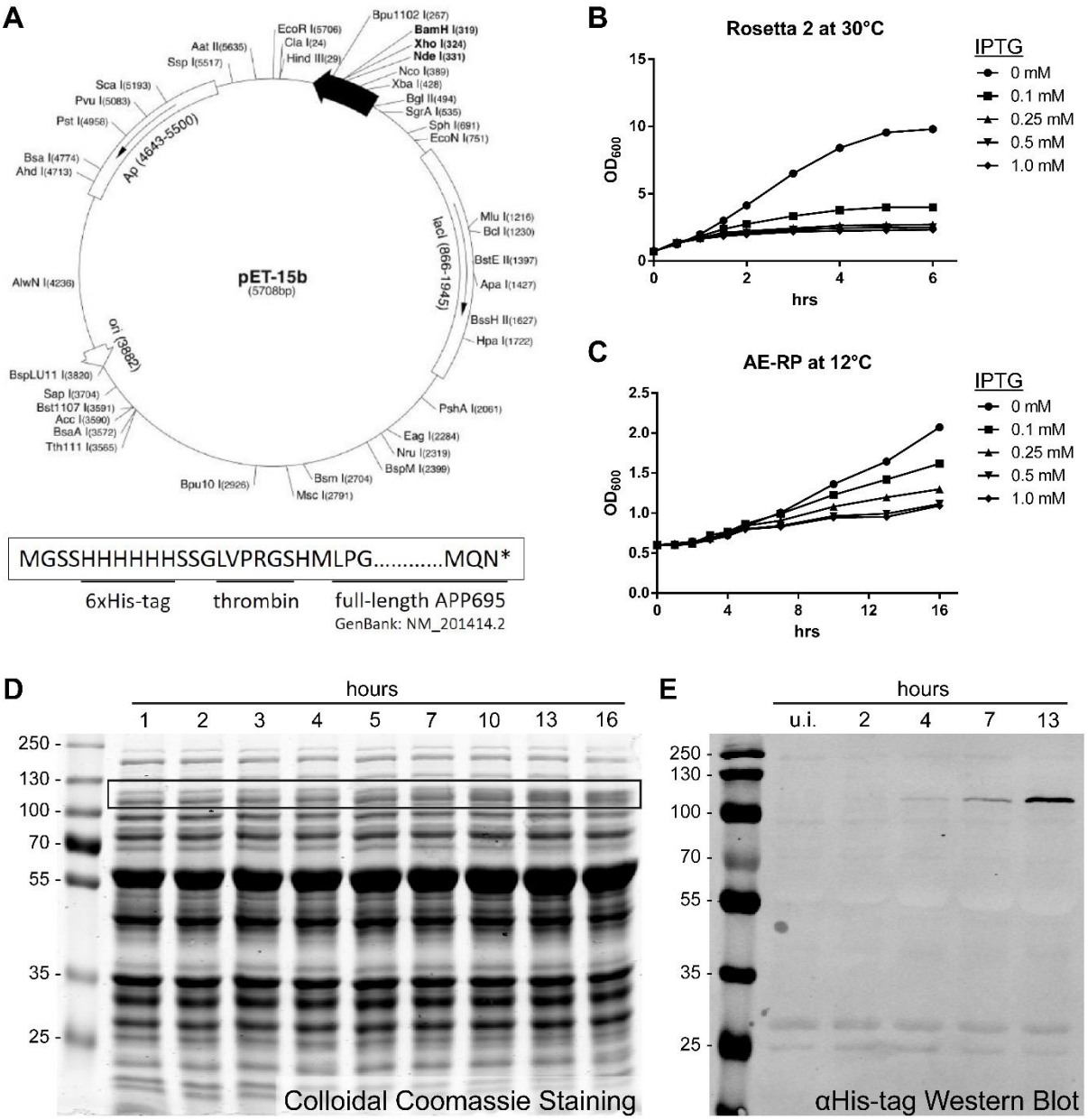

Figure 6. Bacterial expression of recombinant APP_{695}

(A) Vector map of the bacterial expression vector pET-15b including features and unique restriction sites of which NdeI and Bpu1102I were used for insertion of the full-length human APP_{695} cDNA. The final coding sequence is depicted on the bottom of the panel. **(B&C)** Growth curves measured using OD_{600} turbidity of Rosetta 2 (B) and AE-RP (C) competent cells transformed with the completed pET-15b-His_6-Thr-APP_{695} expression vector after induction of expression with different concentrations of IPTG. **(D)** Representative colloidal Coomassie in-gel staining of lysates from ArcticExpress-RP competent cells transformed with pET-15b-His_6-Thr-APP_{695} and induced with 0.1 mM IPTG. The samples were collected at the post-induction timepoints depicted above the image. The black box highlights the area where the His_6-Thr-APP_{695} recombinant protein should run. **(E)** Representative western blot against the 6xHis-tag of His_6-Thr-APP_{695} with selected timepoints from the lysates shown in (D). As in (D), the recombinant protein should run at approximately 120 kDa.

The big advantage of the His_6-tag is not only that it is easily and reproducibly detected by well-established antibodies, but that it can be used to purify a protein possessing the tag using nickel-nitrilotriacetic acid (Ni-NTA) affinity chromatography. The tetradentate chelator NTA binds Ni^{2+} ions using four coordination sites creating a high-affinity ligand for polyhistidine sites. When the Ni-NTA chelate is attached to a support, it can be used to extract captured His-tagged protein rapidly and efficiently from cellular lysates. Washing and recovery of the bound protein is usually accomplished by exposure to varying concentrations of imidazole, which is essentially a histidine without the amino acid peptide backbone. If the downstream applications for the recombinant protein are not dependent on protein activity, denaturing conditions during cell lysis and protein purification are preferred because the affinity for the Ni-NTA chelate is usually better for denatured proteins. Fortunately, these conditions could also be used for isolation of the recombinant APP, as the only downstream applications were in-gel stainings and western blotting, which were both performed under denaturing conditions anyway. After thorough lysis of the AE-RP cells, equilibrated nickel-laden NTA-agarose beads were added to the cell lysate and used to capture the His_6-tagged APP. The beads were harvested from the lysate by centrifugation and washed with increasing concentrations of imidazole to stringently remove non-specifically bound proteins and contaminants. After the final recovery of the recombinant protein, the elution buffer was replaced with PBS, where after glycerol was added for long-term stable storage. Throughout the whole procedure, samples were taken at every step to check for purity and control for loss of protein or degradation during the procedure. Sample collection was done in such a way that each sample remained directly comparable to the others, i.e. for all collected samples the loaded content had the same ratio to the total volume of the experiment at that time. By detecting these samples with an anti-His antibody using western blotting (Figure 7A) and revealing total protein content directly on the gel using colloidal Coomassie (Figure 7B), both the relative content of the recombinant APP as well as its purity in each sample could be visualized. The His-tagged APP was efficiently captured by and liberated from the Ni-NTA agarose beads, as can be observed by comparing the ‘lysate’ with the ‘eluate’ sample in both detection methods. In the Coomassie stained gel, the ‘lysate’ sample shows the complete protein content of the lysed cells, whereas the ‘eluate’ sample shows hardly any protein besides the purified APP. When comparing the ‘lysate’ with ‘supernatant’ sample in the western blot, it becomes obvious that a lot more recombinant APP was present than captured, i.e. only a portion of the available APP could be “fished out” by the amount of beads that was employed. This was intentional and to ensure that the beads were saturated with recombinant APP, while as little as possible non-specific protein could be bound by the Ni-NTA. Additionally, the first wash (’10 mM’) showed a relatively high concentration of His-tagged APP, probably because a lot of material from the cellular lysate, including the recombinant protein, was not specifically bound but still somehow stuck to the beads, which is also indicated by the high signal in

the Coomassie stain. The other washes ('20 mM' to '50 mM') showed an increasing release of APP, but also exhibited steadily increasing purity as revealed by the almost absent signal in the Coomassie stains of the last 2 washes. Unfortunately, the purity of the eluate could not be determined numerically as the signal of the remaining contaminations was so low that they could not be quantified using this methodology. It is, however, safe to assume that the impurities constituted less than 5% in the final product. Lastly, dialysis and addition of glycerol to a concentration of 50% for long-term storage did not affect integrity of the recombinant APP and altered the concentrations thereof as expected.

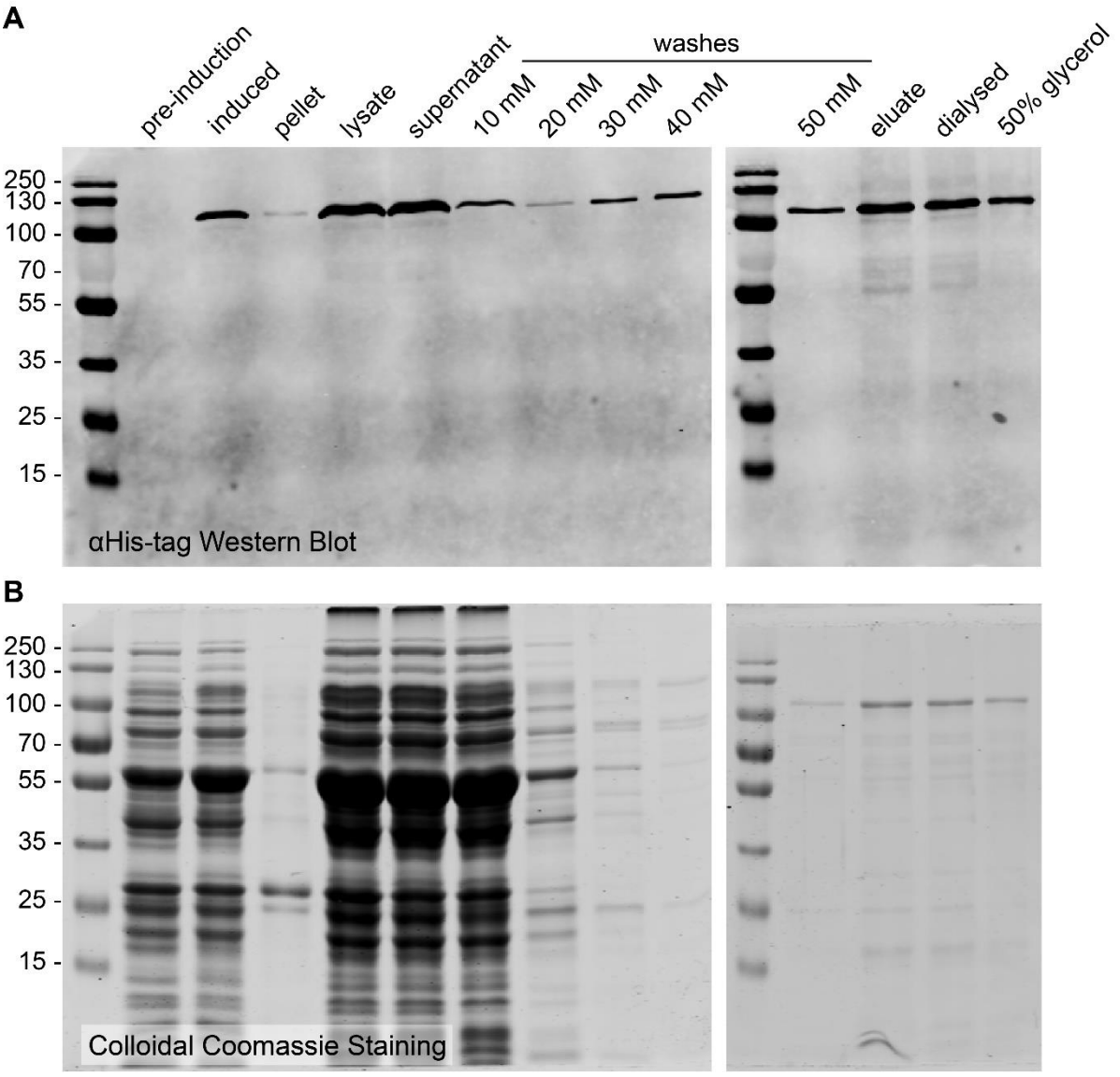

Figure 7. Purification of recombinant APP_{695}

(A) Representative western blot against the 6xHis-tag of recombinant His_6-Thr-APP_{695} with samples taken during selected steps of the Ni-NTA-based purification procedure. **(B)** Representative colloidal Coomassie staining of the same samples presented in (A).

To be able to use the recombinant His-tagged APP as a calibrated standard to estimate the APP content of mammalian cells, its concentration should be meticulously determined. By dissolving exactly weighed quantities of ultra-pure BSA in PBS and sequentially diluting this solution, it could be employed as a calibrated standard to assess the concentration of the purified recombinant APP. To ascertain that the staining method or the dye itself did not affect the quantification, two dyes with distinct protein binding mechanisms were employed. The sequential BSA dilutions together with three dilutions of the recombinant APP were loaded on acrylamide gels and stained with either of the dyes (Figure 8A). By determining the background-corrected signal of each of the BSA bands and plotting these against the amount of BSA that was loaded, a standard curve with which the signal of the APP bands could be correlated to an amount of protein was produced. Of note, both dyes showed linear staining intensities over a 30-fold concentration range. Each of the APP dilutions was quantified separately to account for protein concentration dependent variations in staining intensities and the average of these three dilutions was defined as one replicate. The concentration of the His-tagged APP was 32.47 ± 4.70 ng/µl [average ± standard deviation] when quantified with colloidal Coomassie and 33.41 ± 4.36 ng/µl with Fast Green FCF, which is less than 3% difference (Figure 8B). The evident similarity between these two values and their standard deviations despite the different binding interactions of the dyes confirms the correct estimation of the protein concentration. Finally, because

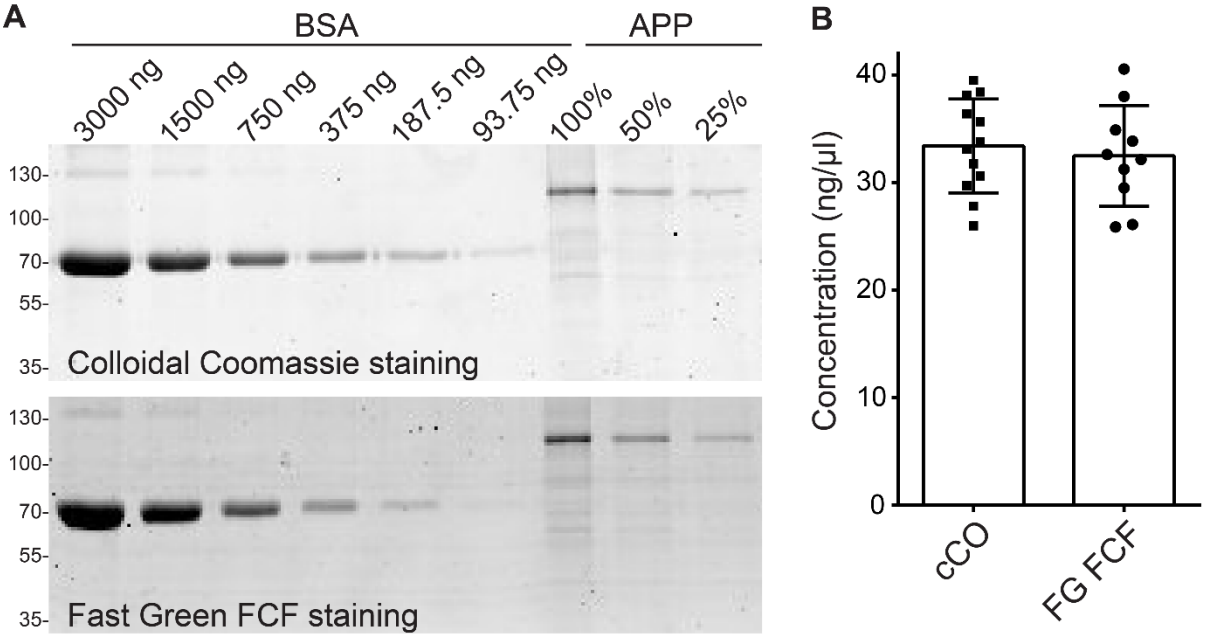

Figure 8. Concentration of recombinant APP_{695}

(A) Representative in-gels stainings of standard dilutions of refined BSA and 3 different concentrations of Ni-NTA purified recombinant APP_{695} (up: colloidal Coomassie; down: Fast Green FCF). **(B)** Quantification of the samples shown in (A). In total 12 colloidal Coomassie and 10 Fast Green FCF in-gel stainings were analyzed. Error bars represent standard deviation.

both staining methods are equally valid, all measurements were averaged to yield the final concentration of 32.98 ± 4.43 ng/µl. By using the theoretical molecular weight of the recombinant His_6-Thr-APP protein (80,840 Da), the found concentration could be transformed into molarity, which was calculated to be 407.5 nM.

4.1.2. APP content of SH-SY5Y plasma membranes

After determining the concentration of the purified APP, the absolute amount of endogenous APP in SH-SY5Y cell lysates could now be assessed. However, to reliably quantify the number of APP molecules per cell, not only the concentration of APP in the lysates, but also the number of cells that constitute each lysate should be accurately resolved. To this end, two different methods to count the number of cells that were subsequently lysed were used in parallel and served as a control for each other. The first counting method utilized the well-established Neubauer cell counting chamber, whereas the second method made use of the Guava easyCyte automated flow cytometer. After acquiring the cell counts, cells were thoroughly lysed in RIPA buffer and the total protein content of each lysate estimated using standardized BCA assays. By plotting the number of cells against the total

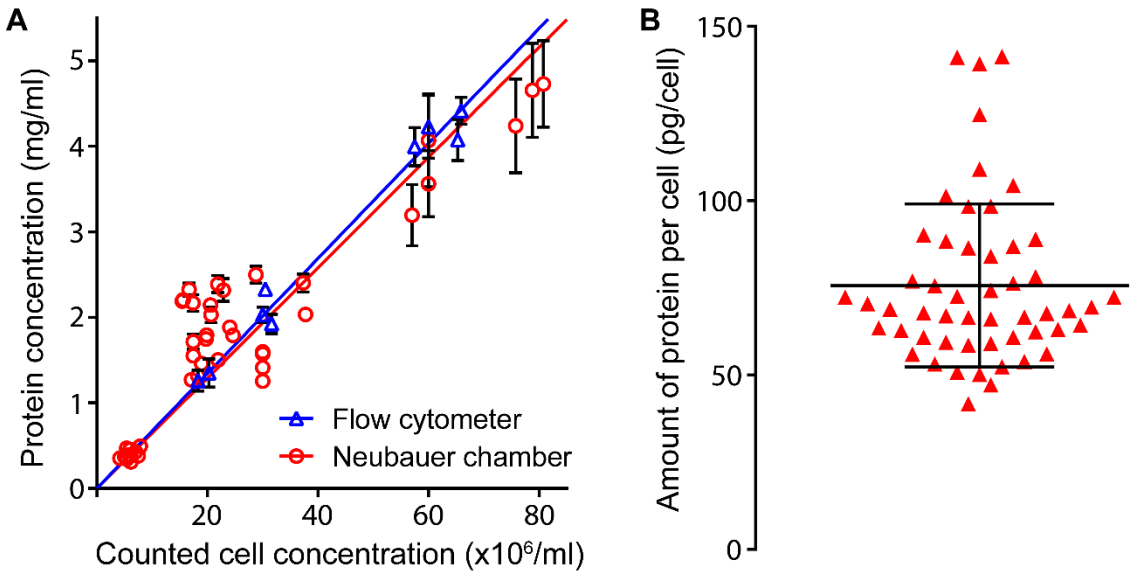

Figure 9. SH-SY5Y total cellular protein content

(A) Correlation of protein concentration with cell concentration for lysates from SH-SY5Y cells counted with either a flow cytometer (blue; 9 biological replicates) or a Neubauer counting chamber (red; 43 biological replicates). The protein concentration of each lysate was quantified with 3 separate BCA assays containing 3 triplicate measurements each (error bars show standard deviation). Cell counts were analyzed with 3 technical replicates for the flow cytometer and 4 technical replicates for the Neubauer counting chamber. Linear regression analysis showed that there was no significant difference between the slopes of the linear fits (p = 0.2987; fit Flow cytometer: y=0.06723, Sy.x=0.2393; fit Neubauer chamber: y=0.06451*x, Sy.x=0.5612). **(B)** Total protein content per SH-SY5Y cell of all 52 samples shown in (A) calculated by dividing protein concentration by cell concentration. Error bars represent standard deviation.

protein content for each lysate and performing linear regression, the accuracy of both counting methods can be directly compared (Figure 9A). The correlations show good linearity over the ~10-fold concentration range, although at higher cellular concentrations counting with the Neubauer counting chamber seems to slightly underestimate the cell counts. Additionally, the automated flow cytometer seems to be more precise as its measurements deviate less from the calculated regression line and have smaller standard deviations for single measurements, especially for the samples with higher cell concentrations. The number of samples counted using the counting chamber, however, seems to compensate for the poorer correlation and it can clearly be observed that both ways of quantification result in the same relationship between protein concentration and cell count. As the methods agree with each other and are equally valid for evaluating the cell counts per lysate, both were pooled for the calculation of the protein content per cell. By dividing the protein concentration through the cell concentration for all lysates and averaging the quotients, the final average total amount of protein per SH-SY5Y cell was determined to be 75.69 ± 23.33 pg/cell (Figure 9B).

After establishing all necessary parameters to quantify both the cell number and the number of APP molecules per SH-SY5Y cell lysate, these parameters were combined to resolve how many APP molecules reside within an SH-SY5Y cell. Using SDS-PAGE followed by western blotting with an antibody against the C-terminus of APP, triplicates of each SH-SY5Y cell lysate of which the cell concentration could efficiently be estimated using the average protein content per cell (refer to Figure 9) were related to sequential dilutions with a known concentration of the recombinant

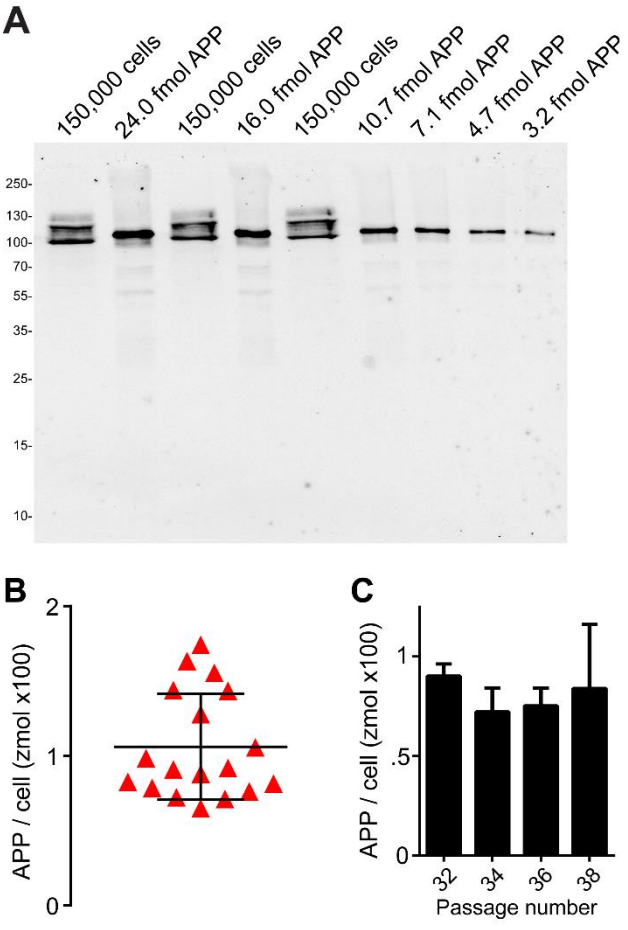

Figure 10. APP copy number per cell

(A) Representative western blot against the C-terminus of APP using serial dilutions of the recombinant APP as a standard curve and 3 technical replicates of an SH-SY5Y cell lysate with a known cell concentration. **(B)** Total APP content per cell was quantified by correlating the average intensity of the total APP signal of the lysates to a standard curve based on the serial dilutions. In total 18 biological replicates were analyzed on separate western blot at least twice and the results averaged. **(C)** A subset of the samples was continuously passaged 6 times with a 1:4 ratio amounting to about 64 population doublings. At selected passages, 3 separate samples were collected and analyzed as technical replicates. ANOVA analysis showed that there were no significant differences between the passages. Error bars represent standard deviation.

APP (refer to Figure 8), which served as a calibration standard (Figure 10A). By assessing the intensities of the bands from the calibration standard and plotting these against the number of APP molecules each band contains, a standard curve was created. Next, the integrated intensity of the combined APP signal, i.e. of all APP isoforms and maturation stages, for each single replicate of a cell lysate was measured against the standard curve. After averaging the replicates, the approximate concentration of APP molecules per cell lysate and, as the cell concentration of each lysate is also known, the number of APP molecules per cell is resolved (Figure 10B). The total amount of APP molecules per SH-SY5Y cells turned out to be 106.1 ± 35.43 zmol/cell. Using Avogadro's constant this number can be transformed into absolute molecule counts and doing so gave 63,889 APP molecules per cell with the 95% confidence interval (95%-CI) between 53,261 and 74,487 molecules per cell. Additionally, because in a different cell model APP levels were found to dwindle with increasing passage number (Kern et al. 2006), a population of SH-SY5Y cells was continuously cultured to cover the number of passages that were typically used for all experiments and analyzed for APP content (Figure 10C). As can be seen, no such trend was observed in SH-SY5Y cells, at least for the passages routinely used for this work.

Of course, only plasmalemmal APP can participate in the formation of plasma membrane clusters, but not all APP molecules that can be found in an SH-SY5Y cell are localized to its plasma membrane. A subpopulation of molecules is always on route towards the plasma membrane, another is actively being endocytosed and a third might be stored in intracellular vesicles ready to be integrated into the plasma membrane. Thus, the percentage of total APP that resides in the plasma membrane should be experimentally determined. By universally biotinylating primary amines, i.e. the sidechain of lysines and the amino termini of the proteins, of all transmembrane and membrane-anchored proteins that possess an extracellular part that is actively displayed on the cell surface, the subpopulation of plasmalemmal APP is also specifically labeled. If the SH-SY5Y cells are subsequently lysed and the labeled APP separated from the non-labeled APP, the ratio between both fractions, and thereby the percentage of plasmalemmal APP, can be determined. Samples were taken at every step of this streptavidin-biotin based segregation procedure not unlike the Ni-NTA protein purification described before and analyzed by western blotting with the same C-terminal APP antibody (Figure 11A). Immediately following cell lysis, a sample is taken ('Raw lysate') and compared to the 'Pellet' and 'Supernatant' fractions emerging after clarification by centrifugation. It can clearly be seen that all APP is extracted from the membrane and well-solubilized, as no signal could be detected from the pellets. Additionally, no significant amount of APP was lost during this procedure as the ratio between 'Pellet + Supernatant' and 'Raw lysate' is remarkably close to 1 (Figure 11B, first column labeled 'Input'). Next, the supernatant was subjected to column chromatography using immobilized streptavidin to isolate the biotinylated proteins. The flow-through should contain all non-biotinylated proteins;

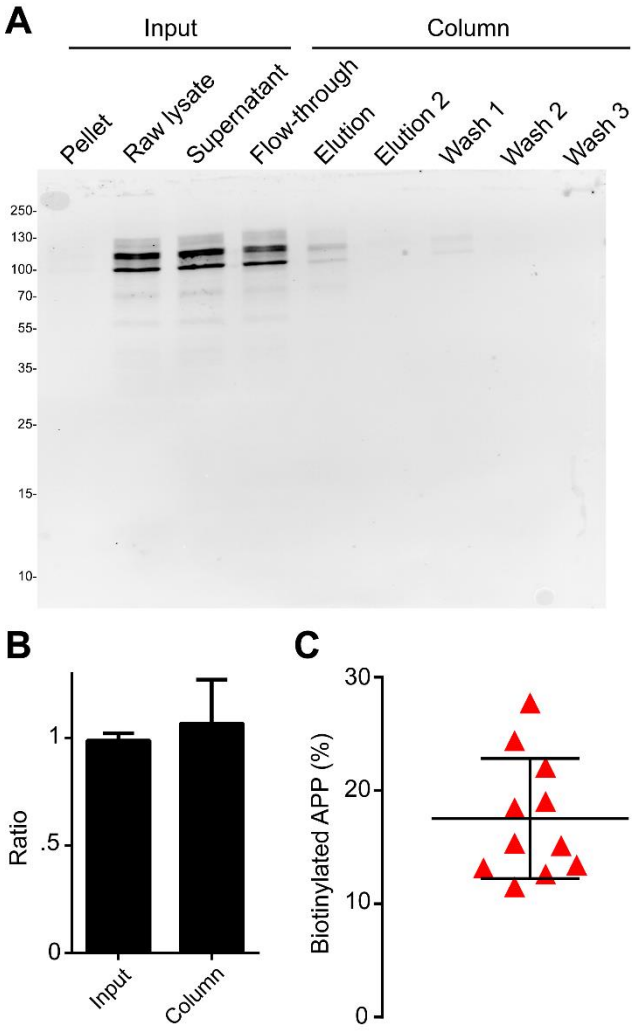

Figure 11. Plasmalemmal APP fraction

(A) Representative western blot against the C-terminus of APP of selected samples collected during the biotin/streptavidin-based cell surface protein isolation procedure. **(B)** Ratios between intensities of specific collected samples from (A). Input is defined as the ratio between 'Pellet + Supernatant' and 'Raw lysate' and Column as the ratio between 'Flow-through + Elution + Wash 1' and 'Supernatant'. Error bars represent standard deviation. **(C)** The percentage biotinylated APP of 11 biological replicates was calculated by dividing 'Elution' by 'Flow-through + Wash 1 + Elution'. Each biological replicate was analyzed on separate western blots at least twice and the results averaged. Error bars represent standard deviation.

whereas the bound biotinylated protein is washed several times before being eluted. The ratio 'Flow-through + Elution + Wash 1' to 'Supernatant' showed more deviation between the biological replicates but was nevertheless close to one (Figure 11B, second column labeled 'Column'), demonstrating that, if at all, only insignificant amounts of APP were lost during the experiment. Of note, the other fractions ('Elution 2', 'Wash 2' and 'Wash 3') gave no quantifiable signals, exemplifying the robustness of the method. By defining the sum of 'Flow-through + Wash 1 + Elution' as 100% and interpreting the signal from 'Wash 1' as residual unbiotinylated APP and thus belonging to 'Flow-through', the percentage of plasmalemmal APP can be calculated by dividing the signal from 'Elution' by 'Flow-through + Wash 1 + Elution' (Figure 11C). It was determined that 17.54% ± 5.31% (with a 95%-CI of between 13.97 and 21.10%) of total APP is localized to the plasma membranes of SH-SY5Y cells.

Combining this finding with the total number of APP molecules per cell found before (refer to Figure 10) gives a final estimate of [63,889 * 0.1754 =] 11,206 molecules per SH-SY5Y plasma membrane. By multiplying the 95%-CI of the cellular APP content with the 95%-CI of the percentage of plasmalemmal APP fraction, the lower and upper limits of the range wherein the actual plasmalemmal APP count may lay with a good degree of certainty can be calculated. This range lies between 7,441 and 15,717 APP molecules, which is quite a narrow range (only about a factor 2) considering the many different parameters and steps the methodology comprises.

4.1.3. Molecular density of APP in the plasma membrane

The prior biochemical experiments finally culminated in the quantification of the number of plasmalemmal APP molecules in SH-SY5Y cells. However, to arrive at the number of APP molecules per cluster, several additional parameters must first be elucidated. First and foremost, the total surface area of the average SH-SY5Y cell should be determined, as it allows calculation of the APP concentration in the cellular plasma membrane. By subsequently combining the plasmalemmal APP density with its cluster density (i.e. the number of APP clusters per unit of surface area), the number of molecules per cluster can be calculated. Another factor that has importance in this respect is the fraction of APP molecules that participates in cluster formation, as it is possible that a significant number of molecules resides in the plasma membrane as monomers.

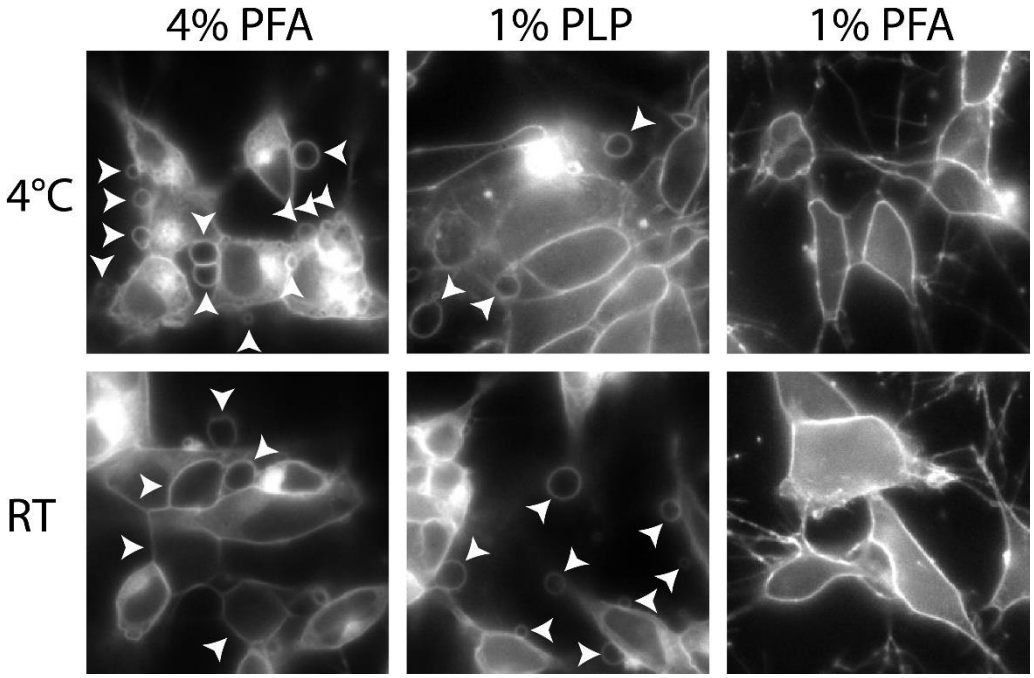

Figure 12. Effect of fixation on cell blebbing

Representative epifluorescence images acquired with the Olympus IX-81 inverted epifluorescence microscope. All conditions were sampled 3 times and each sample was prepared fresh, washed once and immediately imaged. White arrows indicate blebs. Each image constitutes an area of 41.7 x 41.7 µm.

To evaluate the average plasmalemmal surface area of an SH-SY5Y cell, optical sectioning of plasma membranes labeled with a membrane-integrating dye using a confocal microscope seemed the most straightforward method. SH-SY5Y cells were fixated prior to imaging because a good resolution in both the XY and Z-axis is a necessity for accurate recording of the plasma membranes, which could take up to a few minutes per image stack. Without fixation cells are prone to moving within this timeframe. However, in pilot experiments using the established fixation protocol with 4% paraformaldehyde (PFA) in PBS, it could clearly be seen that the fixated cells displayed a lot of small, round and empty structures

that were labelled by the dye and sitting on the extracellular side of the apical plasma membranes (data not shown). This is an indication of so-called 'blebbing', which, while interesting, is not beneficial for this study, as an unknown part of the apical plasma membrane is lost during fixation this way. Therefore, several different fixatives were tested to find one suitable for fixation of SH-SY5Y cells without loss of plasma membrane surface area, namely 4% PFA in PBS, 1% PFA in PBS or 1% periodate-lysine-paraformaldehyde (PLP) in PBS. PLP is a fixative normally employed in electron microscopy and supposed to be able to thoroughly fixate samples without loss of antigenicity or introduction of background fluorescence (McLean and Nakane 1974; Thavarajah et al. 2012). The 3 fixation solutions were also tested at 2 different temperatures, 4°C and 23°C or room temperature (RT). The plasma membranes and blebs were ambiguously labeled using TMA-DPH, a membrane-intercalating dye that only fluoresces when it is incorporated in a lipid bilayer. Of note, it was imperative to only wash the cells once after fixation without too much agitation as the blebs easily detach from the plasma membrane and are then lost. For this experimental set-up, fixation with 1% PFA turned out to be optimal, as no significant blebbing could be detected (Figure 12). Furthermore, because there was no visible difference between fixation at 4°C and RT, there was no reason to fixate at 4°C and risk cell contraction affecting the subsequent experiments.

After establishing the optimal fixation protocol for whole cells, the plasma membrane surface area of SH-SY5Y cells could be investigated. Several membrane dyes, namely TMA-DPH, WGA-Alexa Fluor (AF) 594 conjugate, Fast-DiO and CellMask Deep Red, had been tested in preliminary experiments (data not shown). WGA-AF594 conjugate, although bright and membrane-specific, resulted in a punctate staining pattern, which is not optimal for thresholding or the creation of smooth cell surface models. Fast-DiO also specifically stained the plasma membrane, but the staining intensities of individual cells varied greatly, meaning that for every image stack the microscope settings would have to be adjusted increasing the chance for artifacts and bias. CellMask Deep Red displayed a homogeneous staining of the plasma membranes but had a relatively disappointing signal-to-noise ratio in our set-up that seemed to deteriorate during optical sectioning presumably due to bleaching. In the end, TMA-DPH was chosen as the optimal dye because its staining intensity between cells was comparable, the plasma membranes were stained homogeneously, and signal-to-noise ratio was good. Additionally, staining intensity does not deteriorate during optical sectioning, as TMA-DPH is included in the imaging buffer and therefore continuously refreshed during imaging. Thus, SH-SY5Y cells were seeded at low density on cover slips, allowed to attach for 24 hours and fixated using 1% PFA at RT. High-resolution optical sections were made with a confocal microscope using TMA-DPH to detect the plasma membranes and the resultant images cleaned and prepared for analysis (Figure 13A). Prepared image stacks were processed with the Imaris software package (Bitplane AG 2015) to create 3D cell surface masks from

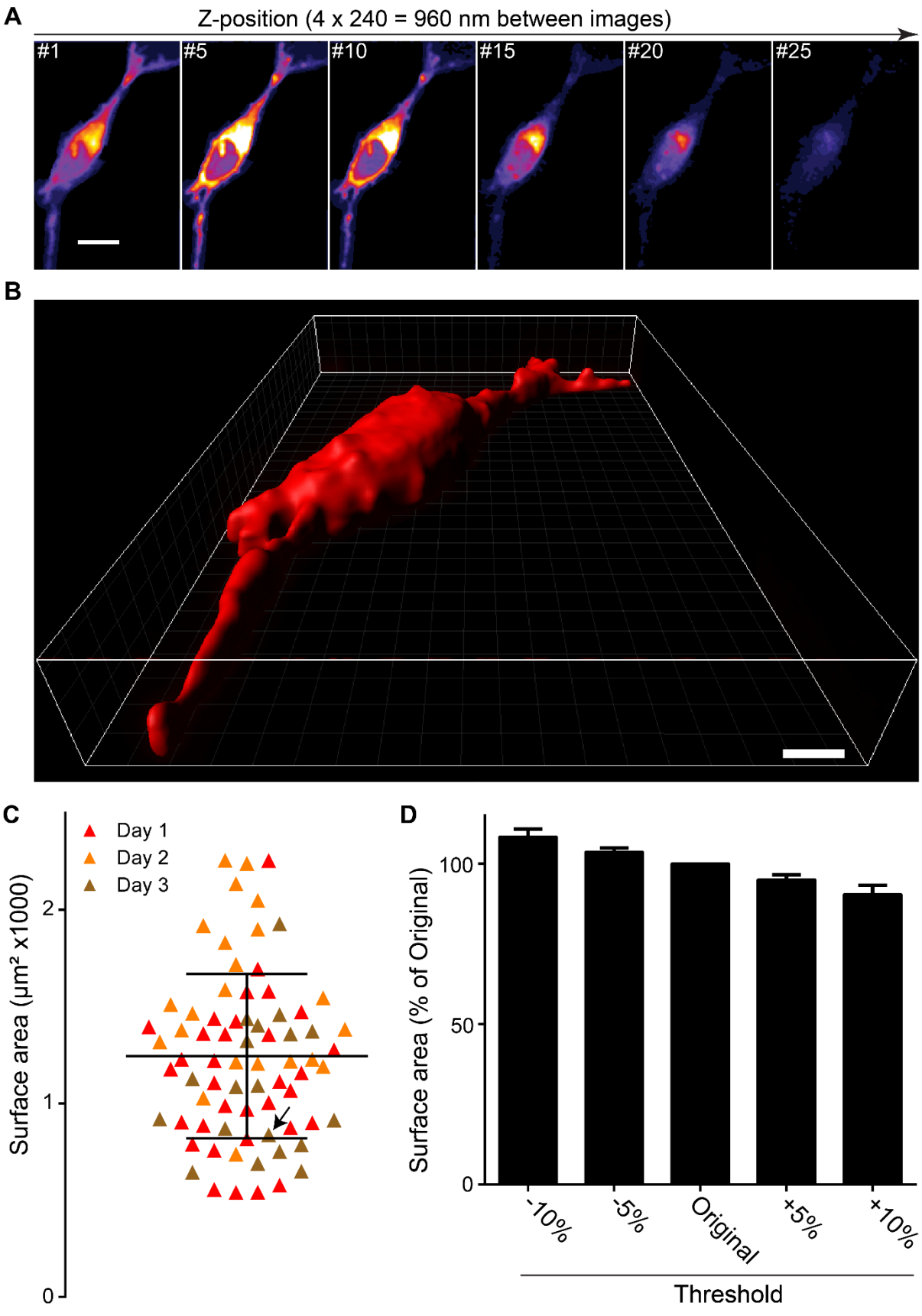
A
Z-position (4 x 240 = 960 nm between images)
#1
#5
#10
#15
#20
#25
B
C
Day 1
Day 2
Day 3
Surface area (µm² x1000)
2
1
0
D
Surface area (% of Original)
100
50
0
-10%
-5%
Original
+5%
+10%
Threshold

Figure 13. SH-SY5Y membrane surface area

(A) Every 5th image, which are 960 nm apart, from a representative stack generated by optical sectioning using the Zeiss AXIO Observer Z1 inverted fluorescence microscope. The "fire" lookup table (LUT) is used to allow simultaneous visualization of strong and weak signals with ample contrast. Scale bar is 10 µm. **(B)** The modelled 3D surface area reconstructed from the entire image stack showcased in (A). Scale bar is 5 µm. **(C)** The surface areas of 74 cells, prepared and imaged on 3 independent experimental days and reconstructed as illustrated in (B), were extracted and averaged. The black arrow marks the cell displayed in (A&B). Error bars represent standard deviation. **(D)** All cell surfaces were reconstructed again using different thresholds (-10%, -5%, +5% and +10% of the original). Results are shown as a percentage of the original average. Error bars represent standard deviation.

optical sections using interpolation algorithms (Figure 13B). Fixation with paraformaldehyde prior to imaging permeabilizes the cells, which allows the dye to also stain cell organelles with membranes, like clearly be seen by the bright intracellular staining of the cell depicted in Figure 13A. This is not a problem, however, as the experimental parameters, i.e. small pinhole size, small pixel size and low power excitation, prohibit excessive carry-over of signal in neighboring pixels or image plains. Additionally, by manually setting the threshold to the lowest possible level that still gives an intact cell surface mask, modelling of the outermost "real" signal coming from the imaged cell, which should be the plasma membrane, is ensured as can be seen in Figure 13B. The software not only creates cell surface masks but can also quantify these in real-world units when the pixel size and axial step size are provided. By doing this for all imaged cells, the average surface area of SH-SY5Y cells can be calculated and was found to be 1,244 ± 425 µm² with the 95%-CI between 1,146 and 1,343 µm² (Figure 13C). However, as the threshold had to be set manually for each cell because of minor differences in staining intensities between cells and homogeneity of the signal within the plasma membranes, one could argue that this methodology might bias the found value. To address this issue, all cells were re-evaluated using 5% and 10% lower and 5% and 10% higher thresholds (Figure 13D). Using higher thresholds, the surface areas decreased mainly because less brightly stained neurites were now often not detected by the algorithm. This effect was partly offset by the introduction of holes in the cell surface masks, which increased surface area. Increasing the threshold thus resulted in a relatively minor difference in the average surface area (about 9.5% for a 10% increase of the threshold value), but the surface masks did not reflect the imaged cells to the same extent anymore. On the other hand, decreasing the thresholds did not alter the shape of the surface masks except for just making them larger and, in some cases, detecting structures that were not part of the investigated cells. The resultant increase in average surface area (about 8.4% for a 10% decrease of the threshold value) was again relatively small yet seemed to be an artificial enlargement caused by the inclusion of diffuse signals around the plasma membrane and recognition of non-cell structures as specific signals. In conclusion, manually setting the threshold to the smallest value producing a still intact cell surface mask proved to be the most accurate method for the quantification of the surface areas.

The number of molecules found to inhabit the plasma membrane of an SH-SY5Y cells (refer to Figure 11) can now be distributed over the average surface area of these cells giving a molecular density of [11,206 / 1,244 =] 9 {9.008} molecules per µm². Considering the lower and upper probability limits of the number of molecules per plasma membrane and the 95%-CI of the membrane surface areas, a lowest estimate of 6 {5.541} and a highest of 14 {13.715} molecules per µm² is obtained. Please note that it is meaningless to talk about fractions of a molecule. However, because a conceptual value based on semi-quantitative experiments is calculated here, values with the correct number of significant figures have been added between accolades and were used for further quantification.

4.1.4. Validation of the methodology for visualization of plasmalemmal APP

Combining the number of molecules per square micrometer of the SH-SY5Y plasma membrane with the percentage monomers and the number of clusters per square micrometer would allow calculation of the number of APP molecules per cluster. As we have already determined the copy number and density of APP in the plasma membrane, it would be beneficial to be able to isolate plasma membranes and specifically analyze only these. Thus, plasma membrane sheet preparations were employed to probe both the fraction of clustered APP molecules as well as the number of clusters per square micrometer using microscopy. However, as this method had not yet been established for SH-SY5Y cells, optimal sonication power, length and tip height had to be determined. After trying multiple combinations of the aforementioned parameters, satisfying settings for the unroofing procedure were found (data not shown). Using these settings, about 80% of the cells in the middle of the cover slips were unroofed, while almost all these plasma membrane sheets presented with smooth, intact surfaces without any obvious holes, vesicles, debris or remnants of other cellular membranes. The left panel of Figure 14A shows a typical SH-SY5Y plasma membrane sheet in the lower half of the panel, while the upper part displays and intact cell. To verify whether the unroofing procedure could be used to quantify and characterize exclusively plasmalemmal APP in this cell line, co-stainings with a few standard markers for cell organelles that typically could contaminate the plasma membrane sheets were performed. To detect APP in these experiments, the same C-terminal antibody that had already been used in the previous experiments was employed. Not only does it detect all APP isoforms equally, its epitope should also be readily detectable on plasma membrane sheets as the C-terminus lies on the exposed cytosolic side. Figure 14A shows an exemplary co-staining of Rab11, a marker for exocytotic, recycling endosomes (Takahashi et al. 2012), in the green channel and APP in the far-red channel. It can clearly be seen in the merged image that, although there is a clear Rab11 signal, there is essentially no overlap between Rab11 and APP, suggesting that the detected APP does not reside in recycling endosomes. Similarly, Caveolin, a marker of caveolae membranes which participate in receptor-independent endocytosis (Copeland et al. 2017), Rab5, a marker of early endosomes (Huotari and

Helenius 2011) and Calnexin, a marker for ER (Wada et al. 1991), were also investigated. Furthermore, Clathrin, a marker for Clathrin-coated vesicles and -related structures, such as pits (Pearse 1976), was included as a positive control, as APP has been shown to be endocytosed from the plasma membrane via this mechanism and, therefore, a certain amount of colocalization is to be expected (Schreiber et al. 2012). The association of APP with the markers was quantified by pixel intensity spatial correlation analysis based on the Pearson Correlation Coefficient (PCC), where +1 means perfect overlap or correlation, 0 no correlation and -1 perfect anti-correlation (Li et al. 2004). Apparently, APP does not associate markedly with any of the markers (Figure 14B), suggesting that most of the APP in the plasma

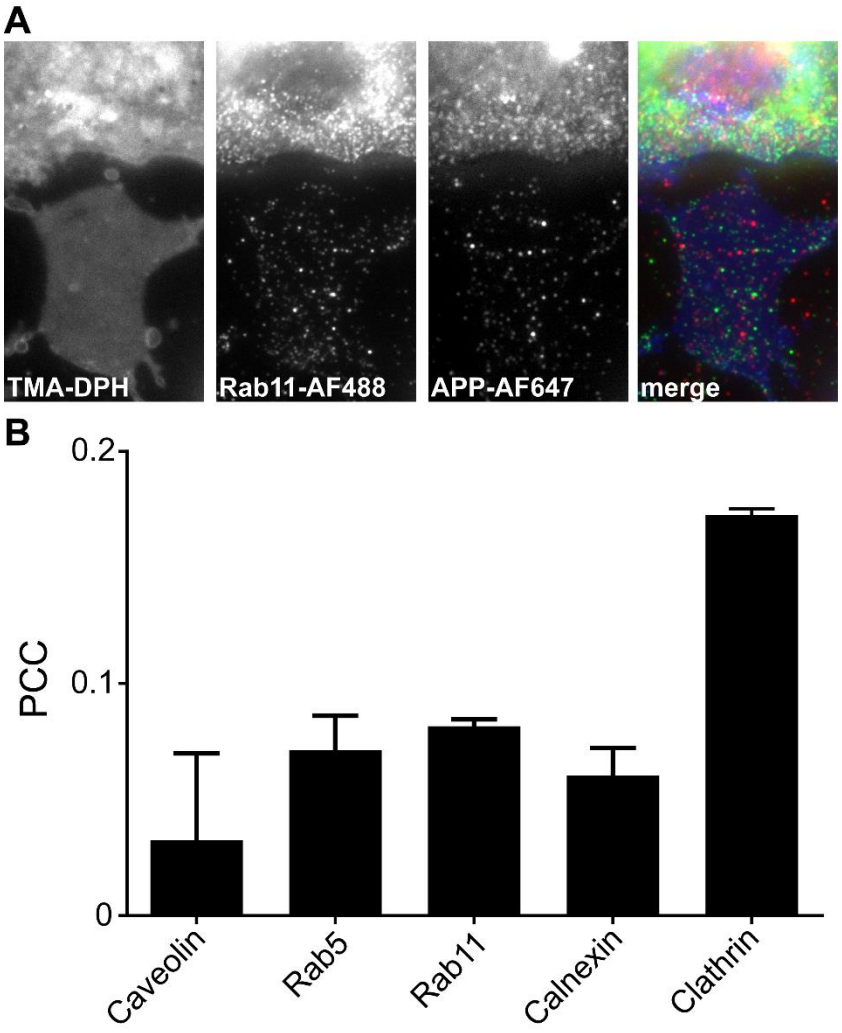

Figure 14. Purity of plasma membrane sheets

(A) Representative multi-channel image of the membrane dye TMA-DPH in the blue channel, the recycling endosome marker Rab11 in the green channel and APP in the red channel acquired using the Olympus IX-81 inverted microscope. The last panel shows the merged image of all three color channels. Of note, on the lower two-thirds of the images the plasma membrane sheet that was analyzed can be observed, whereas in the upper third an intact cell can be discerned. The images each depict and area of 20 x 37.5 µm. **(B)** For each marker, 2 independent experimental days with 20-30 images each were evaluated and the PCCs averaged. Error bars represent standard deviation. No statistical test was performed because only 2 independent experimental days were analyzed.

membrane does not reside in caveolae membranes, early or recycling endosomes, ER or even Clathrin-coated pits or vesicles. Interestingly, the correlation of APP with Clathrin does seem to be substantially higher than with the other markers (PCC ~ 0.17; while all others have a PCC < 0.10), indicating that there is at least some association of APP with Clathrin.

One striking aspect of the experiments presented in Figure 14 was the relatively low signal levels of endogenous APP in the plasma membrane sheets. While the biochemical quantification of plasmalemmal APP did demonstrate that only about 9 APP molecules should be present per square micrometer (refer to Figure 13), one could still doubt that the situation depicted in the images does not reflect the biological situation well. One reason could be that the conformation of the epitope between denaturing conditions (as is the case in western blot experiments) and more-or-less native conditions (as is the case in immunocytochemistry experiments) does significantly change or impact its interaction with the antibody. Furthermore, the proximity of the epitope to the plasma membrane, membrane-associated structures or other proteins could sterically hinder binding of the antibody. To determine the validity of labeling APP with the C-terminal antibody on plasma membrane sheets, SH-SY5Y cells were electroporated with a plasmid encoding APP_{695} C-terminally fused to an emerald Green Fluorescent Protein (emGFP) via a small 18 amino acid linker region. SH-SY5Y cells overexpressing this construct were unroofed and labeled with the C-terminal antibody and a secondary AF647-coupled antibody (Figure 15A). Evaluation of both channels (green: GFP and far-red: AF647) clearly shows the similarity of the two signal patterns. Moreover, a line scan through the merged image demonstrates the prominent overlap of both signals (Figure 15B), indicating that the antibody can detect most of the APP molecules. The amount of conformity between the green and far-red channels was also quantified using the PCC and equaled 0.72, a remarkable correlation considering the technical limitations of these experiments. In earlier studies, a correlation between a protein tagged with both myc and GFP a lesser value of 0.63 was found (Sieber et al. 2006). Thus, the impressive similarity between the signals confirms that not only the oligomers are detected by the C-terminal antibody but also most of the single APP molecules, confirming the suitability of the APP C-terminal antibody for immunocytochemistry. Interestingly, there seem to be two distinct regions designated ‘higher’ and ‘lower’ within the imaged plasma membrane sheet that indicate regions that display a lot of APP signal and markedly less, respectively (Figure 15B). Whether these are a fusion of plasma membranes of what were originally two individual cells, or they are differentially regulated areas of the same cell cannot be determined using the available information. The lack of AF647-only signal in almost all overexpressing cells suggests that the GFP moiety does not or only very weakly interfere with antibody binding and that there is much more overexpressed APP-GFP present than endogenous APP. It could be shown that on average 27-fold more AF647 signal per µm² was detected in the overexpressing

compared to endogenous cells (Figure 15C, left panel). Conversely, there are some spots that only appear in the GFP channel, several of which seem to be outside of the plasma membrane sheet. It could be that these are APP-GFP molecules that did not reside in the plasma membrane but in closed organelles with the GFP moiety and the C-terminal epitope facing inwards at the time of unroofing. Alternatively, they could be GFP molecules that have somehow been liberated from their APP fusion protein. Both cannot be detected by the antibody as either the epitope is inaccessible or absent. During sonication, these vesicles and/or solitary GFP molecules could then have been scattered over the coverslip outside of the plasma membrane sheets. This also means that some of the GFP-only spots that appear within the boundaries of the plasma membrane sheet may originate from these same sources. However, given that not much signal from marker proteins for endocytic compartments was detected on the plasma membrane sheets (refer to Figure 14) and that emGFP has been reported to only have weak dimerization properties (Shaner et al. 2005), makes it unlikely that these biases contribute significantly to the observed signals. Interestingly, independent from the level of overexpression, the GFP and AF647 signals always showed a spotty pattern with a high variability in brightness of the individual spots. At higher expression levels, these spots appear on top of a more-or-less uniform signal (compare Figure 14A with Figure 15A&B). A possible way to quantify this effect is to calculate the relative standard deviation (RSD), which can be determined by dividing the standard deviation of the pixel intensities of a ROI by the average pixel intensity of that same ROI. Thus, the RSD is a measure of the variability of the signal within a given area normalized to the total signal brightness. In other words, a high RSD means a spotty signal and, therefore, a more clustered state, whereas a low RSD indicates a quite homogeneous signal and therefore a quite well-distributed state of the labeled molecules in question. The striking difference in average RSD between endogenous and overexpressed APP (Figure 15C, right panel) demonstrates what can also be observed by examining the images by eye. Of note, the average RSD calculated for the AF647 channel (0.34 ± 0.04) is remarkably similar to the average RSD of the GFP channel (0.43 ± 0.02; data not shown). The minor discrepancy can most likely be attributed to the few more GFP-only spots discussed before or the fact that the antibody might not be able to reach all the epitopes especially at the center of the spots due to steric hindrance or both. By extent, this again suggests that the antibody detects virtually all APP molecules that make up the homogeneous signal between the brighter spots, which are assumed to be monomeric and lower order oligomeric APP molecules. By plotting the RSD of each ROI against its average intensity, the dependence of the RSD on the total intensity can be visualized. When combining the endogenous and the overexpressed samples this way, it can clearly be seen that when the total amount of plasmalemmal APP rises its RSD decreases (Figure 15D), indicating that overexpression alters APP clustering dynamics. Therefore, to study the characteristics of an APP cluster using samples where APP is expressed only in endogenous quantities is preferred.

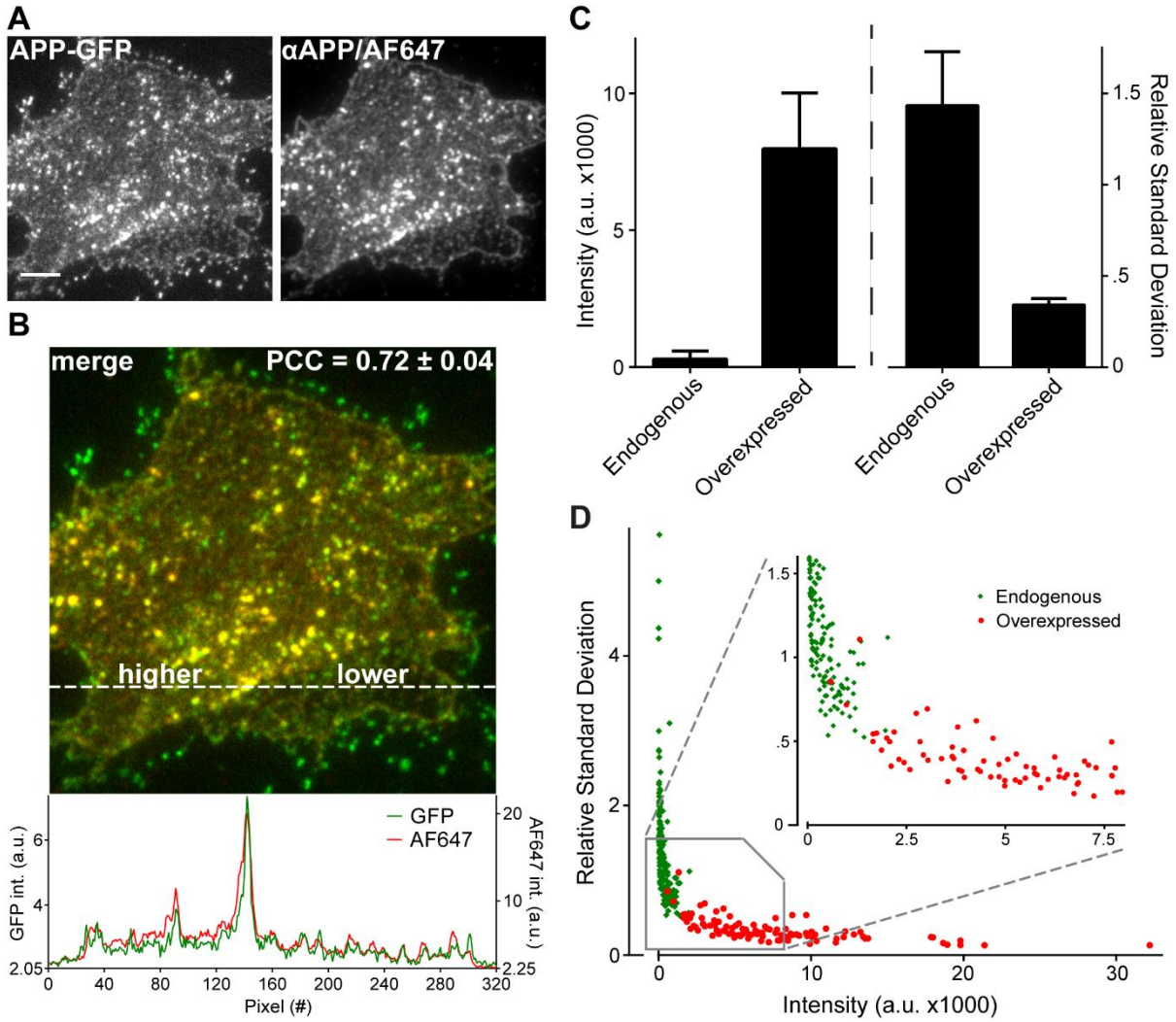

Figure 15. Validity of APP overexpression and the C-terminal antibody

(A) Representative dual-channel image of the fusion protein APP_{695}-emGFP in the green channel and APP labelled with the C-terminal antibody and detected with an AF647-coupled secondary antibody in the red channel acquired using the Olympus IX-81 inverted microscope. The scale bar is 4 µm. **(B)** The merged image of both color channels. The intensity profiles of both channels along a line scan (dashed white line) are presented below the image. The similarity between the signals was analyzed by calculating the PCCs from 107 images equally distributed over 3 independent experimental days (upper-right corner). **(C)** From the images analyzed in (B) and 206 images equally distributed over 8 distinct coverslips generated on 2 independent experimental days of endogenous APP detected by the same antibody used for overexpressed APP (A), the background-corrected intensities and RSDs were calculated and averaged. Error bars represent standard deviation. **(D)** For every image, the relative standard deviation of the antibody channel was plotted against the intensity. The zoom-in exemplifies that there is barely any overlap between the two populations.

It could already be established that the APP C-terminal antibody can detect most of the APP molecules present and that fixated plasma membrane sheets constitute a biologically relevant model system for our research question. However, there is also a drawback to this approach. Certain proteins embedded or attached to the membrane sheets cannot be fixated well anymore by standard aldehyde fixation, because of a lack of cytosol. In pilot photoactivated localization microscopy (PALM)

experiments, a not quantified but significant fraction of APP molecules displayed movement in plasma membrane sheets even after fixation with 4% PFA (data not shown). Thus, the aforementioned 1% PLP fixative was tried in this respect as well. Additional cross-linking of the added aldehyde groups created by the oxidation of polysaccharide chains of glycoproteins, which are predominantly found in the plasma membrane, should make it a prime candidate for thorough fixation of plasma membrane sheets. Additionally, preliminary experiments had shown that performing the unroofing procedure at 4°C produced larger and superior (less perforations and smoother surface) sheets (data not shown). Thus, plasma membrane sheets were unroofed and fixated with 1% PFA at either RT or 4°C, with 4% PFA at 4°C and with 1% PLP at 4°C, subjected to primary-secondary antibody staining and imaged using super-resolution time-gated stimulated emission depletion (gSTED) microscopy. The APP signals were evaluated using an automated ImageJ macro that can detect and count individual maxima, delineate the maxima, and subsequently measure various features, like average intensity and size, of these maxima (Figure 16A-F). Because all thresholds are equal and all calculations the same between the different samples, this is an unbiased approach to assess both the number of APP maxima as well as their defining characteristics. Fixation with 1% PLP at 4°C resulted in the most detected maxima per µm² (Figure 16G) and the highest average intensity of the maxima (Figure 16H). Combining these results with the knowledge that the same amount of APP molecules had to be available in the other samples, suggests that with 1% PLP at 4°C fixation the least amount of aggregation artifacts occur while the antigenicity is preserved best. Additionally, the standard deviation of the intensity of the maxima is also the largest, meaning that using this fixation method a larger dynamic range of possible maxima brightnesses can be detected, which presumably reflects the real biological situation better. A light trend towards a marginally bigger full width at half maximum (FWHM) can also be observed (Figure 16I). The FWHM is measured by the ImageJ macro by overlaying an intensity line scan in both the horizontal and vertical directions over the middle of an identified maximum. This intensity profile should ideally follow a gaussian distribution with the maximum intensity corresponding to the middle of the analyzed spot. Both line scans are than fitted to match a gaussian distribution and the one that matches best, so either the horizontal or the vertical, is used for further analysis. If none of the line scans had an R^2 above 0.9 or if the intensity peak deviated to far from the middle of the line scan, the maximum was not analyzed for FWHM, but was included in the other calculations. The FWHM is the golden standard to probe the dimensions of an object in fluorescence microscopy if not many other parameters are known and is, hence, the best method for approximating the size of the detected maxima. The slightly larger FWHM and standard deviation (Figure 16I) suggest that less artificial aggregation takes place when fixating with 1% PLP and, ergo, that the APP clusters preserved their original proportions better. Interestingly, the number of maxima per µm² is higher using 4% PFA at 4°C than with 1% PFA at 4°C (Figure 16G), maybe because with 1% PFA more APP molecules are not well

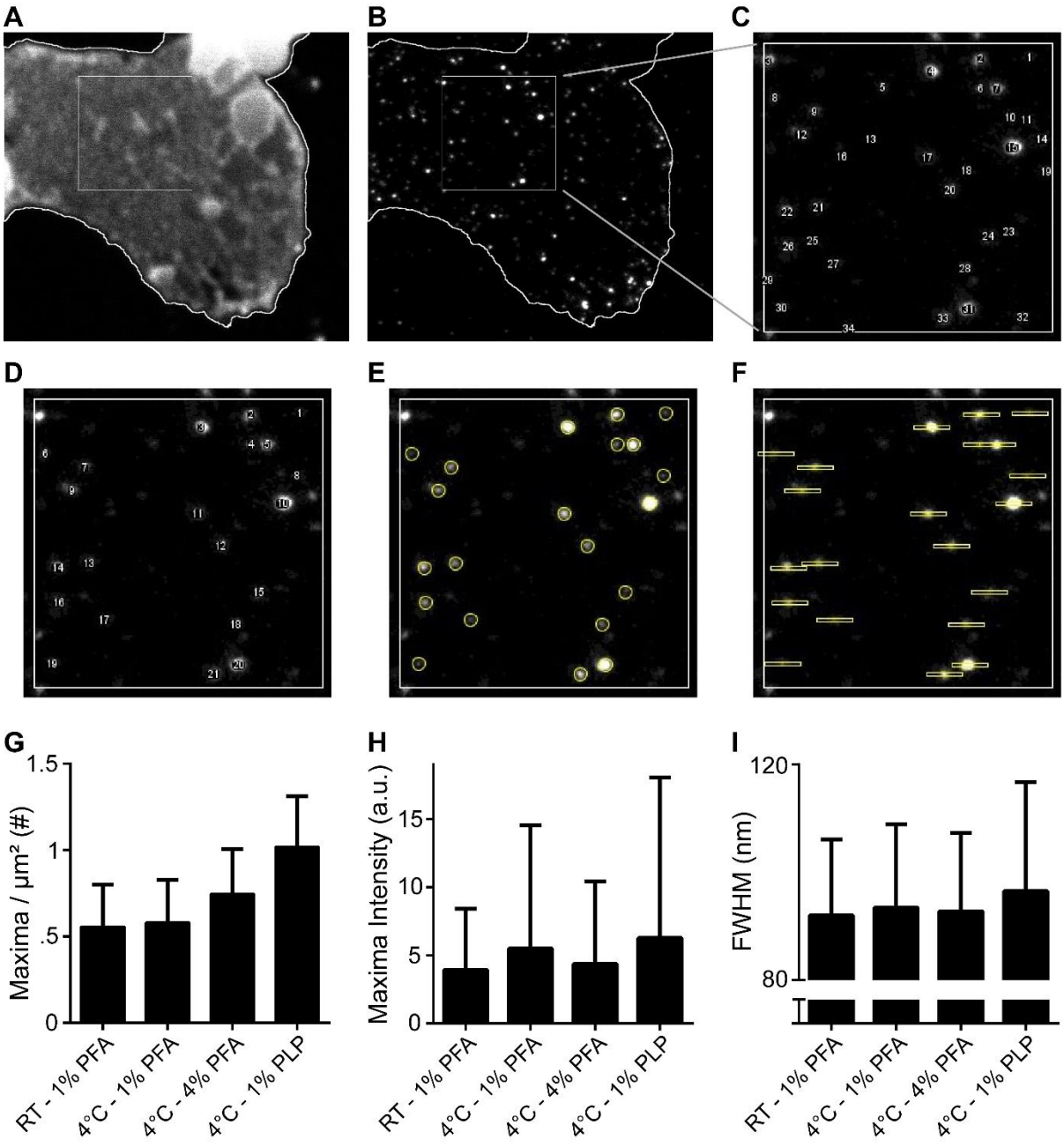

Figure 16. Reliable analysis and immobilization of plasmalemmal APP

(A) Representative image acquired with the Abberior easy3D STED microscope of a plasma membrane sheet fixated with 1% PLP and visualized using the green membrane dye Fast-DiO. The white square marks the ROI that is subsequently analyzed by the ImageJ macro. The profile of the cell is automatically delineated with a white line by employing a simple thresholding algorithm. The imaged area comprises 11.4 x 10.2 µm. **(B)** The same cell presented in (A) imaged in the red channel, revealing APP detected via primary-secondary AF647-coupled antibody labelling. The profile of the cell determined in (A) is depicted here again for reference. **(C)** A zoom-in of the ROI from (B), which constitutes an area of 250 x 250 pixels or 3.75 x 3.75 µm. The ImageJ macro automatically detects maxima and counts them. **(D)** By setting a threshold level for intensity, dim maxima are discarded. **(E)** Remaining maxima are delineated using a circle with a pre-set radius. The total intensity within this circle is measured and defined as the intensity of the maximum. **(F)** One horizontal and one vertical line scan is drawn around the weighted center of the maxima (horizontal line scan shown). The line scans are fitted using a Gaussian profile and the one that provided the best fit is used for calculation of the FWHM. **(G)** Average number of maxima per µm² as determined by the ImageJ macro of antibody labelled APP following 4 distinct fixation protocols. In

total 3 independent experimental days with 22-25 membrane sheets per condition per day were analyzed, amounting to between 480 and 871 analyzed maxima for each condition. **(H)** Average maximum intensity of the maxima detected in (G). **(I)** Average FWHM of the maxima detected in (G). Error bars represent standard deviation.

fixated causing post-fixation aggregation artifacts upon antibody labelling. On the other hand, the average intensity of the maxima is higher and the range of its standard deviation larger with 1% PFA (Figure 16H), implying that with this fixation method the antigenicity is better preserved. To conclude, all results strongly suggest that fixation with 1% PLP at 4°C can fixate proteins in plasma membrane sheets efficiently while maintaining their antigenicity and, therefore, is best suited to analyze plasmalemmal APP clusters.

4.1.5. Size and molecular density of the plasmalemmal APP clusters

After determination of the number of APP molecules per µm² of an SH-SY5Y plasma membrane and having established the optimal parameters for visualization of APP molecules in plasma membrane sheets of SH-SY5Y cells, the molecular density of an APP cluster could finally be probed. However, our methodology heavily relies on microscopy and the resultant images do not only contain oligomeric APP molecules, but presumably also monomers which should be excluded before the molecular density of an APP cluster can examined. To elucidate the percentage of monomeric APP, an alternative approach based on relative stochastic labelling was established. To illustrate our methodology, 3 situations for detecting an epitope in a biological sample using a monoclonal primary and a polyclonal secondary antibody should be considered:

1. In the first situation, a sample is incubated with an abundance of primary antibody over available epitopes, which is how immunocytochemistry is performed in 99% of published cases and is therefore henceforth called the “standard” condition. Here, almost all accessible epitopes will be labelled with a primary antibody and each primary antibody will be detected by multiple secondary antibodies. Additionally, dependent on the specificity of both primary and secondary antibodies, there will be some non-specific deposition of primary-secondary antibody complexes or single secondary antibodies that will result in signals as well.
2. In the second situation only a fraction of the amount of primary antibody compared to the first situation is used, preferably in a range that only a small percentage (somewhere between 1 and 5%) of genuine epitopes will be labelled. This “stochastic” condition is, of course, quite difficult to predict as it is dependent on many parameters and should be determined experimentally using a dilution series. If the correct concentration is found, however, solitary primary antibodies will be enriched in the sample. Even though multiple epitopes might be near each other, as is the case in homo-oligomers for example, the chance that only one primary antibody labelled this aggregate of epitopes is increased. Furthermore, non-specific

deposition of primary antibody also favors single antibodies especially at lower antibody concentrations. Subsequent incubation with the same concentration of secondary antibody used in the first situation followed by visualization and intensity analysis, will result in an increase of the occurrence of a certain range of intensities that correspond to a single primary antibody labelled with the typical number of secondary antibodies specific to the experimental conditions. The consensus seems to be that this typical number is somewhere between 2 and 6 polyclonal secondary antibodies per primary antibody, however the exact number will always be subject to the particular experimental circumstances.

3. The third situation constitutes the case where the primary antibody is omitted completely, thus creating a condition that only allows the non-specific deposition of secondary antibody. When visualized and analyzed, detected signals can only be background noise or secondary antibodies, which is why it will be termed “background”. The signal coming from secondary antibodies will be relatively dim but still span a considerable range as fluorescent secondary antibodies generally have between 2 and 10 fluorescent chemical dyes covalently bound to them. The third situation can be used to normalize the other 2 situations by subtracting the signals that arise from non-specifically deposited secondary antibody and other background noise.

To obtain the largest possible dynamic range of intensities, not only was 1% PLP used for fixating the plasma membrane sheets (refer to Figure 16), every single analyzed image was an average of 10 micrographs taken in quick succession with an epifluorescence microscope using a magnification of 83,3 nm per pixel. By averaging multiple images, fluctuations in signal intensities coming from either the inherent quantum nature of photon-electron interactions or the temporary variations within biological samples or the technical apparatus are minimized. Furthermore, the signal-to-noise ratio is increased, as noise is usually random while signal tends to be more consistent. The pixel size is about 4x lower than the spatial resolution limit in the far-red channel and thereby on the lower end of the suggested range for high resolution imaging (usually a 2.5 to 3 times oversampling is recommended). Furthermore, the far-red dye AF647 was explicitly chosen for the secondary antibody, as in these wavelengths autofluorescence of the samples is usually negligible. In our case, the first condition, wherein explicitly more primary antibody is offered than epitopes are present, constituted the standard antibody labelling protocol with a 1 in 200 dilution of the primary antibody directed against the APP C-terminal followed by a 1 in 200 dilution of a secondary antibody directed against mouse IgG and harboring AF647 fluorescent dyes. For the second situation, stochastic labelling was found to be ideal around a 1 in 8000 dilution of the primary antibody, i.e. 40-fold less than in the first situation. A 1 in 4000 dilution still contained many bright spots where definitely more than 1 primary antibody

labelled multiple epitopes in close proximity to each other; whereas a 1 in 16,000 dilution looked remarkably similar to the situation without primary antibody (data not shown).

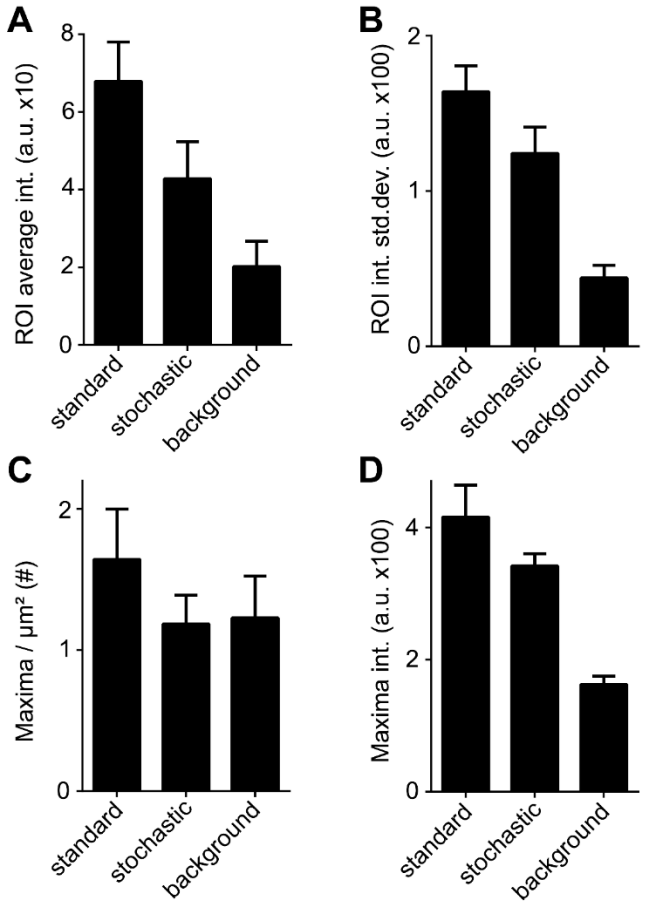

Figure 17. Detection of APP under variable labelling conditions

(A) Average intensity of the ROIs from images taken of plasma membrane sheets after fixation with 1% PLP and either standard (1:200 primary antibody), stochastic (1:8000 primary antibody) or background (no primary antibody) labelling of APP acquired with the Olympus IX-81 inverted microscope used with settings for high signal-to-noise imaging. Between 92 and 170 membrane sheets equally distributed over 3 independent experimental days were analyzed per labelling condition. **(B)** Analysis of the integrated standard deviation of the same ROIs shown in (A). **(C)** The number of maxima per µm² as detected by the ImageJ macro in the same ROIs. Between 564 and 1413 maxima were detected per condition. **(D)** The average intensities of the maxima presented in (C). Error bars represent standard deviation.

To examine the validity of the method, ROIs were placed within plasma membrane sheets in an unbiased way and analyzed mean gray value or, in other words, average intensity. The average intensity and, by extent, also the total intensity, was highest for the standard labelling, lowest for the background labelling and somewhere in between for the stochastic labelling (Figure 17A). This indicates that less antibody was bound in the stochastic compared to the standard condition, but still considerably more than in the background condition, demonstrating that the detected signal mainly depends on the primary antibody concentration. These results were expected because of the inherent

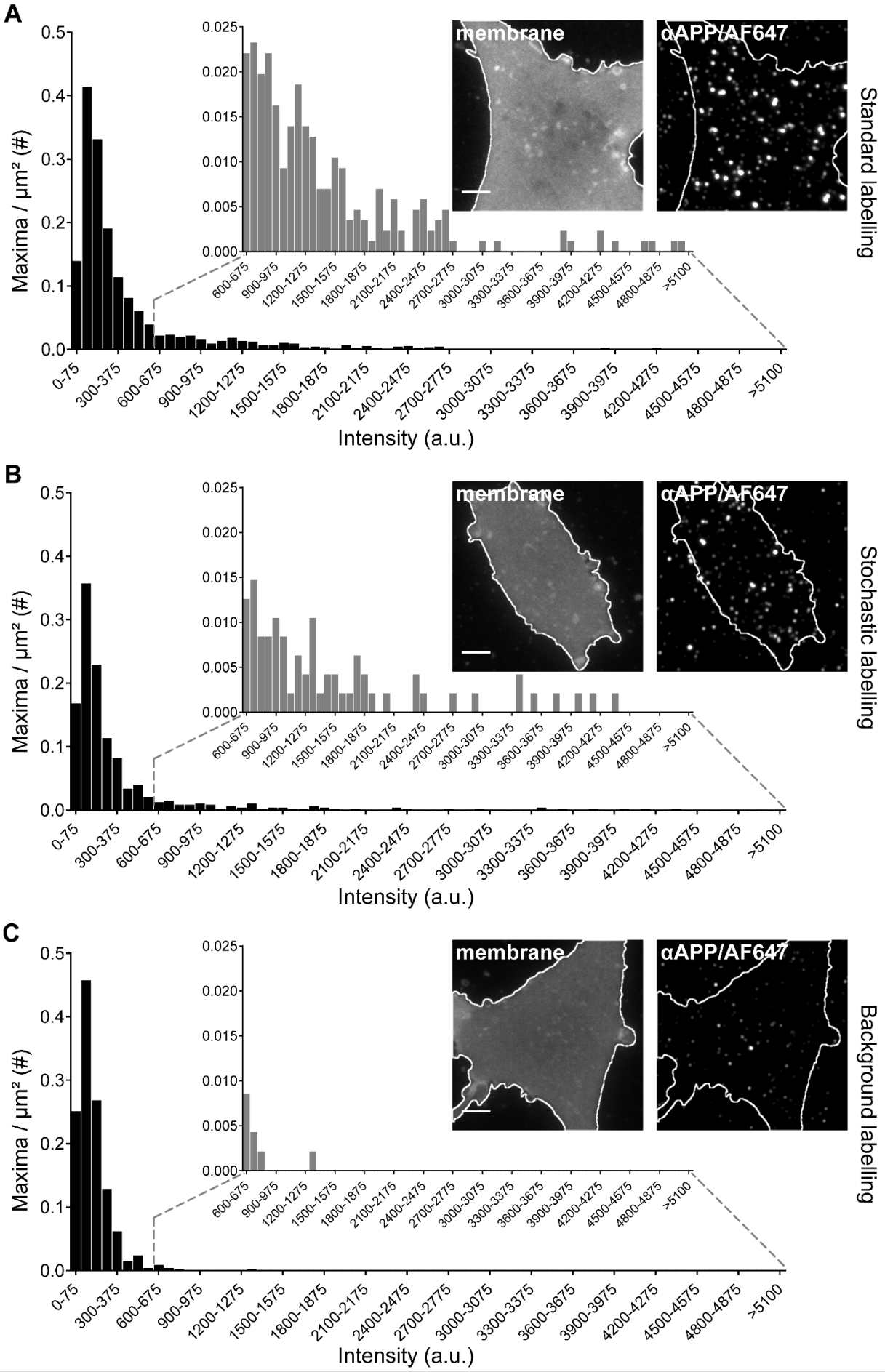
A
B
C
membrane
αAPP/AF647
Standard labelling
Stochastic labelling
Background labelling
Maxima / µm² (#)
Intensity (a.u.)
0-75
300-375
600-675
900-975
1200-1275
1500-1575
1800-1875
2100-2175
2400-2475
2700-2775
3000-3075
3300-3375
3600-3675
3900-3975
4200-4275
4500-4575
4800-4875
>5100

Figure 18. Labelling condition-dependent brightness of APP maxima

(A) The number of maxima per µm² of the standard labelling condition (1:200 primary antibody), as already presented in Figure 17C&D, binned using their intensity values. For each intensity bin the number of maxima per µm² that fell within that bin are summed. A zoom-in of the higher intensity ranges allows better appreciation of the lower counts. The inset displays a representative cell, wherein the membrane is labelled with TMA-DPH, the cell profile is detected using a thresholding algorithm and the scale bar is 2 µm. **(B)** The same for the stochastic labelling condition (1:8000 primary antibody). **(C)** The same for the background labelling condition (no primary antibody).

signal amplification resulting from primary-secondary antibody labelling, which multiplies signal intensities to levels easily exceeding those of noise, most artifacts or non-specifically deposited secondary antibodies. A second parameter of interest was the gray value standard deviation or the standard deviation of the pixel intensities, which is a measure for the variation in pixel brightness within an image (Figure 17B). A similar pattern as was observed for the ROI intensities could also be observed here, albeit that the pixel brightness variability of the stochastic condition was notably closer to the standard condition than to the background condition. This suggests that, although significantly less primary antibody was offered in the stochastic condition, there were still plenty substantially brighter pixels than in the background condition. Nevertheless, the ROI intensity standard deviation of the stochastic condition did not reach the level of the standard condition, revealing that especially the brightest signals were lacking in the stochastic condition. The only other explanation could be that the pixels without any apparent signal (the "background" pixels) were considerably darker in the stochastic condition compared to the background condition, which was not the case (compare the insets of Figure 18A-C). It is important to note that, up until now, only pixel intensities have been assessed, which is not analogues to the maxima intensities. The ImageJ macro introduced earlier (refer to Figure 16) can analyze intensity maxima in an unbiased way, allowing direct comparison of different labelling conditions. To investigate APP maxima, the ImageJ macro was employed to analyze the same ROIs analyzed for Figure 17A&B. Interestingly, about the same number of maxima (1.1852 maxima per µm²) were counted in the stochastic condition compared to the background condition (1.2281 maxima per µm²), both of which were markedly less than the 1.6418 maxima per µm² found in the standard condition (Figure 17C). This could only mean that less primary antibody was offered than there were epitopes available in the stochastic condition, resulting in some lower-order oligomeric APP aggregates and/or monomeric APP not being labelled and thus, not detected. If examined for their intensities, however, it was obvious that many of the identified maxima from the stochastic condition were much brighter than those from the background condition and almost but not quite up to the intensity levels of the standard labelling condition (Figure 17D). It is no coincidence that this graph and the ROI intensity standard deviation graph (refer to Figure 17B) look so similar and the reasoning behind these results is also the same. Many distinctly brighter maxima are detected in the stochastic condition

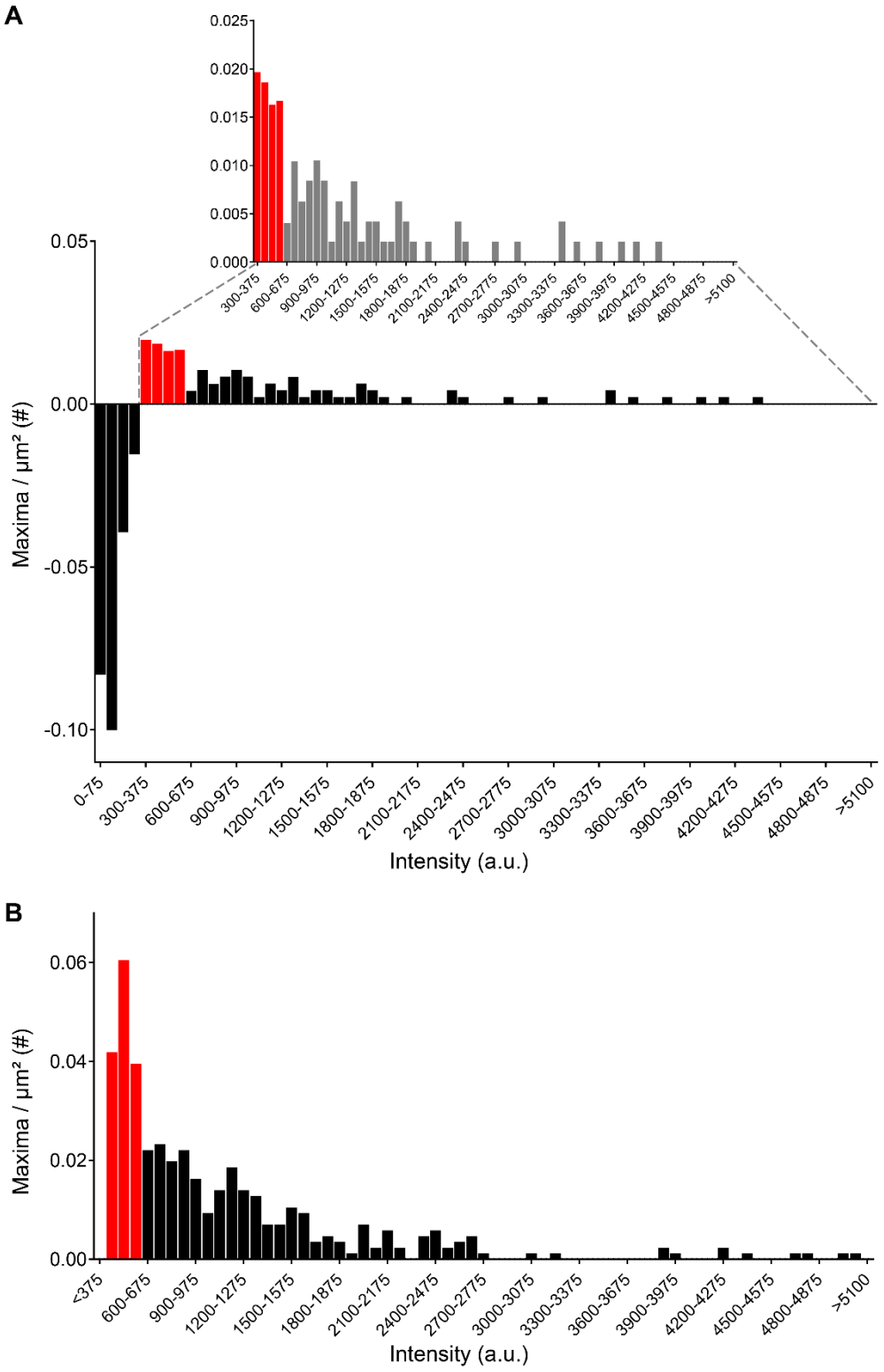

Figure 19. Monomeric fraction of plasmalemmal APP

(A) The maxima per µm² from the background labelling condition were subtracted from the maxima per µm² from the stochastic labelling condition on a per bin basis (refer to Figure 18B&C). A zoom-in of the higher intensity ranges allows better appreciation of the lower counts. The red bars highlight the intensity range that is enriched in the stochastic labelling condition. **(B)** The 356 maxima from the standard labelling condition remaining after background correction were distributed over the same intensity bins used before. The intensity range that was found enriched in (A) is also highlighted in red here and defined as the intensity range in which monomeric APP should be present.

compared to the background condition, but the brightest maxima seen in the standard condition seem to be lacking. The logical explanation hereof must be that especially of the higher-order oligomers not all epitopes get labelled by primary antibodies. By extent, this means that there must be more APP entities in the stochastic labelling condition where only a single primary antibody bound. Taken together, it seems that stochastic labelling is a promising method to probe the intensity range of single primary antibodies.

As said before, our methodology requires elucidation of the intensity range of a single primary antibody labelled with the typical number of secondary antibodies for our samples to be able to find the percentage of monomeric APP. As it is near impossible to find this range by examining individual maxima intensities, the maxima identified in Figure 17C&D were distributed over intensity bins. Subsequently, histograms can be constructed which allow the quantification of the number of maxima that occupy a certain intensity range. The maxima intensity distribution of the standard condition showed many dim spots in the range between 0 to 600 arbitrary units (a.u.; intensity counts), but also many maxima between 600 to 2700 a.u., with some maxima going up to ~5000 a.u. (Figure 18A). Using the stochastic labelling, about similar quantities of dim spots, but significantly less bright maxima could be detected compared to the first condition (Figure 18B). However, plenty of brighter maxima with intensities over 600 a.u. could still be observed. These results confirmed the speculated loss of mainly the brighter maxima between the standard and stochastic conditions (refer to Figure 17B&D). Finally, the background condition, where only secondary antibody was employed, showed essentially only dim spots of up to a maximum of 700 a.u. (Figure 18C).

To find the range of maxima intensities that is enriched in the stochastic labelling condition, the maxima intensity distribution of the condition without primary antibody was subtracted from the intensity distribution of the stochastic condition on a per bin basis (Figure 19A). The reason for this is that by subtraction of only the maxima that belong to the same intensity range, the bins with significantly more maxima in the stochastic condition compared to the background condition become apparent. The maxima intensity bins between 300 and 600 a.u. are clearly enriched and have been colored red to visually highlight this. Given the rationale behind the stochastic condition, these 4 intensity bins represent the range of intensities that a single primary antibody bound by the number of secondary antibodies typical for our experimental conditions could encompass. For the first 4 intensity bins the subtraction resulted in negative numbers, for which possible reasons will be discussed later. Determination of the percentage of monomeric APP was subsequently accomplished by first subtracting the number of maxima per μm^2 that represent background noise and non-specific deposits, i.e. the background condition, from the standard condition. This time, however, this was not done on a per bin basis, because only the detected maxima that represent at least 1 primary antibody

were of interest. Thus, not the enrichment of a certain intensity range was probed, but the background-corrected pool of maxima was to be identified and analyzed. As can also be seen in Figure 17C, [1.2281 / 1.6418 * 100% =] 74.802% of the number of identified maxima in the standard condition were also detected in the background condition. By omitting the dimmest 74.802% of spots from the standard condition, the population of maxima that constitute at least one primary antibody and, by extent, at least one APP molecule, was determined and calculated to be 0.4137 maxima per µm². These were subsequently organized into a maxima intensity distribution wherein the same intensity range representing single primary antibodies established in Figure 19A was again highlighted in red (Figure 19B). The percentage of monomeric maxima was determined by calculating what fraction the maxima from the highlighted bins comprise within the total population of maxima and was found to be 34.27%.

Accurate information about the size of an APP cluster, in other words the area that its molecules occupy within the plasma membrane, is still missing, prohibiting calculation of the molecular density within an APP cluster. To this end, gSTED microscopy seems to be the technique of choice, as it is especially well-suited to resolving bright structures on a dark background with a resolution many times better than epifluorescence microscopy. Coverslips with SH-SY5Y plasma membrane sheets were again fixated with 1% PLP and labelled with the same primary antibody against the C-terminus of APP followed by a polyclonal antibody carrying AF594. AF594 was chosen because it has a higher quantum yield and longer fluorescent lifetime than AF647 (Thermo Fisher Scientific) and thus performs better in experiments where time-gating is combined with stimulated emission depletion. gSTED micrographs were recorded using 10 line accumulations for the same reason discussed earlier. Additionally, the depletion laser was used at 70% of its possible maximum and continuously on, whereas the fluorescent detection was time-gated, meaning that detection only started 1.25 ns after the excitation laser had turned off. Using this set-up, a highly stringent inquiry of the sizes of fluorescent objects was assured and a resolution of down to ~20 nm could be achieved with optimized DNA origamis (data not shown). It is unlikely though that this resolution will also be realized in the biological samples as they are not perfectly optimized for super-resolution detection like the origamis. Nevertheless, it should be close to it, which is also illustrated by the difference in size of the maxima from gSTED imaging compared to the confocal picture (Figure 20A). Of note, the upper left maximum in the confocal image (middle panel; white arrow) looks like a single object, while in the gSTED image it can clearly be seen that it is 2 maxima in close proximity to each other (right panel; white arrow). This perfectly highlights the main advantage of gSTED microscopy. Using the same ImageJ macro for an unbiased approach for the detection and analysis of the maxima, 0.9452 maxima per µm² were detected in the standard labelling condition, whereas 0.4528 maxima per µm² were identified in the background condition (Figure 20B). The average intensity of the maxima from the standard condition was almost 4-fold that of the

background condition (Figure 20C), indicating that significantly more bright maxima must have been present in the standard condition. The density of background-corrected APP maxima could now be estimated and was found to be [0.9452 - 0.4528 =] 0.4924 maxima per µm², only a relatively minor difference (~20%) with the 0.4137 APP maxima per µm² resulting from the epifluorescence data (refer to Figure 17C), exemplifying the robustness of both methods. By putting the number of APP molecules per µm², the percentage of monomeric maxima and the number of maxima per µm² in relation to each other, the average number of APP molecules per cluster can now finally be calculated:

Equation 1.

$$\#APP\ per\ cluster = \frac{APP\ per\ \mu m^2 - (maxima\ per\ \mu m^2 * percentage\ monomers)}{maxima\ per\ \mu m^2 - (maxima\ per\ \mu m^2 * percentage\ monomers)}$$

The copy number of APP within SH-SY5Y plasma membrane sheets was established in Figure 13, namely 9.008 APP molecules per µm². The percentage monomeric maxima had been resolved in Figure 19 and was demonstrated to be 34.27%, while the maxima density was demonstrated to be 0.4924 maxima per µm² in Figure 20B. As a monomeric maximum is per definition also a monomeric APP molecule, the number of oligomeric APP molecules per µm² is determined by subtracting the monomeric maxima from the number of APP molecules per µm², which can be found in the numerator of the formula. Similarly, the number of maxima that represent an oligomeric APP entity can be calculated by subtracting the monomeric maxima from the total maxima per µm², which can be found in the denominator. Subsequently, the division of the oligomeric APP molecules per µm² by the oligomeric maxima per µm² results in the average number of APP molecules per cluster. Completing the formula thus gives [(9.008 - (0.4924 * 0.3427)) / (0.4924 - (0.4924 * 0.3427)) =] 27.31 or ~27 APP molecules per cluster. Additionally, the number of monomeric APP molecules can now be used to calculate what percentage of APP molecules is monomeric. The number of monomeric maxima turned out to be [0.4924 * 0.3427 =] 0.1687 molecules per µm² and the total SH-SY5Y cell surface is 1244 µm² (refer to Figure 13), which means that there are on average [0.1687 * 1244 =] 210 APP molecules per cell surface that are not oligomerized. Because the total number of APP molecules per SH-SY5Y cell membrane was 11,206 (refer to Figure 11), the percentage of monomeric APP must be [210 / 11,206 * 100% =] 1.87% and, conversely, 98.13% of APP must be present in an oligomerized state.

Given the wide range of observed maxima intensities in virtually all microscopy experiments, it seems that there is a high variability in number of APP molecules per clusters. Consequently, the aforementioned average does not reflect this variance properly nor does it appropriately acknowledge the thorough quantifications up until now. Thus, the wide range of observed maxima intensities should

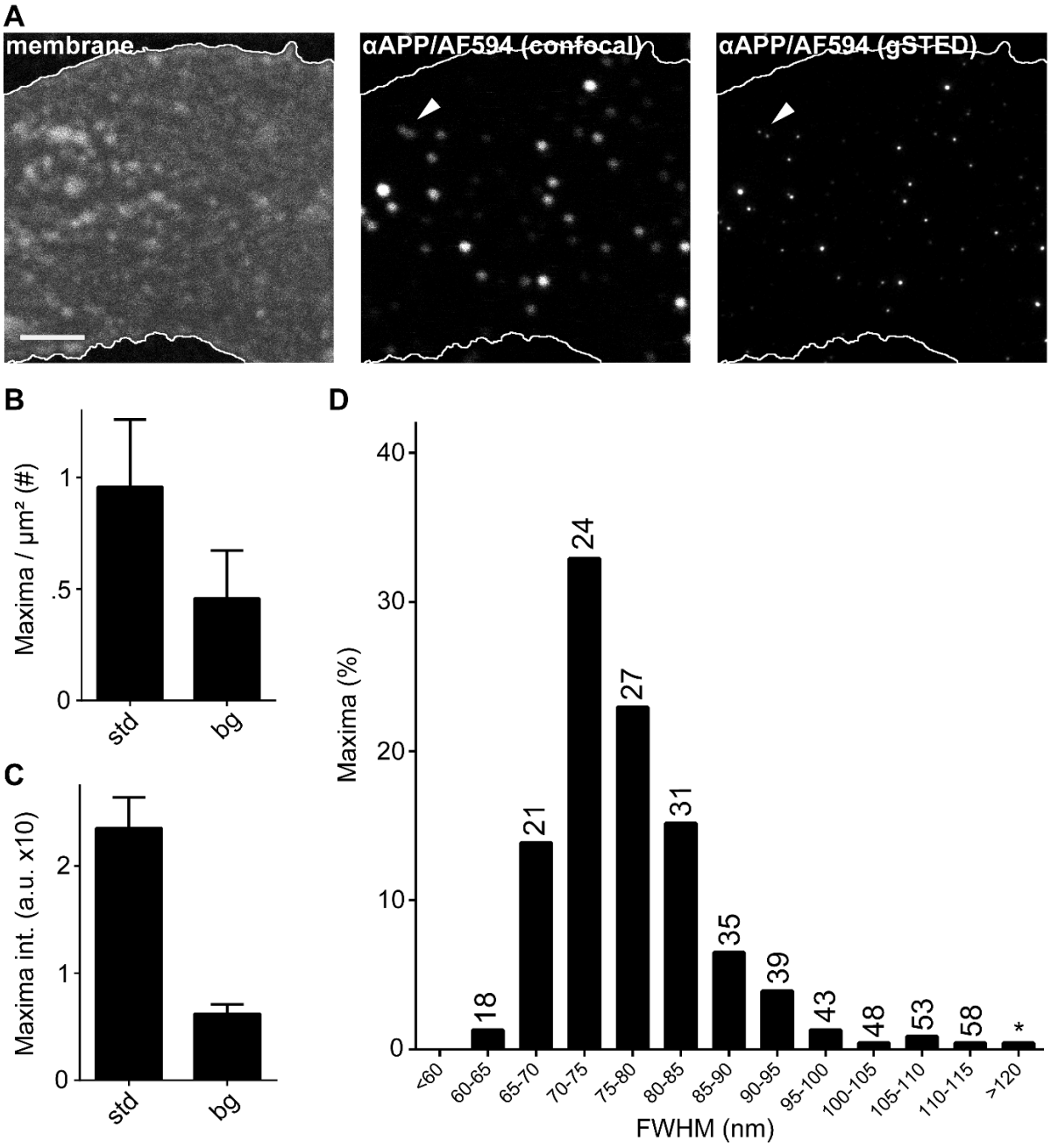

Figure 20. Density and size of APP clusters in the plasma membrane

(A) Representative images of a plasma membrane sheet acquired using the Abberior easy3D STED microscope. The left panel shows the plasma membrane sheet visualized using Fast-DiO and the cell profile is detected using a thresholding algorithm. The scale bar is 2 µm. The middle panel displays APP detected by conventional primary-secondary AF594-coupled antibody labelling using the microscope in confocal mode. The right panel shows the same membrane sheet as the middle panel imaged using the microscope in gSTED mode. The white arrows point to a structure that can only be resolved in the gSTED image. **(B)** The number of maxima per µm² identified using the ImageJ macro after gSTED imaging. Standard (1:200 primary antibody) and background (no primary antibody) labelling conditions were also employed here and 60 or 18 membrane sheets equally distributed over 3 independent experimental days were analyzed, respectively. In total 675 maxima (standard) and 97 (background) were analyzed. **(C)** Maxima intensity for the same labelling conditions described in (B). Error bars represent standard deviation. **(D)** The maxima from the standard labelling condition were background- and monomer-corrected. The remaining 231 maxima were distributed in bins based on their FWHM. The number of APP molecules that a cluster of a certain size contains is displayed above the corresponding bars.

somehow be translated in a distribution of the APP molecules over the diverse clusters, which can be accomplished by taking the size of the APP clusters into account. The subset of oligomeric maxima was quickly identified using the methodology that was also already employed in Figure 19. By taking the 0.4924 background-corrected maxima per µm² and subsequently omitting the 34.27% dimmest maxima to correct for the monomers, the [0.4924 - (0.4924 * 0.3427) =] 0.3237 maxima per µm² that represent oligomeric APP objects remain. The FWHM of these maxima were categorized in size bins of 5 nm and plotted as a percentage histogram to show the relative distribution of the various sizes that an oligomeric APP object can assume (Figure 20D). It can be observed that no cluster was smaller than 60 nm (which is still at least double the resolution limit), that most of the clusters have a diameter of between 65 and 85 nm and that there is quite a range of bigger clusters. Now, if the assumptions are made that all analyzed maxima are perfectly circular and APP molecules within a cluster are spread evenly over the area that each cluster occupies, the number of APP molecules associated with each cluster size can be calculated. By distributing the [0.3237 * 1244 =] 403 APP oligomers per SH-SY5Y cell over the frequency bins, the absolute number of clusters per cell for each size bin can be found. Per size bin, the area that each cluster covers can easily by calculated using the diameter, i.e. the FWHM, and the formula for the area of a circle ($A = ¼ \pi d^2$). For example, each cluster of the size bin from 70-75 nm occupies [$¼ * \pi * 72.5^2$ =] 4128.26 nm² on average and, given that [32.9% * 403 =] 132.6 clusters fall within this bin, a total area occupancy of [132.6 * 4128.26 =] 547,360.6 nm² is to be expected for this size bin in each SH-SY5Y cell. Next, the sum of the products of the cluster number and the average cluster area per bin, in other words, performing the aforementioned example for each bin and adding all together, equals a total area of 1,891,133 nm² or 1.89 µm² per cell. Interestingly, this means that about 0.15% of the total SH-SY5Y cell surface area is associated with APP clusters. Finally, the [11,206 - 210 =] 10,996 oligomeric APP molecules per SH-SY5Y plasma membrane, can be distributed evenly over the total APP cluster area per cell and then be translated back to the typical number of APP molecules constituting the average cluster of each size bin by dividing through the total area that each size bin occupies (Figure 20D; the numbers above each bar). Furthermore, the average molecular density of an APP cluster can be determined by dividing the oligomeric APP molecules by the total cluster area and is [10,996 / 1.89 =] 5814 molecules per µm² or, conversely, 1 molecule per 172 nm², which constitutes a circle with a radius of only 7.4 nm. Of note, the bin representing clusters with a FWHM above 120 nm (marked with an asterisk) comprised a single maximum with a FWHM of ~162 nm. As it was much larger with quite a gap until the next largest clusters, it could be argued that this was an artifact rather than a real APP maximum and the cluster was therefore omitted from any calculations. Should it have been an actual APP cluster, however, it would have contained 118 APP molecules. Inclusion into the calculations would not have affected any of the presented outcomes significantly.

4.2. Significance of the A673T mutant for plasmalemmal APP

After having extensively characterized and validated the average APP cluster in human neuronal cells and demonstrating that many molecules must aggregate together to form such a cluster, the second part of this work focusses on the dynamics of the plasmalemmal APP cluster. To this end, not only is there more emphasis on functional assays, but an important APP mutant, the A673T or Icelandic mutation, which is the only mutation described to protect against AD to date (see Chapter 1.4.5.), was employed to exemplify how these clustering dynamics are regulated and might possibly be exploited to combat AD.

4.2.1. Effect of the A673T mutation on APP clustering

First, wild-type APP_{695} and APP_{695}-A673T (henceforth called WT and A673T respectively) both fused C-terminally to emGFP were overexpressed in HepG2 cells to be able to compare their intrinsic clustering characteristics outside of the neuronal background. It should be highlighted here that, although all used constructs were based on the wild-type neuronal APP_{695} isoform, the nomenclature of APP_{770} was still used for the mutants to streamline referencing to literature. The emGFP-tag was initially chosen to facilitate live cell imaging, cleavage assays and FRAP imaging, but was also used here to allow selective imaging of the overexpressed APP only, as significant levels of endogenous APP_{751} and APP_{770} are present in HepG2 cells (refer to the mock-transfected conditions of Figure 26B). It should be noted that it is to be expected that the endogenous isoforms intermingle with the overexpressed APP. Additionally, because emGFP alone is quite dim and sensitive to bleaching using the laser intensities typical for gSTED microscopy, emGFP was labelled with an anti-GFP primary antibody followed by a secondary antibody linked to the AF488 dye to amplify and stabilize the APP signal for super-resolution microscopy. To investigate the differences between the WT and A673T clusters, gSTED imaging of plasma membrane sheets followed by ROI analysis and maxima analysis using the ImageJ macro described earlier were utilized. The average intensities of the ROIs were remarkably similar, suggesting that the plasma membrane sheets contain similar amounts of overexpressed WT and A673T (Figure 21A). Analysis of the maxima of both variants showed that, although not significant, a few more WT maxima per µm² were detected than A673T maxima (Figure 21B). To determine whether the observed small difference between ROI intensities is solely dependent on the number of detected maxima and not any other factors, the number of maxima per µm² of a ROI was divided by the average intensity of that ROI and plotted against this ROI intensity (Figure 21C). This methodology is akin to the analysis from Figure 15D and allows correlation of the maxima per µm² to the ROI intensity. Seeing the extreme conformity between both trendlines, one can only conclude that the dependence of the ROI intensity on the number of maxima per µm² dominates the small observed difference between WT and A673T and, thus, that the maxima themselves must be

comparable intensity-wise. Given that there was essentially no difference between the average brightness of the maxima and its standard deviation (Figure 21D), it seems likely that, despite the fact there is slightly less A673T in the plasma membranes, the clusters are fairly identical. The average FWHM of the clusters formed by WT and A673T is also considerably similar, albeit that both the

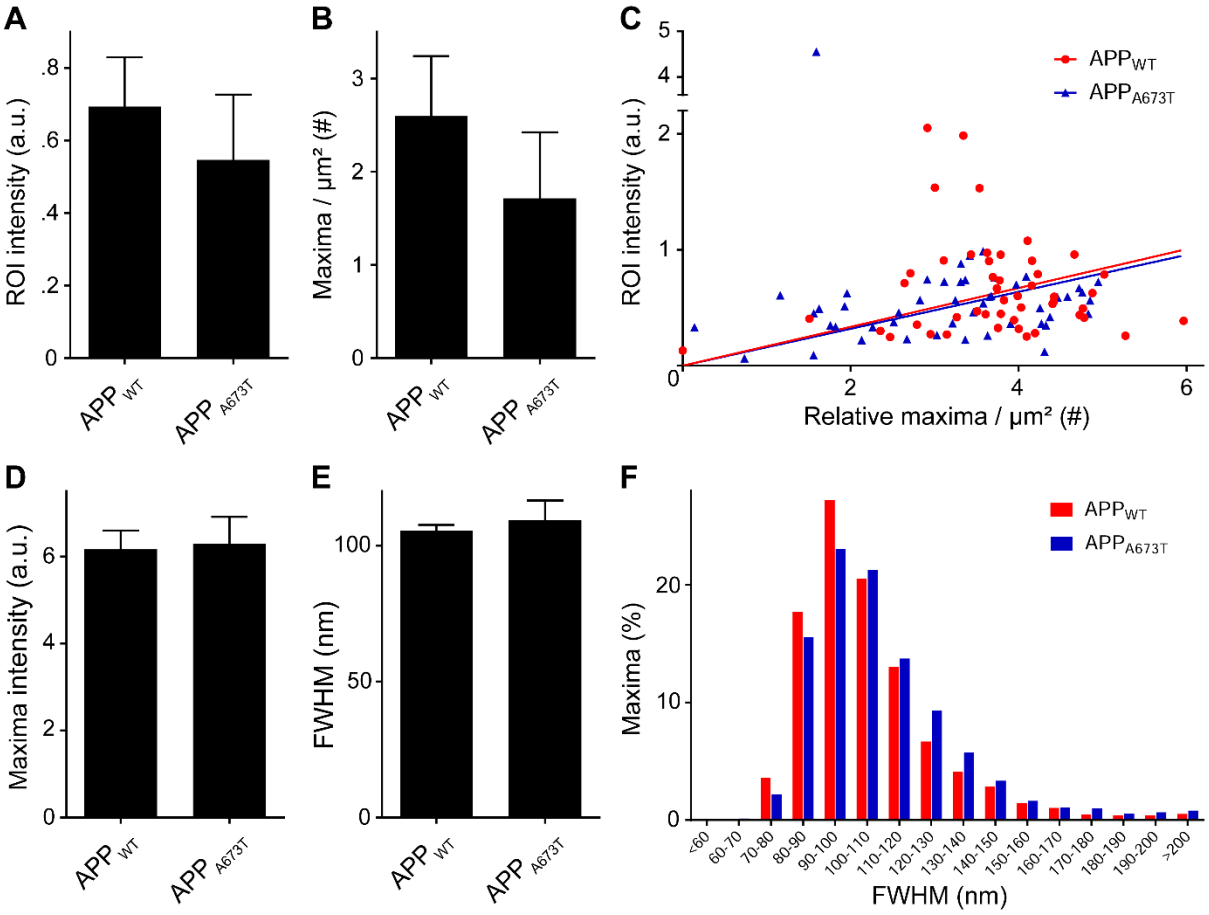

Figure 21. Influence of the A673T mutation on APP cluster size

(A) Plasma membrane sheets from HepG2 cells overexpressing either full-length WT or A673T APP C-terminally fused to emGFP were fixated with 1% PLP, labelled with an anti-GFP primary-secondary AF488-coupled antibody labelling for signal amplification and imaged with the Leica TCS SP8 gated-STED microscope. For each condition, 48-49 images distributed over 3 independent experimental days were acquired and the average ROI intensities analyzed. The difference between the conditions was not significant (p=0.32; unpaired two-tailed t test; n=3). **(B)** By use of the ImageJ macro the number of maxima per µm² was also evaluated for both conditions. In total, 2517 and 1887 maxima were identified for WT and A673T, respectively. The difference between the conditions was not significant (p=0.18; unpaired two-tailed t test; n=3). **(C)** For every image, the relative maxima per µm² is calculated by dividing the number of maxima by the intensity of the ROI, which is then plotted against the ROI intensity. Linear regression analysis showed that there was no significant difference between the slopes of the linear fits (p=0.7993; fit WT: y=0.1675*x, Sy.x=0.4557, n=48; fit AT: y=0.1593*x, Sy.x=0.6613, n=49). **(D)** Average intensity of the maxima identified in (B) as calculated by the ImageJ macro. The difference between the conditions was not significant (p=0.78; unpaired two-tailed t test; n=3). **(E)** Average FWHM of the maxima identified in (B) as calculated by the ImageJ macro. The difference between the conditions was not significant (p=0.42; unpaired two-tailed t test; n=3). **(F)** Maxima identified in (B) were distributed in bins based on their FWHM. Error bars represent standard deviation. Data were collected in collaboration with Hannes F. Maib.

maxima size and its standard deviation appear slightly larger for the A673T mutant (Figure 21D). Yet, the minor increase in FWHM and its standard deviation when APP harbors the A673T mutation do imply that the proportions of these clusters differ from WT clusters. To better resolve this variation, the same relative maxima intensity distribution used in Figure 20D was employed here as well to compare the clusters from both variants (Figure 21F). The tendency of the WT construct to form somewhat smaller clusters than the mutant can now clearly be observed. Of note, no background corrections for non-specific signals were performed in these experiments, as the relative nature of the inquiry does not necessarily require background normalization. In other words, the background signal that is detected should be the same in both conditions and, therefore, cancel out.

The indication that A673T clusters might be less dense than WT clusters suggests that A673T might exist in a more diffuse state overall in the plasma membrane. Because gSTED microscopy is not the ideal method to study this, high signal-to-noise epifluorescence microscopy (refer to Figure 17&18) was again employed to delve a little deeper into the typical appearance of both variants. WT and A673T fused to emGFP were again overexpressed not only in HepG2 cells, but also in SH-SY5Y cells to investigate potential differences in a neuronal background as well. Furthermore, no additional labelling was done, as the fused emGFP is perfectly suited for direct imaging using epifluorescence microscopy. By calculating the RSD and plotting the RSD against the average intensity for each ROI, the intensity-normalized distribution of signal from WT and A647T APP can be presented and compared. It is immediately obvious that WT has a higher RSD, i.e. appears more punctate, than A673T in HepG2 cells for the whole intensity range (Figure 22A). The trendlines have almost identical slopes with a highly significant difference in off-set regarding the RSD, which means that, when the same amount of APP is available, WT molecules always present more clustered or less diffuse than the A673T molecules. Strikingly, the same experiment in SH-SY5Y cells resulted in the exact same outcome (Figure 22B), demonstrating that the A673T mutant is less clustered than the WT also in the neuronal background and that neither the cell type nor the lineage matter for this oligomerization mechanism. Averages can also be determined using the available data and, by averaging the ROI intensity, the level of overexpression can be gauged for both variants and was found to be notably similar in both HepG2 cells (Figure 22C, left panel) and SH-SY5Y cells (Figure 22D, left panel). Thus, similar quantities of molecules must have been available in the plasma membranes of HepG2 and SH-SY5Y for both the WT and A673T variants, revealing that differences in plasmalemmal molecular density cannot explain these observations. Though maybe a bit redundant, the average of the RSD can also be calculated and, even if not normalized to intensity, still demonstrated a significant dissimilarity between WT and A673T in HepG2 cells (Figure 22C, right panel) as well as SH-SY5Y cells (Figure 22D, right panel).

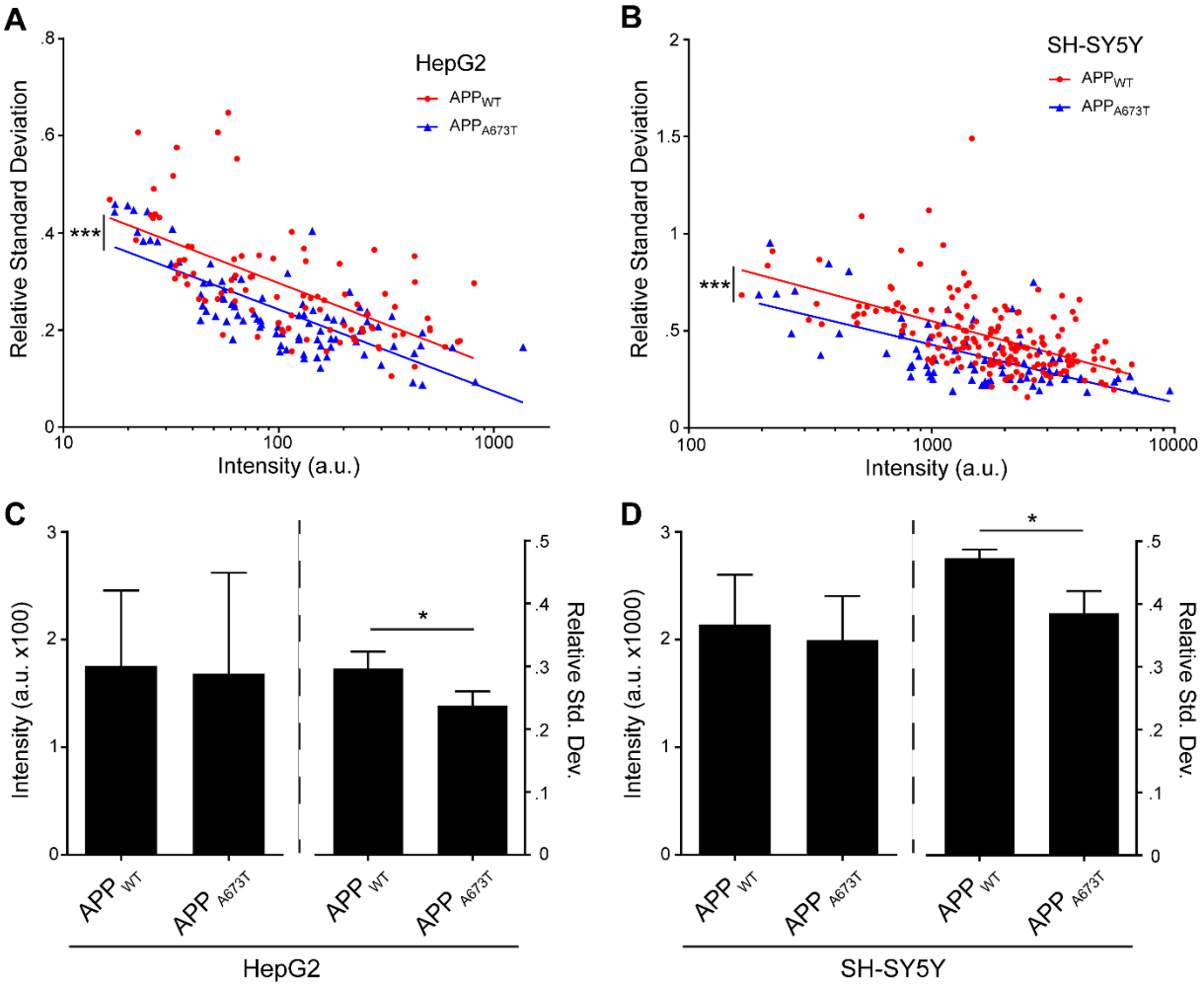

Figure 22. Plasmalemmal distribution of APP_{WT} and APP_{A673T}

(A) Plasma membrane sheets prepared from HepG2 cells overexpressing either full-length WT or A673T APP C-terminally fused to emGFP were fixated and imaged with the Olympus IX-81 inverted microscope used with settings for high signal-to-noise detection. The RSD is plotted against the average intensity for each ROIs. For WT and A673T conditions 92 and 88 membrane sheets equally distributed over 3 independent experimental days respectively were evaluated. Semilog non-linear regression analysis showed that there was no significant difference between the slopes of the fits (p=0.4373), while the difference between the Y-intercepts of the curves was highly significant (p<0.0001; semilog fit WT: y=-0.1708*x+0.6384, R^2=0.402, n=92; semilog fit AT: y=-0.1687*x+0.5798, R^2=0.599, n=88). **(B)** Plasma membrane sheets prepared from SH-SY5Y cells with the exact same conditions and imaging parameters shown in (A). The RSD is plotted against the average intensity for each ROIs. For WT and A673T conditions 174 and 77 membrane sheets equally distributed over 3 experimental days respectively were evaluated. Semilog non-linear regression analysis showed that there was no significant difference between the slopes of the fits (p=0.287), while the difference between the Y-intercepts of the curves was highly significant (p<0.0001; semilog fit WT: y=-0.3352*x+1.556, R^2=0.2959, n=174; semilog fit AT: y=-0.2978*x+1.323, R^2=0.4184, n=77). **(C)** Average intensities and RSDs of the ROIs specified in (A). The RSD shows a significant difference between the two conditions (p=0.0458; unpaired two-tailed t test; n=3). **(D)** Average intensities and RSDs of the ROIs specified in (B). The RSD shows a significant difference between the two conditions (p=0.0159; unpaired two-tailed t test; n=3). Error bars represent standard deviation.

The previous observations were all fixated “snap-shots” of conditions that in a biological setting are dynamic. They are, therefore, prone to artifacts generated mainly due to the fixation procedure and generally lack information about how a situation evolves over time. One of the methods best

suited for investigating mobility and clustering dynamics in a specific, restricted area of a living cell is fluorescence recovery after photobleaching (FRAP) microscopy. This technique usually utilizes a confocal microscope to observe a fluorophore-tagged protein over time in (part of) a living cell. First, a few baseline images are made, where after a specific area is bleached and subsequently monitored for recovery of fluorescence. Recovery can only occur through diffusion and exchange of intact fluorescent molecules from the surrounding environment for photobleached ones from the bleached area. The recovery kinetics are dependent on many factors, like membrane fluidity and composition, transient and longer-lived protein binding mechanisms and membrane skeleton and anchors. As such, this technique is perfectly suited to probe for differences in clustering dynamics between WT APP and the A673T mutant in living cells. Both emGFP-fused constructs were again overexpressed in HepG2 and SH-SY5Y cells and used in FRAP microscopy experiments. The typical experimental procedure is depicted in Figure 23A. A ROI is carefully placed wholly within a cell and outside the nucleus and the average three pre-bleach recordings, called frames, taken as the baseline fluorescent intensity measurement (Figure 23A, first panel). Next, the ROI is bleached (Figure 23A, second panel) and a frame taken every second (Figure 23A, third and fourth panel). The average intensity of the bleached ROI is measured every frame and presented in a graph as a percentage between the pre-bleach average and the post-bleach frame taken at the start of the recording for both HepG2 cells (Figure 23B) and SH-SY5Y cells (Figure 23C). Recovery of the A673T mutant was significantly faster in both cell lines with comparable half-times between the cell lines for each construct (Figure 23D&E, right panel). Besides the recovery half-time, another important parameter that can be extracted from the data is the maximum recovery. The fraction of intensity that cannot be replenished by diffusion is a measure for the immobile fraction or, in other words, the percentage of molecules that cannot diffuse. The immobile fraction of WT and A673T did not diverge significantly in HepG2 cells (Figure 23D, left panel) despite the apparent large discrepancy between the line graph in Figure 23C. The explanation hereof is that for the line graphs all cells from an experimental day are averaged per timepoint and subsequently the average of the three experimental days is calculated, whereas the bar graph shows the average of the maximum recovery which is calculated using fitted data for each experimental day independently. The maximum recovery of both variants in SH-SY5Y cells was remarkably similar (Figure 23E, left panel), leaving no room for doubt that equally large immobile fractions exist for WT and A673T here. Interestingly, although the maximum recovery did not differ much when comparing the APP variants with each other, the maximum recovery was noticeably, albeit not significantly, higher in HepG2 cells than in SH-SY5Y cells for both constructs (p = 0.23 for WT, p = 0.10 for A673T; unpaired two-tailed t test). This suggests that there is an evidently higher immobile fraction of APP molecules in SH-SY5Y cells than in HepG2 cells regardless of the used construct. A possible explanation could be that SH-SY5Y cells express more adaptor or chaperone proteins that somehow stimulate APP clustering.

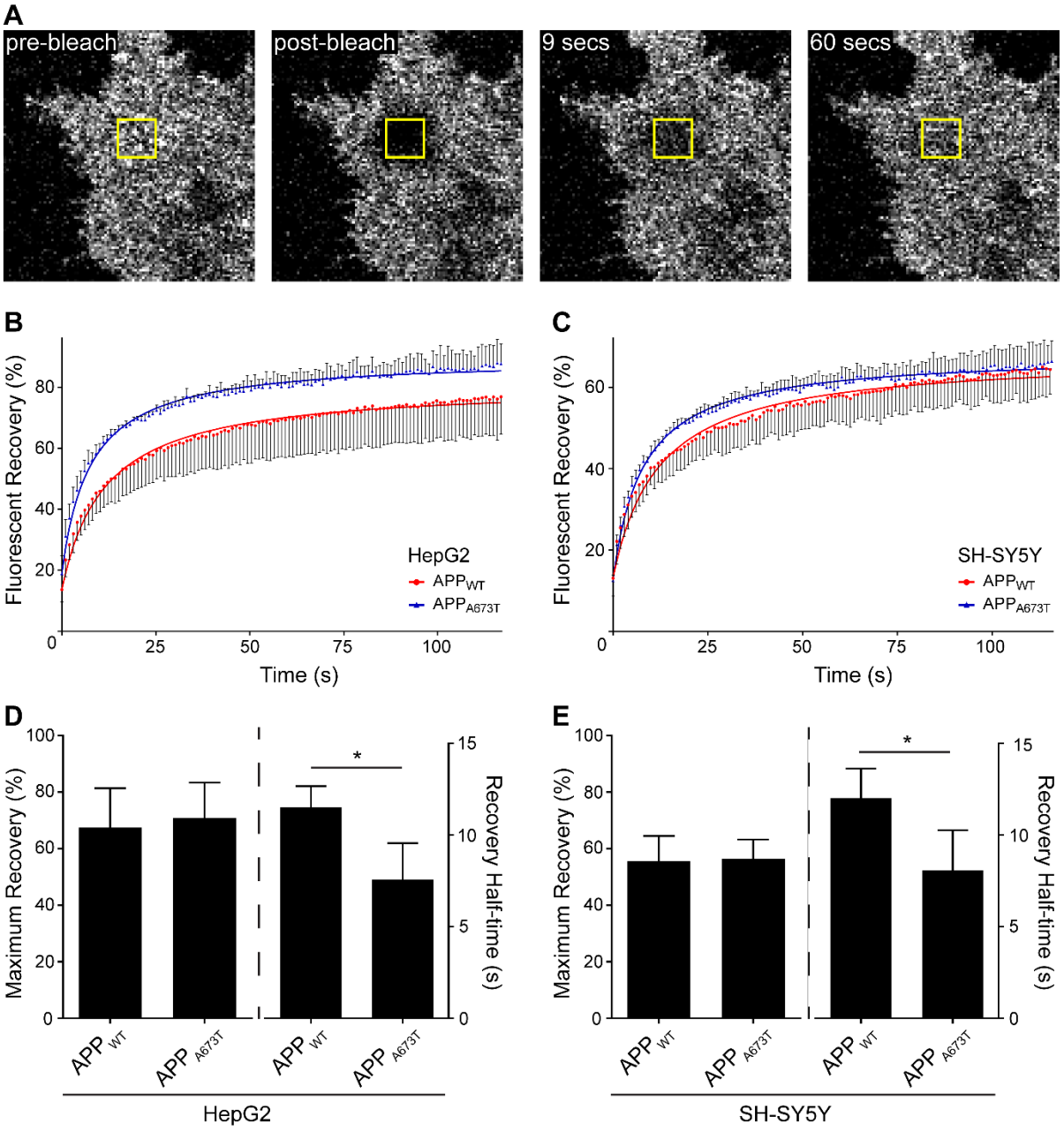

Figure 23. Mobility of APP_{WT} and APP_{A673T} in the plasma membrane

(A) Representative images of a FRAP experiment of HepG2 overexpressing full-length WT C-terminally fused to emGFP acquired with the Olympus Fluoview 1000 laser scanning microscope. The first panel shows the last frame preceding bleaching, the second panel shows the frame immediately after bleaching, the third panel shows the frame taken 9 secs after bleaching and the last panel shows the frame 60 secs after bleaching. The yellow square highlights the photobleached and analyzed area. **(B)** WT and A673T C-terminally fused to emGFP were overexpressed in HepG2 cells and subjected to FRAP imaging. Relative fluorescent recovery is plotted over time. For each condition, 8-12 cells were evaluated on each of 3 independent experimental days. **(C)** The same experiment described in (B) with SH-SY5Y cells. For each condition, 8-11 cells were evaluated on each of 4 independent experimental days. **(D)** Maximum fluorescence recovery and recovery half-times calculated from the samples presented in (B) were averaged. The difference in recovery half-time between WT and A673T was significant (p=0.0419; unpaired two-tailed t test; n=3). **(E)** The same analysis described in (D) for the SH-SY5Y cells presented in (C). The difference in recovery half-time between WT and A673T was significant (p=0.0283; unpaired two-tailed t test; n=4). Error bars represent standard deviation. Data were collected in collaboration with Hannes F. Maib.

Other reasons could be that SH-SY5Y cells have more cytoskeleton, more or denser membrane architecture or a distinct membrane fluidity and/or composition, which would probably make the observed difference not unique for APP.

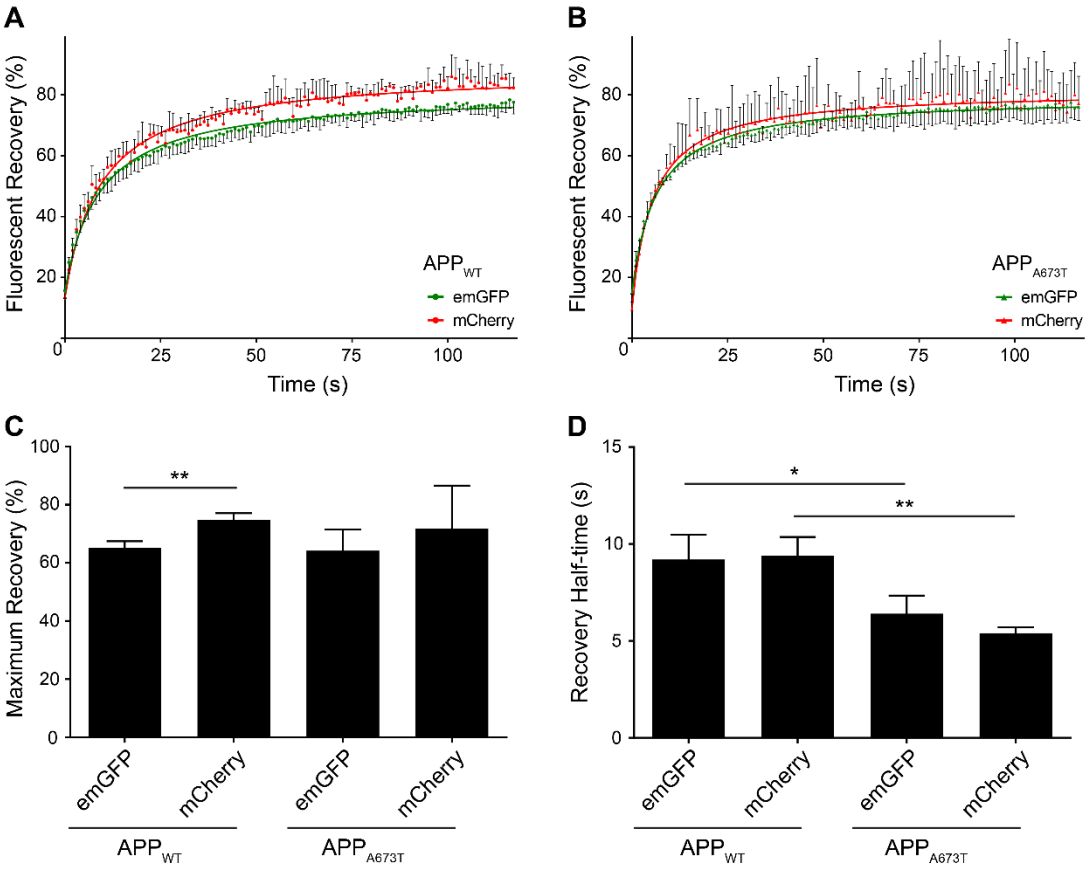

Figure 24. Relevance of APP processing for plasmalemmal mobility

(A) APP_{WT} C-terminally fused to emGFP and N-terminally fused to mCherry were overexpressed in HepG2 cells and subjected to FRAP imaging with the Olympus Fluoview 1000 laser scanning microscope. Both fluorophores are measured simultaneously and their relative fluorescent recovery is plotted over time. In total, 36 cells equally distributed over 3 independent experimental days were evaluated. **(B)** The same experiment described in (A) for APP_{A673T} C-terminally fused to emGFP and N-terminally fused to mCherry. In parallel to WT, 36 cells equally distributed over the same 3 independent experimental described in (A) were evaluated. **(C)** Maximum fluorescence recovery calculated from the samples presented in (A&B) was averaged. The difference in maximum fluorescence recovery between the emGFP and mCherry channels was significant for WT (p=0.0072; unpaired two-tailed t test; n=3). **(D)** Recovery half-times calculated from the samples presented in (A&B) was averaged. The difference in recovery half-time between WT and A673T was significant in both the emGFP (p=0.0393; unpaired two-tailed t test; n=3) and mCherry (p=0.0023; unpaired two-tailed t test; n=3). Please note that an ANOVA statistical analysis would not be correct here, as it would include the comparison between, for example, WT-emGFP and A673T-mCherry in its algorithm and this correlation should not be probed here. Error bars represent standard deviation. Data were collected in collaboration with Hannes F. Maib.

To address whether the results for plasma membrane mobility probed by FRAP microscopy were genuine for full-length APP, the FRAP experiment was repeated with a minor alteration just in HepG2 cells. Instead of a single fused C-terminal green fluorophore, a secondary red fluorophore was fused

to the N-terminus of both APP variants. mCherry was chosen as it is a bright red fluorophore with no spectral overlap with emGFP that has a decent quantum yield and great photostability. Because it is attached to the N-terminal end of the APP molecules and this end is removed upon α- or β-cleavage, mCherry allows imaging of the full-length APP only. By subsequently comparing the recovery half-times of emGFP with mCherry, the possible presence and influence of α-CTF can be gauged. Pilot experiments showed that the double fused APP is still readily overexpressed and incorporated into the plasma membrane by HepG2 cells (data not shown). For both the WT and A673T variants, the curves of emGFP and mCherry look remarkably similar (Figure 24A&B). However, regarding the maximum recovery, there is a significant difference between emGFP and mCherry for the WT variant and a trend in the same direction for the A673T mutant (Figure 24C). The recovery half-times demonstrate that the earlier found contrast between WT and A673T is valid, as the dissimilarity between the variants in the mCherry channel is even more significant than in the emGFP channel (Figure 24D). Additionally, the emGFP and mCherry values were decidedly similar for each construct, highlighting that, should there be any α-CTF present in the plasma membranes, it did not influence the FRAP measurements to any noteworthy degree.

4.2.2. Functional differences of the APP variants

An important mechanism in the life cycle of APP is its endocytosis from the plasma membrane into intracellular vesicles. It is generally accepted that this internalization is executed via Clathrin-mediated endocytosis (Lai et al. 1995; Perez et al. 1999; Ring et al. 2007) and it has been hypothesized that aggregation of APP is a requirement for this process to be initiated (Schreiber et al. 2012). In other words, the APP cluster itself seems to be the functional unit necessary for APP molecules to be made available for β-cleavage. Because of the convincing differences in clustering characteristics between WT and A673T up until now, it could be hypothesized that the variants are also internalized via Clathrin-mediated endocytosis to varying degrees, which could be a mechanism by which the mutant exerts its protective effect. A relatively easy method to investigate this hypothesis is to assess the colocalization of both variants with Clathrin using the PCC, as has been described before (refer to Figure 14 for details). The emGFP-fused constructs were overexpressed in both HepG2 and SH-SY5Y cells and imaged without additional labelling, whereas the Clathrin heavy-chain was detected with a primary antibody followed by an AF594-coupled secondary antibody labelling. Although not significant, a trend towards a lower propensity of A673T to colocalize with Clathrin can be observed in HepG2 cells (Figure 25A). A similar trend could be demonstrated in SH-SY5Y cells; however, it should be noted that due to time constraints this experiment only consisted of 1 experimental day (Figure 25B). Of note, the higher PCC values in these experiments compared to those in Figure 14 can be attributed to the fact that here APP was overexpressed and, therefore, available in much higher

quantities than in the earlier experiment. This automatically increases the PCC as the chance that APP molecules will be near a Clathrin-coated pit will logically be raised. On the other hand, colocalization with Clathrin is, of course, not equivalent to internalization rates and these results should therefore not be over-interpreted.

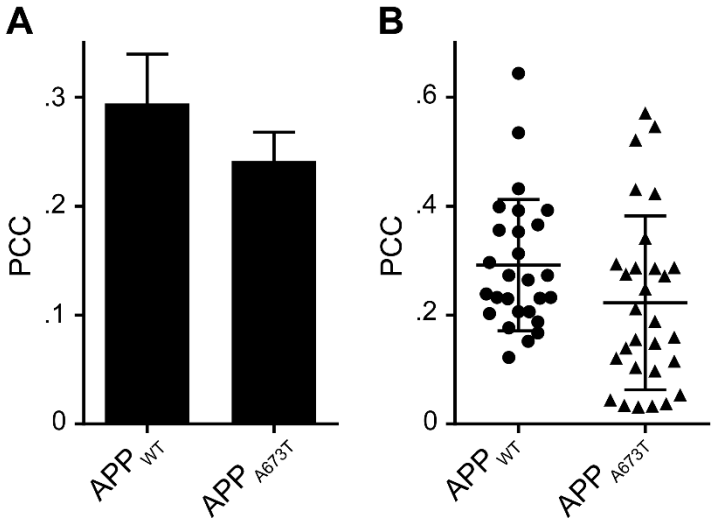

Figure 25. Sorting of APP_{WT} and APP_{A673T} into clathrin structures

(A) Plasma membrane sheet overexpressing WT and A673T C-terminally fused to emGFP were fixated, labelled with an anti-Clathrin-HC antibody which was detected by a secondary antibody couple to AF594 and imaged using the Olympus IX-81 inverted microscope. emGFP and AF594 signals were correlated and expressed as PCC. For each condition, 18-32 membrane sheets were evaluated for each of 3 independent experimental days. The difference between WT and A673T was not significant (p=0.1546; unpaired two-tailed t test; n=3). **(B)** The same experiment as presented in (A) for SH-SY5Y cells. Only 1 experimental day with 27 membrane sheets for WT and 29 for A673T was analyzed. Error bars represent standard deviation.

The foremost possibility for A673T's mechanism of protection against cognitive impairment, is the plausible idea already mentioned more than once before, namely that A673T is more efficiently cleaved by α-secretases. Western blotting was proven to be a robust technique for quantitative estimation of APP levels before and allows differentiation of the different fragments based on size. However, studying α-cleavage rates this way is not as straightforward as one might think. It was not unexpected that no major effects of α-CTF were detected in the earlier FRAP experiments, as cleavage by the γ-secretase usually follows immediately upon α- or β-cleavage (Barthet et al. 2011). Thereby, the APP molecules are liberated completely from the membrane, ending up either in the culture supernatant or in the cytosol. As it is impossible to differentiate between α- and β-cleaved C-terminal γ-cleaved AICD fragments (which is also the part that contains the emGFP tag) based on size, the only intracellular cleavage product is not useful in this respect. The N-terminal sAPP fragments or the p3 and Aβ fragments could theoretically be used to assess α-cleavage, but these would have to be laboriously isolated from the culture supernatant, the inaccuracy of which would most likely eclipse any detectable divergence between WT and A673T. Additionally, the relative size difference between

sAPPα and sAPPβ is less than 3% making it unfeasible to discriminate between them based on size, while the p3 and Aβ fragments are notably small and notoriously difficult to analyze via western blotting. Thus, to be able to investigate α-cleavage efficiencies in cell lysates via western blotting, the γ-secretase inhibitor DAPT was used. Unfortunately, SH-SY5Y cells showed signs of cell toxicity at concentrations of DAPT required to sufficiently inhibit the γ-secretase (data not shown), restricting this experiment to HepG2 cells. This should not be an obstacle, however, as HepG2 cells have been proven to express most of the typical α-secretases as well (Chalaris et al. 2010; Chalupský et al. 2013) and mechanistic similarities between SH-SY5Y cells and HepG2 cells have been demonstrated multiple times throughout this work. Pharmacological treatment of HepG2 cells overexpressing either WT or A673T with DAPT results in inhibition of γ-cleavage allowing the α- and β-CTFs to accumulate and become measurable. Normalization of the α-CTF signal to the total amount of full-length APP as a measure for the extent of overexpression should then facilitate the estimation of the α-cleavage efficiencies of both the WT and A673T variants. As the CTF fragments will increasingly accumulate over time and eventually saturate the plasma membrane, it is imperative that the time span between electroporation, start of DAPT treatment and analysis of the samples was carefully chosen. Pilot experiments revealed that 4 hours post-electroporation was a suitable period to commence DAPT treatment, while 18 hours post-electroporation seemed optimal for harvesting of the cells (data not shown). When stained for emGFP, the western blots revealed that essentially no CTF could be detected without DAPT (Figure 26A&B, DMSO), whereas with DAPT clear bands on the same height as the reference α-CTF-emGFP could clearly be observed (Figure 26A&B, DAPT and α-CTF). Additionally, it seemed that no discernible amounts of β-CTF were enriched during the experiment, suggesting that either DAPT cannot penetrate the late endosomes in which β-cleavage takes place or the rate of β-cleavage is a few orders of magnitude smaller than that of α-cleavage or both (Figure 26A&B, DAPT and β-CTF). To control for the anti-GFP antibody, the same samples were also investigated using the C-terminal APP antibody, which resulted in the exact same picture with the exception that the endogenous APP isoforms were now visible as well (Figure 26B). Due to the underlying endogenous signal when using the APP antibody, all analyses were performed on the blots stained for emGFP. Figure 26C shows the background-corrected signal of the α-CTF bands on top of the full-length APP (fl-APP) bands as stacked bars for each of the 4 experimental days. During evaluation of the results, it quickly became clear that there was quite a lot of deviation between the different experimental days. Whether this was due to a high biological variation or rather a result of the western blotting procedure cannot be resolved, as WT and A673T samples of the same experimental day were always analyzed on the same blot, but different experimental days were unfortunately never put on the same blot together. Total levels, meaning the sum of α-CTF and fl-APP, of WT were always higher than those of A673T, indicating that either less cells were successfully electroporated or the electroporation

procedure was equally efficient for both variants, but the A673T mutant was expressed to a lesser degree or was degraded faster than WT. Nevertheless, by dividing through the fl-APP signal the accumulated α-CTF signal could essentially be normalized for any of the aforementioned discrepancies. By doing this for each experimental day and displaying the results per experimental day, one can easily discern that the ratio is always a bit higher for the A673T mutant (Figure 26D). This means that

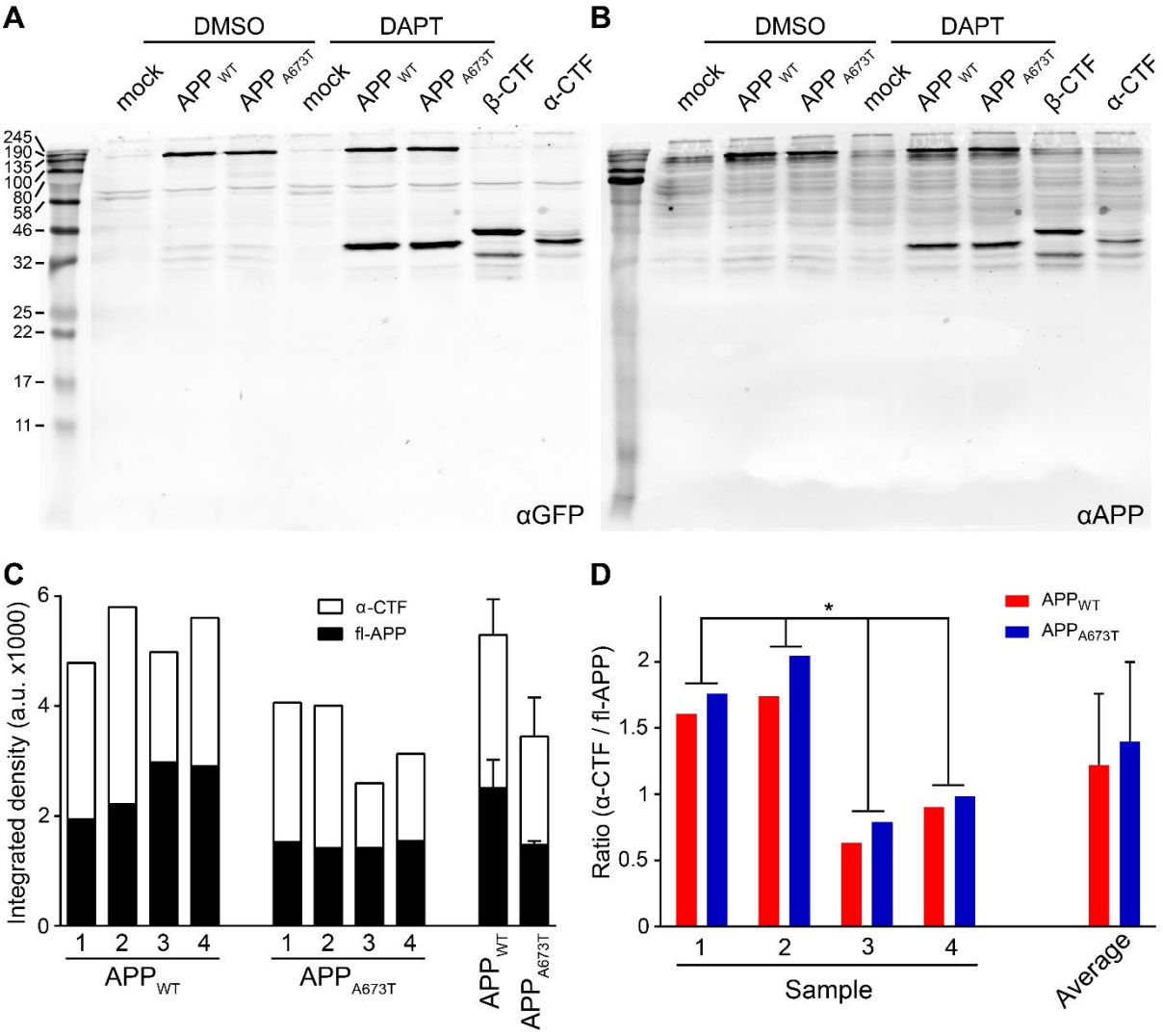

Figure 26. α-processing of APP_{WT} and APP_{A673T}

WT, A673T, β-CTF and α-CTF all fused to emGFP were overexpressed in HepG2 cells, which were subsequently either treated with 10 µM DAPT or vehicle (WT and A673T) or not treated (β- and α-CTF). After cell lysis, samples were subjected to western blotting. **(A)** Representative western blot against emGFP. **(B)** Representative western blot against APP. Note that, because of the emGFP fusion tag all overexpressed APP constructs run approximately 27 kDa higher than untagged variants. **(C)** For both constructs, DAPT treated full-length and α-CTF bands are quantified and presented as stacked bars for each of the 4 experimental days separately and as averages of the experimental days. WT and A673T from the same experimental day were always analyzed together on the same western blots and each of those experimental days was repeated on either 3 or 4 distinct western blots. **(D)** By dividing the in (C) presented α-CTF by fl-APP the ratio can be calculated. The higher the ratio, the more α-CTF is converted from fl-APP. The ratios of WT and APP are shown for each experimental day and as averages of the experimental days. The difference between WT and A673T when evaluated as pairs per experimental day was significant (p=0.0337; paired two-tailed t test; n=4). Error bars represent standard deviation.

irrespective of the amount of overexpressed fl-APP, relatively more ended up being converted into α-CTF if the APP in question carried the A673T mutation. One could argue that since there seems to be a little bit less overexpression of A673T compared to WT (Figure 26C, averages), A673T is also processed more readily. However, it should be noted here that the unmistakable dependence of the ratios of both WT and A673T on the experimental day strongly argues that the technical imprecisions of the western blotting procedure are responsible for the day-to-day variability. Nevertheless, when a paired analysis was performed based on the experimental days to exclude this day-to-day variability from the statistical evaluation, the results could even be demonstrated to be significant (p = 0.034), signifying that the A673T mutant is indeed more readily processed by α-secretases than WT.

5. Discussion

5.1. Validity of the model systems

SH-SY5Y cells were chosen to be the model system to characterize APP oligomerization, because they are one of the best described human cell lines for researching neurodegenerative diseases like Alzheimer's and Parkinson's. These neuroblast-like cells were selected for a neuronal phenotype by subcloning them three times from their parental lineage and can be differentiated into mature dopaminergic neurons by serum deprivation and addition of trophic factors (Teppola et al. 2016; Xie et al. 2010; Encinas et al. 2000). Additionally, in comparison to awfully hard to obtain, maintain and/or manipulate primary neuronal cells and differentiated iPSCs, SH-SY5Y cells are considered to represent human neurons remarkably well without suffering from these disadvantages. Especially, the required number of cells for the many and varied experiments in this work would have been problematic, as primary neurons do not proliferate sufficiently prohibiting the cultivation of large pools of them. iPSCs, on the other hand, do proliferate, but must be differentiated into neuron-like cells using an elaborate protocol which introduces variability between pools and makes it tedious and costly when upscaled. Nevertheless, reproducing at least part of the experiments in other neuronal cell lines, such as IMR-32 or cell models that are closer to the *in vivo* situation should be considered to probe the robustness and biological relevance of the findings. Additionally, another human cell line, namely the HepG2 cell line, which is derived from a liver hepatocellular carcinoma of a 15-year-old Caucasian male, was in the later experiments extensively used besides SH-SY5Y cells. HepG2 cells were mainly chosen because of technical reasons. They are not only easy to culture, manipulate and electroporate, but are relatively large cells that make beautiful membrane sheets and should perform well in the functional assays that were planned. Incidentally, they also functioned as a non-neuronal control for the clustering dynamics of APP, which might be useful for identification of mechanisms that might or might not be unique to neurons. Interestingly, the behavior of the mutant and wild-type APP was overall consistent between SH-SY5Y cells and HepG2 cells, indicating that APP-related processes in the plasma membrane are probably conserved between cell types and organs. This might be relevant considering that some lines of evidence suggest that the source of Aβ does not necessarily has to be a neuron or even a brain-resident cell (Roher et al. 2009). As has been discussed in chapter 1.4.5., the use of rodent cells or cells from other model organisms might not be the most meaningful for the experiments and research questions addressed here.

Another model system extensively used in these experiments is the plasma membrane sheet. One method to obtain authentic cellular membranes is to subject adherent cells to a brief ultrasound pulse,

thereby unroofing them and removing most, if not all, cytosolic components, leaving behind just the basal plasma membrane (Lang 2003). When optimized for a specific cell type, these so-called plasma membrane sheets survive this procedure remarkably well and are viable for at least an hour or longer depending on the cell type. Membrane sheets retain their native protein diffusion dynamics, conserve multi-molecular structures like the SNARE complexes and can still participate in mechanisms like non-vesicular lipid trafficking (Sieber et al. 2007; Lauria et al. 2013; Frick et al. 2007). Additionally, out-of-focus fluorescence coming from other cellular compartments is eliminated and the intracellular side of the plasma membrane can be manipulated and labeled without the need of detergents that could destroy membrane architecture. For these reasons, plasma membrane sheets were employed here as well and could be shown to be a highly relevant tool that allows precise study of plasmalemmal APP clustering mechanisms without disturbing them. Investigation of several typical markers for ER, which has been reported to come into direct proximity with the plasma membrane via ER-PM contact sites (Saheki et al. 2016; Yu et al. 2016; Giordano et al. 2013), and intracellular sorting organelles or structures, like caveolae, Clathrin-coated structures and early- and recycling endosomes, demonstrated only few and faint signals, indicating that only scarce amounts of these entities were present on the membrane sheets (refer to Figure 14). Additionally, plasmalemmal APP did not correlate notably to any of the markers, suggesting that most of it resides in the plasma membrane sheets and not in caveolae, pits or vesicles. Of note, albeit still quite low, the correlation between APP and Clathrin was almost twice that of the other markers, which is not unexpected as Clathrin-mediated endocytosis constitutes APP's canonical reinternalization pathway. Taken together, membrane sheets are relatively pure model systems for isolated plasma membranes in general and for plasmalemmal APP.

5.2. Caveats of standard fixation protocols

The set of experiments, described in chapter 4.1.3., was initially plagued by problems predominantly arising from the fixation procedure. The widely accepted 4% PFA in PBS fixative caused blebbing on whole cells, which is to be expected considering that the osmolarity of 4% PFA in PBS is about 1600 mOsm, which is significantly higher than the ~300 mOsm that is usually reported for the intracellular environment of vertebrate cells (Gagné 2014; Hoffmann et al. 2009; Danziger and Zeidel 2015). The underlying mechanism for blebbing is believed to be the fixation agent already starting to fixate the outer plasma membrane while the discrepancy in osmolarity strongly increases the outwards pressure of the intracellular fluids. This outside pressure than pushes the parts of the plasma membrane that have not yet been so thoroughly fixated outward forming structures reminiscent of balloons. Blebbing as a result of formaline/formaldehyde fixation has already been described in literature a long time ago (Fox et al. 1985), but also more recently (Zeng et al. 2013; Zhao et al. 2014).

Furthermore, incubation of eukaryotic cells with comparable PFA concentrations is also a long-standing established method to produce (giant) plasma membrane vesicles (Scott 1976). It is also not surprising that fixation of 1% PFA turned out to be most favorable, as it has the lowest osmolarity of all tested fixatives, but still has ample fixation capacity to constrain the cells for the required duration of the experiment described in Figure 13. Whether it is a suitable fixative for whole cells that need to undergo permeabilization, multi-day immunocytochemical labelling or longer-term storage is questionable though. The optimal temperature for fixation was also scrutinized because it was suggested that a cold environment makes the cell membranes more rigid, possibly allowing fixation in a more native state. On the other hand, cold treatment is a known inducer of cell contraction, which could favor the formation of blebs in combination with a fixative (Zeng et al. 2013). In the end, the temperature did not seem to matter much for fixation of whole cells in these experiments (refer to Figure 12).

Contrary to whole cells, the plasma membrane sheets were not optimally fixated with either 1% or 4% PFA. This is supposedly because of the loss of cytosol that would normally create a solid interlinked network after fixation, which is able to hold these molecules in place. PALM experiments that did not make it into this work clearly showed that a considerable fraction of APP molecules still moved around after fixation with 4% PFA. These observations are supported by the fact that up to ~40% of Transferrin receptors (TfR), which have an analogous size and a structurally similar intra-extracellular distribution compared to APP, were also found to be mobile even after prolonged fixation with 4% PFA (Tanaka et al. 2010). Residual protein movement in combination with subsequent antibody labelling could induce post-fixation aggregation artifacts that would bias our results (Stanly et al. 2016). Therefore, it was imperative to find a fixation method that allowed complete fixation of plasmalemmal APP without hampering its antigenicity. Addition of low concentrations of glutaraldehyde to the standard formaldehyde fixative seemed the first obvious option to evaluate. Even the addition of only low concentrations of glutaraldehyde seemed to fixate APP quite well. However, its antigenicity seemed to be largely lost and background-fluorescence was significantly increased, especially in the optimal wavelengths for gSTED imaging (data not shown). Both these issues have already been reported extensively in the literature (Jamur et al. 1995; Yokota and Okada 1997). After ruling out glutaraldehyde as a possible solution to the problem, 1% PLP was also tested in this respect and seemed to resolve the problem. PLP was originally proposed by McLean and Nakane in 1974 for immunoelectron microscopy (McLean and Nakane 1974). The combination of lysine with formaldehyde allows the creation of larger polymer structures than formaldehyde alone, these structures cover the plasma membrane sheets like a mesh that somewhat mimics the cytosol. The periodate oxidizes carbohydrate moieties to form aldehydes, which are subsequently cross-linked

either directly by the divalent amine lysine or by the intermediation of the formaldehyde. Supplementary to the fixation of polysaccharide chains of glycoproteins, which are especially abundant in the plasma membrane, paraformaldehyde performs its usual fixation effects by cross-linking the nitrogen atoms of the peptide backbone and sidechains of lysine (Thavarajah et al. 2012) as there is still much more paraformaldehyde than periodate and lysine available in a 1% PLP solution. An additional advantage is that the lower paraformaldehyde concentration without loss of fixation capacity better preserves the antigenicity of many proteins, which has also been reported before (Seftalioglu et al. 2003; Suzuki et al. 2002; Pieri et al. 2002). 1% PLP seemed optimal for fixation of plasma membrane sheets (refer to Figure 16) and was, therefore, used for all experiments that involved analysis of unroofed cells. Interestingly, for generation with subsequent fixation of plasma membrane sheets, temperature did seem to make a difference. Cells unroofed and fixated at 4°C produced larger and more intact sheets (data not shown), which is presumably because of an increased rigidity of cooled lipid bilayers. Additionally, membrane sheet generation at 4°C should also decrease Brownian motion of the proteins, possibly allowing them to be captured in their native arrangement more easily.

5.3. Accuracy of the plasmalemmal copy number

To assess the packing density of plasmalemmal APP clusters the following procedure was conceived and carried out (refer to Figure 6). First, full-length human APP_{695} was cloned in an expression vector adding an N-terminal His_6-tag and a Thrombin recognition site. Given that bacterial growth was inhibited upon induction of the expression vector with IPTG it seems logical that the expressed protein elicited toxic effects on the bacteria. As APP is a mammalian type I transmembrane protein, its incorporation in the cytoplasmic membranes of the bacterial cells or accumulation of aggregates of misfolded APP could lead to cellular toxicity and therefore kill all the cells that produce appreciable amounts of the protein (Dumon-Seignovert et al. 2004; Mulrooney and Waskell 2000). This obstacle was overcome by switching to bacteria that can grow and express proteins at lower temperatures. Moreover, it could be shown that no C-terminally truncated fragments were produced by the bacteria, implying that the subsequent Ni-NTA purification should only isolate the full-length recombinant protein. The lack of contamination as exemplified by both western blotting and colloidal Coomassie stainings of the purification corroborated this prediction (refer to Figure 7). Comparing the western blots against the His_6-tag, which detects the very N-terminus, with the western blots against the C-terminus of the purified APP demonstrates that no other protein than full-length recombinant APP is present (compare Figure 6E&7A with Figure 10A). After production in appropriate bacteria and purification via Ni-NTA, the concentration of the purified APP_{695} was measured by calibrating it against two distinct dyes (refer to Figure 8). It could theoretically be that the distinct binding affinity, staining

protocol and/or employed chemicals of a single dye biases quantification by, for example, preferentially labelling a certain aa that occurs significantly more in one of the proteins. Coomassie G-250 predominantly binds proteins through hydrophobic interactions with tryptophan, phenylalanine and tyrosine (Georgiou et al. 2008); whereas Fast Green FCF primarily binds free, protonated, basic groups of arginine and lysine residues through electrostatic interactions (Alfert and Geschwind 1953; Berlowitz et al. 1970). Additionally, both BSA and APP are not particularly small proteins, which ensures that most of the aa residues are present in comparable abundances. Taken together with the number of replicates, the determination of the concentration of the purified recombinant APP seems reliable.

Next, the recombinant APP was used as a calibrated standard to quantify the amount of APP proteins in SH-SY5Y cell lysates of which the number of cells per volume of lysate was meticulously determined. Because of disruptive factors, like cell clumping, interrogation of cell counts by flow cytometry and especially Neubauer counting chamber becomes more accurate with increasing replicates and by probing multiple dilutions. It is unfeasible to examine cell counts of each collected lysate to be quantified for APP content as thoroughly as the combined analyses of both flow cytometry and Neubauer cell counting over a big range of concentrations. Furthermore, BCA assays show less variability and the protein content of cell lysates can be re-analyzed as often as required; the original cell concentration cannot as the cells are lysed after counting. Thus, it was decided to first determine the protein content per SH-SY5Y cell precisely and then infer the original cell concentration from the total protein content assessed by BCA assay of the whole lysate, instead of directly counting the cell number for each lysate individually (refer to Figure 9). The acquired value of 75.69 ± 23.33 pg/cell is perfectly in line with published values for other cell lines, like 64-95 pg/cell for different dendritic subtypes (Dumortier et al. 2005) and ~60 pg/cell for thymocytes (Salinas et al. 1972), as well as ~150 pg/cell for HeLa cells (Volpe and Eremenko-Volpe 1970), 110-180 pg/cell for A549 cells and 100-190 pg/cell for HepG2 cells (Wiśniewski et al. 2014), the latter 3 all being reportedly bigger than SH-SY5Y. The relatively large spread (and accordingly also the standard deviation) seems odd in comparison to the quite good correlations with the linear regressions. This is likely because if a sample is skewed in the same direction for both parameters, e.g. a lower cell count and a lower protein concentration than the regression or vice versa, the amount of deviation from the average is multiplied by the final division. Nevertheless, given the large number of sampled lysates, the standard error of the mean is only 3.236 pg/cell, which shows that the found average is reliable and likely close to the actual total protein content for SH-SY5Y cells. The APP copy number per cell was determined by making standard dilutions of the recombinant APP and correlating the amount of APP from a cell lysate of which the cell concentration was inferred from the total protein content against the standard curve (refer to Figure 10). It should be noted that the choice of antibody means that all isoforms and maturation stages of

APP are detected and therefore display as a smear with two more prominent bands on the western blots. These two bands reportedly comprise immature APP_{695} (lower) and a combination of mature APP_{695} and immature APP_{751} and APP_{770} (upper), the smear represents all remaining configurations of APP (Jiang et al. 2010; Lewis et al. 2012; Suh et al. 2011). Additionally, the bacterially expressed APP_{695} runs slightly higher than the lower prominent band of the cellular endogenous APP, which is to be expected as it possesses an additional N-terminal His_6-tag and thrombin cleavage site. The found number of APP molecules per SH-SY5Y cell, i.e. 63,889 APP molecules per cell, might strike some as quite low. However, it is in the same order of magnitude as comparable plasmalemmal proteins and it has been demonstrated that especially cell membrane receptors can occur in even lower cellular copy numbers (Zeiler et al. 2012; Beck et al. 2011; Tan et al. 2012; Tennenberg et al. 1988).

Following elucidation of the number of APP molecules per cell, the fraction of these that resides at the plasma membrane of SH-SY5Y cells was to be investigated (refer to Figure 11). All plasmalemmal proteins was biotinylated and subsequently isolated using a streptavidin-based column purification method. As loss of biotinylated APP during the experimental isolation is controlled for, the only expected source of error is the biotinylation step itself. It seems likely that full-length APP can efficiently be biotinylated, because it has a sizeable extracellular domain with plenty of lysine residues (47 to be exact). In similar experimental work, the used experimental set-up has been proven to be robust for proteins that are comparable to APP (Posthumadeboer et al. 2013; Kemper et al. 2010). Nevertheless, it could be that the APP that resides in the center of its plasmalemmal cluster cannot be reached efficiently by the biotin-NHS-ester, although it is a remarkably small molecule. Such an inaccuracy was not controlled for in these experiments, as there were no feasible methodologies available that would not also introduce artifacts of their own. Be that as it may, should this have occurred, it would lead to an underestimation of the plasmalemmal fraction, which in extent would mean that even more APP molecules reside in the plasma membrane than is presented in this work. The determined value of 17.54% appears to corroborate the 10-20% that is often reported (Haass et al. 2012; Thinakaran and Koo 2008; O'Brien and Wong 2011). However, as discussed at the end of paragraph 1.4.2., this is to our knowledge the first experimental exploration of the plasmalemmal APP fraction in human neuronal cells.

To quantitatively distribute the plasmalemmal APP over the cell membranes, the total surface area of SH-SY5Y cells was investigated (refer to Figure 13). Using optimal fixation conditions, artificial loss of parts of the cellular plasma membrane and induction of morphological alterations could be minimized (refer to Figure 12). Moreover, increasing or decreasing the thresholds used to create the 3D models to levels that did not destroy the models either by introducing holes for higher thresholds or by detecting background and non-specific noise as genuine signal, resulted in only minor changes

to the resultant surface areas. Additionally, the evident similarities between the cells when viewed by eye through the microscope and the reconstructed 3D models indicate that the experimentally determined membrane size must be close to the real size. An average surface area of 1,244 ± 425 µm² was detected, which is comparable to experimental data from other cell lines, such as the comparatively small PC-12 cells (~800 µm²) (Knowles et al. 2010) and the relatively big HeLa cells (~1600 µm²) (Puck et al. 1956), further corroborating the validity of the method. It should be accepted, however, that the found size is likely an overestimation as the diffraction of the signal coming from the lipid dye extends a certain distance beyond the actual border of the plasma membrane. As the 3D models are constructed from the outermost detected signal, the calculated surface area will be marginally larger.

To summarize, these findings result in a quite thorough approximation of the total number of APP molecules per square micrometer of SH-SY5Y plasma membrane, namely 9 molecules per µm². However, because this number is an amalgamation of many experimental techniques, a bias in the same direction for several of the experiments could skew the results significantly. A convincing argument for the accuracy of this number are the regions designated 'higher' and 'lower' from Figure 15B. The region labelled 'higher' features a uniform background signal, whereas the region labelled 'lower' displays areas where there is no GFP or AF647 signal, in other words, that contain no overexpressed or endogenous APP molecules. This indicates that the dimmest signals may very well be single, monomeric molecules or lower-order oligomers of APP such as dimers or trimers. Given that the resolution limit in the XY-plane of our epifluorescence microscope is at best ~240 nm in the green channel and ~325 nm in the far-red channel and there should be about 9 molecules per square micrometer in cells that express APP at or close to endogenous levels, this makes sense. If these 9 molecules are perfectly spread over the square micrometer that they occupy, they could just barely fill this area with a uniform signal. When a few of these molecules are clustered together, blank areas without any detectable signal should arise, which is also observed, and the density of the non-clustered molecules becomes so low that resolving them becomes feasible even at diffraction-limited resolution. Thus, these results indicate that the plasma membrane sheets with low levels of overexpressed APP must have a molecular density close to the 9 molecules per µm² found in the biochemical experiments for endogenous APP.

5.4. Implications of APP overexpression

The results discussed for Figure 15 indicate that, with increasing protein copy numbers, more and more APP ends up in the homogeneous background signal underlying the spotty pattern. Consequently, it seems plausible that plasmalemmal APP oligomerization is a process that is either

regulated by co- or adaptor proteins or biophysical properties of the plasma membrane (Destainville et al. 2018). Whichever it should be, it is obvious that APP clustering can easily be saturated by overexpression of the protein, which can be seen here. This is an interesting phenomenon by itself and would make a nice model system to investigate plasmalemmal protein phase separation and biophysical mechanisms governing plasmalemmal protein aggregation. However, the fact that APP overexpression apparently affects its membrane distribution, as can be observed by the fact that there is essentially no overlap between the two pools in Figure 15D, means that it does not constitute a good model system for the aim of this project. It seems that overexpression quickly tips the scales in favor of monomeric APP, making overexpression of APP fusion proteins a method that must be used with caution for the study of APP oligomerization and, by extent, processing. Furthermore, another indication in this work suggests that overexpression of APP, or a part thereof, should be handled with care and findings that are resulting from it interpreted cautiously. For example, the observation from Figure 26 that, although the cells overexpressing either β- or α-CTF were not treated with the γ-secretase inhibitor, ample amounts of both CTFs somehow managed to escape γ-cleavage, whereas full-length APP is completely processed without γ-secretase inhibition. A possible reason could be that, because the CTFs are substantially smaller, considerably more of them is overexpressed compared to full-length APP, leading to saturation of the γ-secretases. Alternatively or maybe synergistically, direct generation of CTFs instead of production at the cell membrane or in the endocytic compartments, might affect their cellular transport in ways allowing them to avoid γ-secretases altogether.

5.5. Microscopic approaches to the molecular cluster density

The set of experiments designed to come from the plasmalemmal copy number to the APP cluster molecular density all depend on microscopy of unroofed cells (refer to 4.1.5.). The use of plasma membrane sheets has been discussed in chapter 5.1., while the choice for a purely microscopical approach is based on the fact that the use of biochemical methods to investigate oligomerization of membrane-bound proteins usually involves some sort of synthetic cross-linking that is likely to induce bias (Gonzalez-Lozano et al. 2020; Eisenberg et al. 2011). Additionally, without the possibility to utilize overexpression, it is notoriously difficult to count molecules packed more-or-less densely together and distinguish lower-order oligomers from monomers even using advanced super-resolution microscopy techniques (Rickman and Duncan 2010; Batoulis et al. 2016; Merklinger et al. 2017; Mattila et al. 2013; Itano et al. 2012). For this reason, the stochastic antibody labelling approach was employed. However, for this approach to be applicable, signals of labelled epitopes should be far enough apart for single spots to be identifiable even in the samples where membrane sheets were submitted to the standard condition with a 1 in 200 dilution of the primary antibody. In other words, if the detected signals are so close together that they overlap each other or a continuous fluorescent background is present (for

example, as is the case in Figure 15B in the area marked “higher”), isolated intensity maxima cannot be detected making it impossible to put the intensity of the maxima in relation to the amount of bound primary antibody. Fortunately, the endogenous expression levels of plasmalemmal APP in SH-SY5Y cells are low enough for single spots to be detected as the many various experiments have shown.

Although this work attempts to attain the best possible approximations of the investigated parameters with the techniques available, it should be noted that some of the concluded results are dependent on assumptions that could not always be tested as they fell outside the scope of this project. One of the major assumptions is that the lowest-order APP object is a monomer. However, some believe that APP is predominantly present as at least a dimer and that the monomeric form does not occur under normal biological conditions (Scheuermann et al. 2001; Gorman et al. 2008; Fogel et al. 2014). Should this be the case, the 0.1687 maxima per µm² that were found to be monomeric must have been dimers, which means that not 1.87% but rather 3.74% of the total plasmalemmal APP molecules would be in the lowest-order, dimeric conformation. To incorporate this change in the calculation using Equation 1, the number of APP molecules that are subtracted in the numerator should be doubled leading to the following result [(9.008 - ((0.4924 * 0.3427) * 2) / (0.4924 - (0.4924 * 0.3427)) =] 26.79 APP molecules per cluster, a marginal difference of only 0.52 molecules per cluster. Therefore, should the dimeric form be the lowest-order conformation of APP, the results concerning the molecular density of the bigger APP oligomers changes only slightly. Additionally, it could be argued that the methodology of determining the percentage of APP monomers using a stochastic labelling

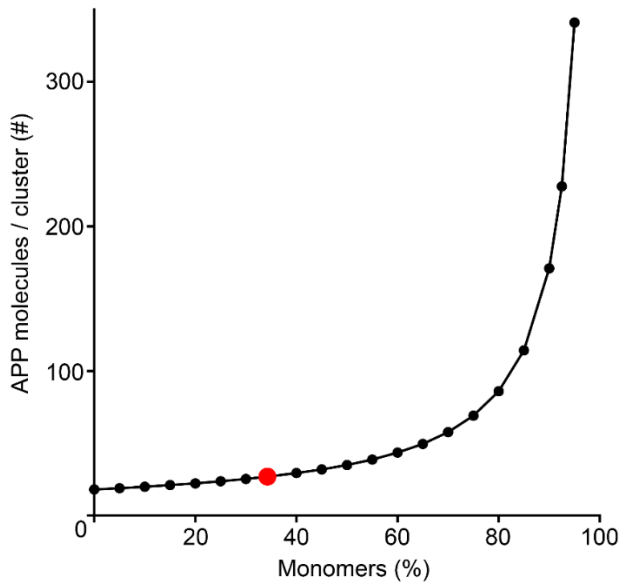

Figure 27. Interaction between monomer fraction and cluster density

The dependence of the number of APP molecules per cluster on the percentage of monomers as described by Equation 1. The monomeric fraction used in this work is marked by a red dot on the curve.

and exclusively microscopic data is probably prone to some margin of error in either direction. To illustrate the effect of contrasting monomeric fractions, Equation 1 was graphically visualized as a plotted graph using the percentage monomers as the unknown parameter (Figure 27). The red spot depicts the value found in this work, 34.27%. The number of APP molecules per cluster is not as dependent on the fraction of monomers as much as one might expect. As can be observed, a monomeric fraction of 0% provides circa 18 molecules per cluster, whereas 60% monomers result in about 44 molecules per cluster. Starting at around 60% monomers the graph starts to skew heavily towards a higher molecular density than seems realistic. Additionally, the observation that many quite dim maxima remain after background subtraction independent of the imaging technique combined with the observed distribution of cluster intensities, indicates that higher monomeric fractions are rather unlikely. It should be noted that these insights do not rely on the size or the distribution of the clusters at all. Thus, at the very least, this work convincingly shows that a large part of the plasmalemmal APP exists in clusters with more than a few to up to 50 molecules, if not more, per cluster.

One might have noticed that the epifluorescence microscopy experiments designed to find the monomeric fraction showed similar numbers of maxima per µm² were detected between the stochastic and background labelling conditions, although no primary antibody was offered in the background labelling condition (refer to Figure 17C). This might seem peculiar as it is generally believed that non-specific deposition of secondary antibody is not dependent on the availability of primary antibody or more general available epitopes. However, this is not necessarily the case. Firstly, because part of the secondary antibodies is sequestered, i.e. bound to primary antibody, in the stochastic condition, there is simply more secondary antibody available for non-specific deposition in the background condition. Secondly, it has been shown before that a complete lack of viable epitope changes the binding dynamics because of an absence of a binding equilibrium (Kaufman and Jain 1992), which results in an increased chance that secondary antibodies will be non-specifically deposited when no epitopes are available. It could be argued that because of these mechanisms too many maxima were subtracted for identification of the pool of non-background, APP maxima in Figure 19B. As these mechanisms should not play a role in the standard labelling condition, it could perhaps have been better to perform the subtraction on a per bin basis as in Figure 19A. Yet, it is impossible to judge how big the influences of these mechanisms might have been and, as discussed before, it is preferred to underestimate the number of molecules per cluster than to overestimate it. Nevertheless, subtraction on a per bin basis would have culminated in a monomeric fraction of 55.25%, about two-thirds more than the original value of 34.27%. By use of Figure 27, it can be deduced that 55.25% monomers results in on average 39 molecules instead of 27 molecules per cluster, an increase of almost 50%.

Furthermore, the increased resolving power of gSTED microscopy exposed that what looked like one cluster in the confocal image was really two clusters near to each other (refer to Figure 20A). This suggests that the results regarding the number of maxima per µm² obtained via epifluorescence microscopy (refer to Figure 17-19) might be an underestimation. However, the comparison between the background-normalized standard and stochastic conditions of Figure 19 regarding the percentage of monomeric maxima should still be valid. The reason for this is that, if there was an error, it must have been the same between all conditions and would "fall out" during the calculations. Still, one cannot assume that none of the detected maxima from the epifluorescence experiments were not 2, 3 or maybe even more maxima near each other. Especially if maxima are notably bright, they automatically appear to occupy a much larger area in epifluorescence microscopy because of the scattering of the many emitted photons. It would therefore be easy for a dimmer maximum to hide under the observed blur of photons emitted by the bright maximum or a bright maximum could be a crowd of multiple more-or-less equally bright maxima. In extent, the error would be more prominent in the higher maxima intensity ranges and could bias quantification of the brighter maxima, which are the maxima of interest. On the other hand, it can be assumed that this effect is not excessively influential due to the low density of maxima in the first place.

A critical point with gSTED microscopy could be that quite dim objects are overlooked as the combination of harsh emission depletion and time-gating would not allow the collection of enough photons from these objects to be detectable. This is a moot point, however, because it has previously been established that the dimmer signals in APP micrographs are mostly non-specific depositions of secondary antibody and random noise from either the instrument or artifacts. The inclusion of a no primary background control condition allows normalization for these entities and it is irrelevant whether a fraction of them is not detected equally in both conditions. Interestingly, the difference between the two conditions for maxima per µm² was found to be more than 2-fold (refer to Figure 20B), while the deviation between the standard and background conditions of the epifluorescence data was only about 1.3-fold (refer to Figure 17C). The observation that the epifluorescence experiment displayed about 70% more maxima per µm² in the standard condition and more than twice the maxima in the background condition, is convincing evidence that especially the dim maxima are not picked up anymore by the ImageJ macro following gSTED imaging and rather not that a lot of maxima were overlooked in the epifluorescence imaging. On the other hand, it nicely emphasizes the high sensitivity in the epifluorescence microscopy experiments. Another criticism that is often heard is that the emission depletion in combination with time-gating would eliminate most of the dynamic range of the intensities of the detected signals. However, a significantly larger disparity was observed between the maxima intensities of the standard and background conditions with gSTED (~4-fold; refer

to 20C) than with epifluorescence imaging (~2.5-fold; refer to Figure 17D), while the standard deviations of the maxima intensities were virtually identical (12.29% and 11.58% of the average, respectively). The larger disparity could be explained by the loss of the dimmer maxima in gSTED imaging, which would not change the average maximum intensity of the background condition much as they are all around the same dim brightness anyway, whereas it would increase the average maximum intensity from the standard condition substantially. Nevertheless, it argues that the dynamic range of maxima intensities is not lost due to the stringent emission depletion and time gating. Taken together, it seems that gSTED microscopy is more robust for counting APP maxima because it is less influenced by background and has a better resolving power. High signal-to-noise epifluorescence microscopy, on the other hand, is more suitable for investigation of the monomeric fraction, as it allowed detection of significantly more maxima especially in the lower intensity ranges.

5.6. Impact of the A673T mutation on clustering and processing

Analysis of the average ROI intensities of the gSTED micrographs from WT and A673T overexpressing HepG2 cells showed a small trend towards less plasmalemmal A673T (refer to Figure 21A), which could be due to several reasons. It might be that the A673T variant is less efficiently expressed, which seems unlikely as it has been shown to beneficial as it provides protection against cell death (Hashimoto and Matsuoka 2014) and there have been no reports of possible toxicity or detrimental effects of this variant. Another reason might be that it is less efficiently trafficked to the plasma membrane from the ER. There are indications that APP is already oligomerized before this trafficking step (Isbert et al. 2012; Plácido et al. 2014), which makes it feasible that clustering could also somehow regulate this mechanism and, thus, be influenced by the A673T mutation. However, the most prominent possibilities must be that it is more efficiently cleaved by α-secretases, which is at the very least suggested by the results in this work, and that there are many more dim A673T maxima that are subsequently not detected by the gSTED imaging, which would indicate that the A673T mutant rather forms lower-order oligomers or monomers. Furthermore, the observations that A673T tends to form slightly larger clusters and that the intensity of the clusters is virtually the same (refer to Figure 21D&E), implies that A673T clusters contain a comparable number of molecules that are spaced a little further apart than in WT clusters or that the clusters actually contain less APP molecules that are better accessible for the antibodies because they are spaced further apart. This is promising, as, by extent, this means that the substitution of a single amino acid can modulate the aggregation characteristics of a large protein. Additionally, it gives insight into other possible molecular mechanisms behind the protective effect of the A673T mutant against age-related cognitive decline. Of note, the discrepancy between the cluster sizes in Figure 20 and Figure 21 are most likely because in Figure 21 APP is overexpressed, which presumably changes its clustering dynamics as discussed in chapter 5.4..

Furthermore, it can never be completely excluded that post-fixation aggregation artifacts skew the results. Especially the required labelling with primary-secondary dye-coupled antibodies to allow stringent gSTED imaging could diminish the observed differences between the two variants. Subsequent investigation of the plasmalemmal distribution of both WT and A673T by directly imaging the emGFP-moiety with high signal-to-noise epifluorescence microscopy (refer to Figure 22) circumvents most of the aforementioned problem with gSTED imaging and has the added benefit that non-specific signal due to off-target deposition of primary and/or secondary antibody is avoided. This methodology found incredibly significant differences between WT and A673T in both cell types, exemplifying that the protective mutant indeed affects the plasmalemmal clustering dynamics of APP regardless of cellular background, which is a strong indication for an intrinsic regulation mode. There was a quite remarkable difference between HepG2 and SH-SY5Y cells, however, namely the about 10-fold difference in average intensity. As the HepG2 cell line is generally able to overexpress most proteins efficiently and no indications of cell toxicity have been observed, this huge discrepancy could maybe be explained by the fact that significantly less APP molecules are trafficked to the plasma membranes of HepG2 cells. Another reason could be that APP molecules are cleaved and/or endocytosed more readily in HepG2 cells.

FRAP measurements demonstrated that the fluorescent recovery half-time is significantly shorter for A673T mutant than for WT in both HepG2 and SH-SY5Y cells (refer to Figure 23). This indicates that the WT variant experiences more hindrance in its lateral diffusion throughout the plasma membrane than the A673T mutant. The most obvious reason for this result is that the WT molecules are retained longer in their corresponding clusters, which means they can spend less time moving around and, therefore, they recover slower. Various mechanisms, such as interactions with the cytoskeleton or with other membrane proteins or lipids, variations in protein secondary or tertiary structure or intracellular transport processes could also play a role. However, since the WT and A673T variants only differ by one amino acid, it seems unlikely that interactions with the cytoskeleton or other membrane proteins are altered. Additionally, it is generally accepted that the region around the mutation site is unstructured (Gralle et al. 2002; Sandbrink et al. 1994), which makes variations in secondary or tertiary structure also improbable explanations. Intracellular transport processes should also not play a huge role because similar results were obtained in preliminary experiments where plasma membrane sheets were used for FRAP microscopy (data not shown). The last remaining mechanism, interactions with membrane lipids, cannot be excluded, especially because there are strong indications that a cholesterol binding site exists close to the mutation site (Barrett et al. 2012). Nevertheless, given that the first 5 amino acids of the Aβ region have been found essential for APP clustering (Schreiber et al.

2012) and the fact that the A673T mutation occurs on the second amino acid of these 5, strongly supports the notion that intrinsic cluster binding dynamics cause the disparity in recovery half-time.

A major criticism on the FRAP experiment could be that the observed difference between the WT and A673T variants in FRAP recovery half-times is due to A673T being cleaved more efficiently by α-secretases leading to significantly more A673T α-CTF than WT α-CTF in the plasma membranes. Because α-CTF is much smaller than full-length APP and the α-CTF fragment still possesses the fused emGFP, a higher ratio of α-CTF would logically result in faster recovery times in FRAP measurements. However, it is quite unlikely that such a mechanism biased our results, because α-processed APP is typically quickly removed from the plasma membrane by subsequent γ-cleavage (Barthet et al. 2011), an observation that is corroborated by the fact that no CTFs were detected on western blots of HepG2 cells overexpressing full-length APP (refer to Figure 26A&B, DMSO). Still, a FRAP microscopy control experiment was devised in which both ends of the APP constructs were differentially fluorescently labelled allowing discrimination between full-length APP and processed species (refer to Figure 24). The significant difference between the maximum recoveries of emGFP and mCherry for the WT construct and a strong trend in the same direction for the A673T mutant could suggest that there is a larger immobile fraction of APP molecules that only possess the mCherry tag, which is the exact opposite of what was expected. However, the most plausible reason is simple and depends on the traits of the fluorophores and the technical set-up, namely mCherry is photobleached more efficiently than emGFP. The threshold for rejecting a measurement is at 20% remaining fluorescence intensity after photobleaching. Now, it seems that in quite a few measurements 10% to 15% of the fluorescence intensity remains in the emGFP channel after photobleaching, whereas the mCherry signal is almost always completely destroyed. Because the pre-bleach signal intensity is defined as 100% and the frame directly after the photobleaching is defined as 0%, any remaining signal after photobleaching lowers the potential maximum recovery by that amount. This is usually not a problem, because the same fluorophore and set-up are used to investigate varying conditions. In this case, these technical discrepancies do play a role, because two fluorophores are directly compared to each other. The observed gap in maximum recovery between emGFP and mCherry is in the same order of magnitude as the difference in photobleaching efficiency, making it highly likely that this is the cause behind it.

As the most prominent processes for APP in the plasma membrane are Clathrin-mediated endocytosis and α-processing, the effect of the A673T mutation on these mechanisms was investigated. A small, but non-significant difference was found for colocalization between APP and Clathrin (refer to Figure 25). However, should this small difference be real and not due to experimental variability, it might be quite relevant. As cognitive decline is normally a slow process taking many years, the effect of miniscule differences in Clathrin-mediated endocytosis efficiency could become quite

significant over a long time. Maybe, if the experimental set-up would not have been dependent on overexpression, which changes APP membrane distribution as discussed in chapter 5.4., and/or endogenous APP could be removed completely from the system, the difference between WT and A673T could reach statistical significance. Moreover, the fact that the molecular density within the clusters is moderately lower for the A673 mutant, it presents more diffusely and can move more freely in the plasma membrane, all point toward the A673T mutant being more accessible purely in a mechanistic way, making it a fundamentally better candidate for α-cleavage than the WT variant. For some of the mutants, it is known that they change the chance that an APP molecule is processed by either the α- or β-secretase, for example, the K687N and Swedish (KM670/671NL) mutant, respectively. The mutation altering the recognition site for the respective secretase, thereby either increasing secretase efficiency or decreasing it, is usually reported as the causative mechanism. However, this cannot be true for all mutations that result in more Aβ production, while these mutations are simply too far away from the cleavage sites. The A673T mutant also seems to be cleaved more efficiently by α-secretases (refer to Figure 26), besides possibly being endocytosed less readily via Clathrin-mediated endocytosis as well. Interestingly, these two modes of regulation should act on the same level and reinforce each other, because less APP should be available for internalization via Clathrin-mediated endocytosis if more is α-cleaved, while APP resides in the plasma membrane longer allowing more chances to be processed by α-secretases if reinternalization is less efficient. Both mechanisms could, thus, act in harmony to mediate the protective effect of the A673T mutation besides the postulated effects of making the mutant-harboring full-length protein a worse substrate for the β-secretase and the lower aggregation propensity of the mutant Aβ species (Jonsson et al. 2012; Benilova et al. 2014; Maloney et al. 2014).

5.7. Conclusion

To our knowledge this is the first time that such an elaborate quantification of the plasmalemmal clusters of APP has been undertaken. Elucidation of the molecular density of these clusters in human neuronal SH-SY5Y cells lead to a cluster copy number of on average 27 APP molecules and a size of between 65 and 85 nm. This results in an area with a mean radius of just 7 nm that each molecule can inhabit within the cluster, which is already quite crowded as can be observed in Figure 28. However, the model assumes that, irrespective of the cluster size, the APP molecules are spread out evenly over the area the cluster occupies, which is not necessarily the case. In the biological situation, it is far more likely that the molecules in the center of the complex are in closer proximity to each other than the ones on the periphery. Moreover, it has been implied that parts of APP curl back onto the plasma membrane (Song et al. 2014), which has already been taken into consideration in the model. It is also plausible that the SH-SY5Y cell surface measurements are an overestimation, while the plasmalemmal

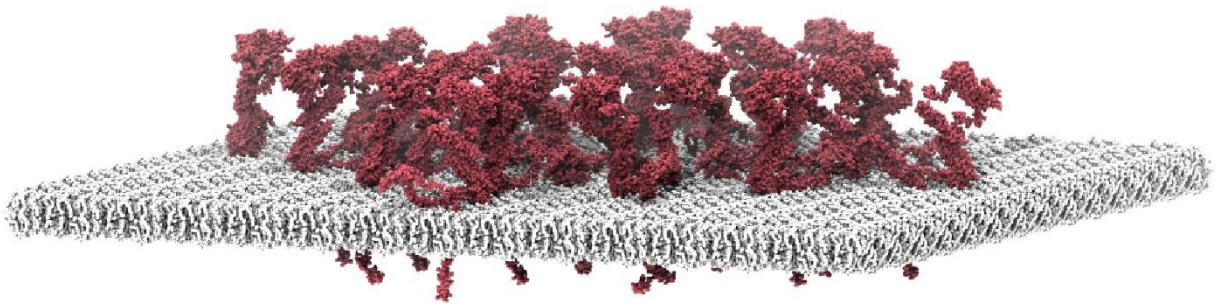

Figure 28. Molecular density of the average APP cluster

A coarse-grain molecular dynamics model that demonstrates the packing density of 27 APP molecules evenly distributed over an area of exactly 77 nm. For details see de Coninck et al. 2018 (Coninck et al. 2018).

APP fraction is probably an underestimate. The size of the clusters, on the other hand, is likely an overestimate because of the reliance on sequential primary-secondary antibody labelling. Additionally, other proteins, such as APLP1 and 2 (Kaden et al. 2009), α-adrenoceptors (Zhang et al. 2017) and low-density lipoprotein receptor-related proteins (Pohlkamp et al. 2017), could be part of the cluster complex as well. All these factors combined contribute to the molecular density within a cluster almost certainly being even higher than demonstrated by the model. Given that the size of the canonical α-secretases is at least comparable to APP, it is extremely reasonable to postulate that the APP molecules not directly at the periphery of the cluster are unavailable for α-processing purely based on steric hindrance. This means that, should one or more physiological parameters in a human being change due to exogenous influences in such a way that APP oligomerization in the cellular plasma membrane is promoted, like plasmalemmal cholesterol build-up during aging, this process might very well be causative in late-onset sporadic AD via this mechanism. Additionally, the to date only protective mutation that has been described in APP, the A673T mutant, has been found to cluster less in the cellular plasma membrane of both neuronal and non-neuronal cells. In live cells, it could also be demonstrated to have an increased plasmalemmal mobility, illustrating the nature of its oligomerization is also more dynamic. Finally, the A673T mutation displayed a slight decrease in correlation to Clathrin-related structures and significantly more cleavage by α-secretases. These last two results link APP clustering dynamics to its processing pathways and strongly imply that clustering is a determinant for the "decision making" whether APP is pathologically cleaved or not, as has also been indicated before (Schneider et al. 2008; Schreiber et al. 2012). Furthermore, this verifies the importance of the N-terminal part of the Aβ domain in the full-length APP for the modulation of clustering and, by extent, its processing. The specific inhibition of plasmalemmal APP clustering, perhaps via pharmacological targeting of the N-terminal Aβ region explicitly, constitutes a novel valid way to combat AD.

5.8. Outlook

In this work the molecular density of plasmalemmal APP cluster was elucidated, which showed that it is highly likely that oligomerization of APP already allows it to evade α-processing. Some factors that could further increase molecular crowding within these clusters have been discussed, but not experimentally addressed here. For example, the possible partner proteins that also reside in these clusters could be identified by immunoprecipitation against a tagged APP followed by mass spectrometry. Colocalization fluorescence microscopy, like the experiment described in Figure 14, could subsequently be used to validate the found proteins. Newly discovered partner proteins could, in addition to increasing molecular cluster density, also uncover novel mechanisms or signaling pathways that APP takes part in, potentially increasing our knowledge regarding its biological function.

There are strong indications for involvement of membrane lipids and especially cholesterol in the development of sporadic AD (Schneider et al. 2008). To deepen our understanding of the effects of membrane lipids on APP oligomerization, these lipids could be enriched or depleted in plasma membranes that overexpress full-length APP coupled to a fluorescent tag. Analysis using the microscopy technique FRAP as presented in Figure 23&24 would uncover any changes in APP mobility due to a changed plasmalemmal microenvironment. This experimental methodology is also well-suited to investigate the effects of various extracellular ion concentrations on APP oligomerization.

To explore whether pharmacological inhibition of APP plasmalemmal clustering is at all feasible, different classes of molecules should be tried. Antibodies directed against the N-terminal Aβ region within the full-length protein are a logical first choice. However, it has already been shown that antibodies directed against other parts of APP induce oligomerization rather than obstruct it. Common anti-aggregation molecules, like Congo Red, curcumin and tannic acid, or more specific ones that have a reported activity against Aβ aggregation, like resveratrol, EGCG and tramiprosate, should also be considered, but are prone to have off-target effects that should be controlled for (Re et al. 2010). Peptide blockers, like the 'Amyloid Blocker' hexamer consisting of the residues QKLVFF available from Sigma Aldrich, on the other hand, could be highly promising in this respect (Mohamed et al. 2016). It is preferable that the read-out for these sorts of screenings is at least somewhat high-throughput such as combining a Förster resonance energy transfer (FRET)-based approach with a fluorescence plate reader.

Better ways to assay APP reinternalization rates are a necessity for the clarification of one of the most important parameters determining amyloidogenic cleavage. One possibility would be a variation on the pulse-chase type experiment utilizing novel fluorescent tag-substrate pairs. For example, by genetically fusing APP to a SNAP-tag from NEB, which is extremely specifically bound by its fluorescent

substrate of which variants exist that are both membrane-impermeable and releasable (Cole and Donaldson 2012). By only briefly incubating overexpressing cells with the substrate, letting the system run for a while, i.e. 30 min, and removing all remaining extracellular substrates again, the only fluorescent signal that should be obtained is that of endocytosed APP. Such a methodology would allow easy and robust quantification of reinternalization rates.

The only mutation that is addressed in this work is the Icelandic A673T variant, however, many more mutations exist close to structures that have been linked to APP oligomerization. Firstly, the A673V, which occurs on the exact same position as the protective mutant but has been described to be pathological. Secondly, the English (H677R), Tottori (D678N) and Taiwanese (D678H) mutations are all close to this N-terminal stretch of 5 aa of the Aβ domain and could theoretically affect APP oligomerization. Thirdly, the set of Flemish (A692G), Arctic (E693G), Dutch (E693Q), Italian (E693K), Osaka (E693Δ) and Iowa (E694N) all occur in or immediately adjacent to a stretch of 6 residues (aa 16-21 of Aβ) that is thought to be the nucleation site of aggregation of the Aβ peptide against which the above-mentioned hexamer peptide is also directed (Mohamed et al. 2016). Lastly, all the mutations that occur close to the GxxxG/A motifs in the TMD (Senes et al. 2004; Munter et al. 2007). Most of these have been linked to altered γ-secretase processing, but they could potentially also affect clustering dynamics because of the postulated importance of these motifs for α-helix oligomerization. In light of the results presented in this work, investigating the effects of these mutations on APP clustering dynamics and, by extent, on cleavage efficiency should provide additional and perhaps novel insights in the relationship between APP oligomerization and processing and might reveal an additional level of regulation by which these mutations exert their pathogenicity.

6. References

Administration on Aging, Administration for Community Living (2016): A Profile of Old Americans. U.S. Department of Health and Human Services, checked on 7/20/2020.

Aizenstein, Howard Jay; Nebes, Robert D.; Saxton, Judith A.; Price, Julie C.; Mathis, Chester A.; Tsopelas, Nicholas D. et al. (2008): Frequent amyloid deposition without significant cognitive impairment among the elderly. In *Archives of neurology* 65 (11), pp. 1509–1517. DOI: 10.1001/archneur.65.11.1509.

Alfert, M.; Geschwind, I. I. (1953): A Selective Staining Method for the Basic Proteins of Cell Nuclei. In *Proceedings of the National Academy of Sciences of the United States of America* 39 (10), pp. 991–999. DOI: 10.1073/pnas.39.10.991.

Ali, Mayssam H.; Imperiali, Barbara (2005): Protein oligomerization: how and why. In *Bioorganic & medicinal chemistry* 13 (17), pp. 5013–5020. DOI: 10.1016/j.bmc.2005.05.037.

Allinson, Tobias M. J.; Parkin, Edward T.; Turner, Anthony J.; Hooper, Nigel M. (2003): ADAMs family members as amyloid precursor protein alpha-secretases. In *Journal of neuroscience research* 74 (3), pp. 342–352. DOI: 10.1002/jnr.10737.

Alois Alzheimer (1911): Über eigenartige Krankheitsfälle des späteren Alters. In *Zeitschrift für die gesamte Neurologie und Psychiatrie* (4), pp. 356–385.

Alzforum: Mutations Database. APP. FBRI LLC. Available online at http://www.alzforum.org/mutations/app, checked on 7/25/2020.

Alzheimer's Association Report (2017): Alzheimer's disease facts and figures (Alzheimer's & Dementia). Available online at https://www.alz.org/media/images/2017-facts-and-figures.pdf, checked on 7/20/2020.

Alzheimer's Disease International (2009): World Alzheimer Report 2009. With assistance of Prof Martin Prince, Mr Jim Jackson. Available online at https://www.alz.co.uk/research/files/WorldAlzheimerReport.pdf.

Anandatheerthavarada, Hindupur K.; Biswas, Gopa; Robin, Marie-Anne; Avadhani, Narayan G. (2003): Mitochondrial targeting and a novel transmembrane arrest of Alzheimer's amyloid precursor protein impairs mitochondrial function in neuronal cells. In *The Journal of cell biology* 161 (1), pp. 41–54. DOI: 10.1083/jcb.200207030.

Ancolio, K.; Dumanchin, C.; Barelli, H.; Warter, J. M.; Brice, A.; Campion, D. et al. (1999): Unusual phenotypic alteration of beta amyloid precursor protein (betaAPP) maturation by a new Val-715 -- Met betaAPP-770 mutation responsible for probable early-onset Alzheimer's disease. In *Proceedings of the National Academy of Sciences of the United States of America* 96 (7), pp. 4119–4124. DOI: 10.1073/pnas.96.7.4119.

Andersen, K.; Launer, L. J.; Dewey, M. E.; Letenneur, L.; Ott, A.; Copeland, J. R. et al. (1999): Gender differences in the incidence of AD and vascular dementia: The EURODEM Studies. EURODEM Incidence Research Group. In *Neurology* 53 (9), pp. 1992–1997. DOI: 10.1212/wnl.53.9.1992.

Ando, K.; Iijima, K. I.; Elliott, J. I.; Kirino, Y.; Suzuki, T. (2001): Phosphorylation-dependent regulation of the interaction of amyloid precursor protein with Fe65 affects the production of beta-amyloid. In *The Journal of biological chemistry* 276 (43), pp. 40353–40361. DOI: 10.1074/jbc.M104059200.

Anstey, Kaarin J.; Lipnicki, Darren M.; Low, Lee-Fay (2008): Cholesterol as a risk factor for dementia and cognitive decline: a systematic review of prospective studies with meta-analysis. In *The American journal of geriatric psychiatry : official journal of the American Association for Geriatric Psychiatry* 16 (5), pp. 343–354. DOI: 10.1097/JGP.0b013e31816b72d4.

Anstey, Kaarin J.; Mack, Holly A.; Cherbuin, Nicolas (2009): Alcohol consumption as a risk factor for dementia and cognitive decline: meta-analysis of prospective studies. In *The American journal of geriatric psychiatry : official journal of the American Association for Geriatric Psychiatry* 17 (7), pp. 542–555. DOI: 10.1097/JGP.0b013e3181a2fd07.

Arialdi M. Minino; Elizabeth Arias; Kenneth D. Kochanek; Sherry L. Murphy; Betty L. Smith (2002): Deaths: Final Data for 2000. Edited by Betty L. Smith. CDC (National Vital Statistics Reports, 15). Available online at https://www.cdc.gov/nchs/data/nvsr/nvsr50/nvsr50_15.pdf, updated on 11/6/2003, checked on 7/20/2020.

Arrighi, Henry Michael; Neumann, Peter J.; Lieberburg, Ivan M.; Townsend, Raymond J. (2010): Lethality of Alzheimer disease and its impact on nursing home placement. In *Alzheimer disease and associated disorders* 24 (1), pp. 90–95. DOI: 10.1097/WAD.0b013e31819fe7d1.

Bamberger, Maria E.; Harris, Meera E.; McDonald, Douglas R.; Husemann, Jens; Landreth, Gary E. (2003): A Cell Surface Receptor Complex for Fibrillar β-Amyloid Mediates Microglial Activation. In *The Journal of neuroscience : the official journal of the Society for Neuroscience* 23 (7), pp. 2665–2674. DOI: 10.1523/JNEUROSCI.23-07-02665.2003.

Bar-On, Dana; Gutman, Menachem; Mezer, Aviv; Ashery, Uri; Lang, Thorsten; Nachliel, Esther (2009): Evaluation of the heterogeneous reactivity of the syntaxin molecules on the inner leaflet of the

plasma membrane. In *The Journal of neuroscience : the official journal of the Society for Neuroscience* 29 (39), pp. 12292–12301. DOI: 10.1523/JNEUROSCI.0710-09.2009.

Barrett, Paul J.; Song, Yuanli; van Horn, Wade D.; Hustedt, Eric J.; Schafer, Johanna M.; Hadziselimovic, Arina et al. (2012): The amyloid precursor protein has a flexible transmembrane domain and binds cholesterol. In *Science (New York, N.Y.)* 336 (6085), pp. 1168–1171. DOI: 10.1126/science.1219988.

Barthet, Gael; Shioi, Junichi; Shao, Zhiping; Ren, Yimin; Georgakopoulos, Anastasios; Robakis, Nikolaos K. (2011): Inhibitors of γ-secretase stabilize the complex and differentially affect processing of amyloid precursor protein and other substrates. In *FASEB journal : official publication of the Federation of American Societies for Experimental Biology* 25 (9), pp. 2937–2946. DOI: 10.1096/fj.11-183806.

Baruch-Suchodolsky, Rozena; Fischer, Bilha (2009): Abeta40, either soluble or aggregated, is a remarkably potent antioxidant in cell-free oxidative systems. In *Biochemistry* 48 (20), pp. 4354–4370. DOI: 10.1021/bi802361k.

Basi, Guriqbal; Frigon, Normand; Barbour, Robin; Doan, Tam; Gordon, Grace; McConlogue, Lisa et al. (2003): Antagonistic effects of beta-site amyloid precursor protein-cleaving enzymes 1 and 2 on beta-amyloid peptide production in cells. In *The Journal of biological chemistry* 278 (34), pp. 31512–31520. DOI: 10.1074/jbc.M300169200.

Batoulis, Helena; Schmidt, Thomas H.; Weber, Pascal; Schloetel, Jan-Gero; Kandt, Christian; Lang, Thorsten (2016): Concentration Dependent Ion-Protein Interaction Patterns Underlying Protein Oligomerization Behaviours. In *Scientific Reports* 6. DOI: 10.1038/srep24131.

Bayer, T. A.; Cappai, R.; Masters, C. L.; Beyreuther, K.; Multhaup, G. (1999): It all sticks together--the APP-related family of proteins and Alzheimer's disease. In *Molecular psychiatry* 4 (6), pp. 524–528. DOI: 10.1038/sj.mp.4000552.

Beck, Martin; Schmidt, Alexander; Malmstroem, Johan; Claassen, Manfred; Ori, Alessandro; Szymborska, Anna et al. (2011): The quantitative proteome of a human cell line. In *Molecular systems biology* 7, p. 549. DOI: 10.1038/msb.2011.82.

Beel, A. J.; Sanders, C. R. (2008): Substrate specificity of gamma-secretase and other intramembrane proteases. In *Cellular and molecular life sciences : CMLS* 65 (9), pp. 1311–1334. DOI: 10.1007/s00018-008-7462-2.

Beel, Andrew J.; Sakakura, Masayoshi; Barrett, Paul J.; Sanders, Charles R. (2010): Direct binding of cholesterol to the amyloid precursor protein: An important interaction in lipid-Alzheimer's disease

relationships? In *Biochimica et biophysica acta* 1801 (8), pp. 975–982. DOI: 10.1016/j.bbalip.2010.03.008.

Beher, D.; Hesse, L.; Masters, C. L.; Multhaup, G. (1996): Regulation of amyloid protein precursor (APP) binding to collagen and mapping of the binding sites on APP and collagen type I. In *The Journal of biological chemistry* 271 (3), pp. 1613–1620. DOI: 10.1074/jbc.271.3.1613.

Belyaev, Nikolai D.; Kellett, Katherine A. B.; Beckett, Caroline; Makova, Natalia Z.; Revett, Timothy J.; Nalivaeva, Natalia N. et al. (2010): The transcriptionally active amyloid precursor protein (APP) intracellular domain is preferentially produced from the 695 isoform of APP in a {beta}-secretase-dependent pathway. In *The Journal of biological chemistry* 285 (53), pp. 41443–41454. DOI: 10.1074/jbc.M110.141390.

Benilova, Iryna; Gallardo, Rodrigo; Ungureanu, Andreea-Alexandra; Castillo Cano, Virginia; an Snellinx; Ramakers, Meine et al. (2014): The Alzheimer disease protective mutation A2T modulates kinetic and thermodynamic properties of amyloid-β (Aβ) aggregation. In *The Journal of biological chemistry* 289 (45), pp. 30977–30989. DOI: 10.1074/jbc.M114.599027.

Benilova, Iryna; Karran, Eric; Strooper, Bart de (2012): The toxic Aβ oligomer and Alzheimer's disease: an emperor in need of clothes. In *Nature neuroscience* 15 (3), pp. 349–357. DOI: 10.1038/nn.3028.

Bergmans, Bruno A.; Shariati, S. Ali M.; Habets, Ron L. P.; Verstreken, Patrik; Schoonjans, Luc; Müller, Ulrike et al. (2010): Neurons generated from APP/APLP1/APLP2 triple knockout embryonic stem cells behave normally in vitro and in vivo: lack of evidence for a cell autonomous role of the amyloid precursor protein in neuronal differentiation. In *Stem cells (Dayton, Ohio)* 28 (3), pp. 399–406. DOI: 10.1002/stem.296.

Berlowitz, L.; Pallotta, D.; Pawlowski, P. (1970): Isolated histone fractions and the alkaline fast green reaction. In *The journal of histochemistry and cytochemistry : official journal of the Histochemistry Society* 18 (5), pp. 334–339. DOI: 10.1177/18.5.334.

Bermejo-Pareja, F.; Benito-León, J.; Vega, S.; Medrano, M. J.; Román, G. C. (2008): Incidence and subtypes of dementia in three elderly populations of central Spain. In *Journal of the neurological sciences* 264 (1-2), pp. 63–72. DOI: 10.1016/j.jns.2007.07.021.

Bertram, Lars; Lange, Christoph; Mullin, Kristina; Parkinson, Michele; Hsiao, Monica; Hogan, Meghan F. et al. (2008): Genome-wide association analysis reveals putative Alzheimer's disease susceptibility loci in addition to APOE. In *American journal of human genetics* 83 (5), pp. 623–632. DOI: 10.1016/j.ajhg.2008.10.008.

Betzaida Tejada-Vera (2013): Mortality From Alzheimer's Disease in the United States. Data for 2000 and 2010. NCHS (Data Brief). Available online at https://www.cdc.gov/nchs/data/databriefs/db116.pdf, checked on 7/20/2020.

Beydoun, M. A.; Beydoun, H. A.; Wang, Y. (2008): Obesity and central obesity as risk factors for incident dementia and its subtypes: a systematic review and meta-analysis. In *Obesity reviews : an official journal of the International Association for the Study of Obesity* 9 (3), pp. 204–218. DOI: 10.1111/j.1467-789X.2008.00473.x.

Beyreuther, K.; Pollwein, P.; Multhaup, G.; Mönning, U.; König, G.; Dyrks, T. et al. (1993): Regulation and expression of the Alzheimer's beta/A4 amyloid protein precursor in health, disease, and Down's syndrome. In *Annals of the New York Academy of Sciences* 695, pp. 91–102. DOI: 10.1111/j.1749-6632.1993.tb23035.x.

Bird, Thomas D. (1993-2020): GeneReviews®. Early-Onset Familial Alzheimer Disease – ARCHIVED CHAPTER, FOR HISTORICAL REFERENCE ONLY. Edited by Margaret P. Adam, Holly H. Ardinger, Roberta A. Pagon, Stephanie E. Wallace, Lora J. H. Bean, Karen Stephens, Anne Amemiya. Seattle (WA). Available online at https://pubmed.ncbi.nlm.nih.gov/20301414/, checked on 7/20/2020.

Bitplane AG (2015): Imaris. Zürich, Switzerland.

Borg, J. P.; Ooi, J.; Levy, E.; Margolis, B. (1996): The phosphotyrosine interaction domains of X11 and FE65 bind to distinct sites on the YENPTY motif of amyloid precursor protein. In *Molecular and cellular biology* 16 (11), pp. 6229–6241. DOI: 10.1128/mcb.16.11.6229.

Braak, H.; Braak, E. (1991): Demonstration of amyloid deposits and neurofibrillary changes in whole brain sections. In *Brain pathology (Zurich, Switzerland)* 1 (3), pp. 213–216. DOI: 10.1111/j.1750-3639.1991.tb00661.x.

Braak, Heiko; Del Tredici, Kelly (2012): Where, when, and in what form does sporadic Alzheimer's disease begin? In *Current opinion in neurology* 25 (6), pp. 708–714. DOI: 10.1097/WCO.0b013e32835a3432.

Bradford, Andrea; Kunik, Mark E.; Schulz, Paul; Williams, Susan P.; Singh, Hardeep (2009): Missed and delayed diagnosis of dementia in primary care: prevalence and contributing factors. In *Alzheimer disease and associated disorders* 23 (4), pp. 306–314. DOI: 10.1097/WAD.0b013e3181a6bebc.

Bressler, S. L.; Gray, M. D.; Sopher, B. L.; Hu, Q.; Hearn, M. G.; Pham, D. G. et al. (1996): cDNA cloning and chromosome mapping of the human Fe65 gene: interaction of the conserved cytoplasmic domains of the human beta-amyloid precursor protein and its homologues with the mouse Fe65 protein. In *Human molecular genetics* 5 (10), pp. 1589–1598. DOI: 10.1093/hmg/5.10.1589.

Bugiani, Orso; Giaccone, Giorgio; Rossi, Giacomina; Mangieri, Michela; Capobianco, Raffaella; Morbin, Michela et al. (2010): Hereditary cerebral hemorrhage with amyloidosis associated with the E693K mutation of APP. In *Archives of neurology* 67 (8), pp. 987–995. DOI: 10.1001/archneurol.2010.178.

Bush, A. I.; Multhaup, G.; Moir, R. D.; Williamson, T. G.; Small, D. H.; Rumble, B. et al. (1993): A novel zinc(II) binding site modulates the function of the beta A4 amyloid protein precursor of Alzheimer's disease. In *The Journal of biological chemistry* 268 (22), pp. 16109–16112.

Cai, H.; Wang, Y.; McCarthy, D.; Wen, H.; Borchelt, D. R.; Price, D. L.; Wong, P. C. (2001): BACE1 is the major beta-secretase for generation of Abeta peptides by neurons. In *Nature neuroscience* 4 (3), pp. 233–234. DOI: 10.1038/85064.

Cai, X. D.; Golde, T. E.; Younkin, S. G. (1993): Release of excess amyloid beta protein from a mutant amyloid beta protein precursor. In *Science (New York, N.Y.)* 259 (5094), pp. 514–516. DOI: 10.1126/science.8424174.

Campion, D.; Dumanchin, C.; Hannequin, D.; Dubois, B.; Belliard, S.; Puel, M. et al. (1999): Early-onset autosomal dominant Alzheimer disease: prevalence, genetic heterogeneity, and mutation spectrum. In *American journal of human genetics* 65 (3), pp. 664–670. DOI: 10.1086/302553.

Casey, David A.; Antimisiaris, Demetra; O'Brien, James (2010): Drugs for Alzheimer's disease: are they effective? In *P & T : a peer-reviewed journal for formulary management* 35 (4), pp. 208–211.

Cebecauer, Marek; Spitaler, Martin; Sergé, Arnauld; Magee, Anthony I. (2010): Signalling complexes and clusters: functional advantages and methodological hurdles. In *Journal of cell science* 123 (Pt 3), pp. 309–320. DOI: 10.1242/jcs.061739.

Chalaris, Athena; Gewiese, Jessica; Paliga, Krzysztof; Fleig, Lina; Schneede, Alex; Krieger, Karsten et al. (2010): ADAM17-mediated shedding of the IL6R induces cleavage of the membrane stub by gamma-secretase. In *Biochimica et biophysica acta* 1803 (2), pp. 234–245. DOI: 10.1016/j.bbamcr.2009.12.001.

Chalupský, K.; Kanchev, I.; Žbodáková, O.; Buryová, H.; Jiroušková, M.; Kořínek, V. et al. (2013): ADAM10/17-dependent release of soluble c-Met correlates with hepatocellular damage. In *Folia biologica* 59 (2), pp. 76–86.

Chang, Keun-A; Kim, Hye-Sun; Ha, Tae-Young; Ha, Ji-Won; Shin, Ki Young; Jeong, Yun Ha et al. (2006): Phosphorylation of Amyloid Precursor Protein (APP) at Thr668 Regulates the Nuclear Translocation of the APP Intracellular Domain and Induces Neurodegeneration. In *Molecular and cellular biology* 26 (11), pp. 4327–4338. DOI: 10.1128/MCB.02393-05.

Chartier-Harlin, M. C.; Crawford, F.; Hamandi, K.; Mullan, M.; Goate, A.; Hardy, J. et al. (1991): Screening for the beta-amyloid precursor protein mutation (APP717: Val----Ile) in extended pedigrees with early onset Alzheimer's disease. In *Neuroscience letters* 129 (1), pp. 134–135. DOI: 10.1016/0304-3940(91)90738-f.

Chen, Wei-Ting; Hong, Chen-Jee; Lin, Ya-Tzu; Chang, Wen-Han; Huang, He-Ting; Liao, Jhih-Ying et al. (2012): Amyloid-beta (Aβ) D7H mutation increases oligomeric Aβ42 and alters properties of Aβ-zinc/copper assemblies. In *PloS one* 7 (4), e35807. DOI: 10.1371/journal.pone.0035807.

Chêne, Geneviève; Beiser, Alexa; Au, Rhoda; Preis, Sarah R.; Wolf, Philip A.; Dufouil, Carole; Seshadri, Sudha (2015): Gender and incidence of dementia in the Framingham Heart Study from mid-adult life. In *Alzheimer's & dementia : the journal of the Alzheimer's Association* 11 (3), pp. 310–320. DOI: 10.1016/j.jalz.2013.10.005.

Chin, Alexander L.; Negash, Selamawit; Hamilton, Roy (2011): Diversity and disparity in dementia: the impact of ethnoracial differences in Alzheimer disease. In *Alzheimer disease and associated disorders* 25 (3), pp. 187–195. DOI: 10.1097/WAD.0b013e318211c6c9.

Cirrito, John R.; Kang, Jae-Eun; Lee, Jiyeon; Stewart, Floy R.; Verges, Deborah K.; Silverio, Luz M. et al. (2008): Endocytosis is required for synaptic activity-dependent release of amyloid-beta in vivo. In *Neuron* 58 (1), pp. 42–51. DOI: 10.1016/j.neuron.2008.02.003.

Cirrito, John R.; Yamada, Kelvin A.; Finn, Mary Beth; Sloviter, Robert S.; Bales, Kelly R.; May, Patrick C. et al. (2005): Synaptic activity regulates interstitial fluid amyloid-beta levels in vivo. In *Neuron* 48 (6), pp. 913–922. DOI: 10.1016/j.neuron.2005.10.028.

Ciuculescu, Eliza-Diana; Mekmouche, Yasmina; Faller, Peter (2005): Metal-binding properties of the peptide APP170-188: a model of the ZnII-binding site of amyloid precursor protein (APP). In *Chemistry (Weinheim an der Bergstrasse, Germany)* 11 (3), pp. 903–909. DOI: 10.1002/chem.200400786.

Clark, M. J.; Gagnon, J.; Williams, A. F.; Barclay, A. N. (1985): MRC OX-2 antigen: a lymphoid/neuronal membrane glycoprotein with a structure like a single immunoglobulin light chain. In *The EMBO journal* 4 (1), pp. 113–118.

Clarris, H. J.; Cappai, R.; Heffernan, D.; Beyreuther, K.; Masters, C. L.; Small, D. H. (1997): Identification of heparin-binding domains in the amyloid precursor protein of Alzheimer's disease by deletion mutagenesis and peptide mapping. In *Journal of neurochemistry* 68 (3), pp. 1164–1172. DOI: 10.1046/j.1471-4159.1997.68031164.x.

Cole, Nelson B.; Donaldson, Julie G. (2012): Releasable SNAP-tag probes for studying endocytosis and recycling. In *ACS chemical biology* 7 (3), pp. 464–469. DOI: 10.1021/cb2004252.

Coninck, Dennis de; Schmidt, Thomas H.; Schloetel, Jan-Gero; Lang, Thorsten (2018): Packing Density of the Amyloid Precursor Protein in the Cell Membrane. In *Biophysical journal* 114 (5), pp. 1128–1141. DOI: 10.1016/j.bpj.2018.01.009.

Copeland, Courtney A.; Han, Bing; Tiwari, Ajit; Austin, Eric D.; Loyd, James E.; West, James D.; Kenworthy, Anne K. (2017): A disease-associated frameshift mutation in caveolin-1 disrupts caveolae formation and function through introduction of a de novo ER retention signal. In *Molecular biology of the cell* 28 (22), pp. 3095–3111. DOI: 10.1091/mbc.E17-06-0421.

Corder, E. H.; Saunders, A. M.; Risch, N. J.; Strittmatter, W. J.; Schmechel, D. E.; Gaskell, P. C. et al. (1994): Protective effect of apolipoprotein E type 2 allele for late onset Alzheimer disease. In *Nature genetics* 7 (2), pp. 180–184. DOI: 10.1038/ng0694-180.

Cossec, Jack-Christophe; Simon, Anne; Marquer, Catherine; Moldrich, Randal X.; Leterrier, Christophe; Rossier, Jean et al. (2010): Clathrin-dependent APP endocytosis and Abeta secretion are highly sensitive to the level of plasma membrane cholesterol. In *Biochimica et biophysica acta* 1801 (8), pp. 846–852. DOI: 10.1016/j.bbalip.2010.05.010.

Crews, Leslie; Masliah, Eliezer (2010): Molecular mechanisms of neurodegeneration in Alzheimer's disease. In *Human molecular genetics* 19 (R1), R12-20. DOI: 10.1093/hmg/ddq160.

Cruchaga, Carlos; Karch, Celeste M.; Jin, Sheng Chih; Benitez, Bruno A.; Cai, Yefei; Guerreiro, Rita et al. (2014): Rare coding variants in the phospholipase D3 gene confer risk for Alzheimer's disease. In *Nature* 505 (7484), pp. 550–554. DOI: 10.1038/nature12825.

Cruts, Marc; Dermaut, Bart; Rademakers, Rosa; van den Broeck, Marleen; Stögbauer, Florian; van Broeckhoven, Christine (2003): Novel APP mutation V715A associated with presenile Alzheimer's disease in a German family. In *Journal of neurology* 250 (11), pp. 1374–1375. DOI: 10.1007/s00415-003-0182-5.

Cureton, David K.; Harbison, Carole E.; Cocucci, Emanuele; Parrish, Colin R.; Kirchhausen, Tom (2012): Limited transferrin receptor clustering allows rapid diffusion of canine parvovirus into clathrin endocytic structures. In *Journal of virology* 86 (9), pp. 5330–5340. DOI: 10.1128/JVI.07194-11.

Dahms, Sven O.; Hoefgen, Sandra; Roeser, Dirk; Schlott, Bernhard; Gührs, Karl-Heinz; Than, Manuel E. (2010): Structure and biochemical analysis of the heparin-induced E1 dimer of the amyloid precursor protein. In *Proceedings of the National Academy of Sciences of the United States of America* 107 (12), pp. 5381–5386. DOI: 10.1073/pnas.0911326107.

Dahms, Sven O.; Könnig, Ina; Roeser, Dirk; Gührs, Karl-Heinz; Mayer, Magnus C.; Kaden, Daniela et al. (2012): Metal binding dictates conformation and function of the amyloid precursor protein (APP) E2 domain. In *Journal of molecular biology* 416 (3), pp. 438–452. DOI: 10.1016/j.jmb.2011.12.057.

Daigle, I.; Li, C. (1993): apl-1, a Caenorhabditis elegans gene encoding a protein related to the human beta-amyloid protein precursor. In *Proceedings of the National Academy of Sciences of the United States of America* 90 (24), pp. 12045–12049. DOI: 10.1073/pnas.90.24.12045.

Danziger, John; Zeidel, Mark L. (2015): Osmotic homeostasis. In *Clinical journal of the American Society of Nephrology : CJASN* 10 (5), pp. 852–862. DOI: 10.2215/CJN.10741013.

Dawson, G. R.; Seabrook, G. R.; Zheng, H.; Smith, D. W.; Graham, S.; O'Dowd, G. et al. (1999): Age-related cognitive deficits, impaired long-term potentiation and reduction in synaptic marker density in mice lacking the beta-amyloid precursor protein. In *Neuroscience* 90 (1), pp. 1–13. DOI: 10.1016/s0306-4522(98)00410-2.

Destainville, Nicolas; Manghi, Manoel; Cornet, Julie (2018): A Rationale for Mesoscopic Domain Formation in Biomembranes. In *Biomolecules* 8 (4). DOI: 10.3390/biom8040104.

Di Fede, Giuseppe; Catania, Marcella; Morbin, Michela; Giaccone, Giorgio; Moro, Maria Luisa; Ghidoni, Roberta et al. (2012): Good gene, bad gene: new APP variant may be both. In *Progress in neurobiology* 99 (3), pp. 281–292. DOI: 10.1016/j.pneurobio.2012.06.004.

Di Fede, Giuseppe; Catania, Marcella; Morbin, Michela; Rossi, Giacomina; Suardi, Silvia; Mazzoleni, Giulia et al. (2009): A recessive mutation in the APP gene with dominant-negative effect on amyloidogenesis. In *Science (New York, N.Y.)* 323 (5920), pp. 1473–1477. DOI: 10.1126/science.1168979.

Dodart, Jean-Cosme; Bales, Kelly R.; Gannon, Kimberley S.; Greene, Stephen J.; DeMattos, Ronald B.; Mathis, Chantal et al. (2002): Immunization reverses memory deficits without reducing brain Abeta burden in Alzheimer's disease model. In *Nature neuroscience* 5 (5), pp. 452–457. DOI: 10.1038/nn842.

Dodge, Hiroko H.; Shen, Changyu; Pandav, Rajesh; DeKosky, Steven T.; Ganguli, Mary (2003): Functional transitions and active life expectancy associated with Alzheimer disease. In *Archives of neurology* 60 (2), pp. 253–259. DOI: 10.1001/archneur.60.2.253.

Drummond, Eleanor; Wisniewski, Thomas (2017): Alzheimer's disease: experimental models and reality. In *Acta neuropathologica* 133 (2), pp. 155–175. DOI: 10.1007/s00401-016-1662-x.

Dulubova, Irina; Ho, Angela; Huryeva, Iryna; Südhof, Thomas C.; Rizo, Josep (2004): Three-dimensional structure of an independently folded extracellular domain of human amyloid-beta precursor protein. In *Biochemistry* 43 (30), pp. 9583–9588. DOI: 10.1021/bi049041o.

Dumon-Seignovert, Laurence; Cariot, Guillaume; Vuillard, Laurent (2004): The toxicity of recombinant proteins in Escherichia coli: a comparison of overexpression in BL21(DE3), C41(DE3), and C43(DE3). In *Protein expression and purification* 37 (1), pp. 203–206. DOI: 10.1016/j.pep.2004.04.025.

Dumortier, Hélène; van Mierlo, Geertje J. D.; Egan, Deirdre; van Ewijk, Willem; Toes, René E. M.; Offringa, Rienk; Melief, Cornelis J. M. (2005): Antigen presentation by an immature myeloid dendritic cell line does not cause CTL deletion in vivo, but generates CD8+ central memory-like T cells that can be rescued for full effector function. In *Journal of immunology (Baltimore, Md. : 1950)* 175 (2), pp. 855–863. DOI: 10.4049/jimmunol.175.2.855.

Eckman, C. B.; Mehta, N. D.; Crook, R.; Perez-tur, J.; Prihar, G.; Pfeiffer, E. et al. (1997): A new pathogenic mutation in the APP gene (I716V) increases the relative proportion of A beta 42(43). In *Human molecular genetics* 6 (12), pp. 2087–2089. DOI: 10.1093/hmg/6.12.2087.

Eggert, Simone; Paliga, Krzysztof; Soba, Peter; Evin, Genevieve; Masters, Colin L.; Weidemann, Andreas; Beyreuther, Konrad (2004): The proteolytic processing of the amyloid precursor protein gene family members APLP-1 and APLP-2 involves alpha-, beta-, gamma-, and epsilon-like cleavages: modulation of APLP-1 processing by n-glycosylation. In *The Journal of biological chemistry* 279 (18), pp. 18146–18156. DOI: 10.1074/jbc.M311601200.

Ehehalt, Robert; Keller, Patrick; Haass, Christian; Thiele, Christoph; Simons, Kai (2003): Amyloidogenic processing of the Alzheimer beta-amyloid precursor protein depends on lipid rafts. In *The Journal of cell biology* 160 (1), pp. 113–123. DOI: 10.1083/jcb.200207113.

Eisenberg, Sharon; Beckett, Alison J.; Prior, Ian A.; Dekker, Frank J.; Hedberg, Christian; Waldmann, Herbert et al. (2011): Raft protein clustering alters N-Ras membrane interactions and activation pattern. In *Molecular and cellular biology* 31 (19), pp. 3938–3952. DOI: 10.1128/MCB.05570-11.

Encinas, M.; Iglesias, M.; Liu, Y.; Wang, H.; Muhaisen, A.; Ceña, V. et al. (2000): Sequential treatment of SH-SY5Y cells with retinoic acid and brain-derived neurotrophic factor gives rise to fully differentiated, neurotrophic factor-dependent, human neuron-like cells. In *Journal of neurochemistry* 75 (3), pp. 991–1003. DOI: 10.1046/j.1471-4159.2000.0750991.x.

Essa, M. Mohamed; Akbar, Mohammed; Guillemin, Gilles (2016): The benefits of natural products for neurodegenerative diseases. Switzerland: Springer (Advances in neurobiology, volume 12).

Ewald, Collin Y.; Raps, Daniel A.; Li, Chris (2012): APL-1, the Alzheimer's Amyloid precursor protein in Caenorhabditis elegans, modulates multiple metabolic pathways throughout development. In *Genetics* 191 (2), pp. 493–507. DOI: 10.1534/genetics.112.138768.

Farrer, L. A.; Cupples, L. A.; Haines, J. L.; Hyman, B.; Kukull, W. A.; Mayeux, R. et al. (1997): Effects of age, sex, and ethnicity on the association between apolipoprotein E genotype and Alzheimer disease. A meta-analysis. APOE and Alzheimer Disease Meta Analysis Consortium. In *JAMA* 278 (16), pp. 1349–1356.

Farrer, L. A.; Myers, R. H.; Cupples, L. A.; St George-Hyslop, P. H.; Bird, T. D.; Rossor, M. N. et al. (1990): Transmission and age-at-onset patterns in familial Alzheimer's disease: evidence for heterogeneity. In *Neurology* 40 (3 Pt 1), pp. 395–403. DOI: 10.1212/wnl.40.3_part_1.395.

Fazzari, Pietro; Horre, Katrien; Arranz, Amaia M.; Frigerio, Carlo Sala; Saito, Takashi; Saido, Takaomi C.; Strooper, Bart de (2017): PLD3 gene and processing of APP. In *Nature* 541 (7638), E1-E2. DOI: 10.1038/nature21030.

Ferrer, Manuel; Chernikova, Tatyana N.; Yakimov, Michail M.; Golyshin, Peter N.; Timmis, Kenneth N. (2003): Chaperonins govern growth of Escherichia coli at low temperatures. In *Nature biotechnology* 21 (11), pp. 1266–1267. DOI: 10.1038/nbt1103-1266.

Ferri, Cleusa P.; Prince, Martin; Brayne, Carol; Brodaty, Henry; Fratiglioni, Laura; Ganguli, Mary et al. (2005): Global prevalence of dementia: a Delphi consensus study. In *Lancet (London, England)* 366 (9503), pp. 2112–2117. DOI: 10.1016/S0140-6736(05)67889-0.

Fiore, F.; Zambrano, N.; Minopoli, G.; Donini, V.; Duilio, A.; Russo, T. (1995): The regions of the Fe65 protein homologous to the phosphotyrosine interaction/phosphotyrosine binding domain of Shc bind the intracellular domain of the Alzheimer's amyloid precursor protein. In *The Journal of biological chemistry* 270 (52), pp. 30853–30856. DOI: 10.1074/jbc.270.52.30853.

Fogel, Hilla; Frere, Samuel; Segev, Oshik; Bharill, Shashank; Shapira, Ilana; Gazit, Neta et al. (2014): APP homodimers transduce an amyloid-β-mediated increase in release probability at excitatory synapses. In *Cell reports* 7 (5), pp. 1560–1576. DOI: 10.1016/j.celrep.2014.04.024.

Fox, C. H.; Johnson, F. B.; Whiting, J.; Roller, P. P. (1985): Formaldehyde fixation. In *The journal of histochemistry and cytochemistry : official journal of the Histochemistry Society* 33 (8), pp. 845–853. DOI: 10.1177/33.8.3894502.

Frick, Manfred; Schmidt, Katja; Nichols, Benjamin J. (2007): Modulation of lateral diffusion in the plasma membrane by protein density. In *Current biology : CB* 17 (5), pp. 462–467. DOI: 10.1016/j.cub.2007.01.069.

Friedman, Esther M.; Shih, Regina A.; Langa, Kenneth M.; Hurd, Michael D. (2015): US Prevalence And Predictors Of Informal Caregiving For Dementia. In *Health affairs (Project Hope)* 34 (10), pp. 1637–1641. DOI: 10.1377/hlthaff.2015.0510.

Fukumori, Akio; Okochi, Masayasu; Tagami, Shinji; Jiang, Jingwei; Itoh, Naohiro; Nakayama, Taisuke et al. (2006): Presenilin-dependent gamma-secretase on plasma membrane and endosomes is functionally distinct. In *Biochemistry* 45 (15), pp. 4907–4914. DOI: 10.1021/bi052412w.

Gagné, François (2014): Tissue Preparation and Subcellular Fractionation Techniques. In François Gagné (Ed.): Biochemical ecotoxicology. Principles and methods / by François Gagné. Amsterdam: Academic Press, pp. 21–31.

Galmes, Romain; Delaunay, Jean-Louis; Maurice, Michèle; Aït-Slimane, Tounsia (2013): Oligomerization is required for normal endocytosis/transcytosis of a GPI-anchored protein in polarized hepatic cells. In *Journal of cell science* 126 (Pt 15), pp. 3409–3416. DOI: 10.1242/jcs.126250.

Gandy, S.; Czernik, A. J.; Greengard, P. (1988): Phosphorylation of Alzheimer disease amyloid precursor peptide by protein kinase C and Ca2+/calmodulin-dependent protein kinase II. In *Proceedings of the National Academy of Sciences of the United States of America* 85 (16), pp. 6218–6221.

Ganguli, Mary; Dodge, Hiroko H.; Shen, Changyu; Pandav, Rajesh S.; DeKosky, Steven T. (2005): Alzheimer disease and mortality: a 15-year epidemiological study. In *Archives of neurology* 62 (5), pp. 779–784. DOI: 10.1001/archneur.62.5.779.

Gefen, Tamar; Peterson, Melanie; Papastefan, Steven T.; Martersteck, Adam; Whitney, Kristen; Rademaker, Alfred et al. (2015): Morphometric and histologic substrates of cingulate integrity in elders with exceptional memory capacity. In *The Journal of neuroscience : the official journal of the Society for Neuroscience* 35 (4), pp. 1781–1791. DOI: 10.1523/JNEUROSCI.2998-14.2015.

Georgiou, Christos D.; Grintzalis, Konstantinos; Zervoudakis, George; Papapostolou, Ioannis (2008): Mechanism of Coomassie brilliant blue G-250 binding to proteins: a hydrophobic assay for nanogram quantities of proteins. In *Analytical and bioanalytical chemistry* 391 (1), pp. 391–403. DOI: 10.1007/s00216-008-1996-x.

Ghidoni, Roberta; Albertini, Valentina; Squitti, Rosanna; Paterlini, Anna; Bruno, Anna; Bernardini, Silvia et al. (2009): Novel T719P AbetaPP mutation unbalances the relative proportion of amyloid-beta peptides. In *Journal of Alzheimer's disease : JAD* 18 (2), pp. 295–303. DOI: 10.3233/JAD-2009-1142.

Ghosal, Kaushik; Vogt, Daniel L.; Liang, Man; Shen, Yong; Lamb, Bruce T.; Pimplikar, Sanjay W. (2009): Alzheimer's disease-like pathological features in transgenic mice expressing the APP intracellular domain. In *Proceedings of the National Academy of Sciences of the United States of America* 106 (43), pp. 18367–18372. DOI: 10.1073/pnas.0907652106.

Giordano, Francesca; Saheki, Yasunori; Idevall-Hagren, Olof; Colombo, Sara Francesca; Pirruccello, Michelle; Milosevic, Ira et al. (2013): PI(4,5)P(2)-dependent and Ca(2+)-regulated ER-PM interactions mediated by the extended synaptotagmins. In *Cell* 153 (7), pp. 1494–1509. DOI: 10.1016/j.cell.2013.05.026.

Glenner, George G.; Wong, Caine W. (1984a): Alzheimer's disease and Down's syndrome: Sharing of a unique cerebrovascular amyloid fibril protein. In *Biochemical and Biophysical Research Communications* 122 (3), pp. 1131–1135. DOI: 10.1016/0006-291X(84)91209-9.

Glenner, George G.; Wong, Caine W. (1984b): Alzheimer's disease: Initial report of the purification and characterization of a novel cerebrovascular amyloid protein. In *Biochemical and Biophysical Research Communications* 120 (3), pp. 885–890. DOI: 10.1016/S0006-291X(84)80190-4.

Goate, A.; Chartier-Harlin, M. C.; Mullan, M.; Brown, J.; Crawford, F.; Fidani, L. et al. (1991): Segregation of a missense mutation in the amyloid precursor protein gene with familial Alzheimer's disease. In *Nature* 349 (6311), pp. 704–706. DOI: 10.1038/349704a0.

Goldgaber, D.; Lerman, M. I.; McBride, O. W.; Saffiotti, U.; Gajdusek, D. C. (1987): Characterization and chromosomal localization of a cDNA encoding brain amyloid of Alzheimer's disease. In *Science (New York, N.Y.)* 235 (4791), pp. 877–880. DOI: 10.1126/science.3810169.

Gonzalez-Lozano, M. A.; Koopmans, F.; Sullivan, P. F.; Protze, J.; Krause, G.; Verhage, M. et al. (2020): Stitching the synapse: Cross-linking mass spectrometry into resolving synaptic protein interactions. In *Science advances* 6 (8), eaax5783. DOI: 10.1126/sciadv.aax5783.

Goodsell, D. S.; Olson, A. J. (2000): Structural symmetry and protein function. In *Annual review of biophysics and biomolecular structure* 29, pp. 105–153. DOI: 10.1146/annurev.biophys.29.1.105.

Gorman, Paul M.; Kim, Sanguk; Guo, Meng; Melnyk, Roman A.; McLaurin, Joanne; Fraser, Paul E. et al. (2008): Dimerization of the transmembrane domain of amyloid precursor proteins and familial Alzheimer's disease mutants. In *BMC Neuroscience* 9, p. 17. DOI: 10.1186/1471-2202-9-17.

Götz, J.; Streffer, J. R.; David, D.; Schild, A.; Hoerndli, F.; Pennanen, L. et al. (2004): Transgenic animal models of Alzheimer's disease and related disorders: histopathology, behavior and therapy. In *Molecular psychiatry* 9 (7), pp. 664–683. DOI: 10.1038/sj.mp.4001508.

Gralle, Matthias; Botelho, Michelle M.; Oliveira, Cristiano L. P. de; Torriani, Iris; Ferreira, Sérgio T. (2002): Solution studies and structural model of the extracellular domain of the human amyloid precursor protein. In *Biophysical journal* 83 (6), pp. 3513–3524. DOI: 10.1016/S0006-3495(02)75351-4.

Gralle, Matthias; Ferreira, Sérgio T. (2007): Structure and functions of the human amyloid precursor protein: the whole is more than the sum of its parts. In *Progress in neurobiology* 82 (1), pp. 11–32. DOI: 10.1016/j.pneurobio.2007.02.001.

Gralle, Matthias; Oliveira, Cristiano L. P.; Guerreiro, Luiz H.; McKinstry, William J.; Galatis, Denise; Masters, Colin L. et al. (2006): Solution conformation and heparin-induced dimerization of the full-length extracellular domain of the human amyloid precursor protein. In *Journal of molecular biology* 357 (2), pp. 493–508. DOI: 10.1016/j.jmb.2005.12.053.

Greenfield, J. P.; Tsai, J.; Gouras, G. K.; Hai, B.; Thinakaran, G.; Checler, F. et al. (1999): Endoplasmic reticulum and trans-Golgi network generate distinct populations of Alzheimer beta-amyloid peptides. In *Proceedings of the National Academy of Sciences of the United States of America* 96 (2), pp. 742–747. DOI: 10.1073/pnas.96.2.742.

Groemer, Teja W.; Thiel, Cora S.; Holt, Matthew; Riedel, Dietmar; Hua, Yunfeng; Hüve, Jana et al. (2011): Amyloid precursor protein is trafficked and secreted via synaptic vesicles. In *PloS one* 6 (4), e18754. DOI: 10.1371/journal.pone.0018754.

Guerreiro, Rita; Wojtas, Aleksandra; Bras, Jose; Carrasquillo, Minerva; Rogaeva, Ekaterina; Majounie, Elisa et al. (2013): TREM2 variants in Alzheimer's disease. In *The New England journal of medicine* 368 (2), pp. 117–127. DOI: 10.1056/NEJMoa1211851.

Guerreiro, Rita Joao; Baquero, Miquel; Blesa, Rafael; Boada, Mercè; Brás, Jose Miguel; Bullido, Maria J. et al. (2010): Genetic screening of Alzheimer's disease genes in Iberian and African samples yields novel mutations in presenilins and APP. In *Neurobiology of aging* 31 (5), pp. 725–731. DOI: 10.1016/j.neurobiolaging.2008.06.012.

Haapasalo, Annakaisa; Kovacs, Dora M. (2011): The many substrates of presenilin/γ-secretase. In *Journal of Alzheimer's disease : JAD* 25 (1), pp. 3–28. DOI: 10.3233/JAD-2011-101065.

Haass, C.; Hung, A. Y.; Selkoe, D. J.; Teplow, D. B. (1994): Mutations associated with a locus for familial Alzheimer's disease result in alternative processing of amyloid beta-protein precursor. In *The Journal of biological chemistry* 269 (26), pp. 17741–17748.

Haass, C.; Koo, E. H.; Mellon, A.; Hung, A. Y.; Selkoe, D. J. (1992): Targeting of cell-surface beta-amyloid precursor protein to lysosomes: alternative processing into amyloid-bearing fragments. In *Nature* 357 (6378), pp. 500–503. DOI: 10.1038/357500a0.

Haass, Christian; Kaether, Christoph; Thinakaran, Gopal; Sisodia, Sangram (2012): Trafficking and proteolytic processing of APP. In *Cold Spring Harbor perspectives in medicine* 2 (5), a006270. DOI: 10.1101/cshperspect.a006270.

Hamer, M.; Chida, Y. (2009): Physical activity and risk of neurodegenerative disease: a systematic review of prospective evidence. In *Psychological medicine* 39 (1), pp. 3–11. DOI: 10.1017/S0033291708003681.

Hardy, J. A.; Higgins, G. A. (1992): Alzheimer's disease: the amyloid cascade hypothesis. In *Science (New York, N.Y.)* 256 (5054), pp. 184–185. DOI: 10.1126/science.1566067.

Hardy, John (2009): The amyloid hypothesis for Alzheimer's disease: a critical reappraisal. In *Journal of neurochemistry* 110 (4), pp. 1129–1134. DOI: 10.1111/j.1471-4159.2009.06181.x.

Harold, Denise; Abraham, Richard; Hollingworth, Paul; Sims, Rebecca; Gerrish, Amy; Hamshere, Marian L. et al. (2009): Genome-wide association study identifies variants at CLU and PICALM associated with Alzheimer's disease. In *Nature genetics* 41 (10), pp. 1088–1093. DOI: 10.1038/ng.440.

Harris, Benjamin; Pereira, Isabel; Parkin, Edward (2009): Targeting ADAM10 to lipid rafts in neuroblastoma SH-SY5Y cells impairs amyloidogenic processing of the amyloid precursor protein. In *Brain Research* 1296, pp. 203–215. DOI: 10.1016/j.brainres.2009.07.105.

Harvey, R. J.; Skelton-Robinson, M.; Rossor, M. N. (2003): The prevalence and causes of dementia in people under the age of 65 years. In *Journal of neurology, neurosurgery, and psychiatry* 74 (9), pp. 1206–1209. DOI: 10.1136/jnnp.74.9.1206.

Hashimoto, Yuichi; Matsuoka, Masaaki (2014): A mutation protective against Alzheimer's disease renders amyloid β precursor protein incapable of mediating neurotoxicity. In *Journal of neurochemistry* 130 (2), pp. 291–300. DOI: 10.1111/jnc.12717.

Heber, S.; Herms, J.; Gajic, V.; Hainfellner, J.; Aguzzi, A.; Rülicke, T. et al. (2000): Mice with combined gene knock-outs reveal essential and partially redundant functions of amyloid precursor protein family members. In *The Journal of neuroscience : the official journal of the Society for Neuroscience* 20 (21), pp. 7951–7963.

Hebert, Liesi E.; Weuve, Jennifer; Scherr, Paul A.; Evans, Denis A. (2013): Alzheimer disease in the United States (2010-2050) estimated using the 2010 census. In *Neurology* 80 (19), pp. 1778–1783. DOI: 10.1212/WNL.0b013e31828726f5.

Herms, Jochen; Anliker, Brigitte; Heber, Sabine; Ring, Sabine; Fuhrmann, Martin; Kretzschmar, Hans et al. (2004): Cortical dysplasia resembling human type 2 lissencephaly in mice lacking all three APP family members. In *The EMBO journal* 23 (20), pp. 4106–4115. DOI: 10.1038/sj.emboj.7600390.

an Herreman; van Gassen, Geert; Bentahir, Mustapha; Nyabi, Omar; Craessaerts, Katleen; Mueller, Ulrike et al. (2003): gamma-Secretase activity requires the presenilin-dependent trafficking of nicastrin through the Golgi apparatus but not its complex glycosylation. In *Journal of cell science* 116 (Pt 6), pp. 1127–1136. DOI: 10.1242/jcs.00292.

Hesse, L.; Beher, D.; Masters, C. L.; Multhaup, G. (1994): The beta A4 amyloid precursor protein binding to copper. In *FEBS letters* 349 (1), pp. 109–116. DOI: 10.1016/0014-5793(94)00658-x.

Hillen, Heinz (2019): The Beta Amyloid Dysfunction (BAD) Hypothesis for Alzheimer's Disease. In *Frontiers in neuroscience* 13, p. 1154. DOI: 10.3389/fnins.2019.01154.

Ho, Angela; Südhof, Thomas C. (2004): Binding of F-spondin to amyloid-beta precursor protein: a candidate amyloid-beta precursor protein ligand that modulates amyloid-beta precursor protein cleavage. In *Proceedings of the National Academy of Sciences of the United States of America* 101 (8), pp. 2548–2553. DOI: 10.1073/pnas.0308655100.

Hoffmann, Else K.; Lambert, Ian H.; Pedersen, Stine F. (2009): Physiology of cell volume regulation in vertebrates. In *Physiological reviews* 89 (1), pp. 193–277. DOI: 10.1152/physrev.00037.2007.

Hofman, Erik G.; Bader, Arjen N.; Voortman, Jarno; van den Heuvel, Dave J.; Sigismund, Sara; Verkleij, Arie J. et al. (2010): Ligand-induced EGF receptor oligomerization is kinase-dependent and enhances internalization. In *The Journal of biological chemistry* 285 (50), pp. 39481–39489. DOI: 10.1074/jbc.M110.164731.

Hollingworth, Paul; Harold, Denise; Sims, Rebecca; Gerrish, Amy; Lambert, Jean-Charles; Carrasquillo, Minerva M. et al. (2011): Common variants at ABCA7, MS4A6A/MS4A4E, EPHA1, CD33 and CD2AP are associated with Alzheimer's disease. In *Nature genetics* 43 (5), pp. 429–435. DOI: 10.1038/ng.803.

Hori, Yukiko; Hashimoto, Tadafumi; Wakutani, Yosuke; Urakami, Katsuya; Nakashima, Kenji; Condron, Margaret M. et al. (2007): The Tottori (D7N) and English (H6R) familial Alzheimer disease mutations accelerate Abeta fibril formation without increasing protofibril formation. In *The Journal of biological chemistry* 282 (7), pp. 4916–4923. DOI: 10.1074/jbc.M608220200.

Hornsten, Angela; Lieberthal, Jason; Fadia, Shruti; Malins, Richard; Ha, Lawrence; Xu, Xiaomeng et al. (2007): APL-1, a Caenorhabditis elegans protein related to the human beta-amyloid precursor

protein, is essential for viability. In *Proceedings of the National Academy of Sciences of the United States of America* 104 (6), pp. 1971–1976. DOI: 10.1073/pnas.0603997104.

Hsieh, Helen; Boehm, Jannic; Sato, Chihiro; Iwatsubo, Takeshi; Tomita, Taisuke; Sisodia, Sangram; Malinow, Roberto (2006): AMPAR removal underlies Abeta-induced synaptic depression and dendritic spine loss. In *Neuron* 52 (5), pp. 831–843. DOI: 10.1016/j.neuron.2006.10.035.

Hsu, Simon; Gordon, Brian A.; Hornbeck, Russ; Norton, Joanne B.; Levitch, Denise; Louden, Adia et al. (2018): Discovery and validation of autosomal dominant Alzheimer's disease mutations. In *Alzheimer's research & therapy* 10 (1), p. 67. DOI: 10.1186/s13195-018-0392-9.

Hu, Nan; Yu, Jin-Tai; Tan, Lin; Wang, Ying-Li; Sun, Lei; Tan, Lan (2013): Nutrition and the risk of Alzheimer's disease. In *BioMed research international* 2013, p. 524820. DOI: 10.1155/2013/524820.

Huang, Li-Kai; Chao, Shu-Ping; Hu, Chaur-Jong (2020): Clinical trials of new drugs for Alzheimer disease. In *Journal of biomedical science* 27 (1), p. 18. DOI: 10.1186/s12929-019-0609-7.

Hung, A. Y.; Haass, C.; Nitsch, R. M.; Qiu, W. Q.; Citron, M.; Wurtman, R. J. et al. (1993): Activation of protein kinase C inhibits cellular production of the amyloid beta-protein. In *The Journal of biological chemistry* 268 (31), pp. 22959–22962.

Huotari, Jatta; Helenius, Ari (2011): Endosome maturation. In *The EMBO journal* 30 (17), pp. 3481–3500. DOI: 10.1038/emboj.2011.286.

Hurd, Michael D.; Martorell, Paco; Langa, Kenneth M. (2013): Monetary costs of dementia in the United States. In *The New England journal of medicine* 369 (5), pp. 489–490. DOI: 10.1056/NEJMc1305541.

Huse, Jason T.; Liu, Kangning; Pijak, Donald S.; Carlin, Dan; Lee, Virginia M-Y; Doms, Robert W. (2002): Beta-secretase processing in the trans-Golgi network preferentially generates truncated amyloid species that accumulate in Alzheimer's disease brain. In *The Journal of biological chemistry* 277 (18), pp. 16278–16284. DOI: 10.1074/jbc.M111141200.

Igbavboa, U.; Sun, G. Y.; Weisman, G. A.; He, Yan; Wood, W. G. (2009): Amyloid beta-protein stimulates trafficking of cholesterol and caveolin-1 from the plasma membrane to the Golgi complex in mouse primary astrocytes. In *Neuroscience* 162 (2), pp. 328–338. DOI: 10.1016/j.neuroscience.2009.04.049.

Imbimbo, Bruno P. (2009): An update on the efficacy of non-steroidal anti-inflammatory drugs in Alzheimer's disease. In *Expert opinion on investigational drugs* 18 (8), pp. 1147–1168. DOI: 10.1517/13543780903066780.

Isbert, Simone; Wagner, Katja; Eggert, Simone; Schweitzer, Andrea; Multhaup, Gerd; Weggen, Sascha et al. (2012): APP dimer formation is initiated in the endoplasmic reticulum and differs between APP isoforms. In *Cellular and molecular life sciences : CMLS* 69 (8), pp. 1353–1375. DOI: 10.1007/s00018-011-0882-4.

Itano, Michelle S.; Steinhauer, Christian; Schmied, Jürgen J.; Forthmann, Carsten; Liu, Ping; Neumann, Aaron K. et al. (2012): Super-resolution imaging of C-type lectin and influenza hemagglutinin nanodomains on plasma membranes using blink microscopy. In *Biophysical journal* 102 (7), pp. 1534–1542. DOI: 10.1016/j.bpj.2012.02.022.

Ittner, Lars M.; Götz, Jürgen (2011): Amyloid-β and tau--a toxic pas de deux in Alzheimer's disease. In *Nature reviews. Neuroscience* 12 (2), pp. 65–72. DOI: 10.1038/nrn2967.

Ittner, Lars M.; Ke, Yazi D.; Delerue, Fabien; Bi, Mian; Gladbach, Amadeus; van Eersel, Janet et al. (2010): Dendritic function of tau mediates amyloid-beta toxicity in Alzheimer's disease mouse models. In *Cell* 142 (3), pp. 387–397. DOI: 10.1016/j.cell.2010.06.036.

Jamur, M. C.; Faraco, C. D.; Lunardi, L. O.; Siraganian, R. P.; Oliver, C. (1995): Microwave fixation improves antigenicity of glutaraldehyde-sensitive antigens while preserving ultrastructural detail. In *The journal of histochemistry and cytochemistry : official journal of the Histochemistry Society* 43 (3), pp. 307–311. DOI: 10.1177/43.3.7868860.

Janssen, J. C.; Beck, J. A.; Campbell, T. A.; Dickinson, A.; Fox, N. C.; Harvey, R. J. et al. (2003): Early onset familial Alzheimer's disease: Mutation frequency in 31 families. In *Neurology* 60 (2), pp. 235–239. DOI: 10.1212/01.wnl.0000042088.22694.e3.

Janus, C.; Pearson, J.; McLaurin, J.; Mathews, P. M.; Jiang, Y.; Schmidt, S. D. et al. (2000): A beta peptide immunization reduces behavioural impairment and plaques in a model of Alzheimer's disease. In *Nature* 408 (6815), pp. 979–982. DOI: 10.1038/35050110.

Jiang, Ying; Mullaney, Kerry A.; Peterhoff, Corrinne M.; Che, Shaoli; Schmidt, Stephen D.; Boyer-Boiteau, Anne et al. (2010): Alzheimer's-related endosome dysfunction in Down syndrome is Abeta-independent but requires APP and is reversed by BACE-1 inhibition. In *Proceedings of the National Academy of Sciences of the United States of America* 107 (4), pp. 1630–1635. DOI: 10.1073/pnas.0908953107.

Jonghe, C. de; Zehr, C.; Yager, D.; Prada, C. M.; Younkin, S.; Hendriks, L. et al. (1998): Flemish and Dutch mutations in amyloid beta precursor protein have different effects on amyloid beta secretion. In *Neurobiology of disease* 5 (4), pp. 281–286. DOI: 10.1006/nbdi.1998.0202.

Jonsson, Thorlakur; Atwal, Jasvinder K.; Steinberg, Stacy; Snaedal, Jon; Jonsson, Palmi V.; Bjornsson, Sigurbjorn et al. (2012): A mutation in APP protects against Alzheimer's disease and age-related cognitive decline. In *Nature* 488 (7409), pp. 96–99. DOI: 10.1038/nature11283.

Jonsson, Thorlakur; Stefansson, Hreinn; Steinberg, Stacy; Jonsdottir, Ingileif; Jonsson, Palmi V.; Snaedal, Jon et al. (2013): Variant of TREM2 associated with the risk of Alzheimer's disease. In *The New England journal of medicine* 368 (2), pp. 107–116. DOI: 10.1056/NEJMoa1211103.

Joshi, Powrnima; Liang, Jennifer O.; DiMonte, Kristine; Sullivan, John; Pimplikar, Sanjay W. (2009): Amyloid precursor protein is required for convergent-extension movements during Zebrafish development. In *Developmental biology* 335 (1), pp. 1–11. DOI: 10.1016/j.ydbio.2009.07.041.

Kaden, Daniela; Munter, Lisa Marie; Reif, Bernd; Multhaup, Gerd (2012): The amyloid precursor protein and its homologues: structural and functional aspects of native and pathogenic oligomerization. In *European journal of cell biology* 91 (4), pp. 234–239. DOI: 10.1016/j.ejcb.2011.01.017.

Kaden, Daniela; Voigt, Philipp; Munter, Lisa-Marie; Bobowski, Karolina D.; Schaefer, Michael; Multhaup, Gerd (2009): Subcellular localization and dimerization of APLP1 are strikingly different from APP and APLP2. In *Journal of cell science* 122 (Pt 3), pp. 368–377. DOI: 10.1242/jcs.034058.

Kamal, A.; Almenar-Queralt, A.; LeBlanc, J. F.; Roberts, E. A.; Goldstein, L. S. (2001): Kinesin-mediated axonal transport of a membrane compartment containing beta-secretase and presenilin-1 requires APP. In *Nature* 414 (6864), pp. 643–648. DOI: 10.1038/414643a.

Kamal, A.; Stokin, G. B.; Yang, Z.; Xia, C. H.; Goldstein, L. S. (2000): Axonal transport of amyloid precursor protein is mediated by direct binding to the kinesin light chain subunit of kinesin-I. In *Neuron* 28 (2), pp. 449–459. DOI: 10.1016/s0896-6273(00)00124-0.

Kametani, Fuyuki; Hasegawa, Masato (2018): Reconsideration of Amyloid Hypothesis and Tau Hypothesis in Alzheimer's Disease. In *Frontiers in neuroscience* 12, p. 25. DOI: 10.3389/fnins.2018.00025.

Kang, J.; Lemaire, H. G.; Unterbeck, A.; Salbaum, J. M.; Masters, C. L.; Grzeschik, K. H. et al. (1987): The precursor of Alzheimer's disease amyloid A4 protein resembles a cell-surface receptor. In *Nature* 325 (6106), pp. 733–736. DOI: 10.1038/325733a0.

Kanoski, Scott E.; Davidson, Terry L. (2011): Western diet consumption and cognitive impairment: links to hippocampal dysfunction and obesity. In *Physiology & behavior* 103 (1), pp. 59–68. DOI: 10.1016/j.physbeh.2010.12.003.

Karch, Celeste M.; Goate, Alison M. (2015): Alzheimer's disease risk genes and mechanisms of disease pathogenesis. In *Biological psychiatry* 77 (1), pp. 43–51. DOI: 10.1016/j.biopsych.2014.05.006.

Karran, Eric; Strooper, Bart de (2016): The amyloid cascade hypothesis: are we poised for success or failure? In *Journal of neurochemistry* 139 Suppl 2, pp. 237–252. DOI: 10.1111/jnc.13632.

Katzman, R.; Terry, R.; DeTeresa, R.; Brown, T.; Davies, P.; Fuld, P. et al. (1988): Clinical, pathological, and neurochemical changes in dementia: a subgroup with preserved mental status and numerous neocortical plaques. In *Annals of neurology* 23 (2), pp. 138–144. DOI: 10.1002/ana.410230206.

Kaufman, E. N.; Jain, R. K. (1992): Effect of bivalent interaction upon apparent antibody affinity: experimental confirmation of theory using fluorescence photobleaching and implications for antibody binding assays. In *Cancer research* 52 (15), pp. 4157–4167.

Kemper, Kristel; Sprick, Martin R.; Bree, Martijn de; Scopelliti, Alessandro; Vermeulen, Louis; Hoek, Maarten et al. (2010): The AC133 epitope, but not the CD133 protein, is lost upon cancer stem cell differentiation. In *Cancer research* 70 (2), pp. 719–729. DOI: 10.1158/0008-5472.CAN-09-1820.

Kenneth D. Kochanek; Sherry L. Murphy; Jiaquan Xu; Betzaida Tejada-Vera (2016): Deaths: Final Data for 2014. CDC (National Vital Statistics Reports, 4). Available online at https://www.cdc.gov/nchs/data/nvsr/nvsr65/nvsr65_04.pdf?s_cid=cs_064, updated on 6/30/2016, checked on 7/20/2020.

Kern, Andreas; Roempp, Birgit; Prager, Kai; Walter, Jochen; Behl, Christian (2006): Down-regulation of endogenous amyloid precursor protein processing due to cellular aging. In *The Journal of biological chemistry* 281 (5), pp. 2405–2413. DOI: 10.1074/jbc.M505625200.

Kim, Minji; Suh, Jaehong; Romano, Donna; Truong, Mimy H.; Mullin, Kristina; Hooli, Basavaraj et al. (2009): Potential late-onset Alzheimer's disease-associated mutations in the ADAM10 gene attenuate {alpha}-secretase activity. In *Human molecular genetics* 18 (20), pp. 3987–3996. DOI: 10.1093/hmg/ddp323.

Kimura, Ayano; Hata, Saori; Suzuki, Toshiharu (2016): Alternative Selection of β-Site APP-Cleaving Enzyme 1 (BACE1) Cleavage Sites in Amyloid β-Protein Precursor (APP) Harboring Protective and Pathogenic Mutations within the Aβ Sequence. In *The Journal of biological chemistry* 291 (46), pp. 24041–24053. DOI: 10.1074/jbc.M116.744722.

Kinoshita, Ayae; Fukumoto, Hiroaki; Shah, Tejal; Whelan, Christa M.; Irizarry, Michael C.; Hyman, Bradley T. (2003): Demonstration by FRET of BACE interaction with the amyloid precursor protein at

the cell surface and in early endosomes. In *Journal of cell science* 116 (Pt 16), pp. 3339–3346. DOI: 10.1242/jcs.00643.

Kivipelto, M.; Solomon, A. (2006): Cholesterol as a risk factor for Alzheimer's disease - epidemiological evidence. In *Acta neurologica Scandinavica. Supplementum* 185, pp. 50–57. DOI: 10.1111/j.1600-0404.2006.00685.x.

Knowles, M. K.; Barg, S.; Wan, L.; Midorikawa, M.; Chen, X.; Almers, Wolfhard (2010): Single secretory granules of live cells recruit syntaxin-1 and synaptosomal associated protein 25 (SNAP-25) in large copy numbers. In *Proceedings of the National Academy of Sciences of the United States of America* 107 (48), pp. 20810–20815. DOI: 10.1073/pnas.1014840107.

Koch, C. S. von; Zheng, H.; Chen, H.; Trumbauer, M.; Thinakaran, G.; van der Ploeg, L. H. et al. (1997): Generation of APLP2 KO mice and early postnatal lethality in APLP2/APP double KO mice. In *Neurobiology of aging* 18 (6), pp. 661–669. DOI: 10.1016/s0197-4580(97)00151-6.

Kojro, E.; Gimpl, G.; Lammich, S.; Marz, W.; Fahrenholz, F. (2001): Low cholesterol stimulates the nonamyloidogenic pathway by its effect on the alpha -secretase ADAM 10. In *Proceedings of the National Academy of Sciences of the United States of America* 98 (10), pp. 5815–5820. DOI: 10.1073/pnas.081612998.

Komarova, Natalia L.; Thalhauser, Craig J. (2011): High degree of heterogeneity in Alzheimer's disease progression patterns. In *PLoS computational biology* 7 (11), e1002251. DOI: 10.1371/journal.pcbi.1002251.

Koo, E. H.; Sisodia, S. S.; Archer, D. R.; Martin, L. J.; Weidemann, A.; Beyreuther, K. et al. (1990): Precursor of amyloid protein in Alzheimer disease undergoes fast anterograde axonal transport. In *Proceedings of the National Academy of Sciences of the United States of America* 87 (4), pp. 1561–1565. DOI: 10.1073/pnas.87.4.1561.

Koo, E. H.; Squazzo, S. L. (1994): Evidence that production and release of amyloid beta-protein involves the endocytic pathway. In *The Journal of biological chemistry* 269 (26), pp. 17386–17389.

Kornberg, L. J.; Earp, H. S.; Turner, C. E.; Prockop, C.; Juliano, R. L. (1991): Signal transduction by integrins: increased protein tyrosine phosphorylation caused by clustering of beta 1 integrins. In *Proceedings of the National Academy of Sciences of the United States of America* 88 (19), pp. 8392–8396.

Krafft, Grant A.; Klein, William L. (2010): ADDLs and the signaling web that leads to Alzheimer's disease. In *Neuropharmacology* 59 (4-5), pp. 230–242. DOI: 10.1016/j.neuropharm.2010.07.012.

Krone, Mary Griffin; Baumketner, Andrij; Bernstein, Summer L.; Wyttenbach, Thomas; Lazo, Noel D.; Teplow, David B. et al. (2008): Effects of familial Alzheimer's disease mutations on the folding nucleation of the amyloid beta-protein. In *Journal of molecular biology* 381 (1), pp. 221–228. DOI: 10.1016/j.jmb.2008.05.069.

Kumar-Singh, S.; Jonghe, C. de; Cruts, M.; Kleinert, R.; Wang, R.; Mercken, M. et al. (2000): Nonfibrillar diffuse amyloid deposition due to a gamma(42)-secretase site mutation points to an essential role for N-truncated A beta(42) in Alzheimer's disease. In *Human molecular genetics* 9 (18), pp. 2589–2598. DOI: 10.1093/hmg/9.18.2589.

Kusumi, Akihiro; Nakada, Chieko; Ritchie, Ken; Murase, Kotono; Suzuki, Kenichi; Murakoshi, Hideji et al. (2005): Paradigm shift of the plasma membrane concept from the two-dimensional continuum fluid to the partitioned fluid: high-speed single-molecule tracking of membrane molecules. In *Annual review of biophysics and biomolecular structure* 34, pp. 351–378. DOI: 10.1146/annurev.biophys.34.040204.144637.

Kwok, J. B.; Li, Q. X.; Hallupp, M.; Whyte, S.; Ames, D.; Beyreuther, K. et al. (2000): Novel Leu723Pro amyloid precursor protein mutation increases amyloid beta42(43) peptide levels and induces apoptosis. In *Annals of neurology* 47 (2), pp. 249–253. DOI: 10.1002/1531-8249(200002)47:2<249::aid-ana18>3.0.co;2-8.

Lai, A.; Sisodia, S. S.; Trowbridge, I. S. (1995): Characterization of sorting signals in the beta-amyloid precursor protein cytoplasmic domain. In *The Journal of biological chemistry* 270 (8), pp. 3565–3573.

Lambert, J. C.; Ibrahim-Verbaas, C. A.; Harold, D.; Naj, A. C.; Sims, R.; Bellenguez, C. et al. (2013): Meta-analysis of 74,046 individuals identifies 11 new susceptibility loci for Alzheimer's disease. In *Nature genetics* 45 (12), pp. 1452–1458. DOI: 10.1038/ng.2802.

Lambert, Jean-Charles; Heath, Simon; Even, Gael; Campion, Dominique; Sleegers, Kristel; Hiltunen, Mikko et al. (2009): Genome-wide association study identifies variants at CLU and CR1 associated with Alzheimer's disease. In *Nature genetics* 41 (10), pp. 1094–1099. DOI: 10.1038/ng.439.

Lambert, M. P.; Barlow, A. K.; Chromy, B. A.; Edwards, C.; Freed, R.; Liosatos, M. et al. (1998): Diffusible, nonfibrillar ligands derived from Abeta1-42 are potent central nervous system neurotoxins. In *Proceedings of the National Academy of Sciences of the United States of America* 95 (11), pp. 6448–6453. DOI: 10.1073/pnas.95.11.6448.

Lang, T. (2003): Imaging SNAREs at work in 'unroofed' cells--approaches that may be of general interest for functional studies on membrane proteins. In *Biochemical Society transactions* 31 (Pt 4), pp. 861–864. DOI: 10.1042/bst0310861.

Lang, Thorsten; Rizzoli, Silvio O. (2010): Membrane protein clusters at nanoscale resolution: more than pretty pictures. In *Physiology (Bethesda, Md.)* 25 (2), pp. 116–124. DOI: 10.1152/physiol.00044.2009.

Lauria, Ines; van Üüm, Jan; Mjumjunov-Crncevic, Esmina; Walrafen, David; Spitta, Luis; Thiele, Christoph; Lang, Thorsten (2013): GLTP mediated non-vesicular GM1 transport between native membranes. In *PloS one* 8 (3), e59871. DOI: 10.1371/journal.pone.0059871.

Lazarov, Orly; Morfini, Gerardo A.; Lee, Edward B.; Farah, Mohamed H.; Szodorai, Anita; DeBoer, Scott R. et al. (2005): Axonal transport, amyloid precursor protein, kinesin-1, and the processing apparatus: revisited. In *The Journal of neuroscience : the official journal of the Society for Neuroscience* 25 (9), pp. 2386–2395. DOI: 10.1523/JNEUROSCI.3089-04.2005.

Lee, Jiyeon; Retamal, Claudio; Cuitiño, Loreto; Caruano-Yzermans, Amy; Shin, Jung-Eun; van Kerkhof, Peter et al. (2008): Adaptor protein sorting nexin 17 regulates amyloid precursor protein trafficking and processing in the early endosomes. In *The Journal of biological chemistry* 283 (17), pp. 11501–11508. DOI: 10.1074/jbc.M800642200.

Lee, Yunhwan; Back, Joung Hwan; Kim, Jinhee; Kim, Si-Heon; Na, Duk L.; Cheong, Hae-Kwan et al. (2010): Systematic review of health behavioral risks and cognitive health in older adults. In *International psychogeriatrics* 22 (2), pp. 174–187. DOI: 10.1017/S1041610209991189.

Lewis, J.; Dickson, D. W.; Lin, W. L.; Chisholm, L.; Corral, A.; Jones, G. et al. (2001): Enhanced neurofibrillary degeneration in transgenic mice expressing mutant tau and APP. In *Science (New York, N.Y.)* 293 (5534), pp. 1487–1491. DOI: 10.1126/science.1058189.

Lewis, J.; McGowan, E.; Rockwood, J.; Melrose, H.; Nacharaju, P.; van Slegtenhorst, M. et al. (2000): Neurofibrillary tangles, amyotrophy and progressive motor disturbance in mice expressing mutant (P301L) tau protein. In *Nature genetics* 25 (4), pp. 402–405. DOI: 10.1038/78078.

Lewis, Victoria; Whitehouse, Isobel J.; Baybutt, Herbert; Manson, Jean C.; Collins, Steven J.; Hooper, Nigel M. (2012): Cellular prion protein expression is not regulated by the Alzheimer's amyloid precursor protein intracellular domain. In *PloS one* 7 (2), e31754. DOI: 10.1371/journal.pone.0031754.

Leyssen, Maarten; Ayaz, Derya; Hébert, Sébastien S.; Reeve, Simon; Strooper, Bart de; Hassan, Bassem A. (2005): Amyloid precursor protein promotes post-developmental neurite arborization in the Drosophila brain. In *The EMBO journal* 24 (16), pp. 2944–2955. DOI: 10.1038/sj.emboj.7600757.

Li, Chaoyun; Ebrahimi, Azadeh; Schluesener, Hermann (2013): Drug pipeline in neurodegeneration based on transgenic mice models of Alzheimer's disease. In *Ageing research reviews* 12 (1), pp. 116–140. DOI: 10.1016/j.arr.2012.09.002.

Li, Qi; Lau, Anthony; Morris, Terence J.; Guo, Lin; Fordyce, Christopher B.; Stanley, Elise F. (2004): A syntaxin 1, Galpha(o), and N-type calcium channel complex at a presynaptic nerve terminal: analysis by quantitative immunocolocalization. In *The Journal of neuroscience : the official journal of the Society for Neuroscience* 24 (16), pp. 4070–4081. DOI: 10.1523/JNEUROSCI.0346-04.2004.

Li, Xueyuan; Bao, Xinjie; Wang, Renzhi (2016): Experimental models of Alzheimer's disease for deciphering the pathogenesis and therapeutic screening (Review). In *International journal of molecular medicine* 37 (2), pp. 271–283. DOI: 10.3892/ijmm.2015.2428.

Liao, Hsin-Kai; Wang, Ying; Noack Watt, Kristin E.; Wen, Qin; Breitbach, Justin; Kemmet, Chelsy K. et al. (2012): Tol2 gene trap integrations in the zebrafish amyloid precursor protein genes appa and aplp2 reveal accumulation of secreted APP at the embryonic veins. In *Developmental dynamics : an official publication of the American Association of Anatomists* 241 (2), pp. 415–425. DOI: 10.1002/dvdy.23725.

Lichtenthaler, Stefan F.; Haass, Christian; Steiner, Harald (2011): Regulated intramembrane proteolysis--lessons from amyloid precursor protein processing. In *Journal of neurochemistry* 117 (5), pp. 779–796. DOI: 10.1111/j.1471-4159.2011.07248.x.

Lingwood, Daniel; Simons, Kai (2010): Lipid rafts as a membrane-organizing principle. In *Science (New York, N.Y.)* 327 (5961), pp. 46–50. DOI: 10.1126/science.1174621.

Lorenzo, A.; Yuan, M.; Zhang, Z.; Paganetti, P. A.; Sturchler-Pierrat, C.; Staufenbiel, M. et al. (2000): Amyloid beta interacts with the amyloid precursor protein: a potential toxic mechanism in Alzheimer's disease. In *Nature neuroscience* 3 (5), pp. 460–464. DOI: 10.1038/74833.

Lourenço, F. C.; Galvan, V.; Fombonne, J.; Corset, V.; Llambi, F.; Müller, U. et al. (2009): Netrin-1 interacts with amyloid precursor protein and regulates amyloid-beta production. In *Cell death and differentiation* 16 (5), pp. 655–663. DOI: 10.1038/cdd.2008.191.

Lu, Feng-Ping; Lin, Kun-Pei; Kuo, Hsu-Ko (2009): Diabetes and the risk of multi-system aging phenotypes: a systematic review and meta-analysis. In *PloS one* 4 (1), e4144. DOI: 10.1371/journal.pone.0004144.

Luo, L. Q.; Martin-Morris, L. E.; White, K. (1990): Identification, secretion, and neural expression of APPL, a Drosophila protein similar to human amyloid protein precursor. In *The Journal of neuroscience : the official journal of the Society for Neuroscience* 10 (12), pp. 3849–3861.

Lyckman, A. W.; Confaloni, A. M.; Thinakaran, G.; Sisodia, S. S.; Moya, K. L. (1998): Post-translational processing and turnover kinetics of presynaptically targeted amyloid precursor superfamily proteins in the central nervous system. In *The Journal of biological chemistry* 273 (18), pp. 11100–11106. DOI: 10.1074/jbc.273.18.11100.

Mahley, Robert W.; Weisgraber, Karl H.; Huang, Yadong (2006): Apolipoprotein E4: a causative factor and therapeutic target in neuropathology, including Alzheimer's disease. In *Proceedings of the National Academy of Sciences of the United States of America* 103 (15), pp. 5644–5651. DOI: 10.1073/pnas.0600549103.

Maloney, Janice A.; Bainbridge, Travis; Gustafson, Amy; Zhang, Shuo; Kyauk, Roxanne; Steiner, Pascal et al. (2014): Molecular mechanisms of Alzheimer disease protection by the A673T allele of amyloid precursor protein. In *The Journal of biological chemistry* 289 (45), pp. 30990–31000. DOI: 10.1074/jbc.M114.589069.

Martin-Morris, L. E.; White, K. (1990): The Drosophila transcript encoded by the beta-amyloid protein precursor-like gene is restricted to the nervous system. In *Development (Cambridge, England)* 110 (1), pp. 185–195.

Matsuda, Shuji; Matsuda, Yukiko; D'Adamio, Luciano (2003): Amyloid beta protein precursor (AbetaPP), but not AbetaPP-like protein 2, is bridged to the kinesin light chain by the scaffold protein JNK-interacting protein 1. In *The Journal of biological chemistry* 278 (40), pp. 38601–38606. DOI: 10.1074/jbc.M304379200.

Mattila, Pieta K.; Feest, Christoph; Depoil, David; Treanor, Bebhinn; Montaner, Beatriz; Otipoby, Kevin L. et al. (2013): The actin and tetraspanin networks organize receptor nanoclusters to regulate B cell receptor-mediated signaling. In *Immunity* 38 (3), pp. 461–474. DOI: 10.1016/j.immuni.2012.11.019.

Mattson, M. P. (1997): Cellular actions of beta-amyloid precursor protein and its soluble and fibrillogenic derivatives. In *Physiological reviews* 77 (4), pp. 1081–1132. DOI: 10.1152/physrev.1997.77.4.1081.

Mayeda, Elizabeth Rose; Glymour, M. Maria; Quesenberry, Charles P.; Whitmer, Rachel A. (2016): Inequalities in dementia incidence between six racial and ethnic groups over 14 years. In *Alzheimer's & dementia : the journal of the Alzheimer's Association* 12 (3), pp. 216–224. DOI: 10.1016/j.jalz.2015.12.007.

Maynard, Christa J.; Bush, Ashley I.; Masters, Colin L.; Cappai, Roberto; Li, Qiao-Xin (2005): Metals and amyloid-beta in Alzheimer's disease. In *International journal of experimental pathology* 86 (3), pp. 147–159. DOI: 10.1111/j.0959-9673.2005.00434.x.

McDonald, Jessica M.; Cairns, Nigel J.; Taylor-Reinwald, Lisa; Holtzman, David; Walsh, Dominic M. (2012): The levels of water-soluble and triton-soluble Aβ are increased in Alzheimer's disease brain. In *Brain Research* 1450, pp. 138–147. DOI: 10.1016/j.brainres.2012.02.041.

McGuinness, Bernadette; Craig, David; Bullock, Roger; Malouf, Reem; Passmore, Peter (2014): Statins for the treatment of dementia. In *The Cochrane database of systematic reviews* (7), CD007514. DOI: 10.1002/14651858.CD007514.pub3.

McLean, I. W.; Nakane, P. K. (1974): Periodate-lysine-paraformaldehyde fixative. A new fixation for immunoelectron microscopy. In *The journal of histochemistry and cytochemistry : official journal of the Histochemistry Society* 22 (12), pp. 1077–1083. DOI: 10.1177/22.12.1077.

Mendez, Mario F. (2012): Early-onset Alzheimer's disease: nonamnestic subtypes and type 2 AD. In *Archives of medical research* 43 (8), pp. 677–685. DOI: 10.1016/j.arcmed.2012.11.009.

Merklinger, Elisa; Schloetel, Jan-Gero; Weber, Pascal; Batoulis, Helena; Holz, Sarah; Karnowski, Nora et al. (2017): The packing density of a supramolecular membrane protein cluster is controlled by cytoplasmic interactions. In *eLife* 6. DOI: 10.7554/eLife.20705.

Mills, J.; Reiner, P. B. (1999): Regulation of amyloid precursor protein cleavage. In *Journal of neurochemistry* 72 (2), pp. 443–460. DOI: 10.1046/j.1471-4159.1999.0720443.x.

Miravalle, L.; Tokuda, T.; Chiarle, R.; Giaccone, G.; Bugiani, O.; Tagliavini, F. et al. (2000): Substitutions at codon 22 of Alzheimer's abeta peptide induce diverse conformational changes and apoptotic effects in human cerebral endothelial cells. In *The Journal of biological chemistry* 275 (35), pp. 27110–27116. DOI: 10.1074/jbc.M003154200.

Mohamed, Tarek; Shakeri, Arash; Rao, Praveen P. N. (2016): Amyloid cascade in Alzheimer's disease: Recent advances in medicinal chemistry. In *European journal of medicinal chemistry* 113, pp. 258–272. DOI: 10.1016/j.ejmech.2016.02.049.

Mölsä, P. K.; Marttila, R. J.; Rinne, U. K. (1995): Long-term survival and predictors of mortality in Alzheimer's disease and multi-infarct dementia. In *Acta neurologica Scandinavica* 91 (3), pp. 159–164. DOI: 10.1111/j.1600-0404.1995.tb00426.x.

Morgan, D.; Diamond, D. M.; Gottschall, P. E.; Ugen, K. E.; Dickey, C.; Hardy, J. et al. (2000): A beta peptide vaccination prevents memory loss in an animal model of Alzheimer's disease. In *Nature* 408 (6815), pp. 982–985. DOI: 10.1038/35050116.

Müller, Thorsten; Concannon, Caoimhin G.; Ward, Manus W.; Walsh, Ciara M.; Tirniceriu, Anca L.; Tribl, Florian et al. (2007): Modulation of gene expression and cytoskeletal dynamics by the amyloid

precursor protein intracellular domain (AICD). In *Molecular biology of the cell* 18 (1), pp. 201–210. DOI: 10.1091/mbc.e06-04-0283.

Müller, Thorsten; Meyer, Helmut E.; Egensperger, Rupert; Marcus, Katrin (2008): The amyloid precursor protein intracellular domain (AICD) as modulator of gene expression, apoptosis, and cytoskeletal dynamics-relevance for Alzheimer's disease. In *Progress in neurobiology* 85 (4), pp. 393–406. DOI: 10.1016/j.pneurobio.2008.05.002.

Müller, U.; Cristina, N.; Li, Z. W.; Wolfer, D. P.; Lipp, H. P.; Rülicke, T. et al. (1994): Behavioral and anatomical deficits in mice homozygous for a modified beta-amyloid precursor protein gene. In *Cell* 79 (5), pp. 755–765. DOI: 10.1016/0092-8674(94)90066-3.

Mulrooney, S. B.; Waskell, L. (2000): High-level expression in Escherichia coli and purification of the membrane-bound form of cytochrome b(5). In *Protein expression and purification* 19 (1), pp. 173–178. DOI: 10.1006/prep.2000.1228.

Multhaup, G.; Bush, A. I.; Pollwein, P.; Masters, C. L. (1994): Interaction between the zinc (II) and the heparin binding site of the Alzheimer's disease beta A4 amyloid precursor protein (APP). In *FEBS letters* 355 (2), pp. 151–154. DOI: 10.1016/0014-5793(94)01176-1.

Multhaup, G.; Schlicksupp, A.; Hesse, L.; Beher, D.; Ruppert, T.; Masters, C. L.; Beyreuther, K. (1996): The amyloid precursor protein of Alzheimer's disease in the reduction of copper(II) to copper(I). In *Science (New York, N.Y.)* 271 (5254), pp. 1406–1409. DOI: 10.1126/science.271.5254.1406.

Munter, Lisa-Marie; Voigt, Philipp; Harmeier, Anja; Kaden, Daniela; Gottschalk, Kay E.; Weise, Christoph et al. (2007): GxxxG motifs within the amyloid precursor protein transmembrane sequence are critical for the etiology of Abeta42. In *The EMBO journal* 26 (6), pp. 1702–1712. DOI: 10.1038/sj.emboj.7601616.

Murrell, J.; Farlow, M.; Ghetti, B.; Benson, M. D. (1991): A mutation in the amyloid precursor protein associated with hereditary Alzheimer's disease. In *Science (New York, N.Y.)* 254 (5028), pp. 97–99. DOI: 10.1126/science.1925564.

Murrell, J. R.; Hake, A. M.; Quaid, K. A.; Farlow, M. R.; Ghetti, B. (2000): Early-onset Alzheimer disease caused by a new mutation (V717L) in the amyloid precursor protein gene. In *Archives of neurology* 57 (6), pp. 885–887. DOI: 10.1001/archneur.57.6.885.

Naj, Adam C.; Jun, Gyungah; Beecham, Gary W.; Wang, Li-San; Vardarajan, Badri Narayan; Buros, Jacqueline et al. (2011): Common variants at MS4A4/MS4A6E, CD2AP, CD33 and EPHA1 are associated with late-onset Alzheimer's disease. In *Nature genetics* 43 (5), pp. 436–441. DOI: 10.1038/ng.801.

Narindrasorasak, S.; Lowery, D. E.; Altman, R. A.; Gonzalez-DeWhitt, P. A.; Greenberg, B. D.; Kisilevsky, R. (1992): Characterization of high affinity binding between laminin and Alzheimer's disease amyloid precursor proteins. In *Laboratory investigation; a journal of technical methods and pathology* 67 (5), pp. 643–652.

Nehlig, Astrid (2013): The neuroprotective effects of cocoa flavanol and its influence on cognitive performance. In *British Journal of Clinical Pharmacology* 75 (3), pp. 716–727. DOI: 10.1111/j.1365-2125.2012.04378.x.

Nikolaev, Anatoly; McLaughlin, Todd; O'Leary, Dennis D. M.; Tessier-Lavigne, Marc (2009): APP binds DR6 to trigger axon pruning and neuron death via distinct caspases. In *Nature* 457 (7232), pp. 981–989. DOI: 10.1038/nature07767.

Nilsberth, C.; Westlind-Danielsson, A.; Eckman, C. B.; Condron, M. M.; Axelman, K.; Forsell, C. et al. (2001): The 'Arctic' APP mutation (E693G) causes Alzheimer's disease by enhanced Abeta protofibril formation. In *Nature neuroscience* 4 (9), pp. 887–893. DOI: 10.1038/nn0901-887.

Ninomiya, H.; Roch, J. M.; Sundsmo, M. P.; Otero, D. A.; Saitoh, T. (1993): Amino acid sequence RERMS represents the active domain of amyloid beta/A4 protein precursor that promotes fibroblast growth. In *The Journal of cell biology* 121 (4), pp. 879–886. DOI: 10.1083/jcb.121.4.879.

Niu, H.; Álvarez-Álvarez, I.; Guillén-Grima, F.; Aguinaga-Ontoso, I. (2017): Prevalencia e incidencia de la enfermedad de Alzheimer en Europa: metaanálisis. In *Neurologia (Barcelona, Spain)* 32 (8), pp. 523–532. DOI: 10.1016/j.nrl.2016.02.016.

Nochlin, D.; van Belle, G.; Bird, T. D.; Sumi, S. M. (1993): Comparison of the severity of neuropathologic changes in familial and sporadic Alzheimer's disease. In *Alzheimer disease and associated disorders* 7 (4), pp. 212–222.

O'Brien, Richard J.; Wong, Philip C. (2011): Amyloid precursor protein processing and Alzheimer's disease. In *Annual review of neuroscience* 34, pp. 185–204. DOI: 10.1146/annurev-neuro-061010-113613.

Oddo, Salvatore; Caccamo, Antonella; Kitazawa, Masashi; Tseng, Bertrand P.; LaFerla, Frank M. (2003): Amyloid deposition precedes tangle formation in a triple transgenic model of Alzheimer's disease. In *Neurobiology of aging* 24 (8), pp. 1063–1070. DOI: 10.1016/j.neurobiolaging.2003.08.012.

Okado, H.; Okamoto, H. (1992): A Xenopus homologue of the human beta-amyloid precursor protein: developmental regulation of its gene expression. In *Biochemical and Biophysical Research Communications* 189 (3), pp. 1561–1568. DOI: 10.1016/0006-291x(92)90254-i.

Ono, Kenjiro; Condron, Margaret M.; Teplow, David B. (2010): Effects of the English (H6R) and Tottori (D7N) familial Alzheimer disease mutations on amyloid beta-protein assembly and toxicity. In *The Journal of biological chemistry* 285 (30), pp. 23186–23197. DOI: 10.1074/jbc.M109.086496.

Pardossi-Piquard, Raphaëlle; Checler, Frédéric (2012): The physiology of the β-amyloid precursor protein intracellular domain AICD. In *Journal of neurochemistry* 120 Suppl 1, pp. 109–124. DOI: 10.1111/j.1471-4159.2011.07475.x.

Parvathy, S.; Hussain, I.; Karran, E. H.; Turner, A. J.; Hooper, N. M. (1999): Cleavage of Alzheimer's amyloid precursor protein by alpha-secretase occurs at the surface of neuronal cells. In *Biochemistry* 38 (30), pp. 9728–9734. DOI: 10.1021/bi9906827.

Peacock, M. L.; Warren, J. T.; Roses, A. D.; Fink, J. K. (1993): Novel polymorphism in the A4 region of the amyloid precursor protein gene in a patient without Alzheimer's disease. In *Neurology* 43 (6), pp. 1254–1256. DOI: 10.1212/wnl.43.6.1254.

Pearse, B. M. (1976): Clathrin: a unique protein associated with intracellular transfer of membrane by coated vesicles. In *Proceedings of the National Academy of Sciences of the United States of America* 73 (4), pp. 1255–1259. DOI: 10.1073/pnas.73.4.1255.

Perez, R. G.; Soriano, S.; Hayes, J. D.; Ostaszewski, B.; Xia, W.; Selkoe, D. J. et al. (1999): Mutagenesis identifies new signals for beta-amyloid precursor protein endocytosis, turnover, and the generation of secreted fragments, including Abeta42. In *The Journal of biological chemistry* 274 (27), pp. 18851–18856. DOI: 10.1074/jbc.274.27.18851.

Perrin, Richard J.; Fagan, Anne M.; Holtzman, David M. (2009): Multimodal techniques for diagnosis and prognosis of Alzheimer's disease. In *Nature* 461 (7266), pp. 916–922. DOI: 10.1038/nature08538.

Pieri, L.; Sassoli, C.; Romagnoli, P.; Domenici, L. (2002): Use of periodate-lysine-paraformaldehyde for the fixation of multiple antigens in human skin biopsies. In *European journal of histochemistry : EJH* 46 (4), pp. 365–375. DOI: 10.4081/1749.

Plácido, A. I.; Pereira, C. M. F.; Duarte, A. I.; Candeias, E.; Correia, S. C.; Santos, R. X. et al. (2014): The role of endoplasmic reticulum in amyloid precursor protein processing and trafficking: implications for Alzheimer's disease. In *Biochimica et biophysica acta* 1842 (9), pp. 1444–1453. DOI: 10.1016/j.bbadis.2014.05.003.

Pohlkamp, Theresa; Wasser, Catherine R.; Herz, Joachim (2017): Functional Roles of the Interaction of APP and Lipoprotein Receptors. In *Frontiers in molecular neuroscience* 10, p. 54. DOI: 10.3389/fnmol.2017.00054.

Posthumadeboer, J.; Piersma, S. R.; Pham, T. V.; van Egmond, P. W.; Knol, J. C.; Cleton-Jansen, A. M. et al. (2013): Surface proteomic analysis of osteosarcoma identifies EPHA2 as receptor for targeted drug delivery. In *British journal of cancer* 109 (8), pp. 2142–2154. DOI: 10.1038/bjc.2013.578.

Puck, T. T.; Marcus, P. I.; Cieciura, S. J. (1956): Clonal growth of mammalian cells in vitro; growth characteristics of colonies from single HeLa cells with and without a feeder layer. In *The Journal of experimental medicine* 103 (2), pp. 273–283. DOI: 10.1084/jem.103.2.273.

Puzzo, Daniela; Lee, Linda; Palmeri, Agostino; Calabrese, Giorgio; Arancio, Ottavio (2014): Behavioral assays with mouse models of Alzheimer's disease: practical considerations and guidelines. In *Biochemical pharmacology* 88 (4), pp. 450–467. DOI: 10.1016/j.bcp.2014.01.011.

Qi-Takahara, Yue; Morishima-Kawashima, Maho; Tanimura, Yu; Dolios, Georgia; Hirotani, Naoko; Horikoshi, Yuko et al. (2005): Longer forms of amyloid beta protein: implications for the mechanism of intramembrane cleavage by gamma-secretase. In *The Journal of neuroscience : the official journal of the Society for Neuroscience* 25 (2), pp. 436–445. DOI: 10.1523/JNEUROSCI.1575-04.2005.

Qiu, Chengxuan; Winblad, Bengt; Fratiglioni, Laura (2005): The age-dependent relation of blood pressure to cognitive function and dementia. In *The Lancet. Neurology* 4 (8), pp. 487–499. DOI: 10.1016/S1474-4422(05)70141-1.

Rapoport, Mark; Dawson, Hana N.; Binder, Lester I.; Vitek, Michael P.; Ferreira, Adriana (2002): Tau is essential to beta -amyloid-induced neurotoxicity. In *Proceedings of the National Academy of Sciences of the United States of America* 99 (9), pp. 6364–6369. DOI: 10.1073/pnas.092136199.

Re, F.; Airoldi, C.; Zona, C.; Masserini, M.; La Ferla, B.; Quattrocchi, N.; Nicotra, F. (2010): Beta amyloid aggregation inhibitors: small molecules as candidate drugs for therapy of Alzheimer's disease. In *Current medicinal chemistry* 17 (27), pp. 2990–3006. DOI: 10.2174/092986710791959729.

Reinhard, Constanze; Hébert, Sébastien S.; Strooper, Bart de (2005): The amyloid-beta precursor protein: integrating structure with biological function. In *The EMBO journal* 24 (23), pp. 3996–4006. DOI: 10.1038/sj.emboj.7600860.

Renner, Marianne; Lacor, Pascale N.; Velasco, Pauline T.; Xu, Jian; Contractor, Anis; Klein, William L.; Triller, Antoine (2010): Deleterious effects of amyloid beta oligomers acting as an extracellular scaffold for mGluR5. In *Neuron* 66 (5), pp. 739–754. DOI: 10.1016/j.neuron.2010.04.029.

Rickman, Colin; Duncan, Rory R. (2010): Munc18/Syntaxin interaction kinetics control secretory vesicle dynamics. In *The Journal of biological chemistry* 285 (6), pp. 3965–3972. DOI: 10.1074/jbc.M109.040402.

Ring, Sabine; Weyer, Sascha W.; Kilian, Susanne B.; Waldron, Elaine; Pietrzik, Claus U.; Filippov, Mikhail A. et al. (2007): The secreted beta-amyloid precursor protein ectodomain APPs alpha is sufficient to rescue the anatomical, behavioral, and electrophysiological abnormalities of APP-deficient mice. In *The Journal of neuroscience : the official journal of the Society for Neuroscience* 27 (29), pp. 7817–7826. DOI: 10.1523/JNEUROSCI.1026-07.2007.

Robakis, N. K.; Ramakrishna, N.; Wolfe, G.; Wisniewski, H. M. (1987): Molecular cloning and characterization of a cDNA encoding the cerebrovascular and the neuritic plaque amyloid peptides. In *Proceedings of the National Academy of Sciences of the United States of America* 84 (12), pp. 4190–4194. DOI: 10.1073/pnas.84.12.4190.

Roberson, Erik D.; Scearce-Levie, Kimberly; Palop, Jorge J.; Yan, Fengrong; Cheng, Irene H.; Wu, Tiffany et al. (2007): Reducing endogenous tau ameliorates amyloid beta-induced deficits in an Alzheimer's disease mouse model. In *Science (New York, N.Y.)* 316 (5825), pp. 750–754. DOI: 10.1126/science.1141736.

Roberts, Blaine R.; Ryan, Timothy M.; Bush, Ashley I.; Masters, Colin L.; Duce, James A. (2012): The role of metallobiology and amyloid-β peptides in Alzheimer's disease. In *Journal of neurochemistry* 120 Suppl 1, pp. 149–166. DOI: 10.1111/j.1471-4159.2011.07500.x.

Rocca, Walter A.; Mielke, Michelle M.; Vemuri, Prashanthi; Miller, Virginia M. (2014): Sex and gender differences in the causes of dementia: a narrative review. In *Maturitas* 79 (2), pp. 196–201. DOI: 10.1016/j.maturitas.2014.05.008.

Roher, Alex E.; Esh, Chera L.; Kokjohn, Tyler A.; Castaño, Eduardo M.; van Vickle, Gregory D.; Kalback, Walter M. et al. (2009): Amyloid beta peptides in human plasma and tissues and their significance for Alzheimer's disease. In *Alzheimer's & dementia : the journal of the Alzheimer's Association* 5 (1), pp. 18–29. DOI: 10.1016/j.jalz.2008.10.004.

Rossjohn, J.; Cappai, R.; Feil, S. C.; Henry, A.; McKinstry, W. J.; Galatis, D. et al. (1999): Crystal structure of the N-terminal, growth factor-like domain of Alzheimer amyloid precursor protein. In *Nature structural biology* 6 (4), pp. 327–331. DOI: 10.1038/7562.

Rotz, Ruth C. von; Kohli, Bernhard M.; Bosset, Jérôme; Meier, Michelle; Suzuki, Toshiharu; Nitsch, Roger M.; Konietzko, Uwe (2004): The APP intracellular domain forms nuclear multiprotein complexes and regulates the transcription of its own precursor. In *Journal of cell science* 117 (Pt 19), pp. 4435–4448. DOI: 10.1242/jcs.01323.

Rushworth, Jo V.; Hooper, Nigel M. (2010): Lipid Rafts: Linking Alzheimer's Amyloid-β Production, Aggregation, and Toxicity at Neuronal Membranes. In *International journal of Alzheimer's disease* 2011, p. 603052. DOI: 10.4061/2011/603052.

Saheki, Yasunori; Bian, Xin; Schauder, Curtis M.; Sawaki, Yujin; Surma, Michal A.; Klose, Christian et al. (2016): Control of plasma membrane lipid homeostasis by the extended synaptotagmins. In *Nature cell biology* 18 (5), pp. 504–515. DOI: 10.1038/ncb3339.

Sakono, Masafumi; Zako, Tamotsu (2010): Amyloid oligomers: formation and toxicity of Abeta oligomers. In *The FEBS journal* 277 (6), pp. 1348–1358. DOI: 10.1111/j.1742-4658.2010.07568.x.

Salinas, F. A.; Smith, L. H.; Goodman, J. W. (1972): Cell size distribution in the thymus as a function of age. In *Journal of cellular physiology* 80 (3), pp. 339–345. DOI: 10.1002/jcp.1040800304.

Sandbrink, R.; Masters, C. L.; Beyreuther, K. (1994): Similar alternative splicing of a non-homologous domain in beta A4-amyloid protein precursor-like proteins. In *The Journal of biological chemistry* 269 (19), pp. 14227–14234.

Santos, Catarina; Costa, João; Santos, João; Vaz-Carneiro, António; Lunet, Nuno (2010): Caffeine intake and dementia: systematic review and meta-analysis. In *Journal of Alzheimer's disease : JAD* 20 Suppl 1, S187-204. DOI: 10.3233/JAD-2010-091387.

Sasaguri, Hiroki; Nilsson, Per; Hashimoto, Shoko; Nagata, Kenichi; Saito, Takashi; Strooper, Bart de et al. (2017): APP mouse models for Alzheimer's disease preclinical studies. In *The EMBO journal* 36 (17), pp. 2473–2487. DOI: 10.15252/embj.201797397.

Sastre, M.; Steiner, H.; Fuchs, K.; Capell, A.; Multhaup, G.; Condron, M. M. et al. (2001): Presenilin-dependent gamma-secretase processing of beta-amyloid precursor protein at a site corresponding to the S3 cleavage of Notch. In *EMBO reports* 2 (9), pp. 835–841. DOI: 10.1093/embo-reports/kve180.

Savva, George M.; Stephan, Blossom C. M. (2010): Epidemiological studies of the effect of stroke on incident dementia: a systematic review. In *Stroke* 41 (1), e41-6. DOI: 10.1161/STROKEAHA.109.559880.

Scheinfeld, Meir H.; Roncarati, Roberta; Vito, Pasquale; Lopez, Peter A.; Abdallah, Mona; D'Adamio, Luciano (2002): Jun NH2-terminal kinase (JNK) interacting protein 1 (JIP1) binds the cytoplasmic domain of the Alzheimer's beta-amyloid precursor protein (APP). In *The Journal of biological chemistry* 277 (5), pp. 3767–3775. DOI: 10.1074/jbc.M108357200.

Scheuermann, S.; Hambsch, B.; Hesse, L.; Stumm, J.; Schmidt, C.; Beher, D. et al. (2001): Homodimerization of amyloid precursor protein and its implication in the amyloidogenic pathway of Alzheimer's disease. In *The Journal of biological chemistry* 276 (36), pp. 33923–33929. DOI: 10.1074/jbc.M105410200.

Scheuner, D.; Eckman, C.; Jensen, M.; Song, X.; Citron, M.; Suzuki, N. et al. (1996): Secreted amyloid beta-protein similar to that in the senile plaques of Alzheimer's disease is increased in vivo by the

presenilin 1 and 2 and APP mutations linked to familial Alzheimer's disease. In *Nature medicine* 2 (8), pp. 864–870. DOI: 10.1038/nm0896-864.

Schneider, Anja; Rajendran, Lawrence; Honsho, Masanori; Gralle, Matthias; Donnert, Gerald; Wouters, Fred et al. (2008): Flotillin-dependent clustering of the amyloid precursor protein regulates its endocytosis and amyloidogenic processing in neurons. In *The Journal of neuroscience : the official journal of the Society for Neuroscience* 28 (11), pp. 2874–2882. DOI: 10.1523/JNEUROSCI.5345-07.2008.

Schönheit, Bärbel; Zarski, Rosemarie; Ohm, Thomas G. (2004): Spatial and temporal relationships between plaques and tangles in Alzheimer-pathology. In *Neurobiology of aging* 25 (6), pp. 697–711. DOI: 10.1016/j.neurobiolaging.2003.09.009.

Schreiber, Arne; Fischer, Sebastian; Lang, Thorsten (2012): The amyloid precursor protein forms plasmalemmal clusters via its pathogenic amyloid-β domain. In *Biophysical journal* 102 (6), pp. 1411–1417. DOI: 10.1016/j.bpj.2012.02.031.

Scott, R. E. (1976): Plasma membrane vesiculation: a new technique for isolation of plasma membranes. In *Science (New York, N.Y.)* 194 (4266), pp. 743–745. DOI: 10.1126/science.982044.

Seabrook, G. R.; Smith, D. W.; Bowery, B. J.; Easter, A.; Reynolds, T.; Fitzjohn, S. M. et al. (1999): Mechanisms contributing to the deficits in hippocampal synaptic plasticity in mice lacking amyloid precursor protein. In *Neuropharmacology* 38 (3), pp. 349–359. DOI: 10.1016/s0028-3908(98)00204-4.

Seftalioglu, Aysel; Karakus, Sema; Dundar, Semra; Can, Belgin; Erdemli, Esra; Irmak, M. Kemal et al. (2003): Syndecan-1 (CD138) expression in acute myeloblastic leukemia cells--an immuno electron microscopic study. In *Acta oncologica (Stockholm, Sweden)* 42 (1), pp. 71–74. DOI: 10.1080/0891060310002267.

Senes, Alessandro; Engel, Donald E.; DeGrado, William F. (2004): Folding of helical membrane proteins: the role of polar, GxxxG-like and proline motifs. In *Current opinion in structural biology* 14 (4), pp. 465–479. DOI: 10.1016/j.sbi.2004.07.007.

Shaked, G. M.; Kummer, M. P.; Lu, D. C.; Galvan, V.; Bredesen, D. E.; Koo, E. H. (2006): Abeta induces cell death by direct interaction with its cognate extracellular domain on APP (APP 597-624). In *FASEB journal : official publication of the Federation of American Societies for Experimental Biology* 20 (8), pp. 1254–1256. DOI: 10.1096/fj.05-5032fje.

Shaner, Nathan C.; Steinbach, Paul A.; Tsien, Roger Y. (2005): A guide to choosing fluorescent proteins. In *Nature methods* 2 (12), pp. 905–909. DOI: 10.1038/nmeth819.

Shankar, Ganesh M.; Li, Shaomin; Mehta, Tapan H.; Garcia-Munoz, Amaya; Shepardson, Nina E.; Smith, Imelda et al. (2008): Amyloid-beta protein dimers isolated directly from Alzheimer's brains impair synaptic plasticity and memory. In *Nature medicine* 14 (8), pp. 837–842. DOI: 10.1038/nm1782.

Shariati, S. Ali M.; Strooper, Bart de (2013): Redundancy and divergence in the amyloid precursor protein family. In *FEBS letters* 587 (13), pp. 2036–2045. DOI: 10.1016/j.febslet.2013.05.026.

Sharma, Rohit; Dearaugo, Stephanie; Infeld, Bernard; O'Sullivan, Richard; Gerraty, Richard P. (2018): Cerebral amyloid angiopathy: Review of clinico-radiological features and mimics. In *Journal of medical imaging and radiation oncology*. DOI: 10.1111/1754-9485.12726.

Shen, Jie; Kelleher, Raymond J. (2007): The presenilin hypothesis of Alzheimer's disease: evidence for a loss-of-function pathogenic mechanism. In *Proceedings of the National Academy of Sciences of the United States of America* 104 (2), pp. 403–409. DOI: 10.1073/pnas.0608332104.

Shimada, Hiroyuki; Ataka, Suzuka; Tomiyama, Takami; Takechi, Hajime; Mori, Hiroshi; Miki, Takami (2011): Clinical course of patients with familial early-onset Alzheimer's disease potentially lacking senile plaques bearing the E693Δ mutation in amyloid precursor protein. In *Dementia and geriatric cognitive disorders* 32 (1), pp. 45–54. DOI: 10.1159/000330017.

Sieber, Jochen J.; Willig, Katrin I.; Heintzmann, Rainer; Hell, Stefan W.; Lang, Thorsten (2006): The SNARE motif is essential for the formation of syntaxin clusters in the plasma membrane. In *Biophysical journal* 90 (8), pp. 2843–2851. DOI: 10.1529/biophysj.105.079574.

Sieber, Jochen J.; Willig, Katrin I.; Kutzner, Carsten; Gerding-Reimers, Claas; Harke, Benjamin; Donnert, Gerald et al. (2007): Anatomy and dynamics of a supramolecular membrane protein cluster. In *Science (New York, N.Y.)* 317 (5841), pp. 1072–1076. DOI: 10.1126/science.1141727.

Small, D. H.; Clarris, H. L.; Williamson, T. G.; Reed, G.; Key, B.; Mok, S. S. et al. (1999): Neurite-outgrowth regulating functions of the amyloid protein precursor of Alzheimer's disease. In *Journal of Alzheimer's disease : JAD* 1 (4-5), pp. 275–285. DOI: 10.3233/jad-1999-14-508.

Small, D. H.; Nurcombe, V.; Reed, G.; Clarris, H.; Moir, R.; Beyreuther, K.; Masters, C. L. (1994): A heparin-binding domain in the amyloid protein precursor of Alzheimer's disease is involved in the regulation of neurite outgrowth. In *The Journal of neuroscience : the official journal of the Society for Neuroscience* 14 (4), pp. 2117–2127.

Soba, Peter; Eggert, Simone; Wagner, Katja; Zentgraf, Hanswalter; Siehl, Katjuscha; Kreger, Sylvia et al. (2005): Homo- and heterodimerization of APP family members promotes intercellular adhesion. In *The EMBO journal* 24 (20), pp. 3624–3634. DOI: 10.1038/sj.emboj.7600824.

Soldano, Alessia; Okray, Zeynep; Janovska, Pavlina; Tmejová, Kateřina; Reynaud, Elodie; Claeys, Annelies et al. (2013): The Drosophila Homologue of the Amyloid Precursor Protein Is a Conserved Modulator of Wnt PCP Signaling. In *PLoS Biology* 11 (5). DOI: 10.1371/journal.pbio.1001562.

Solfrizzi, Vincenzo; Capurso, Cristiano; D'Introno, Alessia; Colacicco, Anna Maria; Santamato, Andrea; Ranieri, Maurizio et al. (2008): Lifestyle-related factors in predementia and dementia syndromes. In *Expert review of neurotherapeutics* 8 (1), pp. 133–158. DOI: 10.1586/14737175.8.1.133.

Song, Yuanli; Mittendorf, Kathleen F.; Lu, Zhenwei; Sanders, Charles R. (2014): Impact of bilayer lipid composition on the structure and topology of the transmembrane amyloid precursor C99 protein. In *Journal of the American Chemical Society* 136 (11), pp. 4093–4096. DOI: 10.1021/ja4114374.

Stanly, Tess A.; Fritzsche, Marco; Banerji, Suneale; García, Esther; La Bernardino de Serna, Jorge; Jackson, David G.; Eggeling, Christian (2016): Critical importance of appropriate fixation conditions for faithful imaging of receptor microclusters. In *Biology open* 5 (9), pp. 1343–1350. DOI: 10.1242/bio.019943.

Statistisches Bundesamt: Bevölkerung - Demografischer Wandel. Available online at https://www.destatis.de/DE/Themen/Querschnitt/Demografischer-Wandel/_inhalt.html, checked on 7/20/2020.

Stopford, Cheryl L.; Snowden, Julie S.; Thompson, Jennifer C.; Neary, David (2008): Variability in cognitive presentation of Alzheimer's disease. In *Cortex; a journal devoted to the study of the nervous system and behavior* 44 (2), pp. 185–195. DOI: 10.1016/j.cortex.2005.11.002.

Strooper, B. de; Annaert, W. (2000): Proteolytic processing and cell biological functions of the amyloid precursor protein. In *Journal of cell science* 113 (Pt 11), pp. 1857–1870.

Suh, Jaehong; Choi, Se Hoon; Romano, Donna M.; Gannon, Moira A.; Lesinski, Andrea N.; Kim, Doo Yeon; Tanzi, Rudolph E. (2013): ADAM10 missense mutations potentiate β-amyloid accumulation by impairing prodomain chaperone function. In *Neuron* 80 (2), pp. 385–401. DOI: 10.1016/j.neuron.2013.08.035.

Suh, Jaehong; Lyckman, Alvin; Wang, Lirong; Eckman, Elizabeth A.; Guénette, Suzanne Y. (2011): FE65 proteins regulate NMDA receptor activation-induced amyloid precursor protein processing. In *Journal of neurochemistry* 119 (2), pp. 377–388. DOI: 10.1111/j.1471-4159.2011.07419.x.

Sundström, A.; Nilsson, L-G; Cruts, M.; Adolfsson, R.; van Broeckhoven, C.; Nyberg, L. (2007): Increased risk of dementia following mild head injury for carriers but not for non-carriers of the APOE epsilon4 allele. In *International psychogeriatrics* 19 (1), pp. 159–165. DOI: 10.1017/S1041610206003498.

Suzuki, Masami; Katsuyama, Kiyoka; Adachi, Kenji; Ogawa, Yumie; Yorozu, Keigo; Fujii, Etsuko et al. (2002): Combination of fixation using PLP fixative and embedding in paraffin by the AMeX method is useful for histochemical studies in assessment of immunotoxicity. In *The Journal of toxicological sciences* 27 (3), pp. 165–172. DOI: 10.2131/jts.27.165.

Szekely, Christine A.; Town, Terrence; Zandi, Peter P. (2007): NSAIDs for the chemoprevention of Alzheimer's disease. In *Sub-cellular biochemistry* 42, pp. 229–248. DOI: 10.1007/1-4020-5688-5_11.

Takahashi, Senye; Kubo, Keiji; Waguri, Satoshi; Yabashi, Atsuko; Shin, Hye-Won; Katoh, Yohei; Nakayama, Kazuhisa (2012): Rab11 regulates exocytosis of recycling vesicles at the plasma membrane. In *Journal of cell science* 125 (Pt 17), pp. 4049–4057. DOI: 10.1242/jcs.102913.

Takami, Mako; Nagashima, Yu; Sano, Yoshihisa; Ishihara, Seiko; Morishima-Kawashima, Maho; Funamoto, Satoru; Ihara, Yasuo (2009): gamma-Secretase: successive tripeptide and tetrapeptide release from the transmembrane domain of beta-carboxyl terminal fragment. In *The Journal of neuroscience : the official journal of the Society for Neuroscience* 29 (41), pp. 13042–13052. DOI: 10.1523/JNEUROSCI.2362-09.2009.

Tan, Chin Wee; Gardiner, Bruce S.; Hirokawa, Yumiko; Layton, Meredith J.; Smith, David W.; Burgess, Antony W. (2012): Wnt signalling pathway parameters for mammalian cells. In *PloS one* 7 (2), e31882. DOI: 10.1371/journal.pone.0031882.

Tanaka, Kenji A. K.; Suzuki, Kenichi G. N.; Shirai, Yuki M.; Shibutani, Shusaku T.; Miyahara, Manami S. H.; Tsuboi, Hisae et al. (2010): Membrane molecules mobile even after chemical fixation. In *Nature methods* 7 (11), pp. 865–866. DOI: 10.1038/nmeth.f.314.

Tanzi, R. E.; Gusella, J. F.; Watkins, P. C.; Bruns, G. A.; St George-Hyslop, P.; van Keuren, M. L. et al. (1987): Amyloid beta protein gene: cDNA, mRNA distribution, and genetic linkage near the Alzheimer locus. In *Science (New York, N.Y.)* 235 (4791), pp. 880–884. DOI: 10.1126/science.2949367.

Tennenberg, S. D.; Zemlan, F. P.; Solomkin, J. S. (1988): Characterization of N-formyl-methionyl-leucyl-phenylalanine receptors on human neutrophils. Effects of isolation and temperature on receptor expression and functional activity. In *Journal of immunology (Baltimore, Md. : 1950)* 141 (11), pp. 3937–3944.

Teppola, Heidi; Sarkanen, Jertta-Riina; Jalonen, Tuula O.; Linne, Marja-Leena (2016): Morphological Differentiation Towards Neuronal Phenotype of SH-SY5Y Neuroblastoma Cells by Estradiol, Retinoic Acid and Cholesterol. In *Neurochemical research* 41 (4), pp. 731–747. DOI: 10.1007/s11064-015-1743-6.

Thavarajah, Rooban; Mudimbaimannar, Vidya Kazhiyur; Elizabeth, Joshua; Rao, Umadevi Krishnamohan; Ranganathan, Kannan (2012): Chemical and physical basics of routine formaldehyde fixation. In *Journal of oral and maxillofacial pathology : JOMFP* 16 (3), pp. 400–405. DOI: 10.4103/0973-029X.102496.

Thermo Fisher Scientific: Fluorescence Quantum Yields (QY) and Lifetimes (τ) for Alexa Fluor Dyes. Table 1.5 (The Molecular Probes® Handbook). Available online at https://www.thermofisher.com/de/de/home/references/molecular-probes-the-handbook/tables/fluorescence-quantum-yields-and-lifetimes-for-alexa-fluor-dyes.html.

Theuns, J.; Marjaux, E.; Vandenbulcke, M.; van Laere, K.; Kumar-Singh, S.; Bormans, G. et al. (2006): Alzheimer dementia caused by a novel mutation located in the APP C-terminal intracytosolic fragment. In *Human mutation* 27 (9), pp. 888–896. DOI: 10.1002/humu.20402.

Thinakaran, Gopal; Koo, Edward H. (2008): Amyloid precursor protein trafficking, processing, and function. In *The Journal of biological chemistry* 283 (44), pp. 29615–29619. DOI: 10.1074/jbc.R800019200.

Tian, Yuan; Bassit, Bhramdeo; Chau, Deming; Li, Yue-Ming (2010): An APP inhibitory domain containing the Flemish mutation residue modulates gamma-secretase activity for Abeta production. In *Nature structural & molecular biology* 17 (2), pp. 151–158. DOI: 10.1038/nsmb.1743.

Tienari, P. J.; Strooper, B. de; Ikonen, E.; Simons, M.; Weidemann, A.; Czech, C. et al. (1996): The beta-amyloid domain is essential for axonal sorting of amyloid precursor protein. In *The EMBO journal* 15 (19), pp. 5218–5229.

Tomiyama, Takami; Nagata, Tetsu; Shimada, Hiroyuki; Teraoka, Rie; Fukushima, Akiko; Kanemitsu, Hyoue et al. (2008): A new amyloid beta variant favoring oligomerization in Alzheimer's-type dementia. In *Annals of neurology* 63 (3), pp. 377–387. DOI: 10.1002/ana.21321.

Torroja, L.; Packard, M.; Gorczyca, M.; White, K.; Budnik, V. (1999): The Drosophila beta-amyloid precursor protein homolog promotes synapse differentiation at the neuromuscular junction. In *The Journal of neuroscience : the official journal of the Society for Neuroscience* 19 (18), pp. 7793–7803.

Townsend, Matthew; Shankar, Ganesh M.; Mehta, Tapan; Walsh, Dominic M.; Selkoe, Dennis J. (2006): Effects of secreted oligomers of amyloid beta-protein on hippocampal synaptic plasticity: a potent role for trimers. In *The Journal of physiology* 572 (Pt 2), pp. 477–492. DOI: 10.1113/jphysiol.2005.103754.

Trapp, B. D.; Hauer, P. E. (1994): Amyloid precursor protein is enriched in radial glia: implications for neuronal development. In *Journal of neuroscience research* 37 (4), pp. 538–550. DOI: 10.1002/jnr.490370413.

Tremml, P.; Lipp, H. P.; Müller, U.; Ricceri, L.; Wolfer, D. P. (1998): Neurobehavioral development, adult openfield exploration and swimming navigation learning in mice with a modified beta-amyloid precursor protein gene. In *Behavioural brain research* 95 (1), pp. 65–76. DOI: 10.1016/s0166-4328(97)00211-8.

Tsubuki, Satoshi; Takaki, Yoshie; Saido, Takaomi C. (2003): Dutch, Flemish, Italian, and Arctic mutations of APP and resistance of Abeta to physiologically relevant proteolytic degradation. In *Lancet (London, England)* 361 (9373), pp. 1957–1958. DOI: 10.1016/s0140-6736(03)13555-6.

Turner, Paul R.; O'Connor, Kate; Tate, Warren P.; Abraham, Wickliffe C. (2003): Roles of amyloid precursor protein and its fragments in regulating neural activity, plasticity and memory. In *Progress in neurobiology* 70 (1), pp. 1–32. DOI: 10.1016/s0301-0082(03)00089-3.

Valenzuela, Michael J.; Sachdev, Perminder (2006): Brain reserve and dementia: a systematic review. In *Psychological medicine* 36 (4), pp. 441–454. DOI: 10.1017/S0033291705006264.

van Broeckhoven, C.; Haan, J.; Bakker, E.; Hardy, J. A.; van Hul, W.; Wehnert, A. et al. (1990): Amyloid beta protein precursor gene and hereditary cerebral hemorrhage with amyloidosis (Dutch). In *Science (New York, N.Y.)* 248 (4959), pp. 1120–1122. DOI: 10.1126/science.1971458.

van den Hurk, W. H.; Bloemen, M.; Martens, G. J. (2001): Expression of the gene encoding the beta-amyloid precursor protein APP in Xenopus laevis. In *Brain research. Molecular brain research* 97 (1), pp. 13–20. DOI: 10.1016/s0169-328x(01)00279-0.

van Nostrand, W. E.; Schmaier, A. H.; Farrow, J. S.; Cunningham, D. D. (1991): Platelet protease nexin-2/amyloid beta-protein precursor. Possible pathologic and physiologic functions. In *Annals of the New York Academy of Sciences* 640, pp. 140–144. DOI: 10.1111/j.1749-6632.1991.tb00205.x.

Villemagne, Victor L.; Pike, Kerryn E.; Chételat, Gaël; Ellis, Kathryn A.; Mulligan, Rachel S.; Bourgeat, Pierrick et al. (2011): Longitudinal assessment of Aβ and cognition in aging and Alzheimer disease. In *Annals of neurology* 69 (1), pp. 181–192. DOI: 10.1002/ana.22248.

Viola, K. L.; Velasco, P. T.; Klein, W. L. (2008): Why Alzheimer's is a disease of memory: the attack on synapses by A beta oligomers (ADDLs). In *The journal of nutrition, health & aging* 12 (1), 51S-7S. DOI: 10.1007/BF02982587.

Volpe, P.; Eremenko-Volpe, T. (1970): Quantitative studies on cell proteins in suspension cultures. In *European journal of biochemistry* 12 (1), pp. 195–200. DOI: 10.1111/j.1432-1033.1970.tb00837.x.

Wada, I.; Rindress, D.; Cameron, P. H.; Ou, W. J.; Doherty, J. J.; Louvard, D. et al. (1991): SSR alpha and associated calnexin are major calcium binding proteins of the endoplasmic reticulum membrane. In *The Journal of biological chemistry* 266 (29), pp. 19599–19610.

Walsh, Dominic M.; Klyubin, Igor; Fadeeva, Julia V.; Cullen, William K.; Anwyl, Roger; Wolfe, Michael S. et al. (2002): Naturally secreted oligomers of amyloid beta protein potently inhibit hippocampal long-term potentiation in vivo. In *Nature* 416 (6880), pp. 535–539. DOI: 10.1038/416535a.

Walter, J.; Capell, A.; Hung, A. Y.; Langen, H.; Schnölzer, M.; Thinakaran, G. et al. (1997): Ectodomain phosphorylation of beta-amyloid precursor protein at two distinct cellular locations. In *The Journal of biological chemistry* 272 (3), pp. 1896–1903. DOI: 10.1074/jbc.272.3.1896.

Walter, J.; Schindzielorz, A.; Hartung, B.; Haass, C. (2000): Phosphorylation of the beta-amyloid precursor protein at the cell surface by ectocasein kinases 1 and 2. In *The Journal of biological chemistry* 275 (31), pp. 23523–23529. DOI: 10.1074/jbc.M002850200.

Wang, Hong; Reiser, Georg (2003): Thrombin signaling in the brain: the role of protease-activated receptors. In *Biological chemistry* 384 (2), pp. 193–202. DOI: 10.1515/BC.2003.021.

Wang, Qianqian; Jia, Jianping; Qin, Wei; Wu, Liyong; Li, Dan; Wang, Qi; Li, Hanzhi (2015): A Novel AβPP M722K Mutation Affects Amyloid-β Secretion and Tau Phosphorylation and May Cause Early-Onset Familial Alzheimer's Disease in Chinese Individuals. In *Journal of Alzheimer's disease : JAD* 47 (1), pp. 157–165. DOI: 10.3233/JAD-143231.

Wang, Yongcheng; Ha, Ya (2004): The X-ray structure of an antiparallel dimer of the human amyloid precursor protein E2 domain. In *Molecular cell* 15 (3), pp. 343–353. DOI: 10.1016/j.molcel.2004.06.037.

Waring, Stephen C.; Rosenberg, Roger N. (2008): Genome-wide association studies in Alzheimer disease. In *Archives of neurology* 65 (3), pp. 329–334. DOI: 10.1001/archneur.65.3.329.

Watson, D. J.; Selkoe, D. J.; Teplow, D. B. (1999): Effects of the amyloid precursor protein Glu693--Gln 'Dutch' mutation on the production and stability of amyloid beta-protein. In *The Biochemical journal* 340 (Pt 3), pp. 703–709.

Weidemann, Andreas; Eggert, Simone; Reinhard, Friedrich B. M.; Vogel, Markus; Paliga, Krzysztof; Baier, Gottfried et al. (2002): A novel epsilon-cleavage within the transmembrane domain of the Alzheimer amyloid precursor protein demonstrates homology with Notch processing. In *Biochemistry* 41 (8), pp. 2825–2835. DOI: 10.1021/bi015794o.

Wenk, Gary L. (2003): Neuropathologic changes in Alzheimer's disease. In *The Journal of clinical psychiatry* 64 Suppl 9, pp. 7–10.

Wertkin, A. M.; Turner, R. S.; Pleasure, S. J.; Golde, T. E.; Younkin, S. G.; Trojanowski, J. Q.; Lee, V. M. (1993): Human neurons derived from a teratocarcinoma cell line express solely the 695-amino acid amyloid precursor protein and produce intracellular beta-amyloid or A4 peptides. In *Proceedings of the National Academy of Sciences of the United States of America* 90 (20), pp. 9513–9517. DOI: 10.1073/pnas.90.20.9513.

Weyer, Sascha W.; Klevanski, Maja; Delekate, Andrea; Voikar, Vootele; Aydin, Dorothee; Hick, Meike et al. (2011): APP and APLP2 are essential at PNS and CNS synapses for transmission, spatial learning and LTP. In *The EMBO journal* 30 (11), pp. 2266–2280. DOI: 10.1038/emboj.2011.119.

Wiese, Mary; Antebi, Adam; Zheng, Hui (2010): Intracellular trafficking and synaptic function of APL-1 in Caenorhabditis elegans. In *PloS one* 5 (9). DOI: 10.1371/journal.pone.0012790.

Williamson, Jennifer; Goldman, Jill; Marder, Karen S. (2009): Genetic aspects of Alzheimer disease. In *The neurologist* 15 (2), pp. 80–86. DOI: 10.1097/NRL.0b013e318187e76b.

Wisniewski, T.; Ghiso, J.; Frangione, B. (1991): Peptides homologous to the amyloid protein of Alzheimer's disease containing a glutamine for glutamic acid substitution have accelerated amyloid fibril formation. In *Biochemical and Biophysical Research Communications* 180 (3), p. 1528. DOI: 10.1016/s0006-291x(05)81370-1.

Wiśniewski, Jacek R.; Hein, Marco Y.; Cox, Jürgen; Mann, Matthias (2014): A "proteomic ruler" for protein copy number and concentration estimation without spike-in standards. In *Molecular & cellular proteomics : MCP* 13 (12), pp. 3497–3506. DOI: 10.1074/mcp.M113.037309.

Wolff, Jennifer L.; Spillman, Brenda C.; Freedman, Vicki A.; Kasper, Judith D. (2016): A National Profile of Family and Unpaid Caregivers Who Assist Older Adults With Health Care Activities. In *JAMA internal medicine* 176 (3), pp. 372–379. DOI: 10.1001/jamainternmed.2015.7664.

World Health Organization (2004): ICD-10 : international statistical classification of diseases and related health problems : tenth revision. 2nd ed.: World Health Organization.

World Health Organization (2019): Dementia. Available online at https://www.who.int/en/news-room/fact-sheets/detail/dementia, updated on 9/19/2019, checked on 7/20/2020.

Xie, Hong-rong; Hu, Lin-sen; Li, Guo-yi (2010): SH-SY5Y human neuroblastoma cell line: in vitro cell model of dopaminergic neurons in Parkinson's disease. In *Chinese medical journal* 123 (8), pp. 1086–1092.

Xue, Yi; Lee, Sangwon; Ha, Ya (2011): Crystal structure of amyloid precursor-like protein 1 and heparin complex suggests a dual role of heparin in E2 dimerization. In *Proceedings of the National*

Academy of Sciences of the United States of America 108 (39), pp. 16229–16234. DOI: 10.1073/pnas.1103407108.

Yaffe, Kristine; Falvey, Cherie; Harris, Tamara B.; Newman, Anne; Satterfield, Suzanne; Koster, Annemarie et al. (2013): Effect of socioeconomic disparities on incidence of dementia among biracial older adults: prospective study. In *BMJ (Clinical research ed.)* 347, f7051. DOI: 10.1136/bmj.f7051.

Yang, Li; Wang, Zilai; Wang, Baiping; Justice, Nicholas J.; Zheng, Hui (2009): Amyloid precursor protein regulates Cav1.2 L-type calcium channel levels and function to influence GABAergic short-term plasticity. In *The Journal of neuroscience : the official journal of the Society for Neuroscience* 29 (50), pp. 15660–15668. DOI: 10.1523/JNEUROSCI.4104-09.2009.

Yokota, Sadaki; Okada, Yoshiie (1997): Quantitative Evaluation of Preparation Procedures Affecting Immunogold Staining in Post Embedding Immunocytochemistry. In *Acta Histochemica et Cytochemica* 30 (5/6), pp. 497–504. DOI: 10.1267/ahc.30.497.

Yoshikai, S.; Sasaki, H.; Doh-ura, K.; Furuya, H.; Sakaki, Y. (1991): Genomic organization of the human-amyloid beta-protein precursor gene. In *Gene* 102 (2), pp. 291–292. DOI: 10.1016/0378-1119(91)90093-q.

Yu, Cheng-han; Rafiq, Nisha Bte Mohd; Cao, Fakun; Zhou, Yuhuan; Krishnasamy, Anitha; Biswas, Kabir Hassan et al. (2015): Integrin-beta3 clusters recruit clathrin-mediated endocytic machinery in the absence of traction force. In *Nature communications* 6, p. 8672. DOI: 10.1038/ncomms9672.

Yu, Haijia; Liu, Yinghui; Gulbranson, Daniel R.; Paine, Alex; Rathore, Shailendra S.; Shen, Jingshi (2016): Extended synaptotagmins are Ca2+-dependent lipid transfer proteins at membrane contact sites. In *Proceedings of the National Academy of Sciences of the United States of America* 113 (16), pp. 4362–4367. DOI: 10.1073/pnas.1517259113.

Zaleta, Alexandra K.; Carpenter, Brian D.; Porensky, Emily K.; Xiong, Chengjie; Morris, John C. (2012): Agreement on diagnosis among patients, companions, and professionals after a dementia evaluation. In *Alzheimer disease and associated disorders* 26 (3), pp. 232–237. DOI: 10.1097/WAD.0b013e3182351c04.

Zanetti, O.; Solerte, S. B.; Cantoni, F. (2009): Life expectancy in Alzheimer's disease (AD). In *Archives of gerontology and geriatrics* 49 Suppl 1, pp. 237–243. DOI: 10.1016/j.archger.2009.09.035.

Zeiler, Marlis; Straube, Werner L.; Lundberg, Emma; Uhlen, Mathias; Mann, Matthias (2012): A Protein Epitope Signature Tag (PrEST) library allows SILAC-based absolute quantification and multiplexed determination of protein copy numbers in cell lines. In *Molecular & cellular proteomics : MCP* 11 (3), O111.009613. DOI: 10.1074/mcp.O111.009613.

Zeng, Fangfa; Yang, Wen; Huang, Jie; Chen, Yuan; Chen, Yong (2013): Determination of the lowest concentrations of aldehyde fixatives for completely fixing various cellular structures by real-time imaging and quantification. In *Histochemistry and cell biology* 139 (5), pp. 735–749. DOI: 10.1007/s00418-012-1058-5.

Zhang, Bin; Gaiteri, Chris; Bodea, Liviu-Gabriel; Wang, Zhi; McElwee, Joshua; Podtelezhnikov, Alexei A. et al. (2013): Integrated systems approach identifies genetic nodes and networks in late-onset Alzheimer's disease. In *Cell* 153 (3), pp. 707–720. DOI: 10.1016/j.cell.2013.03.030.

Zhang, Fang; Gannon, Mary; Chen, Yunjia; Zhou, Lufang; Jiao, Kai; Wang, Qin (2017): The amyloid precursor protein modulates α2A-adrenergic receptor endocytosis and signaling through disrupting arrestin 3 recruitment. In *FASEB journal : official publication of the Federation of American Societies for Experimental Biology* 31 (10), pp. 4434–4446. DOI: 10.1096/fj.201700346R.

Zhao, Siyuan; Liao, Huanhuan; Ao, Meiying; Wu, Li; Zhang, Xiaojun; Chen, Yong (2014): Fixation-induced cell blebbing on spread cells inversely correlates with phosphatidylinositol 4,5-bisphosphate level in the plasma membrane. In *FEBS Open Bio* 4, pp. 190–199. DOI: 10.1016/j.fob.2014.02.003.

Zheng, H.; Jiang, M.; Trumbauer, M. E.; Sirinathsinghji, D. J.; Hopkins, R.; Smith, D. W. et al. (1995): beta-Amyloid precursor protein-deficient mice show reactive gliosis and decreased locomotor activity. In *Cell* 81 (4), pp. 525–531. DOI: 10.1016/0092-8674(95)90073-x.

Zheng, Hui; Koo, Edward H. (2011): Biology and pathophysiology of the amyloid precursor protein. In *Molecular neurodegeneration* 6 (1), p. 27. DOI: 10.1186/1750-1326-6-27.

Zheng, Xueyun; Liu, Deyu; Roychaudhuri, Robin; Teplow, David B.; Bowers, Michael T. (2015): Amyloid β-Protein Assembly: Differential Effects of the Protective A2T Mutation and Recessive A2V Familial Alzheimer's Disease Mutation. In *ACS chemical neuroscience* 6 (10), pp. 1732–1740. DOI: 10.1021/acschemneuro.5b00171.

Zhou, Lujia; Brouwers, Nathalie; Benilova, Iryna; Vandersteen, Annelies; Mercken, Marc; van Laere, Koen et al. (2011): Amyloid precursor protein mutation E682K at the alternative β-secretase cleavage β'-site increases Aβ generation. In *EMBO molecular medicine* 3 (5), pp. 291–302. DOI: 10.1002/emmm.201100138.

Zhu, Xi-Chen; Tan, Lan; Wang, Hui-Fu; Jiang, Teng; Cao, Lei; Wang, Chong et al. (2015): Rate of early onset Alzheimer's disease: a systematic review and meta-analysis. In *Annals of translational medicine* 3 (3), p. 38. DOI: 10.3978/j.issn.2305-5839.2015.01.19.

Zilly, Felipe E.; Halemani, Nagaraj D.; Walrafen, David; Spitta, Luis; Schreiber, Arne; Jahn, Reinhard; Lang, Thorsten (2011): Ca2+ induces clustering of membrane proteins in the plasma membrane via electrostatic interactions. In *The EMBO journal* 30 (7), pp. 1209–1220. DOI: 10.1038/emboj.2011.53.

Zou, Kun; Gong, Jian-Sheng; Yanagisawa, Katsuhiko; Michikawa, Makoto (2002): A Novel Function of Monomeric Amyloid β-Protein Serving as an Antioxidant Molecule against Metal-Induced Oxidative Damage. In *The Journal of neuroscience : the official journal of the Society for Neuroscience* 22 (12), pp. 4833–4841. DOI: 10.1523/JNEUROSCI.22-12-04833.2002.

7. Summary

Alzheimer's Disease (AD) is a major socio-economic threat to health care systems and society in general. Involvement of the amyloid-beta peptide (Aβ) and its parent, the amyloid precursor protein (APP), in AD seemed obvious since the first time it was described by Alois Alzheimer in 1906 and is corroborated by ample genetic, anatomical and pathophysiological evidence. Unfortunately, to date all efforts to cure, slow or even effectively treat AD have failed, indicating that there is still plenty to be learned about its initiation and progression. Two of the most obvious unknowns that are imperative to resolve are the biological function of APP and its cleavage products as well as the underlying molecular mechanisms that coordinate whether APP undergoes β-secretase-mediated amyloidogenic or α-secretase-mediated non-amyloidogenic processing. Previous publications show that at least part of the APP is present in the plasma membranes of many cell types as higher-order oligomers and that plasmalemmal clustering of APP is a primary cause for amyloidogenic processing. Whether APP oligomerization itself can prevent non-amyloidogenic cleavage simply by sterically prohibiting α-secretases access to the molecules in the center of the cluster or APP is able to evade α-processing by other means and oligomerization and subsequent amyloidogenic processing than merely take place as a secondary effect remains to be uncovered. To answer this question, we set out to elucidate the molecular density of the plasmalemmal APP cluster in a relevant human neuronal cell model, the SH-SY5Y cell line. By employing an elaborate combination of various biochemical techniques and state-of-the-art microscopy, it was found that the cellular copy number of APP is about 63,900 molecules, of which 17.5% or about 11,200 reside in the plasma membrane. The surface area of SH-SY5Y cells was determined to be 1,244 μm^2, giving a plasmalemmal molecular density of 9 molecules per μm^2. Around 34% of the detected APP signals constituted monomeric entities, revealing that over 98% of APP molecules had to be oligomerized. Finally, it could be demonstrated that most clusters have a diameter of between 65 and 85 nm and typically contain between 21 and 31 molecules, with considerably bigger entities of well over 100 nm diameter and more than 50 molecules being detected as well. This means that each molecule occupies an area with a radius of just over 7 nm within the cluster, assuming they are distributed evenly over the cluster area. However, it is plausible that the molecules in the center of the complex are in closer proximity to each other than the ones on the periphery and it has been implied that parts of APP curl back onto the plasma membrane. Besides, it is likely that the found molecular density is an underestimate and that other proteins are part of the cluster complex as well. Taken together, molecular crowding within an APP cluster is presumably substantially higher than our results alone suggest, making it increasingly reasonable that α-secretases are indeed unable to approach APP molecules residing within such a cluster.

Furthermore, preceding research has shown that the tiny region consisting of the first 5 amino acids of the Aβ domain is essential for efficient cluster formation of full-length APP. This is extremely interesting, as the only mutation of APP that has been found to be protective against AD, the Icelandic or A673T variant, occurs on the second amino acid of this region. To probe whether its safeguarding effect is linked to the plasmalemmal oligomerization dynamics of APP, the plasma membrane clusters of APP harboring this mutation were characterized and compared to wild-type clusters. We could show that the A673T mutation results in less compact clusters and a more homogeneous distribution in the plasma membrane, as confirmed by both cluster size and relative standard deviation measurements, respectively. Moreover, the plasmalemmal lateral mobility of the full-length proteins was significantly increased for the A673T mutant. A mild but nonsignificant trend towards a decreased colocalization with clathrin-related structures was observed, indicating that the protective variant might also be less prone to be reinternalized into the endocytic sorting machinery. Finally, it could be demonstrated that the A673T mutation is indeed more efficiently non-amyloidogenically processed than the wild-type protein, exemplifying that a decreased tendency to oligomerize may be a mechanism by which it could exert its protective influence. By extent, these results also reinforce the hypothesis that APP's plasmalemmal clustering regulates more than just clathrin-mediated endocytosis. Our work revealed a novel potential mechanism by which protection against amyloidogenic processing can be granted should it be feasible to address pharmacologically in a specific manner, which could possibly have far-reaching consequences in the battle against AD.

8. Acknowledgments

First and foremost, I cannot thank my supervisor, Prof. Dr. Thorsten Lang, enough for allowing me to spend time in his lab and allow me to work on this interesting project. He was always available for discussion and feedback, was deeply involved in the projects and, especially in my case, has shown extraordinary patience and unwavering support. He is an outstanding scientist that has taught me a lot about science and being a scientist.

I would like to thank Prof. Dr. Jochen Walter for kindly agreeing to be my second supervisor. He has been a constant voice of reason and encouragement throughout not only mine, but also my wife's time as a doctoral student. The other two members of my committee Prof. Dr. Dagmar Wachten and Prof. Dr. Ulrich Kubitscheck also deserve a big thanks for their valuable time and willingness to accept the request to take seat in my committee on such short notice.

I am extremely grateful that I could spend my time in the lab with such great colleagues. Helena Batoulis, Martina Bettio, Yahya Homsi, Nora Karnowski, Elisa Merklinger, Jan-Gero Schloetel, Thomas Schmidt, Jan van Üüm and Pascal Weber, thank you for your insights and help. You are great scientists and even better friends, because of you I always came to work with a smile. I sincerely hope we never lose track of each other. A special thanks goes out to Hannes Maib, without you we would have known a lot less about APP. Furthermore, I want to thank the new generation of the AG Lang and especially Jérôme Finke and Nikolas Hochheimer, we might not have spent that much time together, but enough to tell that you are great and smart persons. Thorsten is lucky to have you.

I greatly appreciate the valuable advice of Dr. Julia Sellin and Dr. Thomas Quast and their help with confocal optical sectioning and construction of the 3D models with Imaris, respectively. I would like to thank Elvira, Jenny and Rita from the scullery for their hard work and always welcome chats. Many thanks also to all members of the LIMES Institute, especially Silvia Hoch, Detlef Ragut, Heike Sievert, Tom Wegner and Michael Lange as well as the whole third floor of the LIMES, AG Kolanus and AG Hoch for the nice working atmosphere, the beautiful Christmas parties and making me feel right at home.

I would like to thank my old pals from Helix and the Mensachiller for the continuous support, laughs and friendship since the start of our bachelor studies in Maastricht. Please never change.

I owe my deepest gratitude to my parents for always supporting me, for having a steadfast belief in me and for never giving up on me. Your love gives me strength and keeps me grounded.

Above all, I would like to thank my wife, Nadja Kemmerling, without whom I would probably never have finished this dissertation. Your patience during these stressful times, your incredible love and your sometimes-required nagging were and are irreplaceable. I am extremely lucky to be with you and I wholeheartedly hope we will stay together forever.